

Exploiting Dynamic Covalent Binding for Strain-Specific Bacterial Recognition

Kelly A. McCarthy

A dissertation
submitted to the Faculty of
the department of Chemistry
in partial fulfillment
of the requirements for the degree of
Doctor of Philosophy

Boston College
Morrissey College of Arts and Sciences
Graduate School

August 2018

Exploiting Dynamic Covalent Binding for Strain-Specific Bacterial Recognition

Kelly A. McCarthy

Advisor: Prof. Jianmin Gao, Ph.D.

Antibiotic resistance of bacterial pathogens poses an increasing threat to the wellbeing of our society and urgently calls for new strategies for infection diagnosis and antibiotic discovery. The overuse and misuse of broad-spectrum antibiotics has contributed to the antibiotic resistance crisis. Additionally, treatment of infections with broad-spectrum antibiotics can cause disruption to the host gut microbiome. The development of narrow-spectrum antibiotics would be ideal to avoid unnecessary cultivation of antibiotic resistance and damage to the human microbiota. Bacteria present many mechanisms of resistance, including modulating their cell surface with amine functionalities. In an age where infections are no longer responding to typical antibiotic treatments, novel drugs that target the characteristics of antibiotic resistance would be beneficial to remedy these defiant infections.

Herein, we describe the utility of iminoboronate formation to target the amine-presenting surface modifications on bacteria, particularly those that display antibiotic resistance. Specifically, multiple 2-acetylphenylboronic acid warheads were incorporated into a peptide scaffold to develop potent peptide probes of bacterial cells. Further, by engineering a phage display library presenting the 2-acetylphenylboronic acid moieties, we were able to perform peptide library screens against live bacterial cells to develop reversible covalent peptide probes of target strains of bacteria. These peptide probes,

which were developed for clinical strains of *Staphylococcus aureus* and *Acinetobacter baumannii* which display resistance, can label the target bacterium at submicromolar concentrations in a highly specific manner and in complex biological milieu. We further show that the identified peptide probes can be readily converted to bactericidal agents that deliver generic toxins to kill the targeted bacterial strain with high specificity.

It is conceivable that this phage display platform is applicable to a wide array of bacterial strains, paving the way to facile diagnosis and development of strain-specific antibiotics. Furthermore, it is intriguing to speculate that even higher potency binding could be accomplished with better designed phage libraries with dynamic covalent warheads. This work is currently underway in our laboratory.

TABLE OF CONTENTS

List of tables	vi
List of figures	viii
List of schemes	xii
List of abbreviations	xiii
Acknowledgements	xviii
1.0 Chapter 1: Introduction	1
1.1 Antimicrobial Drug Development	2
1.1.1 The Golden Age of Antibiotic Discovery	2
1.1.2 Modern Day Antibiotic Discovery	4
1.1.3 Targets of Antibiotics: Broad- vs. Narrow-Spectrum	4
1.2 The Origins and Evolution of Antibiotic Resistance	7
1.2.1 Modes of Antibiotic Resistance	7
1.2.2 The ESAKPE Pathogens	8
1.3 Antimicrobial Peptides	9
1.3.1 Host-Defense Peptides	10
1.3.2 Peptide Natural Products	11
1.3.3 Resistance to Antimicrobial Peptides	13
1.4 Conclusions	14
1.5 References	16
2.0 Chapter 2: Labeling Bacterial Cells via Iminoboronate Formation with Polyvalent Display of APBA on a Peptide Scaffold	19
2.1 Introduction	20
2.1.1 Iminoboronate Chemistry	20
2.2 Targeting Bacteria via Iminoboronate Chemistry of Amine-Presenting Lipids	22

2.2.1	Synthesis of AB1 Derivatives	22
2.2.2	Characterization of AB1 Binding	23
2.2.3	AB1 Synergizes with Cationic Peptides for Potent Bacterial Binding	25
2.3	Multivalent Display of APBA Elicits Powerful <i>S. aureus</i> Binding	28
2.3.1	Multivalency	28
2.3.2	Synthesis and Characterization of Dimer Peptides	28
2.3.3	Troubleshooting Efforts and Synthesis of Peptides Beyond Dimers	30
2.3.4	Increasing Valency Increases <i>S. aureus</i> Labeling Potency	34
2.4	Further Analysis of Albumin Binding by Multivalent Peptides	38
2.4.1	Albumin Binding for Increased Serum Retention Time	38
2.4.2	Assessing the Thermodynamics and Kinetics of Albumin Binding	39
2.4.3	Assessing Serum Protein Selectivity	42
2.5	Conclusions	43
2.6	Experimental Procedures	44
2.6.1	General Methods	44
2.6.2	Synthesis of AB1 Derivatives	45
2.6.3	Synthesis of AB1-containing Peptides	53
2.6.4	Synthesis of Tetramer via CuAAC	55
2.6.5	Synthesis of APBA-OH	55
2.6.6	On-resin Multivalent Peptide Synthesis	58
2.6.7	Flow Cytometry Analysis of Bacterial Binding	60
2.6.8	Fluorescence Microscopy Analysis of Bacterial Binding	60
2.6.9	Fluorescence Anisotropy Binding Assay of Serum	60
2.7	References	61
3.0	Chapter 3: Targeting Lipid II Pentapeptide with APBA-Modified Phage Display Library	64
3.1	Introduction	65
3.1.1	Lipid II Pentapeptide and the Peptidoglycan	65
3.1.2	Phage Display	67
3.2	APBA Dimer Library Construction and Validation	69
3.2.1	Synthesis of APBA-IA and Library Modification	69
3.2.2	Confirmation of APBA Modification of Phage	70
3.3	Panning Against Lipid II Pentapeptide and Hit Validation	71

3.3.1	Synthesis of Biotin-Lipid II	71
3.3.2	Screening Protocol Against Lipid II Pentapeptide	72
3.3.3	Characterization of Peptide Repeats	74
3.4	Conclusions	77
3.5	Experimental Procedures	78
3.5.1	General Methods	78
3.5.2	Synthesis of APBA-IA	79
3.5.3	Modification of C7C Library	82
3.5.4	Streptavidin Capture Assay	82
3.5.5	Synthesis of Biotin-Lipid II Pentapeptide	83
3.5.6	Panning Against Lipid II Pentapeptide	84
3.5.7	Synthesis of Peptide Repeats	85
3.5.8	Fluorescence Microscopy Analysis of Lipid II-Bound Streptavidin Beads	86
3.5.9	Fluorescence Anisotropy Analysis of Lipid II-Bound NeutrAvidin Protein	86
3.5.10	Minimum Inhibitory Concentration Determination	86
3.5.11	Flow Cytometry Analysis of <i>S. aureus</i> Binding	87
3.6	References	87
4.0	Chapter 4: Targeting Live Bacterial Cells with APBA-Modified Phage Display Library for Development of targeted Antibiotics	90
4.1	Introduction	91
4.1.1	Live Cell Panning	91
4.1.2	Amine Surface Modifications: A Mechanism of Resistance	91
4.2	Panning Against <i>S. aureus</i> with the APBA Dimer Library	93
4.2.1	Screening Protocol Against <i>S. aureus</i>	93
4.2.2	Characterization of Binding to <i>S. aureus</i>	97
4.2.3	Comparison to Control Phage Libraries	103
4.3	Generating a Targeted Antibiotic for <i>S. aureus</i>	106
4.3.1	Conjugation of Various Hydrophobic Groups	106
4.3.2	Conjugation to Vancomycin	109
4.3.3	Conjugation to Other Antimicrobials	113
4.3.4	Co-treatment with Antimicrobial Peptides	115
4.3.5	Conjugation of ATCUN Motif	116

4.3.6	Conjugation of a Phototoxin Elicits Cell Death Upon Light Exposure	118
4.4	Strain-Specific Targeting of <i>A. baumannii</i>	121
4.4.1	Screening Against <i>A. baumannii</i> (LOS-)	121
4.4.2	Characterization of <i>A. baumannii</i> (LOS-) Binding	122
4.4.3	Generating a Strain-Specific Antibiotic for <i>A. baumannii</i> (LOS-)	125
4.4.4	Screening Against Other Mutant <i>A. baumannii</i> Strains	126
4.4.5	Characterization of a Colistin-Resistant Sensor Peptide	129
4.4.6	Detection of Colistin Resistance in Blood Serum	132
4.5	Serum Stability of the APBA-Dimer Peptides	133
4.5.1	Serum Stability Assessment of APBA-Presenting Peptides	133
4.6	Conclusions	136
4.7	Experimental Procedures	137
4.7.1	General Methods	137
4.7.2	Panning Against Live Cells	139
4.7.3	Phage-Binding Microscopy	140
4.7.4	Synthesis of Peptide Repeats	140
4.7.5	Flow Cytometry Analysis	143
4.7.6	Fluorescence Microscopy	143
4.7.7	Fluorescence Anisotropy	144
4.7.8	KAM5 Conjugate Synthesis	144
4.7.9	Minimum Inhibitory Concentration Determination	149
4.7.10	Photoinactivation of Bacteria	149
4.7.11	MTT Assay to Assess Mammalian Cell Toxicity	150
4.7.12	Analytical HPLC Analysis of Serum Stability	151
4.8	References	151
5.0	Chapter 5: Construction of Novel Phage Libraries	155
5.1	Introduction	156
5.1.1	Selective N-terminal Cysteine Modification	156
5.2	N-terminal Cysteine Phage Library	157
5.2.1	Construction of the IDGRC5C Library	157
5.2.2	Confirmation of Factor XA Cleavage & FPBA Labeling on Model Peptides	161
5.2.3	Attempt to Confirm Cleavage & Labeling on Phage	165
5.2.4	Exploration of Cyanobenzothiazole Chemistry	167
5.3	Conclusions & Future Work	168

5.3.1	Conclusions on IDGRC5C Library	168
5.3.2	Future Work on IDGRC5C Library	169
5.3.3	Additional Proposed Novel Phage Libraries	169
5.4	Experimental Procedures	170
5.4.1	General Methods	170
5.4.2	Preparation of Electrocompetent Cells	171
5.4.3	Preparation of M13KE Vector	172
5.4.4	Preparation of Library Insert	173
5.4.5	Ligation and Electroporation into Competent Cells	174
5.4.6	Model Peptide Synthesis	174
5.4.7	Cleavage and Labeling Confirmation on Model Peptides	175
5.4.8	Streptavidin Capture Assay	176
5.4.9	Measurement of C5C Peptide Oxidation Kinetics	177
5.4.10	Synthesis of CBT-Bio	177
5.5	References	179
6.0	Chapter 6: Conclusions	181

LIST OF TABLES

1	Introduction	
2	Labeling Bacterial Cells via Iminoboronate Formation with Polyvalent Display of APBA on a Peptide Scaffold	
	2-1 – LC-MS monitoring of trimer synthesis with AB1	31
	2-2 – Albumin dissociation constants and rates for multivalent peptides	41
	2-3 – Mass spec data of fluorophore labeled AB1 derivatives	53
	2-4 – Mass spec data of fluorophore labeled AB1-containing peptides	54
	2-5 – Mass spec data of AF488-labeled multivalent APBA peptides	59
3	Targeting Lipid II Pentapeptide with APBA-Modified Phage Display Library	
	3-1 – Sequencing results of Lipid II pentapeptide screen	74
	3-2 – Mass spec data of Lipid II pentapeptide screen hits	85
4	Targeting Live Bacterial Cells with APBA-Modified Phage Display Library for Development of targeted Antibiotics	
	4-1 – Sequencing results of <i>S. aureus</i> screen	95
	4-2 – Synthesized peptide hits from <i>S. aureus</i> screen	97
	4-3 – Sequencing results of control libraries against <i>S. aureus</i>	105
	4-4 – Synthesized peptide hits from control libraries	105
	4-5 – Synthesized KAM5-vancomycin conjugates	111

4-6	– Sequencing results of <i>A. baumannii</i> (LOS-) screen	121
4-7	– Synthesized peptide hits from <i>A. baumannii</i> (LOS-) screen	122
4-8	– Sequencing results of <i>A. baumannii</i> (EGA-407 and EGA-408) screen ...	127
4-9	– Synthesized peptide hits from EGA-407 and EGA-408 screen	128
4-10	– Sequencing results of <i>A. baumannii</i> (WT) screen	129
4-11	– Mass spec data of <i>S. aureus</i> peptide hits	141
4-12	– Mass spec data from control library screen	142
4-13	– Mass spec data of <i>A. baumannii</i> (LOS-) peptide hits	142
4-14	– Mass spec data of EGA-407 and EGA-408 peptide hits	143
4-15	– Mass spec data hydrophobic KAM5 peptides	145
4-16	– Mass spec data of KAM5 conjugates	148
5	Construction of Novel Phage Libraries	
5-1	– Sequencing results from IDGRC5C library construction	161
5-2	– Mass spec data of model peptides	175
6	Conclusions	

LIST OF FIGURES

1 Introduction	
1-1 – Timeline of antibiotics	2
1-2 – Synthetic tailoring of antibiotics	3
1-3 – Targets of antibiotics	5
1-4 – FDA approval of antibiotics	6
1-5 – Mechanisms of resistance	8
1-6 – Examples of host-defense peptides	11
1-7 – Examples of NRP antibiotics	12
1-8 – Lys-PG production in <i>S. aureus</i>	14
2 Labeling Bacterial Cells via Iminoboronate Formation with Polyvalent Display of APBA on a Peptide Scaffold	
2-1 – Imine versus iminoboronate formation	21
2-2 – Fluorescence anisotropy of liposome binding by AB1	24
2-3 – Fluorescence microscopy analysis of cell staining by AB1	25
2-4 – Flow cytometry analysis and confocal microscopy of <i>S. aureus</i> staining by AB1	27
2-5 – Fluorescence microscopy and flow cytometry analysis of Hlys-AB1	28
2-6 – Flow cytometry analysis of dimer-AB1 peptides	30
2-7 – LC-MS analysis of tetramer synthesized via CuAAC	32
2-8 – Multivalent peptide synthesis via on-resin coupling	34

2-9 – Flow cytometry analysis of multivalent peptides	35
2-10 – Fluorescence microscopy analysis of multivalent peptides	36
2-11 – BSA interference of <i>S. aureus</i> staining by multivalent peptides	37
2-12 – Fluorescence microscopy analysis of cyclic trimers	37
2-13 – Illustration of albumin binding with APBA	39
2-14 – Fluorescence anisotropy of albumin binding by multivalent peptides	40
2-15 – Kinetic association of multivalent peptides to albumin	41
2-16 – Serum protein binding curves by KAM-CT	43
3 Targeting Lipid II Pentapeptide with APBA-Modified Phage Display Library	
3-1 – Illustration of peptidoglycan synthesis	66
3-2 – Illustration of Lipid II structure	67
3-3 – Examples of chemical modifications to phage libraries	68
3-4 – APBA-IA modification of phage	69
3-5 – Confirmation of phage labeling with APBA	71
3-6 – Structure of Biotin-Lipid II	72
3-7 – Illustration of panning protocol against Lipid II pentapeptide	73
3-8 – Fluorescence microscopy of Lipid II pentapeptide binding	75
3-9 – Fluorescence anisotropy of Lipid II pentapeptide binding	76
3-10 – MIC determination and flow cytometry analysis of peptide repeats	77
4 Targeting Live Bacterial Cells with APBA-Modified Phage Display Library for Development of targeted Antibiotics	
4-1 – Amine modification on bacterial cell surfaces	93
4-2 – Illustration of panning protocol against live bacterial cells	94
4-3 – Fluorescence microscopy analysis of phage binding	96
4-4 – Flow cytometry analysis of <i>S. aureus</i> binding by KAM1-KAM5	98
4-5 – Flow cytometry-assessed binding by KAM3 and KAM5 up to 10 μ M	99
4-6 – Flow cytometry comparison of KAM5 to Hlys-AB1	99

4-7 – Flow cytometry comparison of KAM5 to control peptides	100
4-8 – Fluorescence microscopy of <i>S. aureus</i> staining by KAM5	101
4-9 – Comparison of BSA versus HSA in KAM5 <i>S. aureus</i> binding	101
4-10 – Comparison of KAM5 binding to <i>MRSA</i>	102
4-11 – Selectivity of KAM5 towards <i>S. aureus</i> over other bacterial species	103
4-12 – Comparison of control library hits to KAM5	106
4-13 – Panel of hydrophobic KAM5 conjugates synthesized	107
4-14 – MIC assay of hydrophobic KAM5 conjugates	108
4-15 – Structures and MIC assay of vancomycin-alkyne derivatives	109
4-16 – MIC assay of KAM5-vancomycin conjugates	111
4-17 – Structures and MIC assay of vancomycin controls	113
4-18 – Structures of KAM5-Hlys and KAM5-m146	114
4-19 – MIC assay of KAM5-Hlys and KAM5-m146	115
4-20 – MIC assay of PG1 and Daptomycin co-treatment with KAM5	116
4-21 – Structure and MIC assay of ATCUN-KAM5	117
4-22 – Structure and KAM5-Eosin and illustration of photodynamic therapy	118
4-23 – Photoirradiation of <i>S. aureus</i> with KAM5 and controls	119
4-24 – Assessment of mammalian cell toxicity of KAM5 photoirradiation	120
4-25 – Flow cytometry analysis of <i>A. baumannii</i> binding by KAM7-KAM10	123
4-26 – Flow cytometry comparison of KAM8 to control peptides	123
4-27 – Fluorescence microscopy of <i>A. baumannii</i> (LOS-) staining by KAM8	124
4-28 – Selectivity of KAM8 towards <i>A. baumannii</i> over other bacterial species	125
4-29 – Photoirradiation of <i>A. baumannii</i> (LOS-) with KAM8 and controls	126
4-30 – Flow cytometry analysis of all <i>A. baumannii</i> strains	130
4-31 – Flow cytometry analysis of KAM19 compared to controls	131
4-32 – Fluorescence microscopy of all <i>A. baumannii</i> strains by KAM19	132
4-33 – Analysis of KAM19 binding bacterial co-culture in blood serum	133
4-34 – Serum stability of KAM5-Eosin	134
4-35 – Serum stability of KAM8-Eosin and KAM19-FAM	135

5 Construction of Novel Phage Libraries

5-1 – Schematic of Factor XA cleavage and FPBA labeling on phage	157
5-2 – Agarose gel purification of M13KE vector	159
5-3 – Polyacrylamide gel purification of library insert	160
5-4 – Structures of control peptides synthesized	162
5-5 – LC-MS analysis of Factor XA treated IDGRC5C peptide	163
5-6 – LC-MS analysis of FPBA-biotin labeled C5C-FAM peptide	164
5-7 – Streptavidin capture of AC7C versus IDGRC5C library	165
5-8 – Streptavidin capture assay for library modification confirmation	166
5-9 – Oxidation kinetics of C5C-FAM peptide	167
5-10 – LC-MS analysis of CBT-biotin labeled C5C-FAM peptide	168
5-11 – Additional unique phage library designs	170

6 Conclusions

LIST OF SCHEMES

1	Introduction	
2	Labeling Bacterial Cells via Iminoboronate Formation with Polyvalent Display of APBA on a Peptide Scaffold	
	2-1 – Synthesis of AB1 derivatives	23
	2-2 – Synthesis of APBA-OH	33
3	Targeting Lipid II Pentapeptide with APBA-Modified Phage Display Library	
	3-1 – Synthesis of APBA-IA	70
4	Targeting Live Bacterial Cells with APBA-Modified Phage Display Library for Development of targeted Antibiotics	
5	Construction of Novel Phage Libraries	
	5-1 – Synthesis of CBT-Bio	167
6	Conclusions	

LIST OF ABBREVIATIONS

(CF₃SO₂)₂O	Trifluoromethanesulfonic anhydride
AF488	Alexa Fluor 488
Ala, A	Alanine
Alloc	Allyloxycarbonyl
APBA	Acetylphenylboronic acid
Arg, R	Arginine
Asn, N	Asparagine
Asp, D	Aspartic acid
ATCUN	Amino-terminal copper and nickel
B₂pin₂	Bis(pinacolato)diboron
Boc	<i>Tert</i> -butyloxycarbonyl
Bpin	Pinacol ester
BSA	Bovine serum albumin
C-dif	<i>Clostridium difficile</i> infection
CaCl₂	Calcium chloride
CAMP	Cationic antimicrobial peptide
CBT	2-Cyanobenzothiazole
CDC	Centers for Disease Control
cfu	Colony forming units
CuAAC	Copper-catalyzed azide-alkyne cycloaddition
CuSO₄	Copper sulfate
Cys, C	Cysteine

Dap	Diaminopropionic acid
DBU	1,8-Diazabicyclo[5.4.0]undec-7-ene
Dbz	Diaminobenzoic acid
DCM	Dichloromethane
DIC	<i>N,N'</i> -Diisopropylcarbodiimide
DIPEA	<i>N,N</i> -Diisopropylethylamine
DMAP	4-Dimethylaminopyridine
DMF	Dimethylformamide
DMPA	2,2-Dimethoxy-2-phenylacetophenone
DMSO	Dimethylsulfoxide
EDTA	Ethylenediaminetetraacetic acid
ESI	Electrospray ionization
Et₃N	Triethylamine
EtBr	Ethidium bromide
FAM	Carboxyfluorescein
FBS	Fetal bovine serum
FDA	Food and Drug Administration
FITC	Fluorescein isothiocyanate
Fmoc	fluorenylmethyloxycarbonyl
FPBA	Formylphenylboronic acid
gA	Gramicidin A
GlcNAc	<i>N</i> -Acetylglucosamine
Gln, Q	Glutamine
Glu, E	Glutamic acid
Gly, G	Glycine
HBTU	Hexafluorophosphate Benzotriazole Tetramethyl Uronium
HCl	Hydrochloric acid
His, H	Histidine
HSA	Human serum albumin

IA	Iodoacetamide
Ile, I	Isoleucine
IPTG	Isopropyl β -D-1-thiogalactopyranoside
iTCEP	Immobilized TCEP
K₂CO₃	Potassium carbonate
K_d	Equilibrium dissociation constant
KOAc	Potassium acetate
LC-MS	Liquid chromatography-mass spectrometry
Leu, L	Leucine
LOS	Lipooligosaccharide
LPS	Lipopolysaccharide
Lys-PG	Lysyl-phosphatidylglycerol
Lys, K	Lysine
MeOH	Methanol
Met, M	Methionine
MIC	Minimum inhibitory concentration
MprF	Multi-peptide resistance factor
MRSA	Methicillin-resistant <i>S. aureus</i>
MS	Mass spectrometry
MTT	3-(4,5-dimethylthiazol-2-yl)-2,5-diphenyltetrazolium bromide
MurNAc	<i>N</i> -Acetylmuramic acid
Na₂CO₃	Sodium carbonate
Na₂SO₄	Sodium sulfate
NaAsc	Sodium ascorbate
NaCl	Sodium chloride
NaHCO₃	Sodium bicarbonate
Nal	Sodium Iodide
Nbz	<i>N</i> -acyl-benzimidazolinone

NEB	New England Biolabs
NMM	<i>N</i> -Methylmorpholine
NMR	Nuclear Magnetic Resonance spectroscopy
NRP	Non-ribosomal peptide
OD₆₀₀	Optical density measured at 600nm
OSu	Succinimidyl ester
PBPs	Penicillin-binding proteins
PBS	Phosphate-buffered saline
PBST	Phosphate-buffered saline with Tween
Pd(dppf)Cl₂	[1,1'-Bis(diphenylphosphino)ferrocene]dichloropalladium (II)
PE	Phosphatidylethanolamine
PEG	Polyethylene glycol
pfu	plaque-forming units
PG	Phosphatidylglycerol
PG1	Protegrin-1
Phe, F	Phenylalanine
PLP	Pyridoxal phosphate
Pro, P	Proline
PS	Phosphatidylserine
ROS	Reactive oxygen species
RP-HPLC	Reversed-phase high-performance liquid chromatography
Scz	Semicarbazide
SDS-PAGE	Sodium dodecyl sulfate-polyacrylamide gel electrophoresis
Ser, S	Serine
SPPS	Solid-phase peptide synthesis
TA	Teichoic acid
TAE buffer	Tris-acetic acid-EDTA buffer
TAMRA	Carboxytetramethylrhodamine

TBE buffer	Tris-borate-EDTA buffer
TBS	Tris-buffered saline
TBST	Tris-buffered saline with Tween
TCEP	Tris(2-carboxyethyl)phosphine
TE buffer	Tris-EDTA buffer
TFA	Trifluoroacetic acid
THF	Tetrahydrofuran
Thr, T	Threonine
TLC	Thin layer chromatography
Trp, W	Tryptophan
Tyr, Y	Tyrosine
TzB	Thiazolidino boronate
UV-VIS	Ultraviolet-Visible
Val, V	Valine
WT	Wild type
WTA	Wall teichoic acid
Xgal	5-bromo-4-chloro-3-indolyl- β -D-galactopyranoside

ACKNOWLEDGMENTS

First and foremost, I would like to express my sincere gratitude to my advisor Professor Jianmin Gao for his guidance, encouragement, and immense knowledge. His passion and enthusiasm for science has kept me motivated throughout my Ph.D. research.

I would also like to thank my committee, Professor Abhishek Chatterjee and Professor Eranthie Weerapana, for their insightful feedback throughout my time at Boston College and for taking the time to read and review my dissertation.

I would like to thank all of my co-workers for fostering a collaborative and fun lab environment. Their thoughtful suggestions have helped me in many aspects of my research. I especially want to thank Sam Cambray and Dr. Breanna Zerfas for not only being people you can count on to help you with anything science-related, but also for being great friends.

Ultimately, I would like to thank my family, my friends and Chris. Without the love and encouraging words of support from these amazing people, I would not be where I am today. Chris has always kept me smiling with his positive and uplifting personality. Laura and Richie are not only siblings that I have always looked up to, but they are hilarious people who can turn around any bad day. A heartfelt thank you to my mom and dad who have always encouraged me to be the best version of myself, supporting me every step of the way.

CHAPTER 1
INTRODUCTION

1.1 Antimicrobial Drug Development

Most bacteria are harmless to humans, participating in commensal or even mutualistic relationships with their host. However, some bacteria species are pathogenic, causing serious infections that can lead to human morbidity or mortality without proper treatment. Antibiotics have had a major impact on the control of infectious diseases that were the leading causes of illness and death for most of human existence.¹

1.1.1 The Golden Age of Antibiotic Discovery

The rise of modern antimicrobial drug development is often associated with the discovery of sulfa drugs and β -lactams. The systematic screening approach of selectively targeting disease-causing microbes developed by Paul Ehrlich in the early 1900's steered the discovery of sulfa drugs, specifically Prontosil, by scientists in the pharmaceutical industry in 1935.^{1,2} Also during this initial time period, Alexander Fleming serendipitously discovered Penicillin, a β -lactam, which was introduced to the clinic in 1940.² The period of time following these discoveries is often termed the "golden age" of antibiotic discovery, with most new drugs introduced to the clinic around 1950-1960 (Figure 1-1).³

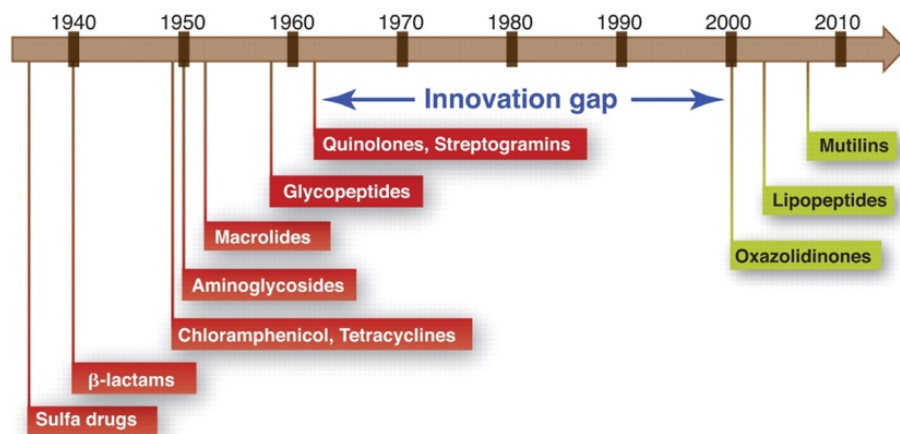


Figure 1-1 Timeline of antibiotic introduction to the clinic (from reference 3).

Originally, the optimal source of new antimicrobial agents was from soil microbes, taking advantage of bacteria's ability to produce their own antibiotics. A discovery platform established by Selman Waksman in the 1940's pioneered this natural product antibiotic discovery with the introduction of streptomycin, the first effective drug for treating tuberculosis and the first aminoglycoside.⁴ Mining soil microbes for antibiotics, mainly *Streptomyces*, was extensively exploited by the pharmaceutical industry during this time period, leading to the discovery of the major classes of antibiotics, such as chloramphenicol and various macrolides; however, the continuous identification of the same compounds eventually suppressed this platform.⁵ Synthetic compounds were also discovered during this time period, particularly quinolones, by the serendipitous discovery of nalidixic acid, a by-product of chloroquine synthesis.⁶ More than two-thirds of clinically used antimicrobial agents today are natural products or their semisynthetic derivatives, based on the chemical scaffolds that were introduced during this era (Figure 1-2).³

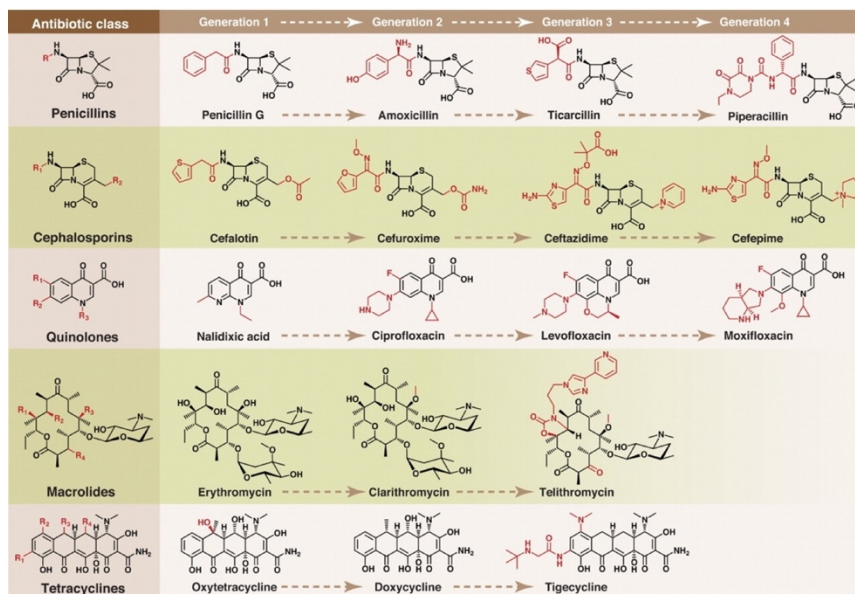


Figure 1-2 Synthetic tailoring of various classes of antibiotics (from reference 3).

1.1.2 Modern Day Antibiotic Discovery

Notably, between 1962 and 2000, no novel major classes of antibiotics were discovered, creating an immense discovery void. New and effective scaffolds were becoming harder to identify using the Waksman platform. Although oxazolidinones, lipopeptides and mutilins were introduced to the clinic in the 2000's, they were discovered two decades prior.³ This lack of development of novel antimicrobial scaffolds overlapped with increased presentation of bacterial resistance mechanisms to nearly all antimicrobial drugs, a major concern in the field of antibiotics. Due to the lack of return on investment, which can be quite high for antibiotic drug discovery, most pharmaceutical companies direct their resources to drug development for chronic use, such as cancer therapeutics.⁷ Encouragingly, novel antibiotics are still being reported, such as teixobactin.⁸ Teixobactin was reported by Lewis and coworkers in 2015 as a cell wall inhibitor discovered in a screen of uncultured bacteria grown in their natural environment using an iChip device, a tool that could revive the Waksman platform of natural product drug discovery.⁸⁻¹⁰ Teixobactin is still in early-development stage; however, there are a handful of antimicrobial drugs in late-stage clinical development.^{7,10-11} Most of these antibiotics in late-stage trials are however intravenous, solely for hospitalized patients⁷; therefore, there is still an urgent need for the continuous development of novel antimicrobial agents to keep up with constantly evolving pathogens.

1.1.3 Targets of Antibiotics: Broad- vs. Narrow-Spectrum

Besides cell wall synthesis, most antibiotics target intracellular pathways, which requires penetration of the bacterial cell. For this reason, many high-throughput screens

of drugs fail to yield potent antimicrobial drugs due to failed penetration of the outer membrane. Additionally, although there are about 200 conserved essential proteins in bacteria, the most successful antibiotics only exploit a small number of conserved metabolic enzymes or pathways (Figure 1-3).^{4,12}

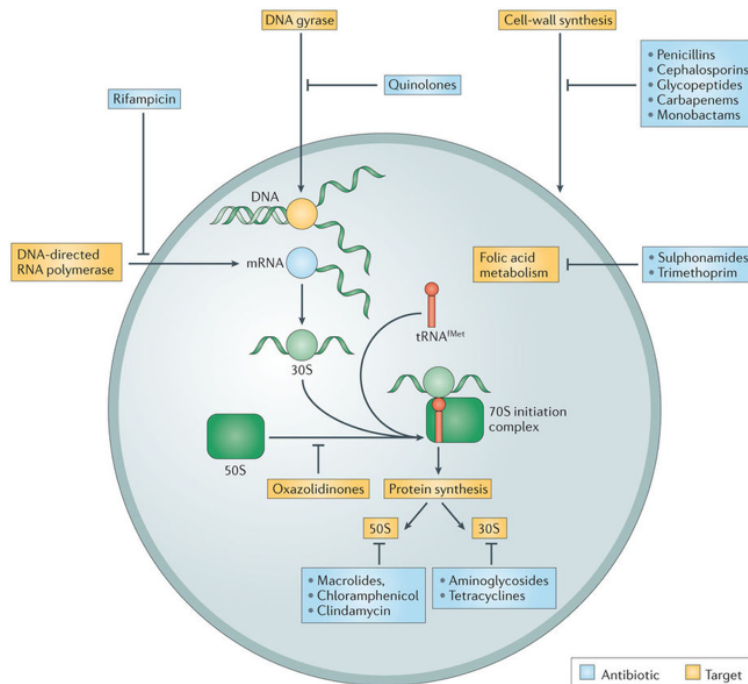


Figure 1-3 Targets of commonly used antibiotics (from reference 4).

A recent study utilizing *Salmonella enterica* as a model pathogen, demonstrated that the total number of new and attractive metabolic enzyme targets for broad-spectrum antimicrobial development is perhaps limited.¹² Although it is likely that some targets still remain unidentified, this study may elucidate why so few new classes of antibiotics have been approved since the golden age of antibiotic discovery. This data supports the robustness of pursuing narrow-spectrum antibiotics that can target a specific virulent-essential entity of a particular bacterial species rather than an enzyme conserved throughout all bacteria. One such example is Bedaquiline (Sirturo), a

diarylquiniline which has narrow-spectrum activity against *Mycobacterium tuberculosis* by inhibiting ATP synthase, introduced to the clinic in 2012.¹³

In addition to establishing a new field of targets that do not need to be conserved throughout pathogenic bacteria, narrow-spectrum antibiotics can overcome some of the pitfalls of broad-spectrum antibiotics. Broad-spectrum antibiotics can disrupt the human microbiome, causing significant damage to commensal gut bacteria, often resulting in health problems such as the notable *Clostridium difficile* (C-dif) infection.¹⁴ Furthermore, although antibiotic resistance occurs naturally, the overuse of broad-spectrum antibiotics in both humans and animals accelerates this process.³ Ideally, to avoid unintentional cultivation of antibiotic resistance and human microbiota damage, it would be advantageous to replace broad-spectrum antibiotics with narrow-spectrum antibiotics. This narrow-spectrum ideology appears to be where the field of antibiotics is heading, given that newest antimicrobial drugs are either selective for one Gram-stain group or pathogen and that only a single broad-spectrum antibiotic was approved by the Food and Drug Administration (FDA) in 2010-2014 (Figure 1-4).¹⁴

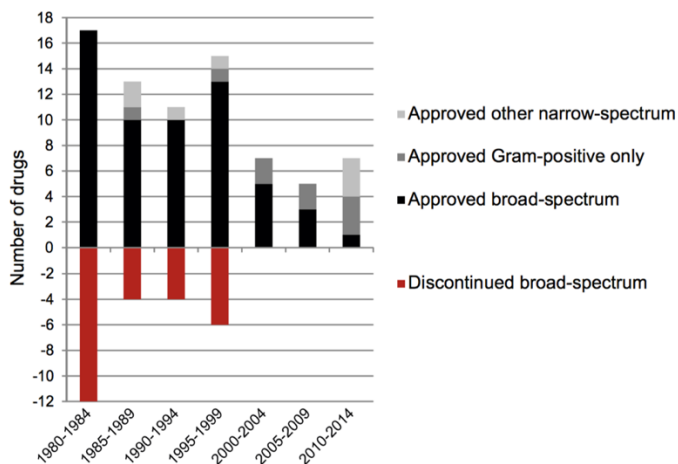


Figure 1-4 United States FDA approval and discontinuation of antibiotics since 1980 (from reference 14).

1.2 The Origins and Evolution of Antibiotic Resistance

Antibiotic resistant bacterial pathogens have become a global threat to public health. Resistance to essentially all current antibiotics has been reported and diverse mechanisms of resistance have been elucidated in recent years and are continuously being discovered.¹⁵ According to the Center for Disease Control (CDC), over 2 million antibiotic resistant infections are reported each year leading to approximately 23,000 deaths in the United States alone.

1.2.1 Modes of Antibiotic Resistance

The rapid manifestation of resistance can be exemplified by the β -lactam class of antibiotics. Shortly after its introduction to the clinic, resistance to penicillin was documented in 1945. This was due to an enzyme penicillinase, a β -lactamase, which inactivates the antibiotic via hydrolysis. Fortunately, the pharmaceutical industry thoroughly investigated β -lactamase inhibitors, leading to a successful co-treatment of various β -lactams and β -lactamase inhibitors, and optimized β -lactamase-stable antibiotics, such as the carbapenems.¹⁶ In addition to this hydrolysis mechanism by bacterial enzymes, β -lactams experienced additional modes of resistance such as drug efflux and target alteration.¹⁷ These modes of resistance, along with others, represent the most common clinically relevant resistance mechanisms (Figure 1-5).⁴

Antibiotic resistance can occur for a variety of reasons. Some bacteria can encompass intrinsic resistance to a particular antibiotic, whereas other bacteria acquire resistance via horizontal gene transfer or through a genetic mutation.¹⁵ The widespread overuse and misuse of antibiotics has allowed bacteria to evolve these diverse resistance

mechanisms. In the presence of an antimicrobial drug, susceptible organisms are eliminated while resistant organisms, and their genetic resistance traits, are selected for.¹⁸ These resistance traits can be transferred among bacteria of different taxonomic and ecological groups via bacteriophages, plasmids, or free DNA. The resistant bacteria continue to propagate under antimicrobial selection to amplify and extend the problem to other hosts and other geographical locations.^{18,19}

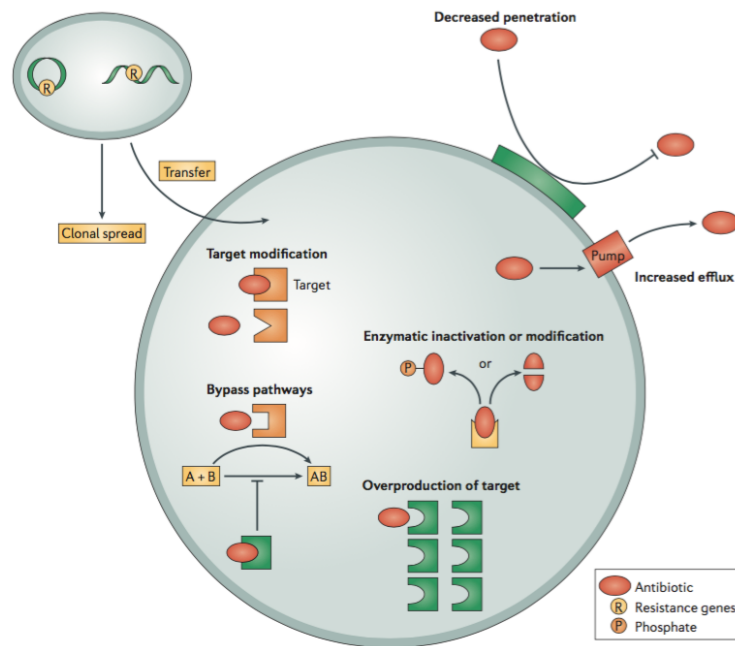


Figure 1-5 Most common mechanisms of resistance (from reference 4).

1.2.2 The ESKAPE Pathogens

There are numerous bacterial species presenting multi-drug resistance on the rise and require immediate attention. Of particular importance are the “ESKAPE pathogens” (*Enterococcus faecium*, *Staphylococcus aureus*, *Klebsiella pneumoniae*, *Acinetobacter baumannii*, *Pseudomonas aeruginosa* and *Enterobacter* species) which exhibit prominent levels of antibiotic resistance and often escape eradication by normal courses of

treatment.^{20,21} These species of bacteria not only cause the majority of infections among society, but are increasingly prevalent in hospitals, causing the majority of nosocomial infections.²⁰ The majority of nosocomial *S. aureus* infections in the United States exhibit methicillin-resistance and are typically multi-drug resistant.^{18,22} According to the CDC, methicillin-resistant *S. aureus* (MRSA) was the cause of approximately 11,000 deaths in the United States in 2011, accounting for nearly half of the antibiotic resistant infection-related deaths. These resistant strains of bacteria are becoming progressively difficult to treat, with effective therapeutic options declining. Many doctors are forced to treat patients with older, discontinued antibiotics, although they typically exhibit significant toxicity to healthy human cells.²¹ For example, colistin (polymyxin E) is now used as a drug of last resort for Gram-negative infections, such as *A. baumannii*.²³ Unfortunately, recent reports have also revealed colistin resistance in *A. baumannii*.²⁴ It is of contemporary importance to overcome the ESKAPE pathogens and their increasing resistance to antibiotics.

1.3 Antimicrobial Peptides

Inspired by nature, there has been considerable interest in the development of peptide therapeutics as antibiotics.²⁵⁻³⁰ Both plants and animals possess potent, broad-spectrum host-defense peptides as part of their innate immune system. Additionally, many microbes produce non-ribosomal natural product peptides with antimicrobial activity. Peptide therapeutics in general are attractive for their advantages over small molecules, in terms of better selectivity and potency, and over antibodies, in terms of their smaller size.³¹ As of 2015, more than 60 peptide therapeutics were introduced to

the market and hundreds of novel peptide drugs were in clinical development for a variety of ailments.³²

1.3.1 Host-Defense Peptides

Host-defense peptides are short, cationic antimicrobial peptides (CAMPs) with amphiphilic properties. They are gene-encoded peptides that are often subjected to post-translational modifications, including proteolytic processing of a precursor sequence, to yield segments of 10-50 amino acid long peptides with an overall positive charge typically ranging from +2 to +9.^{25,26} In general, the mechanism of action of CAMPs involves the initial electrostatic interaction of the cationic peptide with the anionic bacterial cell membrane followed by membrane insertion, after which the peptide can disrupt the physical integrity of the membrane or translocate across the membrane to act on internal targets.²⁶ In mammals, the direct antimicrobial activity of these host-defense peptides is typically weak at physiological conditions, and their ability to participate in immunomodulatory events is more vital.³³ There have been more than 1,500 peptides identified from essentially all species of life that not only display antimicrobial activity, but also modulate the innate immune system.³⁰ These CAMPs exhibit significant diversity (Figure 1-6), yet can be generalized into four broad categories: β -sheet peptides stabilized by 2-4 disulfide bridges, α -helical peptides, extended helices with a predominance of certain amino acids (glycine, proline, tryptophan, arginine and/or histidine), and loop peptides with a disulfide bridge.^{26,29}

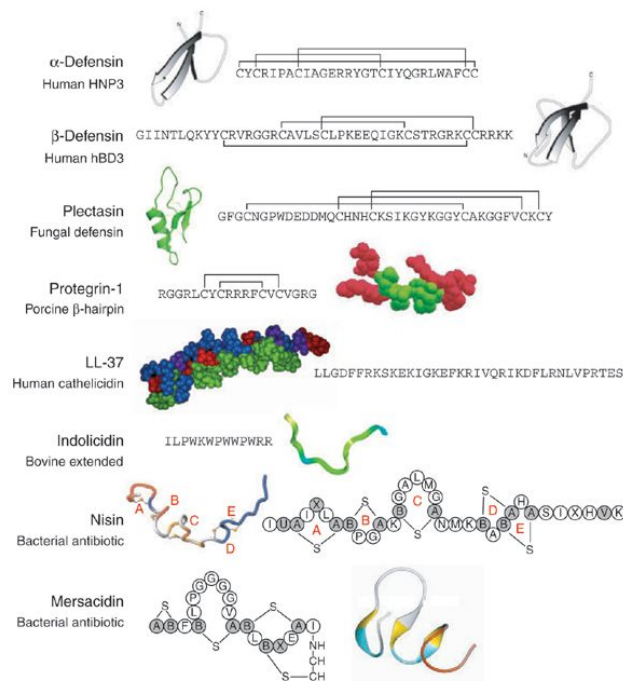


Figure 1-6 Examples of various types of host-defense peptides (adapted from reference 26).

Although successful in nature, the therapeutic use of host-defense peptides as antibiotics is rather limited. For example, the lantibiotic nisin, effective at nanomolar concentrations, is used as an antimicrobial food preservative.^{25,26} Significant efforts have been invested in the design and development of synthetic cationic peptides based on known host-defense peptides. However, there are only a handful of cationic host-defense peptide mimics that have advanced into phase III clinical trials and most are solely for topical use due to cytotoxicity and instability.^{26,27}

1.3.2 Peptide Natural Products

Many powerful antibiotics currently on the market are natural products isolated from various organisms.³⁴ Several of these are non-ribosomal peptides (NRPs) or NRP-polyketide hybrid natural products that are biosynthesized via assembly lines of enzymes and incorporate unnatural functionalities such as cyclizations and D-amino acids.³⁵ Many

of these NRPs are arranged as rigid macrocycles, which allows for high affinity binding with their target due to enhanced conformational stability.³⁶ Among these constrained macrocyclic natural product antibiotics are the well-known polymyxins, gramicidin S, vancomycin, daptomycin and teixobactin (Figure 1-7). Polymyxins and gramicidin S are CAMPs that have been used extensively in the clinic for years in the topical treatment of infections.^{26,29} Vancomycin, the first glycopeptide discovered in 1956, is a non-cationic antibiotic administered intravenously for the treatment of serious Gram-positive infections.³⁷ More recently, the anionic lipopeptide daptomycin (Cubicin) was approved by the FDA in 2003 for the intravenous treatment of complicated Gram-positive skin infections.²⁷ The newly discovered teixobactin, mentioned previously, is a cyclic depsipeptide in clinical development to treat drug resistant Gram-positive infections, currently with no reported or anticipated resistance mechanisms.^{7,8}

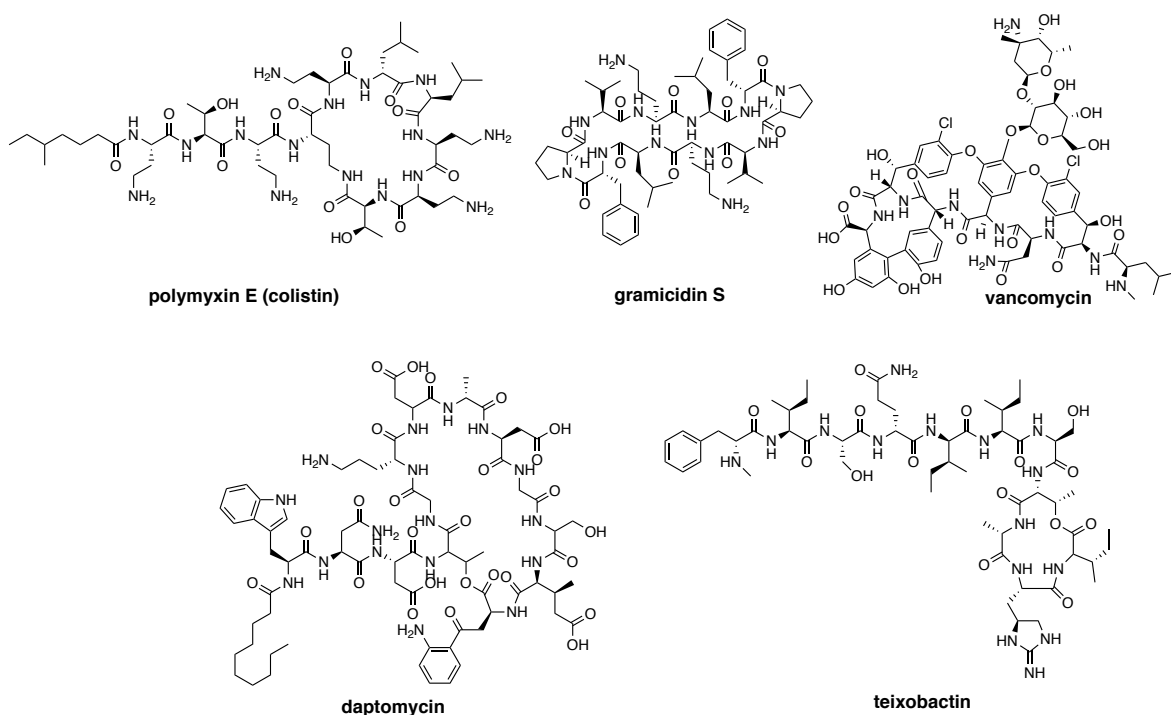


Figure 1-7 Prominent examples of non-ribosomal peptide antibiotics.

1.3.3 Resistance to Antimicrobial Peptides

As discussed previously, bacterial resistance to essentially all current antibiotics via diverse mechanisms has been reported. Due to their fundamental requirement to interact with the bacterial cell membrane and their probability to engage multiple targets, peptide antibiotics are less susceptible to resistance mechanisms compared to other antibiotics.^{25,30} Resistance to these antibiotics would require complete alteration of the membrane or elimination of multiple targets, occurrences that are likely to occur at a lower propensity than the resistance mechanisms exhibited by conventional antibiotics.²⁷

Although antimicrobial peptides are less likely to develop resistance, pathogens have still evolved mechanisms of resistance. Among external trapping mechanisms, membrane efflux pumps, peptidases and down-regulation of host antimicrobial peptide production, a major resistance mechanism that pathogens develop for peptide antibiotics is cell surface modifications to reduce the affinity of the required initial interaction, often by the addition of positively charged amine functionalities.³⁸⁻⁴¹ Gram-positive bacteria instigate charge repulsion by D-alanylation of teichoic acid (TA) and amino-acylation of phosphatidylglycerol (PG), cause steric hindrance by L-rhamnosylation of wall teichoic acid (WTA), and undergo Lipid II modification. Gram-negative bacteria instigate charge repulsion by Lipid A phosphate modification, increase outer membrane rigidity by Lipid A acylation and, similar to Gram-positive pathogens, increase inner membrane rigidity via PG acylation.³⁹ Many regulatory systems and proteins³⁹ have been identified as elements responsible for these bacterial surface modifications. In *S. aureus* for example, the addition of lysine onto the anionic PG, producing lysyl-phosphatidylglycerol (Lys-PG) and

neutralizing the negative charge of the phospholipid, is catalyzed by the integral membrane protein multi-peptide resistance factor (MprF, Figure 1-8).³⁹⁻⁴¹ The synthase domain of MprF catalyzes the addition of lysine from the lysyl-tRNA to PG (or alanine from the alanyl-tRNA) and the flippase domain translocates the lipid to the outer member, resulting in a more positively charged membrane to repel CAMPs.

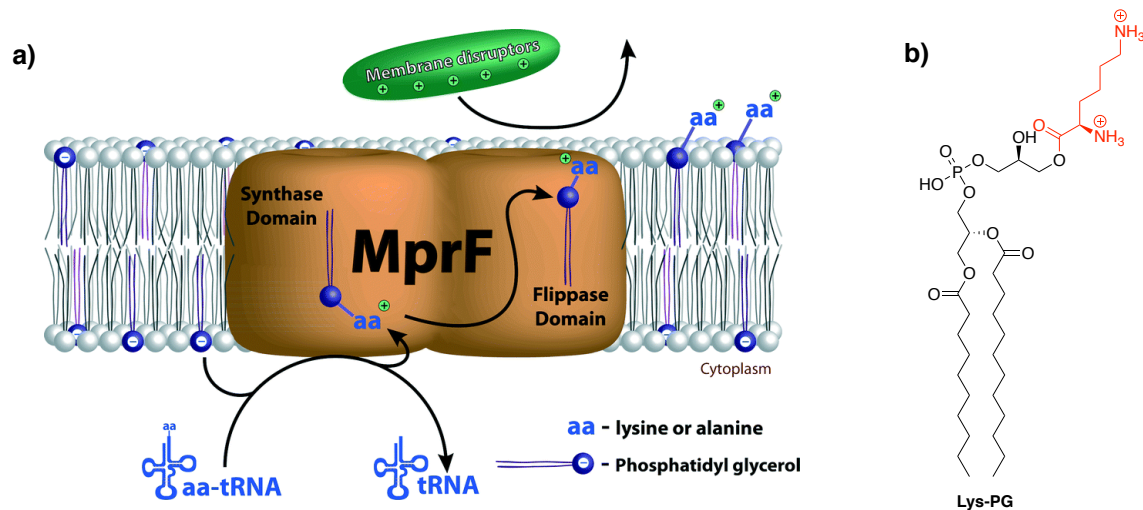


Figure 1-8 (a) Amino-acylation of PG via MprF in *S. aureus*, causing repulsion to CAMPs (from reference 40). (b) Structure of Lys-PG that is presented on the bacterial membrane.

1.4 Conclusions

The continuous rise of bacterial resistance to antibiotics is a global public health threat with no current solution. There is thus an urgent need for the development of novel antimicrobial agents, particularly against drug resistant strains of bacteria such as the ESKAPE pathogens. Peptide antibiotics are an intriguing modality to investigate as antimicrobial agents due to their ease of synthesis, ability to screen as robust peptide libraries, and reduced cultivation of resistance compared to other conventional antibiotics. Peptide antibiotics with narrow-spectrum activity are of particular interest

due to their ability to solely target a culprit species or strain of bacteria, leading to even less occurrence of resistance and no disruption of the human microbiome. Development of these ideal narrow-spectrum antimicrobial peptides requires novel detection methods to identify the infection-causing pathogen. Besides a few advanced diagnostic techniques such as nucleic acid-based and mass spectrometry (MS)-based technologies, pathogen detection is currently limited to the traditional and time-consuming culture-based phenotypic identification.¹⁴

The work described herein investigates the ability to develop peptides for the diagnosis and treatment of specific bacterial pathogens by targeting the characteristic amine-presenting surface modifications of antibiotic resistance. Specifically, we take advantage of iminoboronate chemistry, a novel reversible covalent binding mechanism, between 2-acetylphenylboronic acid (APBA) and the amine functionalities on the bacterial cell surface. Using both rational design and peptide libraries, specifically a chemically-modified phage display library, the following aims were addressed:

- (1) Detecting Lys-PG via iminoboronate formation with a polyvalent display of 2-APBA on a peptide scaffold (**Chapter 2**).
- (2) Attempting to target Lipid II pentapeptide of the peptidoglycan with an APBA-presenting, iminoboronate-capable phage display library (**Chapter 3**).
- (3) Developing targeted antibiotics via live cell screening of the APBA-modified phage display library (**Chapter 4**).
- (4) Designing and constructing novel phage libraries for the discovery of improved peptide probes (**Chapter 5**).

1.5 References

1. Aminov, R. I. A brief history of the antibiotic era: lessons learned and challenges for the future. *Front. Microbiol.* **1**, 1–7 (2010).
2. Gould, K. Antibiotics: from prehistory to the present day. *J. Antimicrob. Chemother.* **71**, 572–575 (2016).
3. Fischbach, M. A. & Walsh, C. T. Antibiotics for Emerging Pathogens. *Science* **325**, 1089–1094 (2009).
4. Lewis, K. Platforms for antibiotic discovery. *Nat. Rev.* **12**, 371–387 (2013).
5. Lewis, K. Recover the lost art of drug discovery. *Nature* **485**, 439–440 (2012).
6. Andriole, V. T. The Quinolones: Past , Present , and Future. *Clin. Infect. Dis.* **41**, S113–119 (2005).
7. Fernandes, P. & Martens, E. Antibiotics in late clinical development. *Biochem. Pharmacol.* **133**, 152–163 (2017).
8. Ling, L. L. *et al.* A new antibiotic kills pathogens without detectable resistance. *Nature* **517**, 455–459 (2015).
9. Nichols, D. *et al.* Use of Ichip for High-Throughput In Situ Cultivation of ‘Uncultivable’ Microbial Species. *Appl. Environ. Microbiol.* **76**, 2445–2450 (2010).
10. Piddock, L. J. V. Teixobactin, the first of a new class of antibiotics discovered by iChip technology? *J. Antimicrob. Chemother.* **70**, 2679–2680 (2015).
11. Donadio, S., Maffioli, S., Monciardini, P., Sosio, M. & Jabes, D. Antibiotic discovery in the twenty-first century: current trends and future perspectives. *J. Antibiot.* **63**, 423–430 (2010).
12. Becker, D. *et al.* Robust Salmonella metabolism limits possibilities for new antimicrobials. *Nature* **440**, 303–307 (2006).
13. Fair, R. J. & Tor, Y. Antibiotics and Bacterial Resistance in the 21st Century. *Perspect. Medicin. Chem.* **6**, 25–64 (2014).
14. Maxson, T. & Mitchell, D. A. Targeted Treatment for Bacterial Infections: Prospects for Pathogen-Specific Antibiotics Coupled with Rapid Diagnostics. *Tetrahedron* **72**, 3609–3624 (2016).

15. Blair, J. M. A., Webber, M. A., Baylay, A. J., Ogbolu, D. O. & Piddock, L. J. V. Molecular mechanisms of antibiotic resistance. *Nat. Rev. Microbiol.* **13**, 42–51 (2015).
16. Docquier, J. & Mangani, S. An update on β -lactamase inhibitor discovery and development. *Drug Resist. Updat.* **36**, 13–29 (2018).
17. Davies, J. & Davies, D. Origins and Evolution of Antibiotic Resistance. *Microbiol. Mol. Biol. Rev.* **74**, 417–433 (2010).
18. Levy, S. B. & Marshall, B. Antibacterial resistance worldwide: causes, challenges and responses. *Nat. Med.* **10**, 122–129 (2004).
19. Levy, S. B. The Challenge of Antibiotic Resistance. *Sci. Am.* 46–53 (1998).
20. Rice, L. B. Federal Funding for the Study of Antimicrobial Resistance in Nosocomial Pathogens: No ESKAPE. *J. Infect. Dis.* **197**, 1079–1081 (2008).
21. Boucher, H. W. *et al.* Bad Bugs, No Drugs: No ESKAPE! An Update from the Infectious Diseases Society of America. *Clin. Infect. Dis.* **48**, 1–12 (2009).
22. Boucher, H. W. & Corey, G. R. Epidemiology of Methicillin-Resistant *Staphylococcus aureus*. *Clin. Infect. Dis.* **46**, S344–S349 (2008).
23. Falagas, M. E., Grammatikos, A. P. & Michalopoulos, A. Potential of old-generation antibiotics to address current need for new antibiotics. *Expert Rev. Anti. Infect. Ther.* **6**, 593–600 (2008).
24. Peleg, A. Y., Seifert, H. & Paterson, D. L. *Acinetobacter baumannii*: Emergence of a successful pathogen. *Clin. Microbiol. Rev.* **21**, 538–582 (2008).
25. Zasloff, M. Antimicrobial Peptides of Multicellular Organisms. *Nature* **415**, 389–395 (2002).
26. Hancock, R. E. W. & Sahl, H. G. Antimicrobial and host-defense peptides as new anti-infective therapeutic strategies. *Nat. Biotechnol.* **24**, 1551–1557 (2006).
27. Marr, A. K., Gooderham, W. J. & Hancock, R. E. Antibacterial peptides for therapeutic use: obstacles and realistic outlook. *Curr. Opin. Pharmacol.* **6**, 468–472 (2006).
28. Scott, R. W., DeGrado, W. F. & Tew, G. N. De novo designed synthetic mimics of antimicrobial peptides. *Curr. Opin. Biotechnol.* **19**, 620–627 (2008).
29. Hancock, R. E. W. Peptide Antibiotics. *Lancet* **349**, 418–422 (1997).

30. Oyston, P. C. F., Fox, M. A., Richards, S. J. & Clark, G. C. Novel peptide therapeutics for treatment of infections. *J. Med. Microbiol.* **58**, 977–987 (2009).
31. McGregor, D. P. Discovering and improving novel peptide therapeutics. *Curr. Opin. Pharmacol.* **8**, 616–619 (2008).
32. Fosgerau, K. & Hoffmann, T. Peptide therapeutics: Current status and future directions. *Drug Discov. Today* **20**, 122–128 (2015).
33. Bowdish, D., Davidson, D. & Hancock, R. A Re-evaluation of the Role of Host Defence Peptides in Mammalian Immunity. *Curr. Protein Pept. Sci.* **6**, 35–51 (2005).
34. Peláez, F. The historical delivery of antibiotics from microbial natural products - Can history repeat? *Biochem. Pharmacol.* **71**, 981–990 (2006).
35. Walsh, C. T. Polyketide and Nonribosomal Peptide Antibiotics: Modularity and Versatility. *Science* **303**, 1805–1810 (2004).
36. Passioura, T., Katoh, T., Goto, Y. & Suga, H. Selection-Based Discovery of Druglike Macrocyclic Peptides. *Annu. Rev. Biochem.* **83**, 727–752 (2014).
37. Breukink, E. & de Kruijff, B. Lipid II as a target for antibiotics. *Nat. Rev. Drug Discov.* **5**, 321–332 (2006).
38. Nizet, V. Antimicrobial Peptide Resistance Mechanisms of Human Bacterial Pathogens. *Curr. Issues Mol. Biol.* **8**, 11–26 (2006).
39. Joo, H. S., Fu, C. I. & Otto, M. Bacterial strategies of resistance to antimicrobial peptides. *Philos. Trans. R. Soc. B Biol. Sci.* **371**, (2016).
40. Steinbuch, K. B. & Fridman, M. Mechanisms of resistance to membrane-disrupting antibiotics in Gram-positive and Gram-negative bacteria. *Med. Chem. Commun.* **7**, 86–102 (2016).
41. Brogden, K. A. Antimicrobial peptides: Pore formers or metabolic inhibitors in bacteria? *Nat. Rev. Microbiol.* **3**, 238–250 (2005).

CHAPTER 2

LABELING BACTERIAL CELLS VIA IMINOBORONATE FORMATION WITH POLYVALENT DISPLAY OF APBA ON A PEPTIDE SCAFFOLD

2.1 Introduction

2.1.1 Iminoboronate Chemistry

Imine or schiff-base formation is an extensively characterized reversible reaction that occurs between a primary amine and an aldehyde or ketone. It is frequently utilized in nature, particularly in pyridoxal phosphate (PLP)-dependent enzymatic reactions.¹ However, without a reduction step to trap the imine², the association is relatively weak and displays unfavorable thermodynamic equilibrium.³ For example, the association constant of acetone and glycine was reported to be $3.3 \times 10^{-3} \text{ M}^{-1}$ (dissociation constant (K_d) $\sim 300 \text{ M}$).⁴ Opportunely, the thermodynamic stability of imine formation can be improved by modifying the adjacent functionalities of the aldehyde or ketone. This phenomenon is exemplified by nature and the PLP cofactor, which has a larger association constant with glycine of 883 M^{-1} ($K_d \sim 1 \text{ mM}$) compared to simple acetone.⁴ This improved thermodynamic stability is attributed with the presence of an *ortho*-phenoxide moiety which the iminium ion can hydrogen bond with.

Inspired by nature, chemists have sought to improve upon imine formation to exploit the advantageous reversible covalent targeting of biological amines.³ One example in particular is iminoboronate chemistry, in which an *ortho*-boronic acid is installed within benzaldehyde or acetophenone, resulting in improved thermodynamic stability due to a nitrogen-boron dative bond where the boronic acid group serves as an electron trap (Figure 2-1). Specifically, the Yatsimirsky group demonstrated that 2-formylphenylboronic acid (FPBA) readily conjugates with aminosugars at sub to low millimolar concentrations.⁵ Additionally, Gois and coworkers reported that both 2-FPBA

and 2-APBA can readily conjugate with the lysine side chains of proteins to form iminoboronates.⁶

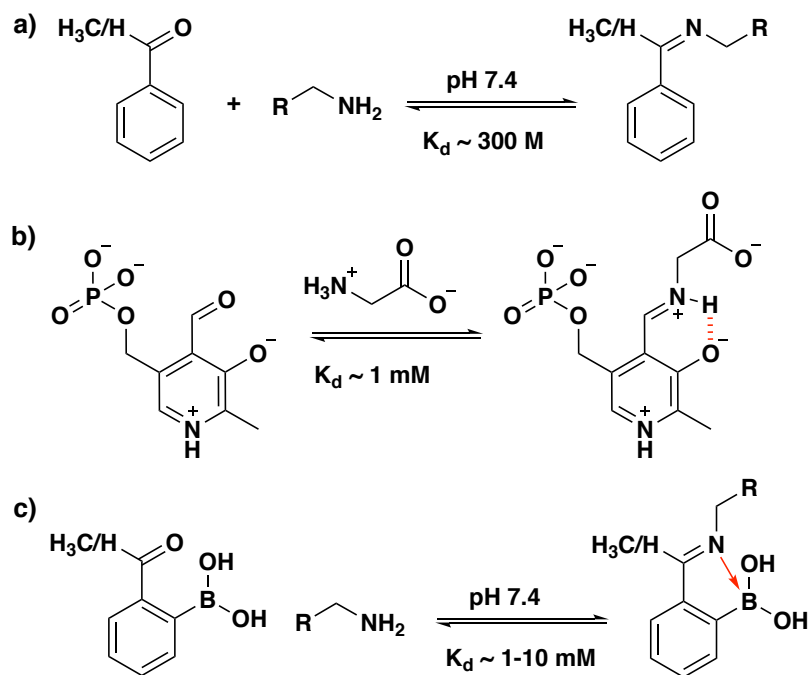


Figure 2-1 Comparison of (a) simple imine formation, (b) PLP-mediated imine formation, and (c) iminoboronate formation.

Our group hypothesized that the amine-presenting phospholipids of bacteria could be targeted with iminoboronate chemistry.⁷ By synthesizing an unnatural amino acid incorporating the 2-APBA warhead, namely AB1, we were able to target Gram-positive bacteria via iminoboronate chemistry. Exploiting multivalency of the APBA-warhead allowed for substantial enhancement in *S. aureus* binding potency, a pathogen known to express a significant amount of Lys-PG on its surface. Overall, the results presented here demonstrate the robust nature of iminoboronate chemistry in targeting bacterial cell membranes.

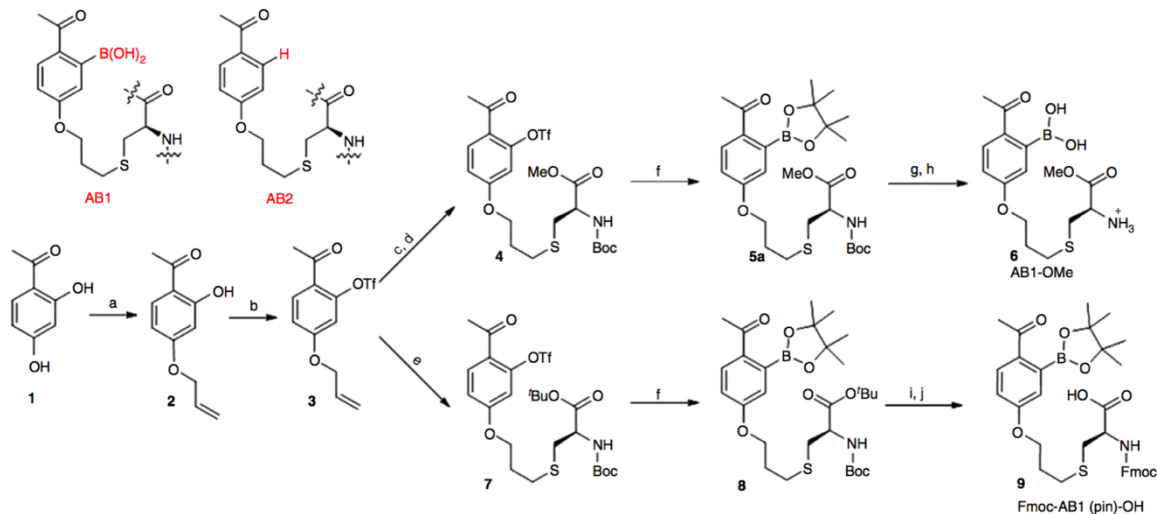
2.2 Targeting Bacteria via Iminoboronate Chemistry of Amine-Presenting Lipids

2.2.1 Synthesis of AB1 Derivatives

The unnatural amino acid AB1 was synthesized via an approach that allowed for fluorophore conjugation and peptide incorporation (Scheme 2-1). For initial binding studies, fluorophore labeled AB1 was synthesized with either fluorescein (FI-AB1-OMe) or Alexa Fluor 488 (AF488-AB1-OMe). For incorporation into peptides, AB1 was synthesized in the proper fluorenylmethoxycarbonyl (Fmoc) and pinacol (pin)-protected form (Fmoc-AB1(pin)-OH) necessary for solid phase synthesis. Both syntheses utilized 2',4'-dihydroxyacetophenone as the starting material, first subjected to regioselective alkylation of the 4'-hydroxyl to install an alkene for thiol-ene click chemistry followed by triflation of the 2'-hydroxyl. The synthesis diverged at this step and thiol-ene chemistry was utilized to attach the correct cysteine derivative. The borylation of the derivatives was then accomplished with Miyaura borylation, which required rigorous temperature control to avoid the protodeboronated product, AB2, which constructively served as a negative control. The final step involved the deprotections/protectations to yield the desired derivatives.

The AB1 methyl ester was subjected to fluorophore labeling with fluorescein isothiocyanate (FITC) or AF488-succinimidyl ester (OSu) at the free N-terminal amine. Solid-phase peptide synthesis (SPPS) was exploited to synthesize peptides incorporating Fmoc-AB1-OH. An N-terminal cysteine (Cys, C) residue was incorporated into each peptide for facile fluorophore labeling by AF488-C₅-maleimide.

Scheme 2-1 Synthesis of AB1 Derivatives.



(a) Allyl bromide, K_2CO_3 , NaI, acetone; 81% yield. (b) $(CF_3SO_2)_2O$, Et_3N , DCM; 95%. (c) Cys-OMe, DMPA, MeOH, ~ 365 nm UV irradiation. (d) Boc anhydride, Na_2CO_3 , THF/water; 80% over two steps. (e) Boc-Cys-OtBu, DMPA, MeOH, ~ 365 nm UV irradiation; 75%. (f) $Pd(dppf)Cl_2/dppf$, B_2Pin_2 , KOAc, dioxane; ~ 70 –80%. (g) 40% TFA in DCM. (h) diethanolamine, 1 N HCl; 74% over two steps. (i) 60% TFA in DCM. (j) Fmoc-Osu, Na_2CO_3 , THF/water; 81% over two steps.

2.2.2 Characterization of AB1 Binding

To assess the binding propensity of AB1 towards various lipids, fluorescence anisotropy against lipid vesicles was employed (Figure 2-2). Lipid vesicle preparation and anisotropy was performed by Dr. Anupam Bandyopadhyay.⁷ As the lipid concentration increased, only the anisotropy values for lipid vesicles containing phosphatidylethanolamine (PE) and Lys-PG, the amine-presenting bacterial lipids, increased in the presence of AB1. Although phosphatidylserine (PS) also contains a primary amine, it is most likely too sterically hindered to elicit iminoboronate formation. Confirming that the binding was due to the 2-APBA head group, AB2 revealed negligible anisotropy changes compared to AB1. The iminoboronate binding mechanism of AB1 with

Lys-PG was confirmed by MS and ^{11}B -Nuclear Magnetic Resonance spectroscopy (NMR) as well (data not shown).⁷

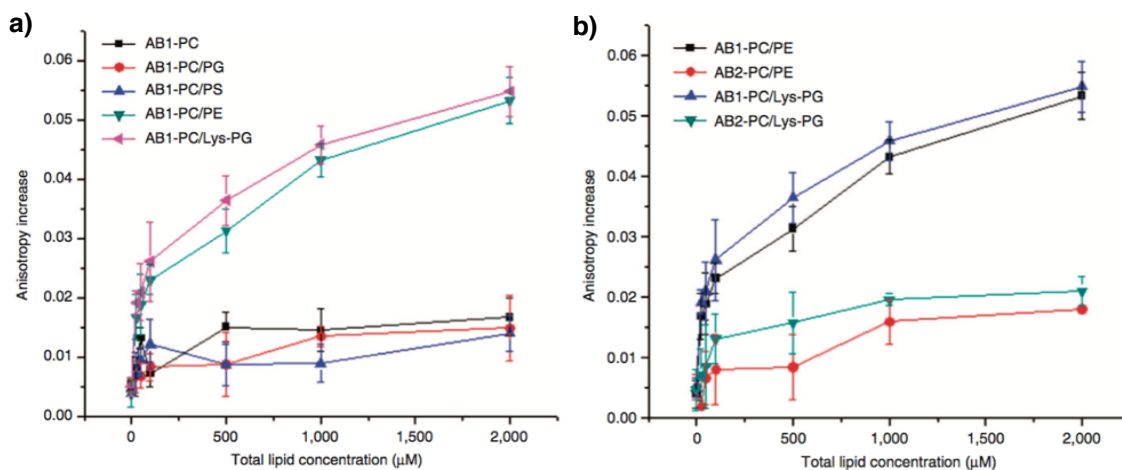


Figure 2-2 Fluorescence anisotropy of liposome binding plotted by Dr. Bandyopadhyay with (a) FI-AB1-OMe (0.5 μM) against various lipids and (b) FI-AB1-OMe versus FI-AB2-OMe.

Once model membrane studies established bacterial lipid binding potential, the ability of AB1 to label bacterial cells was investigated. *S. aureus*, *Bacillus subtilis* and *Escherichia coli* were incubated with AF488-AB1-OMe and analyzed via fluorescence microscopy by Anupam Bandyopadhyay (Figure 2-3a).⁷ AF488-AB1-OMe effectively stained the two Gram-positive bacteria *S. aureus* and *B. subtilis* at concentrations greater than 100 μM. No staining of the Gram-negative *E. coli* was observed, which is most likely due to the inability to penetrate the outer membrane of Gram-negative bacteria to reach the plasma membrane. Importantly, AF488-AB2-OMe failed to stain the Gram-positive bacterial cells at this concentration (data not shown).⁷ Additionally, AF488-AB1-OMe did not bind mammalian cells, demonstrated by confocal microscopy of a co-culture consisting *S. aureus* and Jurkat T lymphocytes, further confirming the Gram-positive bacterial selectivity of the iminoboronate-capable probe (Figure 2-3b).

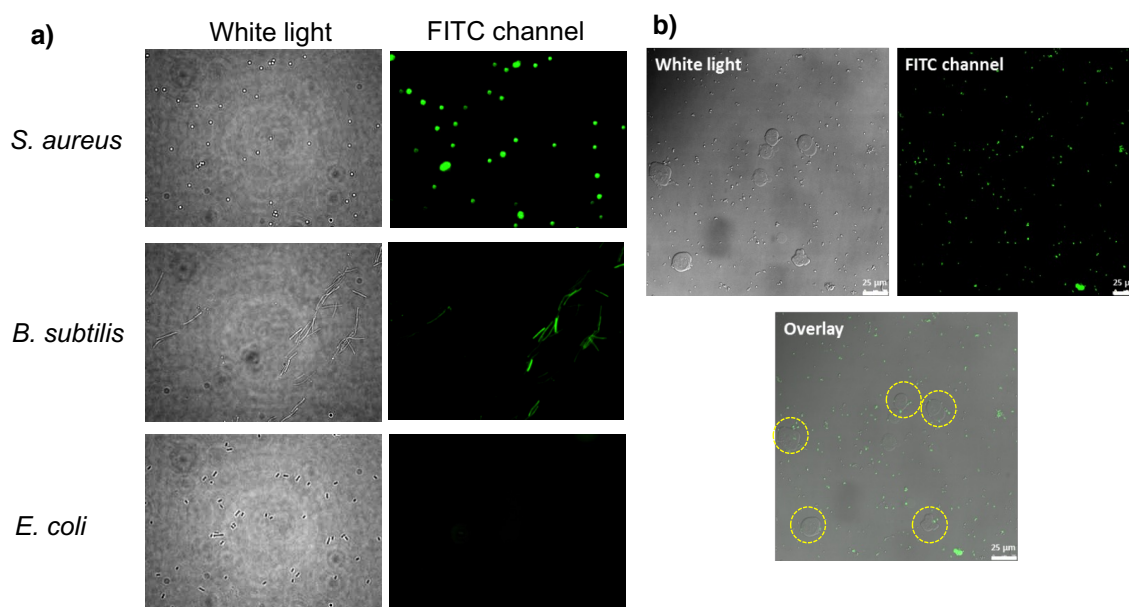


Figure 2-3 Microscopy analysis of AB1 binding performed by Dr. Bandyopadhyay of (a) AF488-AB1-OMe (200 μ M) binding various bacterial species via fluorescence microscopy and (b) AF488-AB1-OMe (100 μ M) staining *S. aureus* and Jurkat co-culture via confocal microscopy.

2.2.3 AB1 Synergizes with Cationic Peptides for Potent Bacterial Labeling

Although selective for Gram-positive bacteria, AF488-AB1-OMe requires high concentrations to effectively label the bacteria. Additionally, due to the iminoboronate binding mechanism of AB1 with primary amines, the probe binds to lysine-containing proteins as well; the staining of *S. aureus* by AF488-AB1-OMe was reduced by 90% in the presence of 10 mg/mL bovine serum albumin (BSA, data not shown).⁷ This is particularly problematic for real applications since albumin is present in human serum at a concentration of 35-50 mg/mL.⁸ The synergistic effect of conjugating a membrane directing entity to AB1 was investigated to determine if more potent binding could be achieved with less protein interference. Since bacterial cell membranes are known to maintain a largely negative charge, cationic conjugates were synthesized to supplement the reversible covalent mechanism of AB1 with noncovalent, electrostatic interactions.

Two peptides were synthesized with Fmoc-AB1(pin)-OH containing either lysine (Lys, K) or arginine (Arg, R), K-AB1 and R-AB1, respectively. Additionally, Fmoc-AB1-OH was incorporated into the CAMP Hlys, which has the sequence RYWVAWRNR. Hlys yields a minimal inhibitory concentration (MIC) of 24 μ M with little hemolytic activity.⁹ A control peptide incorporating a simple glycine (Gly, G) residue was also analyzed.

The panel of AB1-containing peptides were subjected to flow cytometry analysis of *S. aureus* binding at various concentrations of peptide (Figure 2-4a). As expected, the control peptide, G-AB1, elicited minimal staining at 100 μ M, comparable to AB1 alone. K-AB1 additionally revealed little *S. aureus* staining, whereas R-AB1 exhibited much improved *S. aureus* staining. Although both cationic amino acids, the difference in *S. aureus* staining between K-AB1 and R-AB1 is most likely due to the capacity of arginine to effectively interact with phospholipids.¹⁰ A significant improvement of *S. aureus* binding was observed with Hlys-AB1 compared to other conjugates and Hlys alone. Importantly, Hlys-AB1 did not bind Jurkat cells or Gram-negative *E. coli* (data not shown), maintaining its Gram-positive bacteria selectivity. Notably, Hlys-AB1 was assessed for its labeling ability at sub- μ M concentrations, demonstrating potent *S. aureus* labeling at 200 nM via confocal microscopy performed by Dr. Bandyopadhyay (Figure 2-4b). The confocal microscopy also demonstrated membrane localized staining of Hlys-AB1, as expected.⁷

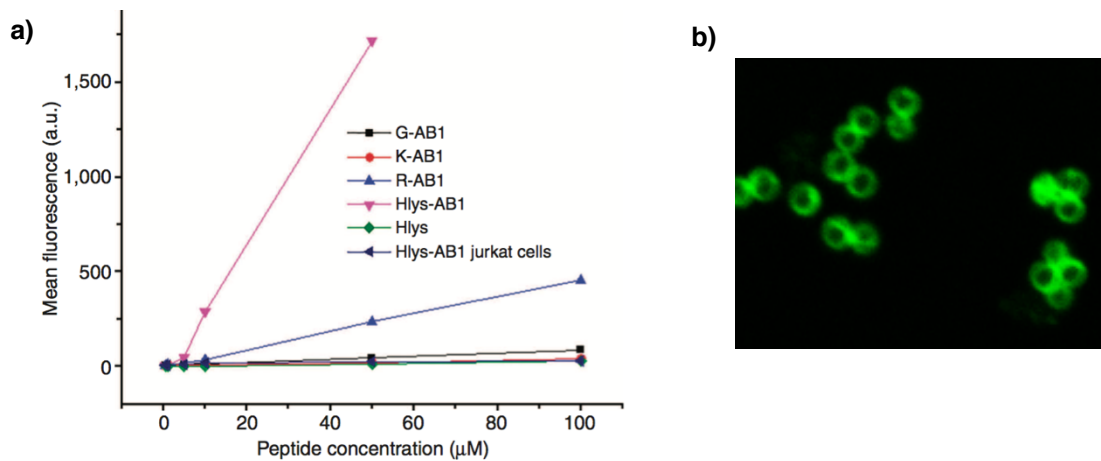


Figure 2-4 (a) Flow cytometry concentration profiles of *S. aureus* staining by AB1-peptides (b) Confocal microscopy of Hlys-AB1 staining *S. aureus* at 200 nM performed by Dr. Bandyopadhyay.

The synergistic mechanism of Hlys-AB1 not only allowed for more potent *S. aureus* binding, but it also allowed for less serum protein interference than AB1 alone. This was demonstrated by fluorescence microscopy and flow cytometry analysis by Dr. Bandyopadhyay (Figure 2-5). In the fluorescence microscope images, although slightly dimmer, the staining of *S. aureus* can still be visualized with 500 nM Hlys-AB1 in the presence of 10% fetal bovine serum (FBS). Consistent with these results, flow cytometry analysis revealed ~30% inhibition of *S. aureus* labeling in 10% FBS with Hlys-AB1, an improvement from 90% inhibition for AB1 alone.

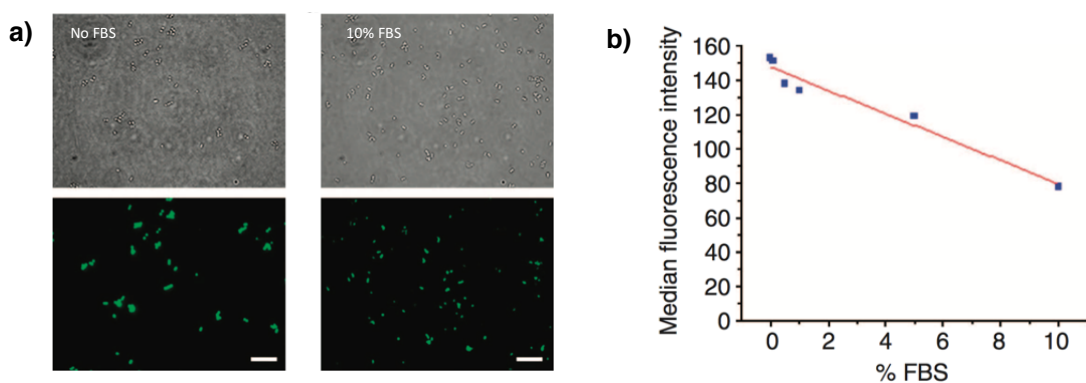


Figure 2-5 Serum protein interference assessed by Dr. Bandyopadhyay via (a) fluorescence microscopy of Hlys-AB1 (500 nM) staining *S. aureus* with or without 10% FBS and (b) flow cytometry of *S. aureus* staining by Hlys-AB1 (200 nM) with increasing % FBS.

2.3 Multivalent Display of APBA Elicits Powerful *S. aureus* Binding

2.3.1 Multivalency

An alternative method to obtain potency and potentially subsequent specificity is by utilizing the multivalency effect. Many biological interactions occur naturally using multivalent binding mechanisms, such as protein-cell interactions, where multiple binding groups can engage with multiple copies of a receptor.¹¹ This allows for avidities that are orders of magnitude stronger than corresponding monovalent interactions and is often accompanied by accelerated kinetics. Synthetic multivalent ligands have proven to be useful in various therapeutic applications ranging from toxin and pathogen inhibitors to disease-relevant receptor modulators.^{12,13}

2.3.2 Synthesis & Characterization of Dimer Peptides

A series of dimers, peptides containing two 2-APBA warheads, were synthesized utilizing SPPS with Fmoc-AB1(pin)-OH to determine the optimal linker length between

each warhead. Each peptide incorporated an N-terminal cysteine for AF488 labeling (represented by C*) and glycine residues flanking the APBA moiety (represented by X) to solely study the effect of the warhead. Additionally, the N- and C-termini of the peptides were acetylated and amidated respectively for increased serum stability. For the dimers, the linker varied between a single glycine residue (C*GXGXG), two glycines (C*GXGGXG), three glycines (C*GXGGGXG) or three alanines (C*GXAAAXG). A monomer (C*GXG) was synthesized for comparison. Flow cytometry analysis of *S. aureus* staining revealed a significant improvement in binding of the dimers over the monomer, particularly for the dimers with a three-residue linker (Figure 2-6a). Similar to results seen by AF488-AB1-OMe, flow cytometry analysis of the dimers demonstrated that the addition of 10% human serum resulted in *S. aureus* binding inhibition; although, not to the same extent as AB1 alone (Figure 2-6b). This data was promising since ~30% *S. aureus* cell staining remained in the presence of 10% human serum by some of the peptides, an improvement from the mere 10% *S. aureus* staining retention exhibited by AB1 alone in the presence of serum proteins. Since C*GXGGGXG demonstrated the most potent staining of *S. aureus* and less serum protein interference within the dimer series, the triple glycine linker was chosen to further study the effect of increasing the valency beyond dimers on *S. aureus* binding.

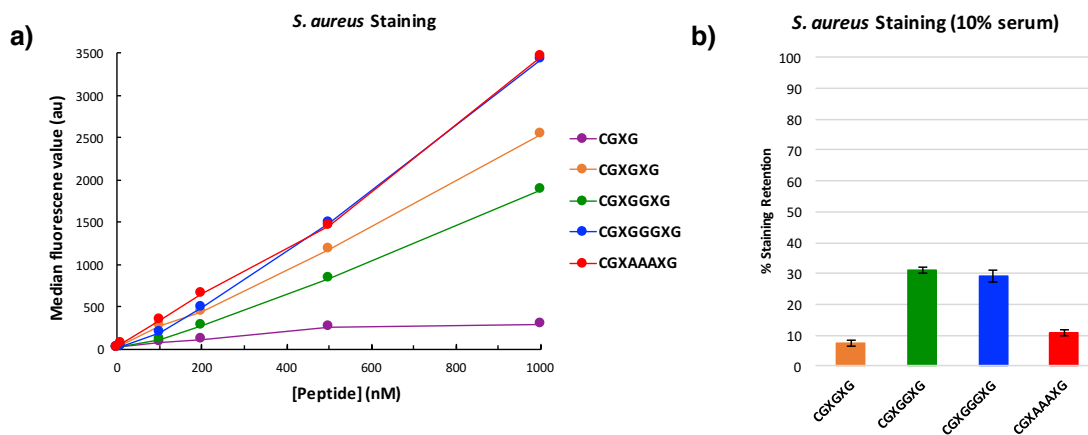
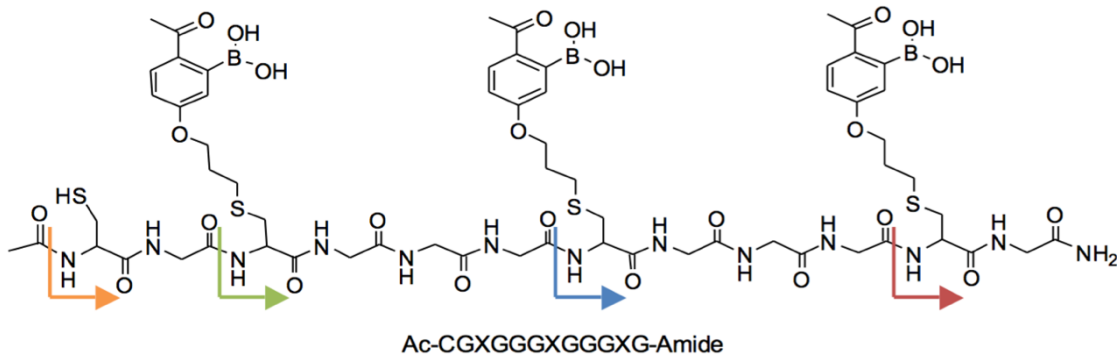


Figure 2-6 Flow cytometry analysis of *S. aureus* staining (a) Concentration profile of dimers and monomer (b) Percent staining retention of peptides (1 μ M) with 10% human serum present.

2.3.3 Troubleshooting Efforts and Synthesis of Peptides Beyond Dimers

With the promising results of the dimer series, a series of multivalent peptides were synthesized. First, SPPS was attempted utilizing Fmoc-AB1(pin)-OH to synthesize a trimer and tetramer employing the same protocol for dimer synthesis. However, synthesis beyond dimers became problematic when using the unnatural amino acid Fmoc-AB1(pin)-OH. In these cases, glycine deletions were observed as the peptide was extended, yielding extremely impure final peptides. For example, monitoring the synthesis of a trimer via liquid chromatography-mass spectrometry (LC-MS) after the addition of each AB1 residue revealed an increase in glycine deletions as synthesis continued, such that so many impurities were present in the final product, the desired peptide could not be purified (Table 2-1). A test peptide incorporating the natural amino acid Fmoc-Tyr(*t*Bu)-OH in the place of AB1 was synthesized with ease and no glycine deletions were observed, indicating Fmoc-AB1(pin)-OH as the problem, not the nature of the peptide sequence.

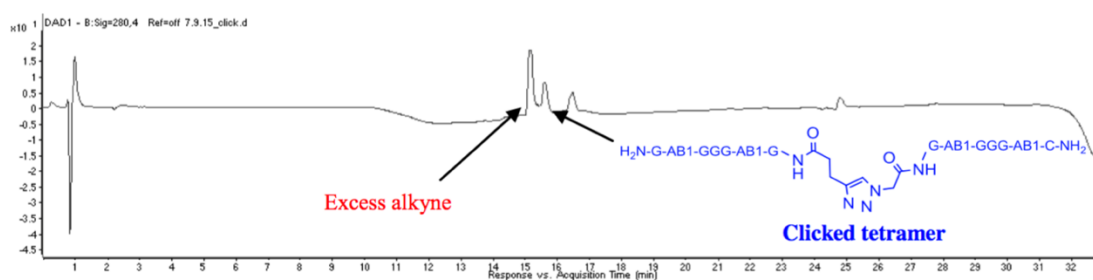
Table 2-1 LC-MS monitoring of trimer synthesis with Fmoc-AB1(pin)-OH

Structure Analyzed	Desired Mass	Observed Mass (main)	Number of peaks (impurities)	Other masses shown
Fmoc-AB1-G-NH ₂	[M-H ₂ O+H] ⁺ 602.216	602.22122	1	n/a
Fmoc-AB1-GGG-AB1-G-NH ₂	[M-2H ₂ O+H] ⁺ 1078.380	1078.36535	2+	1021.33958 (m/z - 57) 964.31667 (m/z - 57x2)
Fmoc-AB1-GGG-AB1-GGG-AB1-G-NH ₂	[M-3H ₂ O+H] ⁺ 1554.5445	1497.49810 (m/z - 57)	4+	1440.47723 (m/z - 57x2) 1554.52301
H ₂ N-CG-AB1-GGG-AB1-GGG-AB1-G-NH ₂	[M-3H ₂ O+H] ⁺ 1493.5149	n/a	9+	n/a

A multitude of troubleshooting efforts were attempted to resolve the glycine deletions with Fmoc-AB1-OH. First, the purity of Fmoc-AB1(pin)-OH was assessed further via LC-MS and demonstrated a small impurity (~5-10%) of a hydroxylated byproduct, in which the pinacol-protected boronic acid (Bpin) was replaced with hydroxyl, potentially causing issues in the synthesis of lengthy peptides due to an unprotected nucleophilic moiety. The final Fmoc protection step of AB1 was altered from aqueous conditions to organic conditions (dichloromethane (DCM) and N-methylmorpholine (NMM)), resulting in the elimination of the hydroxylated byproduct. Unfortunately, improving the purity of Fmoc-AB1(pin)-OH did not solve the problem at hand. Next, to verify that the glycine deletions were not due to incomplete Fmoc deprotection of AB1, the deprotection was monitored via LC-MS, which confirmed complete Fmoc deprotection under standard conditions. The coupling time of Fmoc-Gly-OH was also increased; however, this did not

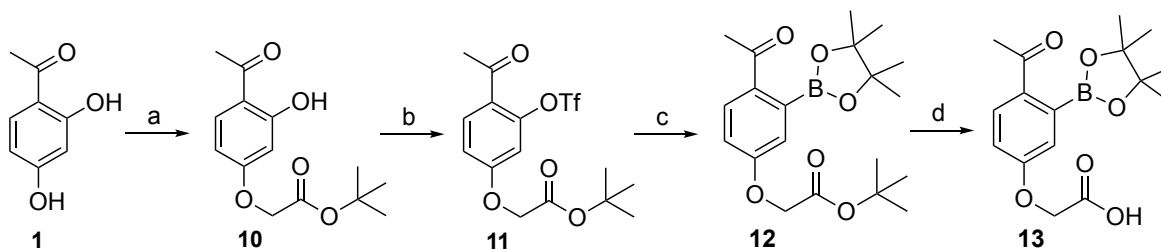
resolve the issue. One potential explanation for these glycine deletions could be the formation of an intramolecular iminoboronate during peptide synthesis. After Fmoc deprotection of the AB1 residue, a free amine is exposed, which could potentially form an iminoboronate complex with an AB1 moiety already coupled to the resin. This would be a difficult hypothesis to investigate and nevertheless, a new and efficient method to obtain these lengthy peptides incorporating more than two AB1 warheads needed to be developed.

The first potential solution investigated to remedy this issue was conjugation chemistry via copper-catalyzed azide-alkyne cycloaddition (CuAAC). An azide handle was attached to one dimer and an alkyne to another via coupling on-resin to the N-terminal amine. Once cleaved from resin, the two peptides were combined and subjected to copper sulfate (CuSO_4) and sodium ascorbate (NaAsc) conditions, yielding a tetramer fused by a triazole linkage. LC-MS analysis demonstrated that the desired clicked product can be obtained in excellent purity utilizing this strategy, although the ratio of azide:alkyne needs optimization (Figure 2-7). This strategy could be utilized with a dimer and a monomer as well to obtain a trimer. Although the CuAAC was a clean reaction and yielded the desired peptide, an alternative method was developed that made the synthesis of multivalent peptides extremely efficient and facile.



The second, more efficient, method that was investigated to remedy the multivalent synthesis issue was the on-resin coupling of the 2-APBA warhead. Towards this end, APBA-OH, a small molecule that displays the 2-APBA warhead and a carboxylic acid for amide bond formation with a free amine, was synthesized (Scheme 2-2).

Scheme 2-2 Synthesis of APBA-OH (13).



(a) *t*-butylbromoacetate, K_2CO_3 , Acetone, NaI; 100%. (b) $(CF_3SO_2)_2O$, DCM, Et_3N ; 80%. (c) $Pd(dppf)Cl_2$, B_2Pin_2 , KOAc, Dioxane; 63%. (d) 60% TFA in DCM; 100%.

By synthesizing this small molecule, facile on-resin coupling could be utilized to accomplish highly efficient preparation of 2-APBA oligomers. In this protocol, the peptides were synthesized with all commercially available building blocks, and APBA-OH was subsequently coupled to the lysine homologue diaminopropionic acid (Dap) after orthogonally deprotecting on resin. This protocol gave the desired peptides in excellent yields, with over 70% purity observed for the crude peptides cleaved off resin. A monomer (KAM-mono), dimer (KAM-di), trimer (KAM-tri) and tetramer (KAM-tetra) were synthesized utilizing this protocol and AF488-labeled following cleavage from resin (Figure 2-8a). Additionally, two cyclized trimers were synthesized, one with the triple glycine linker (KAM-CT) and one with a Gly-Arg-Gly linker (KAM-CT(GRG)) to assess the addition of positive charge to the peptide. The cyclic peptides were synthesized using the Dawson diaminobenzoic acid (Dbz) resin, which afforded the C-terminal activated linear

precursor peptide that was cyclized via intramolecular native chemical ligation (Figure 2-8b).¹⁴

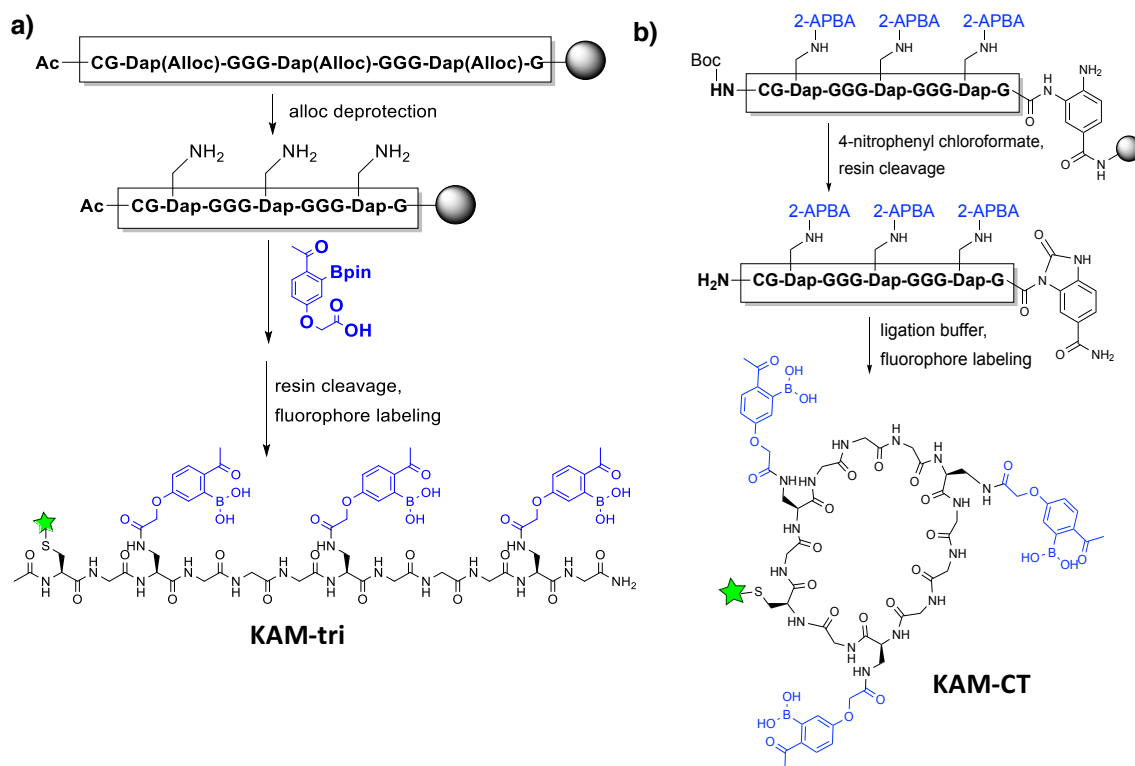


Figure 2-8 Schematic representation of on-resin coupling strategy for the incorporation of 2-APBA into peptides for (a) linear peptide synthesis and (b) cyclic peptide synthesis.

2.3.4 Increasing Valency Increases *S. aureus* Labeling Potency

The panel of multivalent peptides were subjected to flow cytometry analysis of *S. aureus* binding at various concentrations of peptide (Figure 2-9a). Increasing the valency distinctly increases the *S. aureus* staining potency. Interestingly, although it displays fewer warheads, KAM-CT behaves slightly better than KAM-tetra, suggesting that a rigid scaffold is more ideal for *S. aureus* binding than a flexible scaffold. Strikingly, the addition of positive charge to direct the peptide to the negatively charged bacterial cell membrane with KAM-CT(GRG) increased the *S. aureus* staining drastically compared to the other

multivalent peptides. Bacterial membrane labeling saturation was also observed with the cyclic peptides. KAM-CT(GRG) demonstrated significant improvement over rationally designed Hlys-AB1 as well (Figure 2-9b).

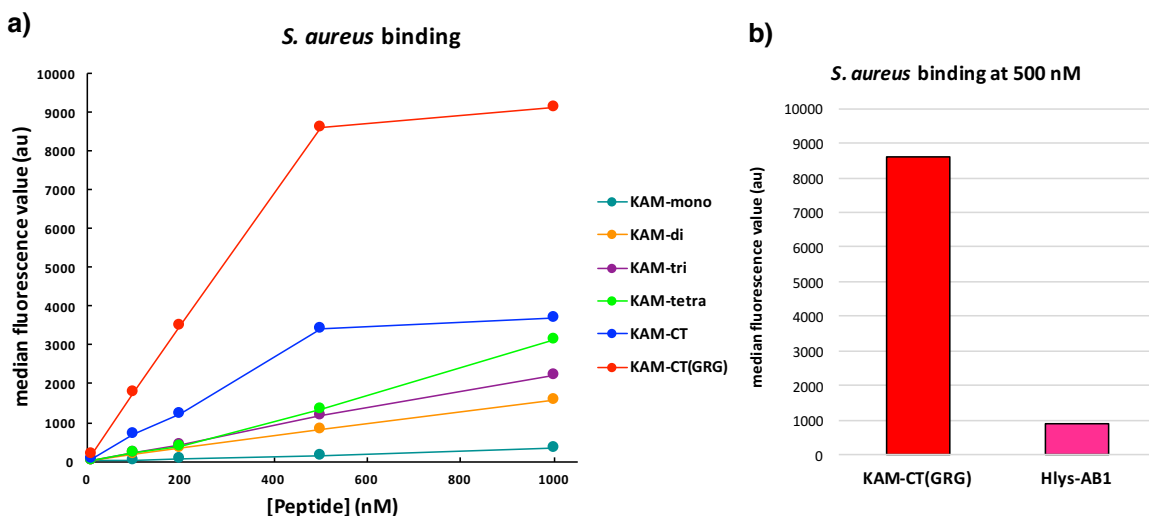


Figure 2-9 Flow cytometry analysis of *S. aureus* staining via (a) concentration profiles of multivalent peptides and (b) comparison of KAM-CT(GRG) to Hlys-AB1 at 500 nM peptide.

Analysis of *S. aureus* staining by the multivalent peptides via fluorescence microscopy corroborated the flow cytometry results (Figure 2-10a). A clear increase in staining intensity can be visualized as the valency increases. Further microscopic analysis of KAM-CT staining of other Gram-positive bacteria revealed effective staining of *S. aureus* and MRSA; however, negligible staining of *B. subtilis* and *Streptococcus pyogenes* was observed (Figure 2-10b). These results are promising, indicating selectivity among Gram-positive bacteria species is possible with iminoboronate-capable peptide probes.

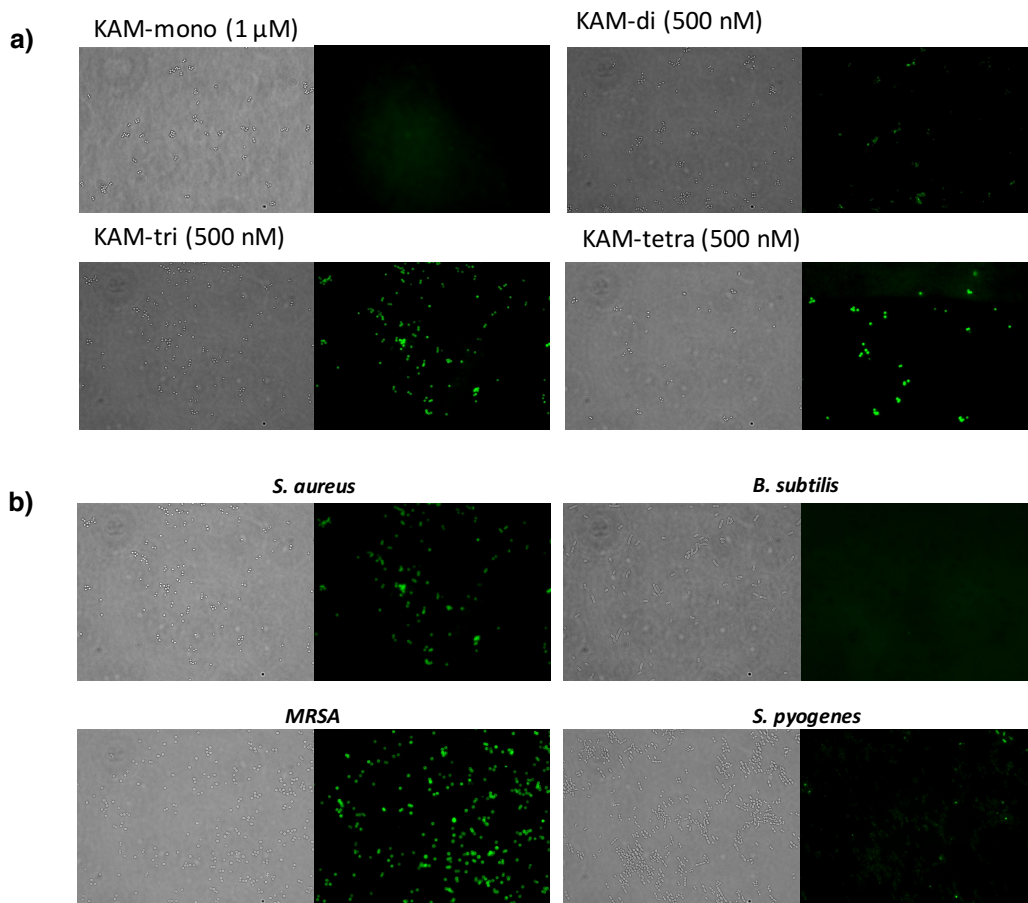


Figure 2-10 Fluorescence microscopy of (a) *S. aureus* staining by multivalent peptides and (b) various Gram-positive bacteria by KAM-tri at 500 nM.

As with AB1 alone, the multivalent peptides were assessed for serum albumin interference with bacterial binding. Each peptide was analyzed for *S. aureus* labeling via flow cytometry with 1 mg/mL BSA present, which diminished the median fluorescent intensity of each sample compared to those with no BSA present. A percent staining retention in the presence of 1 mg/mL BSA was calculated for each peptide (Figure 2-11). Unfortunately, increasing the valency does not increase the selectivity of the peptides towards the bacterial cell membrane. However, compared to the triple glycine linker peptides, KAM-CT(GRG) demonstrates less protein interference.

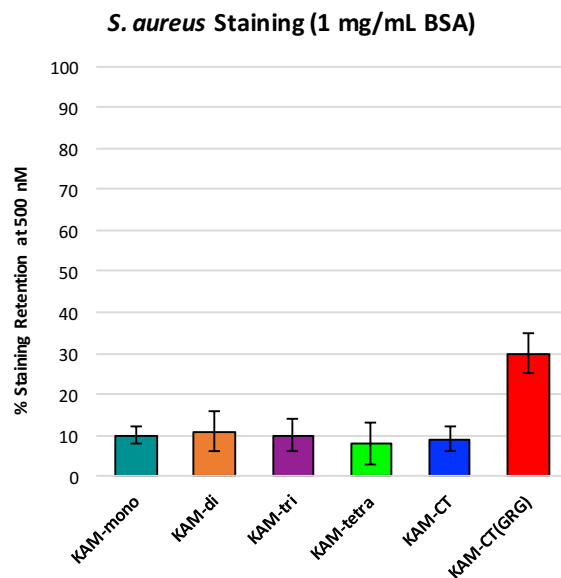


Figure 2-11 BSA interference of *S. aureus* staining by 500 nM multivalent peptides assessed via flow cytometry generated median fluorescence values.

Fluorescence microscopy of the cyclic trimers in the presence of albumin corroborated the flow cytometry results (Figure 2-12). It can be clearly visualized that the KAM-CT(GRG) staining of *S. aureus* remains much more than that of KAM-CT in the presence of 1 mg/mL BSA. Although not ideal, the improvement in albumin interference demonstrates the potential to obtain both potency and bacterial selectivity over serum albumin with iminoboronate-capable peptide probes.

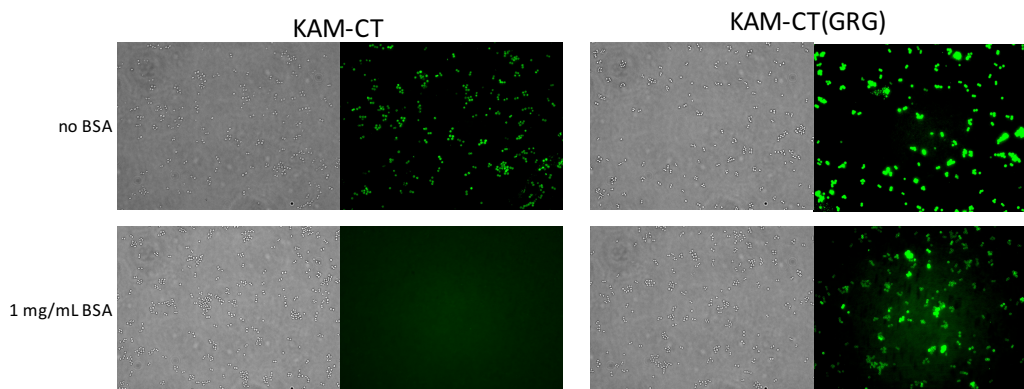


Figure 2-12 Fluorescence microscopy of cyclic trimers with and without albumin present.

2.4 Further Analysis of Albumin Binding by Multivalent Peptides

2.4.1 Albumin Binding for Increased Serum Retention Time

Although not favorable for selective bacterial labeling, the albumin-binding capability of the multivalent peptides could be exploited for increasing the pharmacokinetic properties of low molecular weight compounds. Peptides and other low molecular weight compounds, below 60 kDa, are often subjected to rapid renal clearance from the blood stream, a major drawback associated with peptide therapeutics. Due to its large size (66 kDa), albumin exceeds the renal threshold, resulting in long circulation time. Conjugation to serum proteins, such as albumin, has been explored as a strategy to improve this pharmacokinetic property by increasing the retention time of therapeutics in blood.^{15,16} The clinical impact of utilizing serum proteins as drug carriers has been recognized in therapeutic and diagnostic applications in oncology, diabetes, rheumatoid arthritis and other relevant diseases.¹⁷ Synthetic ligands that target albumin may serve as anchoring motifs for attaching peptide therapeutics. Therefore, targeting albumin with a multivalent iminoboronate display has the potential to allow for a novel and potent binding mechanism which can reversibly dissociate for therapeutic purposes (Figure 2-13). The thermodynamic and kinetic properties of the multivalent peptides were investigated to further study the albumin-binding nature of the peptides.

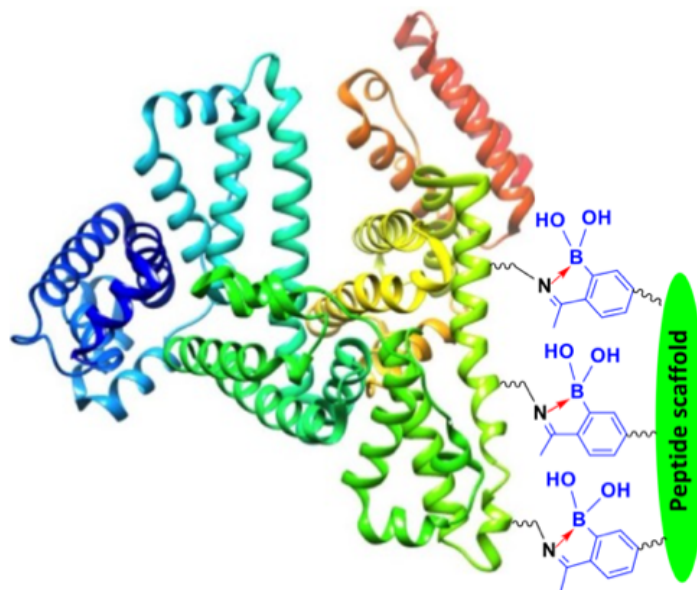


Figure 2-13 Illustration of albumin binding with a multivalent construct of 2-APBA.

2.4.2 Assessing Thermodynamics and Kinetics of Albumin Binding

The peptides were first assessed for albumin binding via titration monitored by fluorescence anisotropy. Varying concentrations of human serum albumin (HSA) were incubated with 200 nM of each peptide and fluorescent anisotropy values were determined, generating a binding curve (Figure 2-14). Curve fitting yielded K_d values for each peptide, denoted on each graph. The data shows that the albumin-binding affinity dramatically increases with increasing valency, with a K_d value of 27 μM for the monomer and about 1 μM for the tetramer. Cyclization favors the peptide's binding to albumin as well, yielding a K_d value of 1 μM for the cyclic trimer, in contrast to 2.4 μM for the linear trimer.

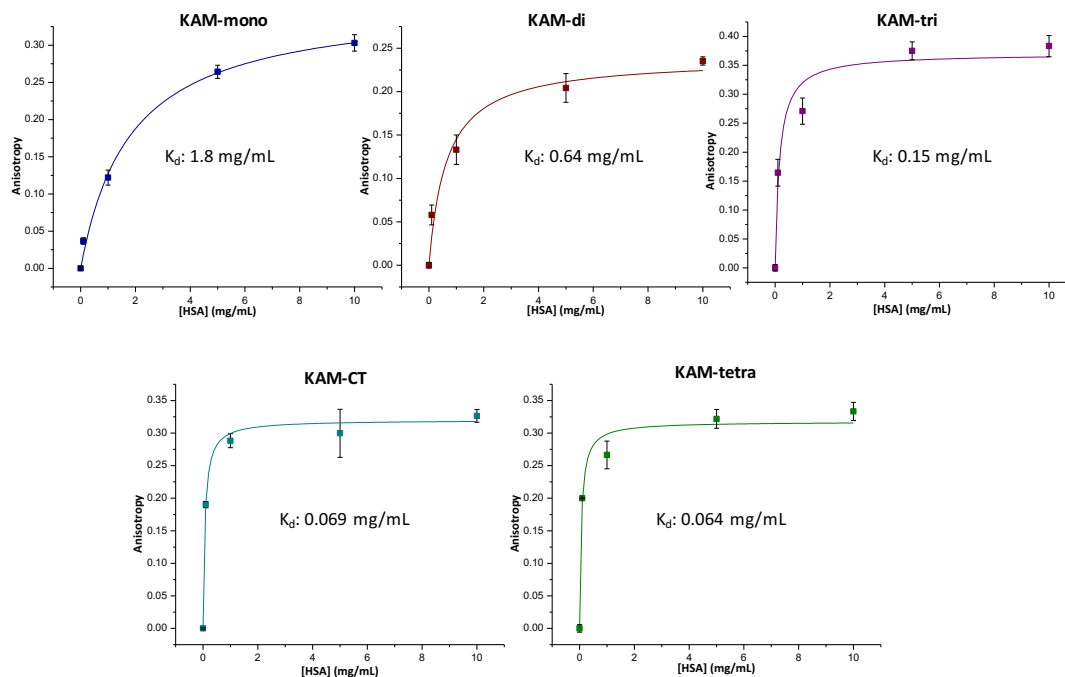


Figure 2-14 Albumin binding curve and calculated K_d value of each peptide generated by fluorescence anisotropy.

To gain further insight on albumin binding by the multivalent peptides, kinetic studies of the peptide-albumin binding were carried out to determine the on and off rates. Each peptide (200 nM) was mixed with HSA at concentrations equivalent to the K_d of the peptide. The anisotropy values were recorded over time, yielding an exponential curve as expected for relaxation kinetics (Figure 2-15). The on rate (k_{on}) and off rate (k_{off}) were determined by fitting the kinetic profiles according to the pseudo first order binding equilibrium and are summarized alongside dissociation constants in Table 2-2. The data shows a small variation (<2.5 fold) for the on rate of the peptides' association with HSA. This indicated that for binding to HSA by each peptide, formation of the first iminoboronate linkage is rate limiting, regardless of the number of 2-APBA groups. In contrast, the off rate gradually decreases as the valency increases, with the tetramer

dissociating 15 times slower than the monomer. The slow dissociation largely accounts for the improved affinity of the multivalent peptides for albumin binding.

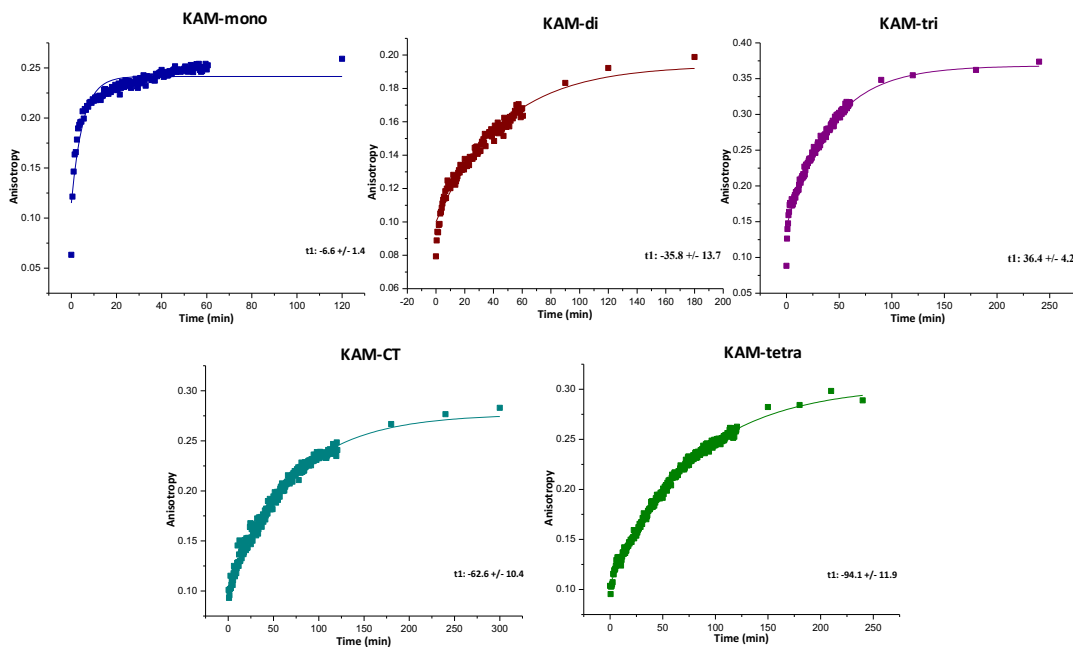


Figure 2-15 Kinetic profile and t1 values of each peptide generated by fluorescence anisotropy.

Table 2-2 Summarized dissociation constants and rates of association/dissociation for each peptide.

Peptide	K_d (mg/mL)	K_d (μ M)	k_{ON} (μ M ⁻¹ min ⁻¹)	k_{OFF} (min ⁻¹)
KAM-mono	1.8 ± 0.33	27 ± 5.0	0.0025 ± 0.0006	0.063 ± 0.015
KAM-di	0.64 ± 0.24	9.6 ± 3.7	0.0024 ± 0.0016	0.017 ± 0.011
KAM-tri	0.15 ± 0.06	2.4 ± 0.9	0.0027 ± 0.0004	0.0079 ± 0.0010
KAM-CT	0.069 ± 0.005	1.0 ± 0.1	0.0063 ± 0.0015	0.0069 ± 0.0013
KAM-tetra	0.064 ± 0.021	0.96 ± 0.3	0.0043 ± 0.0007	0.0043 ± 0.0007

2.4.3 Assessing Serum Protein Selectivity

Albumin is the most abundant protein in serum, encompassing 55% of all serum proteins. However, serum contains a variety of proteins other than albumin, including globulins, fibrinogen, transferrin and other regulatory proteins.⁸ Selective binding to albumin over other proteins is desirable for therapeutic agents in order to avoid interfering with the function of important serum proteins. The selectivity of KAM-CT for albumin was assessed via titration and fluorescence anisotropy, from which binding curves were generated for γ -globulins, fibrinogen and transferrin (Figure 2-16). Globulins, composing 38% of serum proteins, are the second most abundant protein in serum and can be divided into α -globulins, β -globulins and γ -globulins depending on their separation via protein electrophoresis. γ -Globulins, consisting mainly of immunoglobins, make up the majority of globulins and are present in serum at a concentration of 7-16 mg/mL. KAM-CT is about 6-fold more selective for albumin over γ -globulins. Fibrinogen, composing 7% of serum proteins, is the third most abundant protein. It is a 340 kDa glycoprotein present in serum at a concentration of 2-4 mg/mL essential in blood coagulation. KAM-CT is about 12-fold more selective for albumin over fibrinogen. Transferrin is a 78 kDa protein present in serum at a concentration of 2.5-3.5 mg/mL. It is responsible for controlling levels of free iron in serum and is often used as a drug carrier, similar to albumin. KAM-CT is about 13-fold more selective for albumin over transferrin.

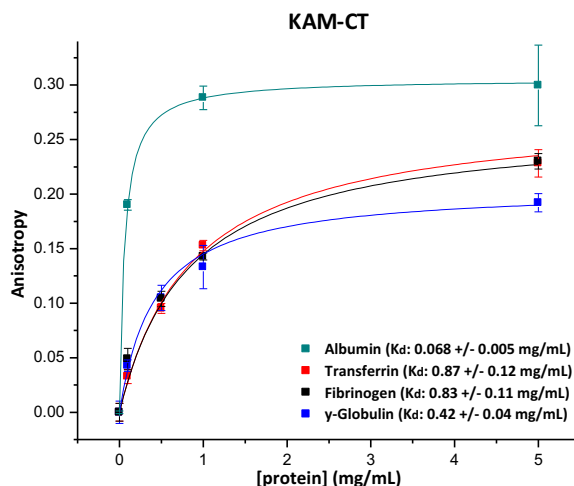


Figure 2-16 Binding curves and calculated K_d values for various serum proteins.

2.5 Conclusions

Iminoboronate chemistry serves as a powerful mechanism to promote ligand binding. We synthesized an unnatural amino acid incorporating the 2-APBA warhead, namely AB1, that allowed for the labeling of amine-presenting phospholipids of bacteria via iminoboronate formation. AB1 demonstrated selectivity towards Gram-positive bacteria over Gram-negative bacteria and mammalian cells. Although exciting and novel, AB1 suffered from the requirement of high concentrations and interference from serum proteins. Conjugation of AB1 to an antimicrobial peptide, Hlys, allowed for potent *S. aureus* staining and demonstrated much less serum protein interference.

Exploiting multivalency of the APBA-warhead allowed for even more potent binding of *S. aureus*. Specifically, KAM-CT(GRG) demonstrated significant improvement in potency over Hlys-AB1 and other multivalent peptides. Most of the multivalent peptides exhibited ~90% *S. aureus* staining interference by albumin. Although not ideal for selective bacterial labeling, the albumin-binding capacity of the multivalent peptides

could be beneficial for increasing the pharmacokinetic properties of peptide therapeutics. KAM-CT(GRG) exhibited less protein interference of *S. aureus* staining, presumably due to the additional positive charge directing the peptide to the bacterial cell membrane. These results are promising, indicating that potent and selective bacterial cell binding is attainable with iminoboronate-capable peptide probes. The ability to completely overcome protein interference with multivalent peptides will be described in a later chapter. Overall, the results presented here demonstrate the robust nature of iminoboronate chemistry in targeting bacterial cell membranes.

2.6 Experimental Procedures

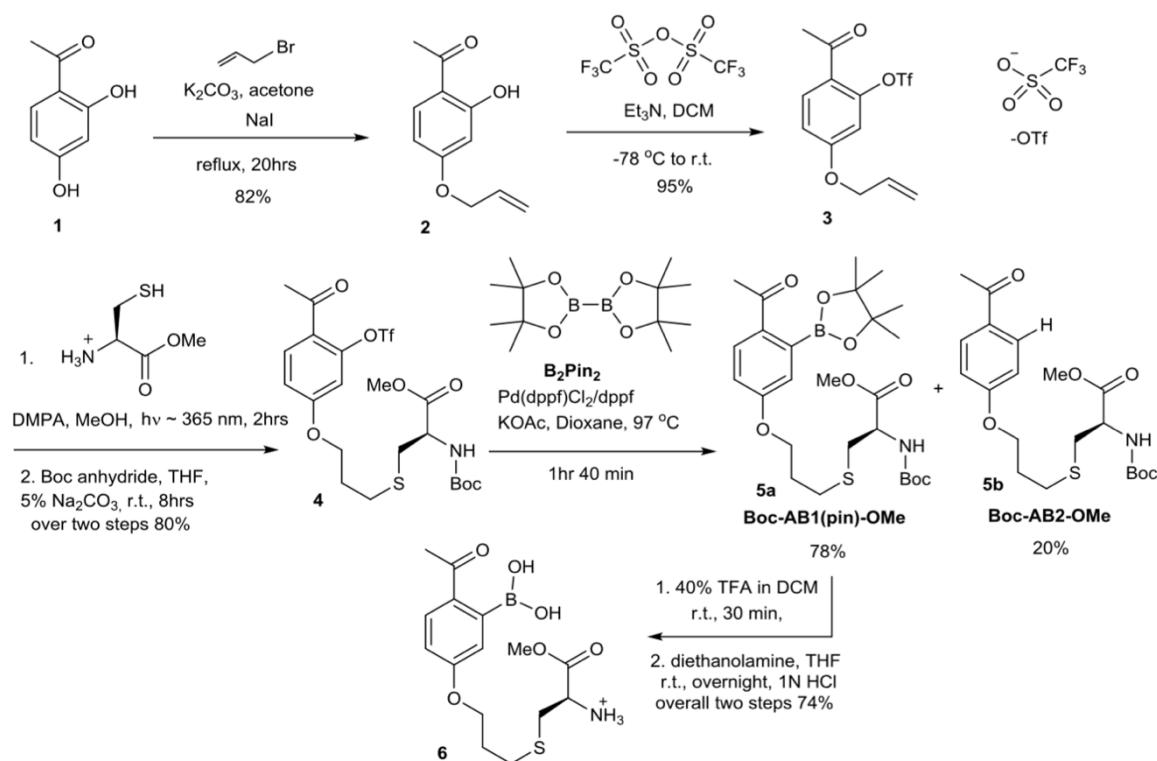
2.6.1 General Methods

Chemical reagents for small molecule and peptide synthesis were purchased from various vendors and used as received. *S. aureus* (ATCC 6538), *B. subtilis* (ATCC 663) and *S. pyogenes* (ATCC 19615) were purchased as lyophilized pellets from Microbiologics (Cloud, MN). MRSA (ATCC 43300) was purchased from ATCC (Manassas, VA). *E. coli* (BL21) was a gift from the laboratory of Professor Mary Roberts. NMR data were collected on a VNMR 500 MHz NMR spectrometer. Mass spectrometry data were generated by using an Agilent 6230 LC TOF mass spectrometer. Peptide synthesis was carried out on a Tribute peptide synthesizer from Protein Technologies and purified via reverse phase high-performance liquid chromatography (RP-HPLC) on a Waters Prep LC with a Jupiter C18 column (Phenomenex) with acetonitrile/water (0.1% trifluoroacetic acid (TFA)) eluent. The peptide concentration of all samples used in these studies were determined by measuring their absorbance at 495 nm ($\epsilon = 73,000 \text{ M}^{-1}\text{cm}^{-1}$ for AF488, $\epsilon = 75,000 \text{ M}^{-1}\text{cm}^{-1}$ for

fluorescein) on a Nanodrop 2000c ultraviolet-visible (UV/VIS) spectrometer. Flow cytometry analysis was carried out on a BD FACSAria cell sorter housed in the Biology Department at Boston College. Fluorescence images were taken on a Zeiss Axio Observer A1 inverted microscope and confocal images were taken on the Leica SP5 confocal microscope housed in the Biology Department at Boston College. The fluorescence anisotropy experiments were performed using a SpectraMax M5 plate reader.

2.6.2 Synthesis of AB1 Derivatives

Synthetic scheme for AB1-OMe (6).



Synthesis of Compound 2. Allyl bromide (4.2 mL, 49.6 mmol) and sodium iodide (NaI, 7.38 g, 49.2 mmol) were heated in acetone (75 mL) to reflux for 1 hr. Subsequently, 2',4'-dihydroxyacetophenone (4.99 g, 32.8 mmol), potassium carbonate (K_2CO_3 , 4.44 g, 32.1

mmol) and acetone (50 mL) were added to the pot. The reaction mixture was refluxed for 20 hr and reaction completion was monitored by thin layer chromatography (TLC). Upon completion, acetone was evaporated to dryness and the resulting residue was dissolved in water (150 mL). The product was extracted with ether (3 × 150 mL). Combined organic layer was washed with 5% sodium thiosulfate (150 mL), then with brine (150 mL) and dried over sodium sulfate (Na₂SO₄). The organic layer was concentrated and purified via silica gel column chromatography using hexane/ethyl acetate (4:1) to yield a viscous colorless oil (5.24 g, 82%); ¹H NMR (CDCl₃) δ: 12.72 (s, 1H), 7.64-7.62 (d, J = 8.9, 1H), 6.48-6.45 (dd, J = 8.9, 2.5 Hz, 1H), 6.43-6.42 (d, J = 2.5 Hz, 1H), 6.07-5.99 (ddt, J = 17.2, 10.6, 5.3 Hz, 1H), 5.44-5.40 (dq, J = 17.3, 1.5 Hz, 1H), 5.34-5.31 (dq, J = 10.6, 1.1 Hz, 1H), 4.58-4.56 (dt, J = 5.3, 1.5 Hz, 2H), 2.56 (s, 3H); ¹³C NMR (CDCl₃) δ: 202.5, 165.2, 165.0, 132.3, 132.2, 118.4, 114.0, 108.0, 101.7, 68.9, 26.2; MS-electrospray ionization (ESI⁺): m/z calculated for C₁₁H₁₃O₃ [M+H]⁺ 193.0864, found 193.0870.

Synthesis of Compound 3. Compound 2 (2.56 g, 13.3 mmol), was dissolved in anhydrous DCM (40 mL) and triethylamine (Et₃N, 7.4 mL, 53.0 mmol) was added. The reaction mixture was cooled to -78 °C and trifluoromethane sulfonic anhydride ((CF₃SO₂)₂O, 4.8 mL, 29.3 mmol) was added slowly over 5 min. The reaction mixture was allowed to stir at room temperature for 30 min under an argon environment. The reaction was subsequently quenched with saturated sodium bicarbonate (NaHCO₃, 60 mL) and the mixture was allowed to stir for 5 min. The product was extracted with DCM (3 × 80 mL). The combined organic layer was washed with brine (100 mL) and dried over Na₂SO₄. The organic layer was concentrated and purified on silica gel using hexane/ethyl acetate (13:1)

to yield a viscous oil (3.95 g, 95%); ^1H NMR (CDCl_3) δ : 7.83-7.82 (d, $J = 8.8$ Hz, 1H), 6.98-6.95 (dd, $J = 8.8, 2.4$ Hz, 1H), 6.84-6.83 (d, $J = 2.4$ Hz, 1H), 6.06-5.98 (ddt, $J = 17.2, 10.6, 5.4$ Hz, 1H), 5.45-5.41 (dd, $J = 17.3, 1.5$ Hz, 1H), 5.37-5.35 (dd, $J = 10.5, 1.2$ Hz, 1H), 4.62-4.60 (dt, $J = 5.4, 1.4$ Hz, 2H), 2.59 (s, 3H); ^{13}C NMR (CDCl_3) δ : 194.9, 162.5, 148.4, 132.6, 131.5, 124.1, 118.9, 117.3, 114.0, 109.5, 69.5, 29.1; MS-ESI $^+$: m/z calculated for $\text{C}_{12}\text{H}_{12}\text{F}_3\text{O}_5\text{S}$ $[\text{M}+\text{H}]^+$ 325.0357, found 325.0353.

Synthesis of Compound 4. Compound 3 (253 mg, 0.781 mmol), cysteine hydrochloride methyl ester (Cys-OMe·HCl, 270 mg, 1.56 mmol), and 2,2-dimethoxy-2-phenylacetophenone (DMPA, 44.1 mg, 0.172 mmol) were dissolved in methanol (MeOH, 440 μL). The reaction mixture was kept under UV light (~ 365 nm) for 2 hr and reaction completion was monitored by TLC. MeOH was evaporated from the reaction mixture under vacuum. The yellow residue was dissolved with 5% sodium carbonate (Na_2CO_3) solution in water (20 mL). Further, di-*tert*-butyl dicarbonate (Boc anhydride, 187 mg, 0.859 mmol) solution in tetrahydrofuran (THF, 20 mL) was added into the reaction mixture at room temperature. The was stirred for 8 hr to reaction completion. The reaction mixture was acidified with 1 M hydrochloric acid (HCl) to pH ~ 2 and the crude product was extracted with ethyl acetate (3 x 60 mL). The combined organic layer was washed with brine (80 mL) and dried over Na_2SO_4 . The organic layer was concentrated under vacuum and purified via silica gel using hexane/ethyl acetate (7:3) to yield a viscous oil (350 mg, 80% over 2 steps); ^1H NMR (CDCl_3) δ : 7.84-7.82 (d, $J = 8.8$ Hz, 1H), 6.96-6.94 (dd, $J = 8.8, 2.4$ Hz, 1H), 6.81 (d, $J = 2.4$ Hz, 1H), 5.33-5.34 (d, $J = 7.6$ Hz, 1H), 4.57- 4.53 (m, 1H), 4.13-4.11 (t, $J = 6.0$ Hz, 2H), 3.76 (s, 3H), 3.03-2.93 (m, 2H), 2.75-2.72 (m, 2H), 2.59

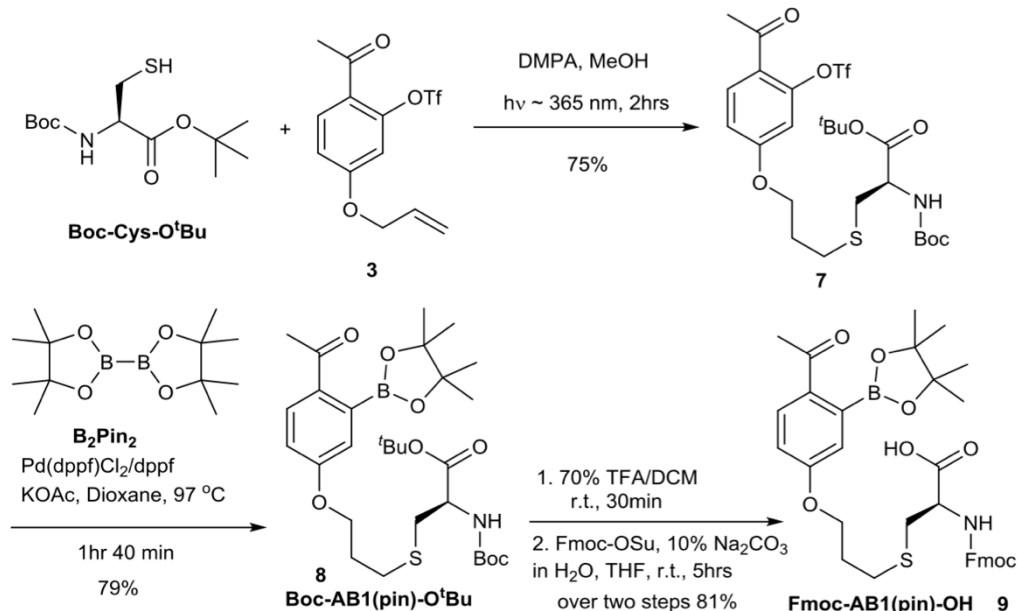
(s, 3H), 2.11-2.06 (m, 2H), 1.45 (s, 9H); ^{13}C NMR (CDCl_3) δ : 194.9, 171.4, 162.7, 148.4, 132.7, 124.1, 119.8, 117.3, 113.6, 109.3, 80.2, 66.9, 53.3, 52.5, 34.6, 29.1, 28.9, 28.6, 28.2; MS-ESI $^+$: m/z calculated for $\text{C}_{16}\text{H}_{21}\text{F}_3\text{NO}_7\text{S}_2$ [M- t-butyloxycarbonyl (Boc) +H] $^+$ 460.0712, found 460.0712.

Synthesis of Boc-AB1(pin)-OMe (5a) and Boc-AB2-OMe (5b). Compound 4 (117 mg, 0.208 mmol) was dissolved in anhydrous dioxane (1.3 mL). Bis(pinacolato)diboron (B_2Pin_2 , 116 mg, 0.458 mmol), [1,1'-Bis(diphenylphosphino)ferrocene]dichloropalladium(II) ($\text{Pd}(\text{dppf})\text{Cl}_2$, 12.3 mg, 0.0168 mmol), dppf (9.3 mg, 0.017 mmol) and potassium acetate (KOAc, 69.2 mg, 0.706 mmol) were added into the solution. Molecular sieves (3 Å, 35 mg) were added into the reaction and the reaction vessel was flushed with argon before reaction mixture was allowed to stir at 97 °C for 1 hr and 40 min. Reaction completion was monitored via LC-MS. Upon completion, water (40 mL) was added to the reaction and the product was extracted with ethyl acetate (3 × 20 mL). The combined organic layer was washed with brine (40 mL) and dried over Na_2SO_4 . The organic layer was concentrated under vacuum and purified on silica gel using hexane/diethylether (2:3) to separate the desired product Boc-AB1(pin)-OMe (5a) (82 mg, 78%, colorless highly viscous liquid) and the protodeboronated product Boc-AB2-OMe (5b) (18 mg, 20%, colorless liquid). Boc-AB1(pin)-OMe(5a) ^1H NMR (CDCl_3) δ : 7.78-7.76 (d, J = 8.6 Hz, 1H), 6.98-6.97 (d, J = 2.4 Hz, 1H), 6.88-6.85 (dd, J = 8.6, 2.5 Hz, 1H), 5.41-5.39 (d, J = 8.0 Hz, 1H), 4.56-4.55 (m, 1H), 4.13-4.11 (t, J = 5.9 Hz, 2H), 3.81-3.75 (s, 3H), 3.18-3.06 (m, 1H), 2.97-3.00 (d, J = 6.0 Hz, 1H), 2.75-2.71 (m, 2H), 2.59 (s, 3H), 2.08-2.03 (dq, J = 13.1, 6.2 Hz, 2H), 1.45 (s, 9H), 1.43 (s, 12H); ^{13}C NMR (CDCl_3) δ 200.6, 168.1, 163.3, 133.2, 130.6, 117.5, 114.4, 109.9, 83.6,

80.5, 66.2, 53.7, 52.6, 34.5, 29.1, 28.9, 28.7, 28.2, 24.7; MS-ESI⁺: m/z calculated for C₂₁H₃₂BNO₆S [M+H]⁺ 538.2646, found 538.2653. Boc-AB2-OMe(5b) ¹H NMR (CDCl₃) δ: 7.93-7.91 (m, 2H), 6.90-6.92 (m, 2H), 5.36-5.34 (d, J = 8.0 Hz, 1H), 4.55-4.53 (d, J = 6.9 Hz, 1H), 4.11-4.09 (t, J = 6.0 Hz, 2H), 3.75 (s, 3H), 2.99-2.93 (td, J = 13.8, 13.0, 5.2 Hz, 2H), 2.74-2.71 (t, J = 6.9, 2H), 2.55 (s, 3H), 2.04-2.09 (m, 2H), 1.44 (s, 9H); ¹³C NMR (CDCl₃) δ: 196.6, 171.4, 162.6, 155.0, 130.5, 130.40, 114.1, 80.1, 66.1, 53.3, 52.5, 34.6, 29.1, 28.9, 28.2, 26.3; MS-ESI⁺: m/z calculated for C₁₅H₂₁NO₄S [M-Boc+H]⁺ 312.1270, found 312.1262.

Synthesis of AB1-OMe (6). Boc-AB1(pin)-OMe (5a) (30 mg, 0.057 mmol) was dissolved in anhydrous DCM (300 μL) and TFA (200 μL) was added. The reaction was allowed to stir at room temperature for 30 min. TFA and DCM were evaporated completely from reaction mixture. The liquid residue was dissolved in water and lyophilized to give a white powder (quantitative). The white powder was dissolved in THF (1 mL) and diethanolamine (36 mg, 0.342 mmol) was added into the solution at room temperature. The reaction was allowed to stir overnight. The reaction was quenched with 1 M HCl (3 mL) and THF was evaporated under vacuum. The compound was purified using RP-HPLC to yield yellow powder after lyophilization (74%, 15 mg). ¹H NMR (DMSO d₆) δ: 8.56 (s, 3H), 7.88-7.86 (d, J = 8.3 Hz, 1H), 6.91-6.89 (dd, J = 8.6, 2.5 Hz, 1H), 6.83 (d, J = 2.2 Hz, 1H), 4.34-4.32 (m, 1H), 4.10-4.08 (t, J = 5.8 Hz, 2H), 3.74 (s, 3H), 3.01-2.99 (m, 2H), 2.70-2.67 (t, J = 5.2 Hz, 2H), 2.46 (s, 3H), 1.98-1.94 (m, 2H); ¹³C NMR (DMSO d₆) δ 198.0, 169.1, 161.7, 133.1, 131.6, 117.4, 113.1, 66.4, 53.4, 31.7, 28.8, 28.5, 26.2. MS-ESI⁺: m/z calculated for C₁₅H₂₃BNO₆S [M+H]⁺ 338.1233, found 338.1469.

Synthetic scheme for Fmoc-AB1(pin)-OH (9).



Synthesis of Compound 7. Boc-Cys-O^tBu was prepared by following a previously reported protocol.¹⁸ Boc-Cys-O^tBu (0.967 g, 3.48 mmol), compound **3** (1.02 g, 3.16 mmol), and DMPA (166 mg, 0.640 mmol) were dissolved in MeOH (1.9 mL) and allowed to react under UV light for 1 hr. Additional DMPA (20 mg, 7.8 mmol) was added and the reaction and allowed to continue under UV light for 15 min. Reaction completion was monitored by TLC and concentrated under vacuum upon completion. The resulting residue was purified via silica gel column chromatography using hexane/ethyl acetate (4:1) to yield a white solid (1.43 g, 75%); ^1H NMR (CDCl_3) δ 7.82 (d, $J = 8.8 \text{ Hz}$, 1H), 6.94 (dd, $J = 8.8, 2.4 \text{ Hz}$, 1H), 6.80 (d, $J = 2.4 \text{ Hz}$, 1H), 5.32 (d, $J = 7.6 \text{ Hz}$, 1H), 4.40 (d, $J = 7.0 \text{ Hz}$, 1H), 4.11 (t, $J = 6.1 \text{ Hz}$, 2H), 3.03 – 2.89 (m, 2H), 2.75 (td, $J = 7.0, 1.4 \text{ Hz}$, 2H), 2.58 (s, 3H), 2.12 – 2.03 (m, 2H), 1.45 (d, $J = 16.2 \text{ Hz}$, 18H); ^{13}C NMR (CDCl_3) δ 194.91, 169.86, 162.80, 148.45, 132.69, 124.10, 119.87, 117.32, 113.63, 109.33, 82.61, 79.90, 66.98, 53.98, 34.72, 29.14, 29.10,

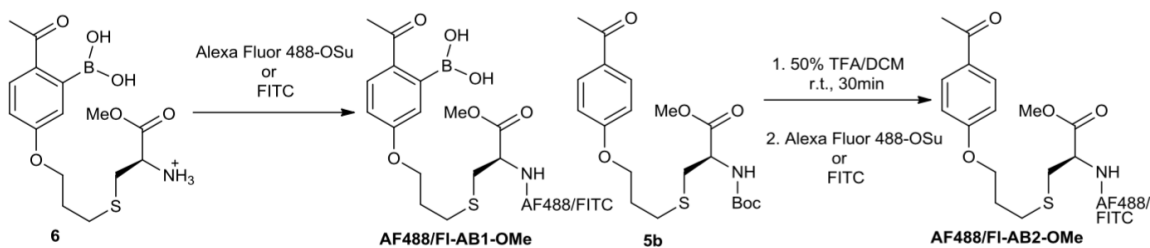
28.71, 28.28, 27.95; Dart (ESI⁺) m/z calculated for C₂₄H₃₅F₃NO₉S₂ [M+H]⁺ 602.1705, found 602.1689.

Synthesis of Compound 8. Compound 7 (1.99 g, 3.31 mmol), B₂pin₂ (2.02 g, 7.97 mmol), Pd(dppf)Cl₂ (202 mg, 0.270 mmol), dppf (151 mg, 0.270 mmol) and KOAc (952 mg, 9.69 mmol) were dissolved in anhydrous dioxane (21 mL). Molecular sieves (3 Å, 500 mg) were added into the reaction and the reaction vessel was flushed with argon. The reaction mixture was allowed to stir at 97 °C for 2 hr and reaction completion was monitored by HPLC. Upon completion, water (150 mL) was added to the reaction mixture and the product was extracted with ethyl acetate (3 × 150 mL). Combined organic layer was washed with brine (200 mL) and dried over Na₂SO₄. The organic layer was concentrated and purified via silica gel column chromatography using hexane/ether (3:2) to yield a viscous oil (1.51 g, 79%). A small amount of the protodeboronated product (Boc-AB2-OtBu) was observed by LC-MS analysis (data not shown), but not isolated. ¹H NMR (CDCl₃) δ 7.78-7.76 (d, J = 8.6 Hz, 1H), 6.96-6.94 (d, J = 2.6 Hz, 1H), 6.87-6.85 (dd, J = 8.6, 2.6 Hz, 1H), 5.41-5.40 (d, J = 7.6 Hz, 1H), 4.43-4.40 (m, 1H), 4.12-4.10 (t, J = 6.0 Hz, 2H), 3.01-2.92 (dt, J = 13.7, 6.8 Hz, 1H), 2.76-2.73 (t, J = 6.2, 2H), 2.55 (s, 3H), 2.08 – 2.03 (m, 2H), 1.48 (s, 9H), 1.44 (s, 15H), 1.26 (s, 6H); ¹³C NMR (CDCl₃) δ 198.39, 169.99, 162.47, 155.13, 133.50, 130.68, 117.95, 113.91, 83.55, 82.54, 79.86, 74.97, 66.16, 53.95, 34.62, 29.33, 29.05, 24.89, 24.77, 24.50; MS-ESI⁺: m/z calculated for C₂₉H₄₇BNO₈S [M+H]⁺ 580.3115, found 580.3115.

Synthesis of Compound 9. Boc-AB1(pin)-OtBu (8) (1.51 g, 2.60 mmol) was dissolved in DCM (15 mL) and placed on ice. TFA (22 mL) was added to the reaction vessel. The reaction

mixture was allowed to stir at room temperature for 2 hr. DCM and TFA were evaporated and the resulting residue was re-dissolved in DCM and evaporated (3 x) to remove the residual TFA. The resulting residue was subsequently dissolved in 10% Na₂CO₃ (30 mL). Fmoc-OSu (878 mg, 2.60 mmol) was dissolved in THF (30 mL), added to the reaction mixture and allowed to stir at room temperature for 5 hr. The resulting mixture was acidified with 2 M HCl and the product was extracted with ethyl acetate (3 × 70 mL). Combined organic layer was washed with brine (100 mL) and dried over Na₂SO₄. Solvent removal gave a yellow oil residue, which was triturated in hexane/ethyl acetate overnight to yield an off- white solid (1.37 g, 81%). ¹H NMR (CDCl₃) δ: 7.74 (dd, J = 12.1, 8.1 Hz, 3H), 7.62 – 7.56 (m, 2H), 7.39 (t, J = 7.4 Hz, 2H), 7.30 (td, J = 7.3, 1.1 Hz, 2H), 7.00 (d, J = 2.5 Hz, 1H), 6.84 (dd, J = 8.6, 2.5 Hz, 1H), 5.65 (d, J = 7.8 Hz, 1H), 4.61 – 4.55 (m, 1H), 4.39 (d, J = 7.2 Hz, 2H), 4.22 (t, J = 7.1 Hz, 1H), 4.18 – 4.09 (m, 2H), 3.07 – 2.92 (m, 2H), 2.70 (t, J = 7.1 Hz, 2H), 2.55 (s, 3H), 2.02 (dt, J = 21.2, 14.2 Hz, 1H), 1.44 (s, 12H), 1.26 (d, J = 4.2 Hz, 1H); ¹³C NMR (CDCl₃) δ: 162.8, 143.6, 141.2, 133.4, 130.5, 127.7, 127.0, 125.0, 119.9, 117.7, 114.9, 83.8, 67.2, 66.0, 47.0, 34.4, 31.5, 29.1, 24.8, 24.8, 24.2, 14.0; MS-ESI⁺: m/z calculated for C₃₅H₄₁BNO₈S [M+H]⁺ 646.2646, found 646.2649.

Fluorophore Labeling of AB1-OMe and AB2-OMe.



AB1-OMe (6) was directly conjugated to FITC and AF488-OSu by following the vendor protocols from Life Technologies (<http://tools.lifetechnologies.com/content/sfs/manuals/mp10168.pdf>). Boc-AB2-OMe (5b) was treated with 50% TFA in DCM to remove Boc. Upon solvent evaporation, the residue was directly subjected to the same labeling conditions as AB1-OMe. The labeled products were purified via RP-HPLC and confirmed via LC-MS for integrity and purity (Table 2-3).

Table 2-3 MS data of fluorophore labeled AB1 derivatives.

AB1 Derivative	Calculated m/z	Observed m/z
Fl-AB1-OMe	727.16 [M-H ₂ O] ⁺	727.15
Fl-AB2-OMe	701.16 [M+H] ⁺	701.16
AF488-AB1-OMe	854.11 [(M-H ₂ O)+H] ⁺	854.12
AF488-AB2-OMe	828.12 [M+H] ⁺	828.11

2.6.3 Synthesis of AB1-containing Peptides

SPPS was performed on a Rink Amide MBHA solid support using Fmoc-*t*Bu chemistry on a 0.05 mmol scale. The N-terminus of each peptide was acetylated. Five equivalents of commercially available amino acids were used for the coupling reaction with hexafluorophosphate benzotriazole tetramethyl uronium (HBTU) as the activating reagent. The incorporation of the unnatural amino acid, Fmoc-AB1(pin)-OH was accomplished by using four equivalents and an extended coupling time (1 hr). The peptides were cleaved off resin and globally deprotected with Reagent B (88% TFA, 5%

water, 2% triisopropylsilane, and 5% phenol). Crude peptides were obtained via ether precipitation and purified via RP-HPLC. For a typical fluorophore labeling experiment, 1.3 mM solution of AF488-C₅-maleimide in dimethylformamide (DMF, 100 μ L) and 3 mM peptide solution (150 μ L) were mixed together with 30 mM NMM (6 μ L) and 15 mM tris(2-carboxyethyl)phosphine (TCEP, 5 μ L). The reaction was stirred at room temperature for 1 hr and reaction completion was monitored by LC-MS. The crude products were purified via RP-HPLC. All peptides were characterized via LC-MS to confirm their identities and excellent purities (>95%, Table 2-4).

Table 2-4 MS data of fluorophore labeled AB1-containing peptides.
Ac: Acetyl; C*: AF488-labeled Cys; X: AB1

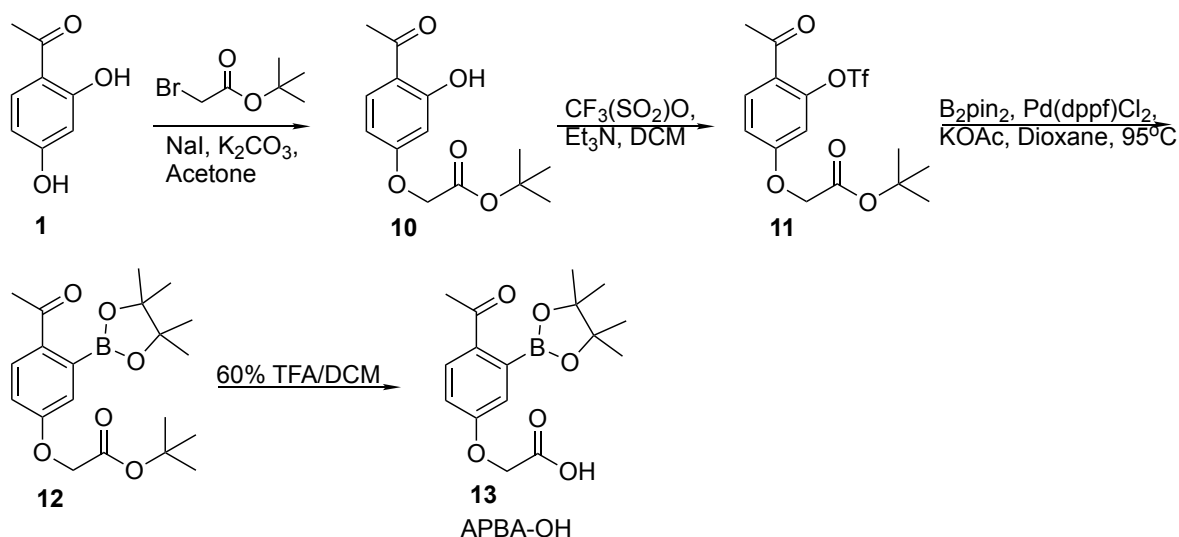
Peptide	Calculated m/z	Observed m/z
G-AB1: Ac-C*GX-NH ₂	1223.26 [M-(H ₂ O)] ⁺	1223.26
K-AB1: Ac-C*KX-NH ₂	1294.34 [M-(H ₂ O)] ⁺	1294.34
R-AB1: Ac-C*RX-NH ₂	1322.35 [M-(H ₂ O)] ⁺	1322.34
Hlys-AB1: Ac-C*RYWVAWRNRGX-NH ₂	1256.47 [M-(H ₂ O)+2H] ²⁺	1256.47
Hlys: Ac-C*RYWVAWRNR-NH ₂	1075.34 [M+2H] ²⁺	1075.34
Ac-C*GXG-NH ₂	1280.19 [M-(H ₂ O)+H] ⁺	1280.29
Ac-C*GXGXG-NH ₂	812.50 [M-(3H ₂ O)+2H] ²⁺	812.70
Ac-C*GXGGXG-NH ₂	841.24 [M-(3H ₂ O)+2H] ²⁺	841.21
Ac-C*GXGGGXG-NH ₂	869.50 [M-(3H ₂ O)+2H] ²⁺	869.71
Ac-C*GXAAAXG-NH ₂	890.80 [M-(3H ₂ O)+2H] ²⁺	890.74

2.6.4 Synthesis of Tetramer via CuAAC

Fmoc-GXGGGXG was subjected to Fmoc deprotection (20% piperidine, 5 min x 2) followed by coupling with 5 equivalents of 4-pentynoic acid with equal equivalents of HBTU in 0.4 M NMM/DMF on resin to yield Alkyne-GXGGGXG. Fmoc-GXGGGXG was subjected to Fmoc deprotection followed by coupling with 5 equivalents of 2-azidoacetic acid with equal equivalents of HBTU in 0.4 M NMM/DMF on resin to yield Azide-GXGGGXG. Both peptides were cleaved from resin with Reagent B and purified via RP-HPLC. Alkyne-GXGGGXG (1.25 mg, 1.2 μ mol) and Azide-GXGGGXG (1.25 mg, 1.2 μ mol) were subjected to click reaction conditions consisting of 4 equivalents NaAsc and 1 equivalent CuSO_4 in HEPES buffer/*t*-butanol (1:1, 300 μ L) for 12 hr under argon. LC-MS confirmed desired clicked tetramer was present.

2.6.5 Synthesis of APBA-OH

Synthetic scheme for APBA-OH (13).



Synthesis of Compound 10. 2,4'-dihydroxyacetophenone (5.00 g, 32.9 mmol), K_2CO_3 (4.51, 32.7 mmol) and acetone (75 mL) were heated to reflux for 2 hr. In a separate flask, *t*-butyl

bromoacetate (4.9 mL, 32.9 mmol) and NaI (5.40, 36.6 mmol) were stirred at room temperature in acetone (75 mL) for 2 hr. The two reaction pots were combined and allowed to reflux overnight and reaction completion was monitored by TLC. Acetone was evaporated to dryness and the resulting residue was dissolved in water (150 mL). The product was extracted with ethyl acetate (3 x 150 mL). The combined organic layer was washed with 5% sodium thiosulfate (150 mL), washed with brine (150 mL) and dried over Na_2SO_4 . The resulting product was concentrated to dryness to yield a pure yellow viscous oil (9.58 g, 100%); ^1H NMR (CDCl_3) δ 12.67 (s, 1H), 7.64 (d, J = 8.9 Hz, 1H), 6.47 (dd, J = 8.9, 2.6 Hz, 1H), 6.34 (d, J = 2.5 Hz, 1H), 4.53 (s, 2H), 2.55 (s, 3H), 1.48 (s, 9H); ^{13}C NMR (CDCl_3) δ 202.66, 167.00, 164.99, 164.16, 132.42, 114.49, 107.70, 101.64, 82.88, 77.27, 77.01, 76.76, 65.39, 28.01, 26.23; MS-ESI⁺: m/z calculated for $\text{C}_{14}\text{H}_{18}\text{O}_5$ $[\text{M}+\text{H}]^+$ 267.1154, found 267.1415.

Synthesis of Compound 11. Compound 10 (9.50 g, 35.6 mmol) was dissolved in anhydrous DCM (100 mL) and Et_3N (20 mL, 42.7 mmol) was added. The reaction mixture was cooled to -78°C and $(\text{CF}_3\text{SO}_2)_2\text{O}$ (11.8 mL, 71.2 mmol) was added drop-wise. The reaction was allowed to stir at room temperature for 1 hr and reaction completion was monitored by TLC. The reaction was quenched with the addition of saturated Na_2CO_3 (100 mL) and the mixture was allowed to stir for 5 min. The product was extracted with DCM (3 x 100 mL). The combined organic layer was washed with brine (100 mL) and dried over Na_2SO_4 . The resulting crude product was concentrated and purified via silica gel column chromatography using hexane/ethyl acetate (9:1) to yield a yellow solid (11.33 g, 80%); ^1H NMR (CDCl_3) δ 7.84 (d, J = 8.8 Hz, 1H), 6.94 (dd, J = 8.8, 2.5 Hz, 1H), 6.83 (d, J = 2.4 Hz,

1H), 4.58 (s, 2H), 2.59 (s, 3H), 1.49 (s, 9H); ^{13}C NMR (CDCl_3) δ 194.95, 166.48, 161.75, 148.31, 132.63, 119.84, 117.29, 113.93, 109.55, 83.29, 77.28, 77.03, 76.77, 65.79, 28.01, 27.83; MS-ESI⁺: m/z calculated for $\text{C}_{15}\text{H}_{17}\text{F}_3\text{O}_7\text{S}$ $[\text{M}+\text{H}]^+$ 399.0647, found 399.07090.

Synthesis of Compound 12. Compound 11 (2.02 g, 5.0 mmol), B_2pin_2 (3.17 g, 12.5 mmol), $\text{Pd}(\text{dppf})\text{Cl}_2$ (367 mg, 0.5 mmol) and KOAc (1.47 g, 15.1 mmol) were dissolved in anhydrous dioxane (30 mL). Molecular sieves (4 Å) were added and the reaction mixture was flushed with argon for 10 min. The reaction mixture was allowed to stir at 95 °C under argon for 2 hr and reaction completion was monitored by TLC. Water (100 mL) was added to the reaction mixture and the product was extracted with ethyl acetate (3 x 100 mL). The combined organic layer was washed with brine (100 mL) and dried over Na_2SO_4 . The resulting crude product was concentrated and purified via silica gel column chromatography using hexane/diethyl ether (3:2) to yield a white solid (1.20 g, 63%); ^1H NMR (CDCl_3) δ 7.76 (d, J = 8.6 Hz, 1H), 6.93 (d, J = 2.6 Hz, 1H), 6.90 – 6.84 (m, 1H), 4.55 (s, 2H), 2.53 (s, 3H), 1.46 (s, 9H), 1.41 (s, 12H); ^{13}C NMR (CDCl_3) δ 198.30, 167.26, 161.37, 134.22, 130.57, 117.76, 114.54, 83.59, 82.65, 77.29, 77.04, 76.78, 65.66, 27.97, 24.88, 24.54; MS-ESI⁺: m/z calculated for $\text{C}_{20}\text{H}_{29}\text{BO}_6$ $[\text{M}+\text{H}]^+$ 377.2057, found 377.21938.

Synthesis of Compound 13. Compound 12 (1.20 g, 3.17 mmol) was dissolved in 60% TFA in DCM (30 mL) and allowed to stir at room temperature for 1 hr. The solvent was evaporated and the residue was dissolved in DCM and evaporated (3 x) to remove residual TFA. The resulting residue was dissolved in water and lyophilized to yield a white solid (1.01 g, 100%). ^1H NMR ($\text{DMSO}-d_6$) δ 7.94 (d, J = 8.6 Hz, 1H), 6.98 (dd, J = 8.6, 2.6 Hz, 1H), 6.85 (d, J = 2.6 Hz, 1H), 4.79 (s, 2H), 2.51 (s, 3H), 1.30 (s, 12H); ^{13}C NMR ($\text{DMSO}-d_6$) δ

198.46, 170.19, 161.54, 133.96, 131.84, 118.25, 114.27, 83.39, 64.99, 40.45, 40.38, 40.28, 40.21, 40.12, 40.04, 39.95, 39.87, 39.78, 39.62, 39.45, 25.46, 25.10; MS-ESI⁺: m/z calculated for C₁₆H₂₁BO₆ [M+H]⁺ 321.1431, found 321.1647.

2.6.6 On-resin Multivalent Peptide Synthesis

SPPS was performed on a Rink Amide MBHA solid support using Fmoc-*t*Bu chemistry on a 0.05 mmol scale. The N-terminus of each peptide was acetylated. Five equivalents of commercially available amino acids were used for the coupling reaction with HBTU as the activating reagent. Dap, orthogonally protected with allyloxycarbonyl (Alloc), was incorporated in the sequence to serve as an attachment for the 2-APBA coupling. Alloc deprotection was achieved upon 1 hr treatment with tetrakis(triphenylphosphine)palladium and phenylsilane in DCM. Following deprotection, APBA-OH was coupled to the Dap residues utilizing 2 equivalents of the small molecule per Dap residue, equal equivalents of HBTU in 0.4M NMM/DMF for 2 hr. The peptides were cleaved off resin and globally deprotected with Reagent B. Crude peptides were obtained through ether precipitation and purified by RP-HPLC. Peptides were labeled with AF488-maleimide following same procedure as above for AB1-containing peptides. All peptides were characterized via LC-MS for excellent purity (>95%) and correct masses (Table 2-5).

Cyclic trimer synthesis was carried out via Fmoc/*t*Bu chemistry with the Dawson dbz resin as the solid support and a Boc protected N-terminal cysteine. The synthesis was carried out on a 0.05 mmol scale. Five equivalents of commercially available amino acids were used for the coupling reaction with HBTU as the activating reagent. Fmoc-

Dap(Alloc)-OH was incorporated in the sequence to serve as an attachment for the 2-APBA moiety. Following Alloc deprotection as described above, six equivalents of APBA-OH were coupled to the Dap residues. The dbz resin was converted to activated N-acylbenzimidazolinone (nbz) resin with 5 equivalents of 4-nitrophenylchloroformate in DCM followed by treatment with 0.5 M diisopropylethylamine (DIPEA) in DMF. Cleavage from resin with Reagent B results in a C-terminal N-acylurea functionality which can undergo rapid thiolysis. Crude peptide was obtained through ether precipitation and purified by RP-HPLC. The pure peptide was subjected to native chemical ligation to obtain head-to-tail cyclization by treatment with thiophenol in the presence of 3 M guanidine HCl, 200mM sodium phosphate, TCEP and DMF at a pH ~ 7-8. Following confirmation of product formation, the peptides were purified by RP-HPLC. The peptides were characterized via LC-MS for excellent purity (>95%) and correct masses (Table 2-5).

Table 2-5 MS data of AF488-labeled on-resin coupled APBA peptides.

Peptide	Calculated m/z	Observed m/z
KAM-mono	1263.32 [M-H ₂ O+H] ⁺	1263.29
KAM-di	852.74 [M-3H ₂ O+2H] ²⁺	852.71
KAM-tri	1082.32 [M-4H ₂ O+2H] ²⁺	1082.30
KAM-tetra	1320.91 [M-4H ₂ O+H] ²⁺	1320.87
KAM-CT	1052.30 [M-4H ₂ O+H] ²⁺	1052.76
KAM-CT(GRG)	1228.97 [M-H ₂ O+H] ²⁺	1228.90

2.6.7 Flow Cytometry Analysis of Bacterial Binding

S. aureus was grown to an optical density measured at 600 nm ($OD_{600} \approx 0.5$), washed and diluted with phosphate-buffered saline (PBS, pH 7.4). The cells ($\sim 1 \times 10^7$ colony-forming units (cfu)/mL) were incubated with various concentrations of AF488-labeled peptide in PBS alone or with 10% FBS, 10% human serum or 1 mg/mL BSA as indicated in each experiment. After incubation for 1 hr, samples were subjected to cytometric analysis. Data obtained were analyzed via BD FACSDiva software and median fluorescent values were computed from the generated histograms. All flow cytometry experiments were repeated and generated consistent results.

2.6.8 Fluorescence Microscopy Analysis of Bacterial Binding

Each bacterial strain was grown to an $OD_{600} \approx 1.0$, washed and diluted with PBS (pH 7.4). The cells ($\sim 1 \times 10^9$ cfu/mL) were incubated with various concentrations of AF488-labeled peptide in PBS alone or with 1 mg/mL BSA, as indicated in each experiment, for 1 hr. White light and fluorescent images were obtained on the Zeiss microscope equipped with filter set 44 (excitation: BP 475/40, emission: BP 530/50) suitable for detection of AF488 fluorescence. Images were captured using the 100X oil immersion objective with a 300 ms exposure time. All images were processed consistently using ImageJ software.

2.6.9 Fluorescence Anisotropy Binding Assay of Serum Proteins

The serum protein of interest was added at various concentrations to a Costar black/clear-bottom 96-well plate from a stock solution in PBS (pH 7.4). The AF488-labeled peptide (200 nM) was added to the 96-well plate. Endpoint fluorescence polarization readings were obtained hourly until they leveled off. Saturation binding curves were plotted with

Origin software to determine K_d values. Errors bar represent standard deviation over 3 trials. The hyperbolic curves generate the equation $y = P1*x/(P2+x)$, where the P2 value is reported as the K_d . For kinetic studies, fluorescence polarization readings were obtained every 30 seconds for early time points, then every 30 min for later time points. Kinetics were plotted with Origin software to determine k_{on} and k_{off} rates. One trial for each peptide is depicted with the average t_1 value (and standard deviation error) generated from an exponential fit over 3 trials. Exponential growth curves generate the equation $y = A1(x/t_1) + y_0$. K_{eq} is calculated assuming peptide is fully bound at 10 mg/mL HSA. Pseudo-first order reaction kinetics derives the equation $1/t_1 = k_{on} [HSA] + k_{off}$, which is used to calculate k_{on} and k_{off} .

2.7 References

1. Vazquez, M. A., Echevarria, G., Munoz, F., Donoso, J. & Blanco, F. G. Kinetic Study of the Schiff-base Formation between Glycine and Pyridoxal 5'- Phosphate (PLP), Pyridoxal (PL), and 5'-Deoxypyridoxal (DPL). *J. Chem. Soc. Perkin Trans. 2* 1617–1622 (1989).
2. Mcfarland, J. M. & Francis, M. B. Reductive Alkylation of Proteins Using Iridium Catalyzed Transfer Hydrogenation. *J. Am. Chem. Soc.* **127**, 13490–13491 (2005).
3. Bandyopadhyay, A. & Gao, J. Targeting biomolecules with reversible covalent chemistry. *Curr. Opin. Chem. Biol.* **34**, 110–116 (2016).
4. Crugeiras, J., Rios, A., Riveiros, E. & Richard, J. P. Substituent Effects on the Thermodynamic Stability of Imines Formed from Glycine and Aromatic Aldehydes: Implications for the Catalytic Activity of Pyridoxal-5'-Phosphate (PLP). *J. Am. Chem. Soc.* **131**, 15815–15824 (2009).

5. Links, D. A., Medrano, F. & Yatsimirsky, A. K. Schiff base formation and recognition of amino sugars, aminoglycosides and biological polyamines by 2-formyl phenylboronic acid in aqueous solution. *Org. Biomol. Chem.* **10**, 6960–6972 (2012).
6. Cal, P. M. S. D., Vicente, J. B., Pires, E., Coelho, A. V., Veiros, L. F., Cordeiro, C. & Gois, P. M. P. Iminoboronates: A New Strategy for Reversible Protein Modification. *J. Am. Chem. Soc.* **134**, 10299–10305 (2012).
7. Bandyopadhyay, A., McCarthy, K. A., Kelly, M. A. & Gao, J. Targeting bacteria via iminoboronate chemistry of amine-presenting lipids. *Nat. Commun.* **6**, 6561 (2015).
8. Kratz, F. & Elsadek, B. Clinical impact of serum proteins on drug delivery. *J. Control. Release* **161**, 429–445 (2012).
9. Gonz, R. & Albericio, F. Improved antimicrobial activity of h-lysozyme (107 – 115) by rational Ala substitution. *J. Pept. Sci.* **16**, 424–429 (2010).
10. Tang, M., Waring, A. J., Lehrer, R. I. & Hong, M. Effects of Guanidinium – Phosphate Hydrogen Bonding on the Membrane-Bound Structure and Activity of an Arginine-Rich Membrane Peptide from Solid-State NMR Spectroscopy. *Angew. Chemie Int Ed* **3202–3205** (2008).
11. Mammen, M., Choi, S. & Whitesides, G. M. Polyvalent Interactions in Biological Systems: Implications for Design and Use of Multivalent Ligands and Inhibitors. *Angew. Chemie Int Ed* **37**, 2754–2794 (1998).
12. Joshi, A., Vance, D., Rai, P., Thiyagarajan, A. & Kane, R. S. The Design of Polyvalent Therapeutics. *Chem. Eur. J.* **14**, 7738–7747 (2008).
13. Levine, P. M., Imberg, K., Garabedian, M. J. & Kirshenbaum, K. Multivalent Peptidomimetic Conjugates: A Versatile Platform for Modulating Androgen Receptor Activity. *J. Am. Chem. Soc.* **134**, 6912–6915 (2012).
14. Blanco-canosa, J. B. & Dawson, P. E. An Efficient Fmoc-SPPS Approach for the Generation of Thioester Peptide Precursors for Use in Native Chemical Ligation. *Angew. Chemie Int Ed* **47**, 6851–6855 (2008).

15. Dennis, M. S., Zhang, M., Meng, Y. G., Kadkhodayan, M., Kirchofer, D., Combs, D. & Damico, L. A. Albumin Binding as a General Strategy for Improving the Pharmacokinetics of Proteins. *J. Biol. Chem.* **277**, 35035–35043 (2002).
16. Panchala, S. C. *et al.* A biomimetic approach for enhancing the in vivo half-life of peptides. *Nat. Chem. Biol.* **11**, 793–798 (2015).
17. Kratz, F. & Elsadek, B. Clinical impact of serum proteins on drug delivery. *J. Control. Release* **161**, 429–445 (2012).
18. Shen, F., Zhang, Z. P., Li, J. Bin, Lin, Y. & Liu, L. Hydrazine-sensitive thiol protecting group for peptide and protein chemistry. *Org. Lett.* **13**, 568–571 (2011).

CHAPTER 3

TARGETING LIPID II PENTAPEPTIDE WITH APBA-MODIFIED PHAGE DISPLAY LIBRARY

3.1 Introduction

3.1.1 Lipid II Pentapeptide and the Peptidoglycan

The cell wall is essential for bacterial survival, providing both protection and structural support. Bacterial cell walls are made of peptidoglycan, a covalent polymer of sugars and amino acids.¹ The peptidoglycan provides a robust barrier for the cell, resisting intracellular osmotic pressure and forming a strong matrix of glycan chains cross-linked with short peptide chains. The glycan chains are composed of alternating N-acetylglucosamine (GlcNAc) and N-acetylmuramic acid (MurNAc) sugar units. A pentapeptide stem chain, attached to the carboxyl functionality of MurNAc, can cross-link with adjacent stem peptides to create the three-dimensional network structure of the peptidoglycan.^{2,3} Bacterial cell wall synthesis is accomplished through a complex set of enzymatic reactions involving the above components and construction of the central building block of peptidoglycan synthesis, Lipid II (Figure 3-1).⁴ Specifically, UDP-GlcNAc is converted by MurA-F synthetases to UDP-MurNAc-pentapeptide on the cytosolic front, which is then conjugated to membrane-bound undecaprenyl phosphate, generating the intermediate Lipid I. The addition of GlcNAc to Lipid I produces Lipid II, which upon subjection to flippases is translocated to periplasmic side of the inner membrane and incorporated into the growing peptidoglycan chain.^{3,4}

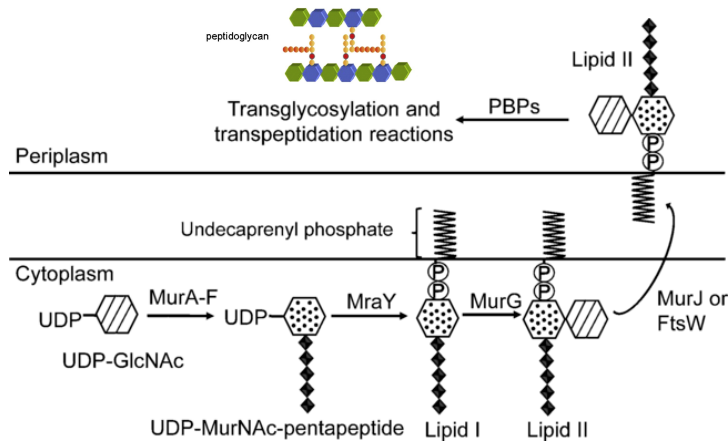


Figure 3-1 Illustration of peptidoglycan biosynthesis (adapted from references 3 & 4).

Cell wall biosynthesis is the target of a variety of antimicrobial agents. For example, β -lactam antibiotics disrupt peptidoglycan synthesis by covalently binding the penicillin-binding proteins (PBPs) involved in the final transpeptidation step.⁵ Lipid II itself is the target of multiple classes of antibiotics (Figure 3-2). Specifically, vancomycin inhibits peptidoglycan synthesis by binding to the D-Ala-D-Ala terminus of the Lipid II pentapeptide via an elaborate hydrogen bond network, preventing further cross-linking.^{4,6} Inspired by these antibiotics, we hypothesized that we could use an APBA-presenting phage display library to target the Lipid II pentapeptide, which displays a lysine residue for iminoboronate conjugation, in an effort to discover peptide binders of bacteria or peptide antibiotics.

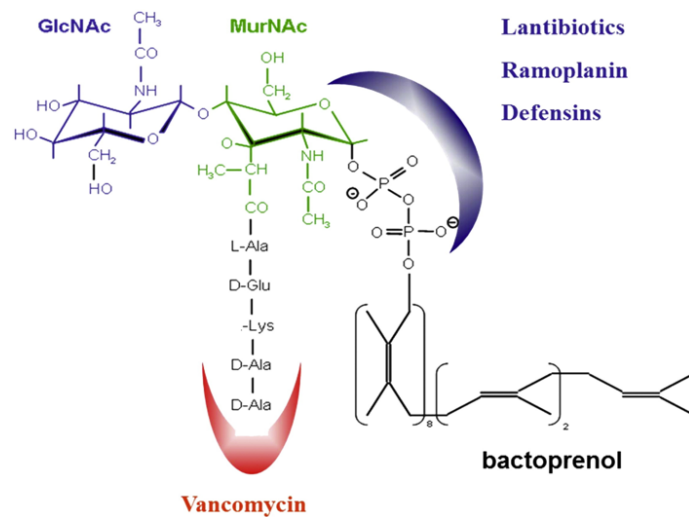


Figure 3-2 Illustration of Lipid II structure and known antibiotic binding sites (from reference 4).

3.1.2 Phage Display

Screening diverse peptide libraries presents a great opportunity for the discovery of potent and selective targeting motifs for a specific target. One such peptide screening strategy is phage display, in which a peptide scaffold of interest is fused to a bacteriophage coat protein, a technique first described by George P. Smith in 1985.⁷ Phage display has been used extensively for various applications including epitope mapping, studying protein-protein interactions and discovering a multitude of peptide ligands for novel targets.^{8,9}

Until recently, phage display technology had been limited to presenting peptides only composed of natural, proteinogenic amino acids. Due to technological advances in the field, phage display libraries can now be chemically and genetically modified to present unnatural entities, which greatly expands the chemical space of phage-displayed molecules (Figure 3-3).¹⁰⁻¹² Early work aimed at modifying the carboxylates of glutamate

or aspartate, the amines of lysines, and the phenol functionalities of tyrosines; however, the lack of site-specificity lead to compromised phage infectivity.¹¹ In addition to chemical modification of natural amino acids, Schultz and co-workers were able to incorporate unnatural amino acids, such as p-azidophenylalanine via amber codon suppression to provide reactive sites on the phage coat proteins.¹³ Other groups have taken advantage of strategically placed natural amino acids to allow for site-selective chemical modifications. For example, the Heinis group strategically engineered three cysteine residues within a phage coat protein, allowing for selective cysteine alkylation to create bicyclic peptide libraries on phage.¹⁴ Similarly, a glycopeptide library was developed by Derda and co-workers through oxidative cleavage of an N-terminal serine or threonine that yields a bioorthogonal aldehyde handle for conjugation to carbohydrates.¹⁵ Further expanding the chemical space of phage display, our group developed a novel phage library that incorporates a pair of 2-APBA moieties, an APBA-dimer library, to screen against the Lipid II pentapeptide.

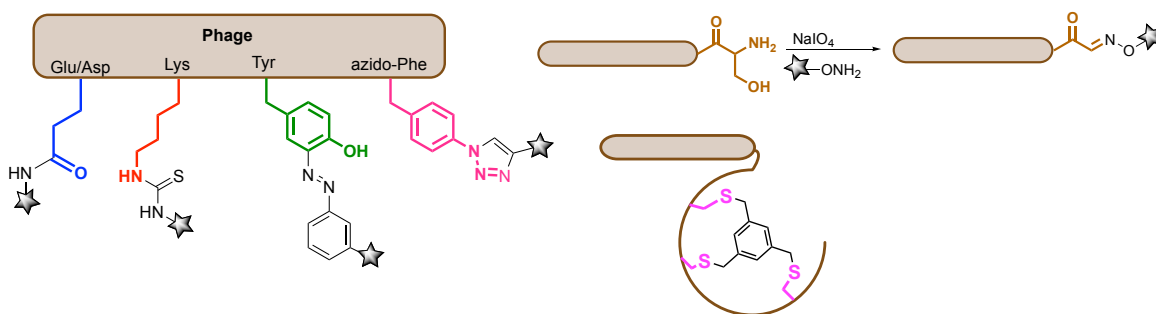


Figure 3-3 Previously reported examples of chemical modifications to phage libraries.

3.2 APBA Dimer Library Construction and Validation

A collaboration with Michael Kelly was established for the construction and validation of the APBA-dimer library.

3.2.1 Synthesis of APBA-IA and Library Modification

The phage library chosen for modification was the commercially available Ph.D.[™]-C7C library, which displays disulfide-cyclized peptides with seven randomized residues that are fused to the pIII minor coat protein of the M13 phage. The library was modified with APBA moieties via disulfide reduction and selective cysteine alkylation originally described by Derda and co-workers.¹⁶ Briefly, the disulfide bond of the C7C peptides was selectively reduced on phage with immobilized TCEP (iTCEP) for 48 hr at 4 °C. The reduced cysteines were then alkylated with an APBA derivative, namely APBA-IA, for 2 hr to yield the APBA-dimer library (Figure 3-4).¹⁷ Briefly, APBA-IA was synthesized from 2',4'-dihydroxyacetophenone as the starting material, first subjected to regioselective alkylation of the 4'-hydroxyl to install an amine functionality followed by triflation of the 2'-hydroxyl. The compound was then subjected to Miyaura borylation, addition of the iodoacetamide to the amine, and deprotection (Scheme 3-1).

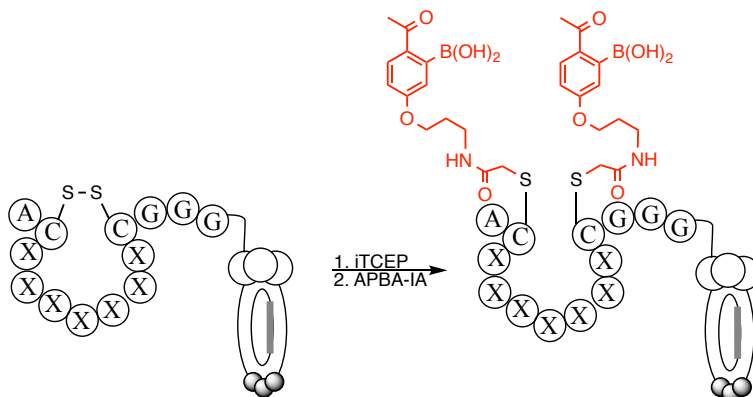
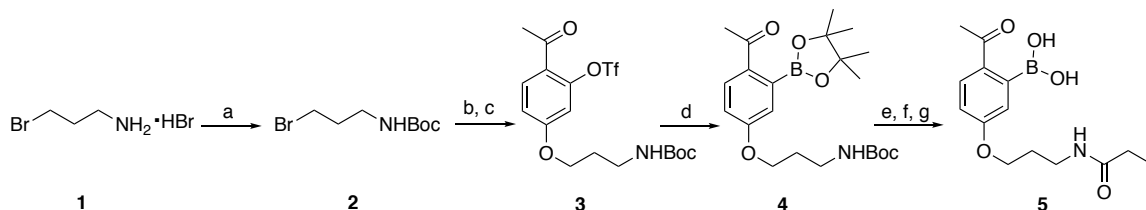


Figure 3-4 Illustration of the cysteine labeling strategy to display 2-APBA on phage.

Scheme 3-1 Synthesis of APBA-IA (5).



(a) Boc anhydride, K_2CO_3 , THF/ H_2O ; 90% yield. (b) 2',4'-dihydroxyacetophenone, acetone, K_2CO_3 . (c) $(CF_3SO_2)_2O$, DCM, Et_3N ; 78% over two steps. (d) B_2pin_2 , $Pd(dppf)Cl_2$, KOAc, dioxane; 85%. (e) 60% TFA in DCM. (f) Iodoacetyl chloride, K_2CO_3 , DCM/ H_2O . (g) 80% TFA in H_2O ; 35% over three steps.

3.2.2 Confirmation of APBA Modification of Phage

The extent of APBA-IA labeling was monitored via a pulse-chase assay in which biotin-iodoacetamide (Biotin-IA) treatment and streptavidin capture after APBA-IA labeling allowed quantification of phage that APBA-IA failed to label. The minimal streptavidin capture of the APBA-IA treated phage compared to Biotin-IA labeled phage indicates complete labeling of cysteines by APBA-IA (Figure 3-5a). Control phage, with no peptide insert, and reduced/untreated phage additionally yielded no capture. More direct evidence of APBA conjugation was established by Michael Kelly by treating the modified phage with a fluorophore labeled semicarbazide (Scz-FITC), which Dr. Anupam Bandyopadhyay and Samantha Cambray recently synthesized and reported to conjugate with APBA chemoselectively to form a stable diazaborine.¹⁸ The labeled phage was heat denatured and the coat proteins were subjected to fluorescence gel electrophoresis analysis. Reduced phage with and without Biotin-IA labeling were included as negative controls to confirm on the APBA-semicarbazide conjugation. For the APBA labeled phage, a single distinct band was observed that corresponds to the pIII protein (Figure 3-5b), which is known to run on sodium dodecyl sulfate-polyacrylamide gel electrophoresis

(SDS-PAGE) with an apparent molecular weight of 60–65 kDa, larger than its actual molecular weight of 43 kDa.¹⁹

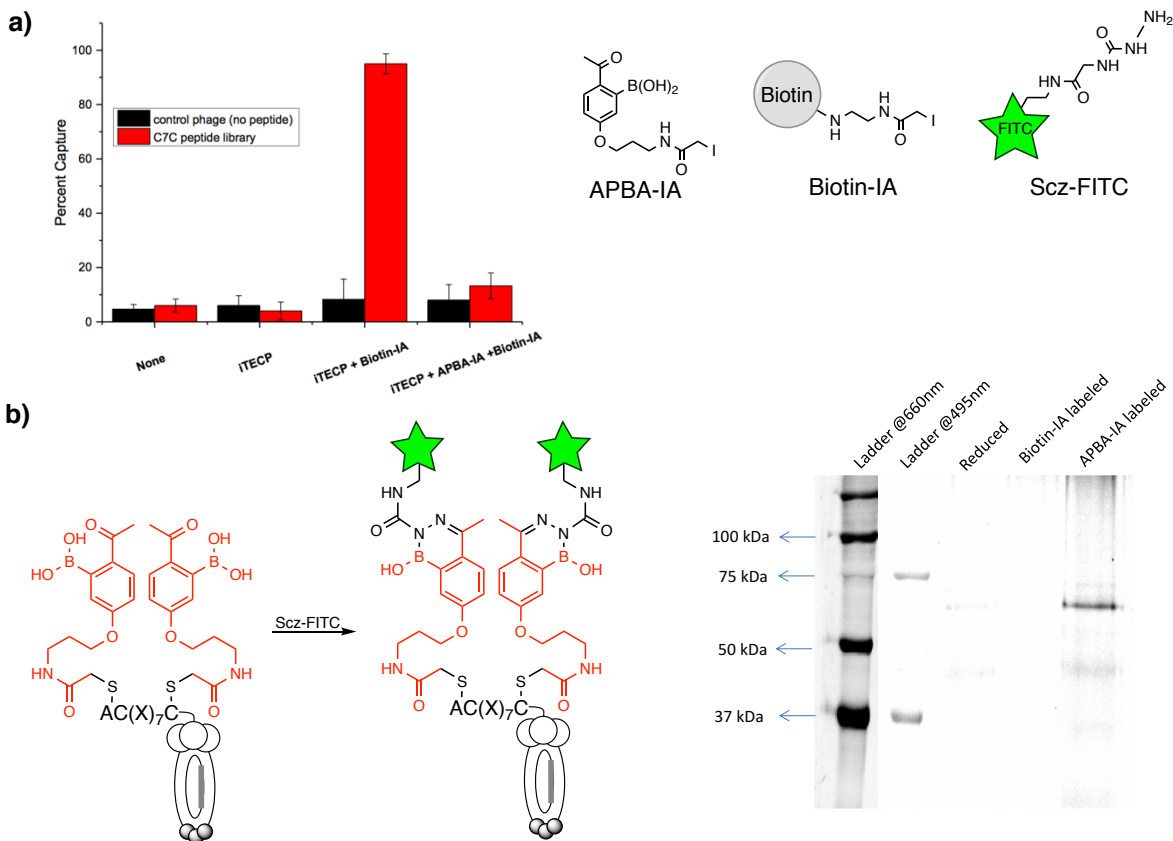


Figure 3-5 Confirmation of phage labeling with 2-APBA functionalities via (a) streptavidin pulse-chase assay and (b) fluorescent gel analysis by Michael Kelly.

3.3 Panning Against Lipid II Pentapeptide and Hit Validation

3.3.1 Synthesis of Biotin-Lipid II

To screen against Lipid II pentapeptide with the APBA-dimer library, target immobilization via streptavidin agarose resin was chosen as the panning strategy; therefore, Lipid II pentapeptide was synthesized with a biotin handle (Biotin-Lipid II, Figure 3-6). The pentapeptide was synthesized on a Wang Resin via SPPS followed by a hexanoic acid linker and conjugation of biotin.

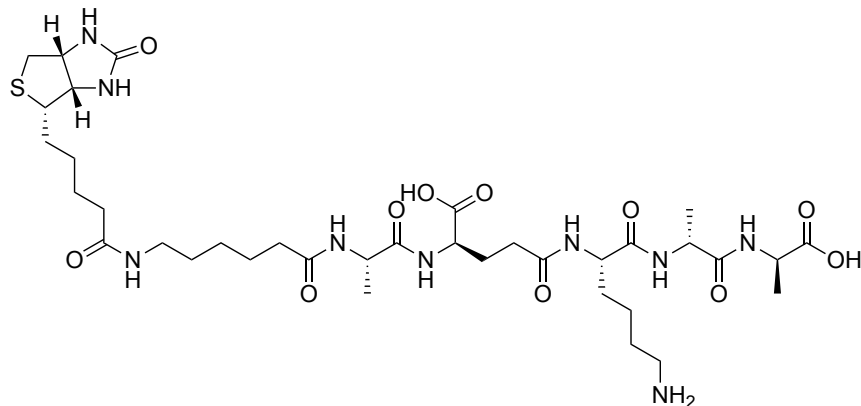


Figure 3-6 Structure of Biotin-Lipid II for phage panning.

3.3.2 Screening Protocol Against Lipid II Pentapeptide

Three rounds of affinity selection were initiated with an input population of $\sim 10^{10}$ plaque forming units (pfu) in each round along with extensive washing steps to eliminate non-binders. Biotin-Lipid II was immobilized on streptavidin agarose resin and the APBA-dimer library was subsequently incubated with the resin for 1 hr. After washing, the phage were eluted from the resin-immobilized target with acid treatment. The output population typically ranged from 10^3 to 10^6 pfu. The recovered phage were amplified, labeled with APBA-IA and subjected to the next round of panning (Figure 3-7). The pulse-chase assay described above was performed after subjection to APBA-IA to confirm library labeling for the next round. Starting in the second round of panning, a negative selection was introduced, which involved screening the library against biotin-bound streptavidin, in an effort to eliminate strong nonspecific streptavidin binders.

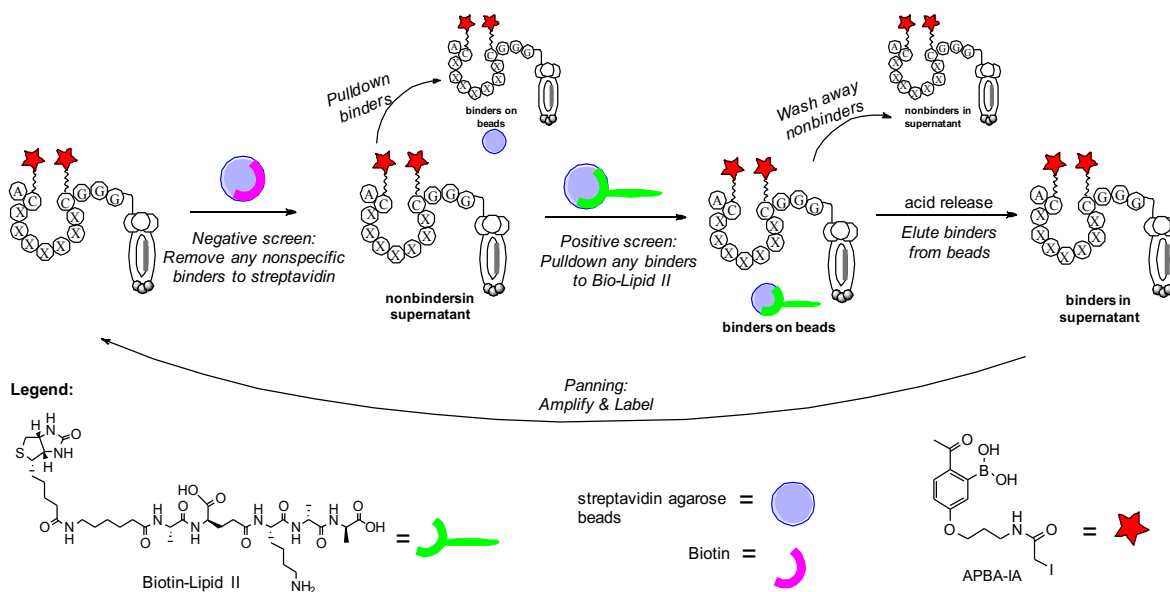


Figure 3-7 Illustration of panning protocol against Lipid II pentapeptide.

After three rounds of affinity selection, 60 colonies were randomly selected from the output population, the DNA was isolated and subjected to Sanger sequencing (Table 3-1a). Five colonies did not yield any peptide sequences and nineteen colonies yielded blank phage, with no C7C peptide insert. Three peptide sequences were observed repeatedly and chosen for analysis off phage (Table 3-1b). Synthesis was performed on a rink amide resin incorporating an orthogonally protected Dap residue on the C-terminus, which allowed for on-resin coupling of fluorescein as a fluorescent reporter. A triple glycine linker was installed between Dap and the core C7C peptide to minimize interference of the fluorophore. After peptide synthesis, the pair of cysteines was subsequently modified with APBA-IA.

Table 3-1 (a) Sequencing results from third round screen against Lipid II pentapeptide
(b) Sequence consensus observed and peptides synthesized.

C_m: APBA-IA modified Cys, Dap*: fluorescein-modified Dap residue.

a)

1. ACTLPQAPNC	21. blank	40. blank
2. blank	22. ACADPSSQTC	41. ACGPTAKYIC
3. ACNSHTQGKC	23. ACGPTAKYIC	42. blank
4. ACSGVQPFQC	24. blank	43. ACTTKLPNSC
5. AC SLNHTVNC	25. blank	44. ACLSNANSAC
6. ACNIKSSHVC	26. ACNIKSSHVC	45. ACSKMKIDHC
7. ACGPTAKYIC	27. ACGPTAKYIC	46. ACLPTKFRSC
8. blank	28. ACQSASPHTC	47. blank
9. ACTLGPAFSC	29. blank	48. ACPKGDENTC
10. blank	30. blank	49. blank
11. ACDRAQAKVC	31. ACSKMKIDHC	50. blank
12. ACNWMINKEC	32. ACDSKHVPFC	51. ACKNIVAPWC
13. ACNKFLASC	33. ACHASHAHVC	52. blank
14. blank	34. ACPDMCVSCC	53. ACNNHSRSTC
15. ACNVMSKRLC	35. ACGPTAKYIC	54. ACGPTAKYIC
16. blank	36. ACTPHMPAQC	55. ACSKMKIDHC
17. blank	37. ACSKMKIDHC	
18. ACNSHRHGAC	38. blank	
19. blank	39. ACHHKGFGVC	
20. ACDFKNRNTC		

b)

NAME	PEPTIDE SYNTHESIZED	RD. 3 FREQUENCY
KAM-GPT	AC _m GPTAKYIC _m GGGDap*	6
KAM-SKM	AC _m SKMKIDHC _m GGGDap*	4
KAM-NIK	AC _m NIKSSHVC _m GGGDap*	2

3.3.3 Characterization of Peptide Repeats

To assess binding of the peptide repeats to the Lipid II pentapeptide, fluorescence microscopy of the streptavidin agarose beads (45-165 μM) was investigated. Towards this end, Biotin-Lipid II or unconjugated biotin was immobilized on the streptavidin beads

followed by incubation with each peptide for 1 hr at 1000 nM and 100 nM. The beads were then directly subjected to fluorescence microscopy analysis to visualize fluorescent peptide binding (Figure 3-8). At 1000 nM, KAM-GPT showed potential of differentiation between Lipid II-bound streptavidin compared to just biotin-bound streptavidin, with slightly brighter beads. On the contrary, KAM-NIK yielded brighter staining of the biotin-bound beads compared to the Lipid II-bound beads. At 100 nM, conflicting results were observed. Particularly, KAM-SKM showed extremely bright staining of the Lipid II-bound streptavidin, which was not observed at the higher concentration. These data proved streptavidin bead fluorescence microscopy was not the most effective method for assessing Lipid II pentapeptide binding.

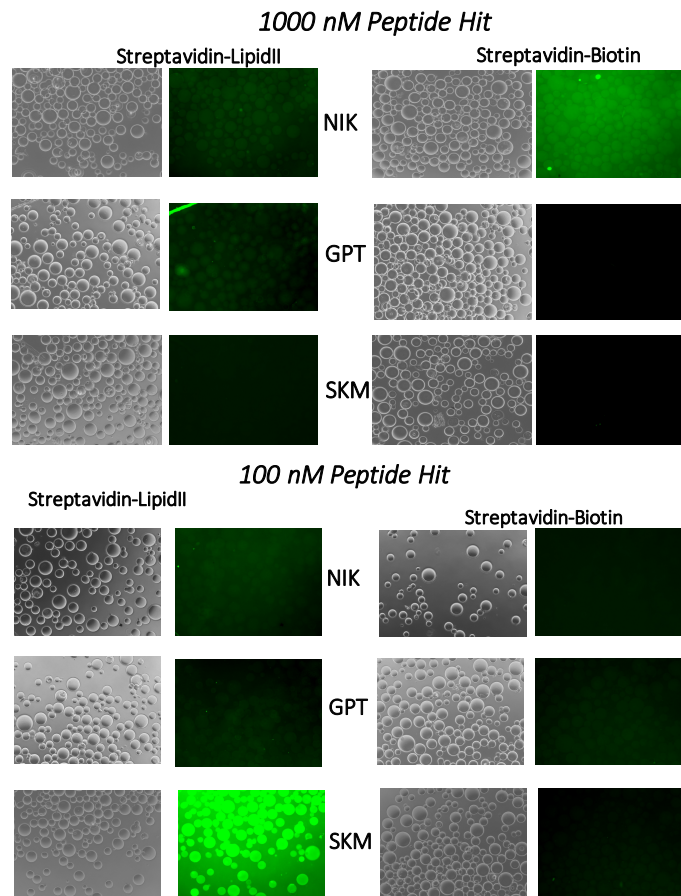


Figure 3-8 Fluorescence microscopy of Lipid II- and biotin-bound streptavidin binding.

Due to conflicting results with fluorescence microscopy, fluorescence polarization was utilized to assess the binding of the peptides to Lipid II pentapeptide. The anisotropy increase to NeutrAvidin-bound Biotin-Lipid II elicited by each peptide was calculated (Figure 3-9). NeutrAvidin is an economical, de-glycosylated surrogate of streptavidin. As a control, the binding capability of each peptide to biotin-bound NeutrAvidin was also assessed. Inopportunately, the binding of each peptide to the Lipid II pentapeptide compared to biotin alone showed very little discrepancies in anisotropy response. Lipid-II pentapeptide binders would show a significant anisotropy increase with the Biotin-Lipid II-bound NeutrAvidin compared to the biotin-bound protein.

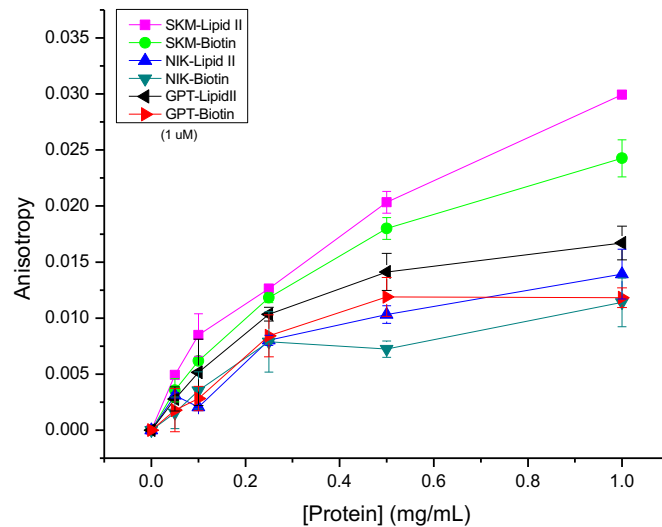


Figure 3-9 Fluorescence anisotropy of Biotin-Lipid II and biotin binding.

In final efforts to elucidate the binding capability of these peptides, cell-based assays were assessed. First, if these peptides were to bind Lipid II, they could potentially cause cell death, as vancomycin does. Therefore, the MIC was calculated for each peptide against *S. aureus* via a microdilution growth inhibition assay (Figure 3-10a). Compared to

a positive control of wild-type gramicidin (gA-WT), the three peptides did not elicit any *S. aureus* cell death with up to 25 μM peptide. To determine if these peptides were even binding to *S. aureus* cells, flow cytometry was utilized (Figure 3-10b). Compared to KAM-di, the APBA dimer peptide separated by a triple glycine linker described in Chapter 2, the peptides elicited little to no bacterial staining, although they also incorporate a pair of APBA warheads.

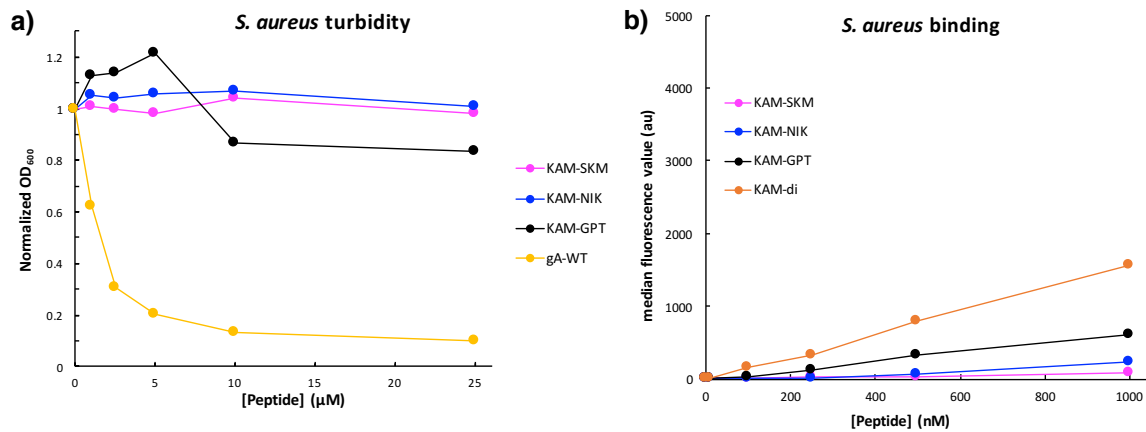


Figure 3-10 (a) MIC assay of Lipid II peptide repeats against *S. aureus* (b) Flow cytometry assessment of *S. aureus* binding by Lipid II peptide repeats.

3.4 Conclusions

Although the APBA-dimer library was successfully generated and APBA modification was confirmed, peptide binders to the Lipid II pentapeptide were not discovered from screening the novel library. The inconsistent results from fluorescence microscopy and lack of differentiation of anisotropy increase between Biotin-Lipid II-bound protein and biotin-bound protein suggest that these peptides may simply bind streptavidin, although a negative screen was introduced to avoid such a problem. The lack of *S. aureus* killing or binding by these peptides further confirms the lack of Lipid-II pentapeptide binding. In retrospect, perhaps the target is simply too small. A short C7C

peptide does not have much opportunity to bind a short pentapeptide sequence, which may not be properly exposed on the streptavidin resin. A solution to this setback is described in the following chapter, where screening against the whole cell, instead of a specific target, yielded potent peptide binders.

3.5 Experimental Procedures

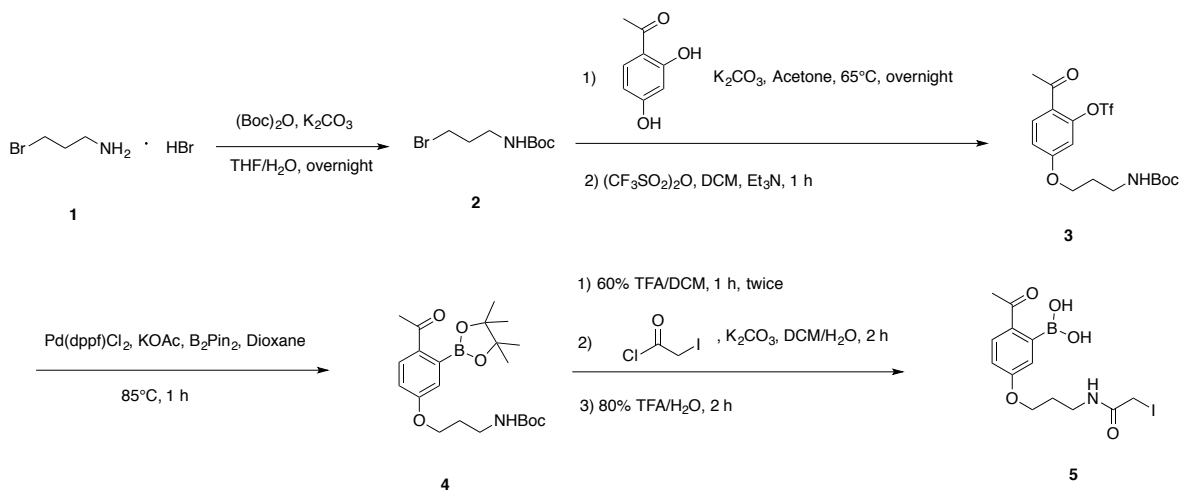
3.5.1 General Methods

The Ph.D.[™]-C7C Phage Display Peptide Library Kit and the *E. coli* K12 ER2738 strain were purchased from New England Biolabs (NEB). All ER2738 strains were grown with 20 µg/mL tetracycline. Chemical reagents for small molecule, library modification and confirmation, and peptide synthesis were purchased from various vendors and used as received. *S. aureus* (ATCC 6538) was purchased as a lyophilized pellet from Microbiologics (Cloud, MN). All titering experiments were plated on Isopropyl β-D-1-thiogalactopyranoside (IPTG)/5-bromo-4-chloro-3-indolyl-β-D-galactopyranoside (Xgal)-containing agar. NMR data were collected on a VNMR 500 MHz NMR spectrometer. Mass spectrometry data were generated by using an Agilent 6230 LC TOF mass spectrometer. Peptide synthesis was carried out on a Tribute peptide synthesizer from Protein Technologies and purified via RP-HPLC on a Waters Prep LC with a Jupiter C18 column (Phenomenex) with acetonitrile/water (0.1% TFA) eluent. The peptide concentration of all samples used in these studies were determined by measuring their absorbance at 495 nm ($\epsilon = 75,000 \text{ M}^{-1} \text{ cm}^{-1}$ for fluorescein) on a Nanodrop 2000c UV/VIS spectrometer. The fluorescence anisotropy experiments and MIC assays were analyzed on a SpectraMax M5 plate reader. Fluorescence images were taken on a Zeiss Axio Observer A1 inverted microscope. Flow

cytometry analysis was carried out on a BD FACSria cell sorter housed in the Biology Department at Boston College.

3.5.2 Synthesis of APBA-IA

Synthetic scheme for APBA-IA (5).



Synthesis of Compound 2. 3-Bromopropylamine hydrobromide (7.00 g, 32.0 mmol) was dissolved in 10% Na_2CO_3 (60 mL) solution and placed on ice for 5 min, to which Boc-anhydride (6.50 g, 29.8 mmol in 60 mL THF) was added. The reaction was kept at room temperature overnight. THF in the reaction mixture was then evaporated. The residual solution was acidified to $\text{pH} \sim 3$ by 1 N HCl and the product was extracted with ethyl acetate (3×150 mL). The combined organic layer was washed with brine (200 mL) and dried over Na_2SO_4 . Solvent removal yielded a white solid (6.40 g, 90% yield). ^1H NMR (CDCl_3) δ 4.79 (br, 1H), 3.40 (t, $J = 6.5$ Hz, 2H), 3.22 (q, $J = 6.4$ Hz, 2H), 2.01 (m, $J = 6.6$ Hz, 2H), 1.39 (s, 9H). ^{13}C NMR (CDCl_3) δ 155.95, 79.29, 38.96, 32.70, 30.74, 28.34. MS-ESI $^+$: m/z calculated for $\text{C}_4\text{H}_9\text{BrNO}_2$ [$\text{M}-t\text{Bu}+\text{H}$] $^+$ 181.9817, found 181.9795.

Synthesis of Compound 3. Compound 2 (3.00 g, 12.6 mmol) and 2,4-dihydroxyacetophenone (2.13 g, 14.0 mmol) were dissolved in acetone (30 mL). K_2CO_3 (7.74 g, 56.0 mmol) was added and the reaction was allowed to reflux at 65 °C overnight. Acetone was evaporated and the residue was dissolved in water (100 mL). The product was extracted with ethyl acetate (3 × 100 mL). The combined organic layer was washed with brine (200 mL) and dried over Na_2SO_4 . Solvent removal yielded an off-white solid (3.78 g). 2.00 g of the crude product was directly dissolved in anhydrous DCM (40 mL). Et_3N (2.17 g, 21.5 mmol) was added to the solution and the mixture was kept at -78 °C for 5 min. $(CF_3SO_2)_2O$ (3.52 g, 12.4 mmol) was added slowly over 5 min. The reaction was warmed up to room temperature and allowed to stir for 1 hr. The reaction was quenched with saturated Na_2CO_3 (40 mL), stirred for 5 min and the product was subsequently extracted with DCM (3 × 100 mL). The combined organic layer was washed with brine (100 mL) and dried over Na_2SO_4 . The solvent was removed and the product was purified via silica gel column chromatography using hexane/ethyl acetate (4:1) to give the desired product as a light orange solid (2.29 g, 78% yield over two steps). 1H NMR ($CDCl_3$) δ 7.82 (d, J = 8.7 Hz, 1H), 6.96 – 6.91 (dd, 1H), 6.80 (d, J = 2.4 Hz, 1H), 4.71 (br, 1H), 4.08 (t, J = 6.1 Hz, 2H), 3.32 (q, J = 6.5 Hz, 2H), 2.58 (s, 3H), 2.01 (m, J = 6.3 Hz, 2H), 1.43 (s, 9H). ^{13}C NMR ($CDCl_3$) δ 195.12, 162.98, 156.13, 148.62, 132.86, 124.24, 119.82, 117.69, 113.82, 109.46, 79.60, 66.79, 37.68, 29.60, 29.26, 28.50. MS-ESI⁺: m/z calculated for $C_{13}H_{15}F_3NO_7S$ [M - tBu +H]⁺ 386.0521, found 386.0494.

Synthesis of Compound 4. Compound 3 (1.00 g, 2.27 mmol), B_2pin_2 (1.40 g, 5.51 mmol), $Pd(dppf)Cl_2$ (0.20 g, 0.27 mmol) and KOAc (0.8 g, 8.16 mmol) were dissolved in anhydrous

dioxane (20 mL), to which ~100 mg of 3 Å molecular sieves were added. The reaction was bubbled with argon for 15 min and allowed to stir for 1 hr at 85 °C. The reaction was cooled to room temperature and water (50 mL) was added. The product was extracted with ethyl acetate (3 × 100 mL). The combined organic layer was washed with brine (100 mL) and dried over Na₂SO₄. The solvent was removed and the product was purified via silica gel column chromatography using hexane/ethyl acetate (7:3) to give the desired product as a light yellow viscous liquid (0.81 g, 85% yield). ¹H NMR (CDCl₃) δ 7.69 (d, *J* = 8.6 Hz, 1H), 6.88 (d, *J* = 2.5 Hz, 1H), 6.77 (dd, *J* = 8.6, 2.6 Hz, 1H), 4.91 (br, 1H), 3.98 (t, *J* = 6.1 Hz, 2H), 3.21 (q, *J* = 6.5 Hz, 2H), 2.46 (s, 3H), 1.89 (m, *J* = 6.9 Hz, 2H), 1.36 (d, *J* = 1.6 Hz, 21H). ¹³C NMR (CDCl₃) δ 198.26, 162.41, 155.99, 133.47, 130.68, 117.92, 113.83, 83.49, 83.48, 79.03, 65.80, 37.64, 29.39, 28.33, 24.86. MS-ESI⁺: *m/z* calculated for C₁₆H₂₃BNO₅ [M-Pin-H₂O+H]⁺ 320.1669, found 320.1857.

Synthesis of Compound 5. Compound 4 (250 mg, 0.60 mmol) was dissolved in DCM (2 mL) and TFA (3 mL). The reaction was stirred at room temperature for 1 hr. TFA and DCM were removed and the residue was treated with 60% TFA/DCM (5 mL) for another hour. After solvent removal, K₂CO₃ (500 mg, 2.89 mmol) was added to the residue. The mixture was dissolved in DCM/H₂O (2:1, 6 mL) and kept on ice for 20 min. Iodoacetyl chloride (533 mg, 2.62 mmol) was added slowly over 5 min to the reaction. The mixture was allowed to stir at room temperature for 2 hr. The solution was acidified to pH 3 by 1 N HCl and the product was extracted with DCM (3 x 100 mL). The combined organic layer was washed with brine (100 mL) and dried over Na₂SO₄. DCM was removed and the residue was treated with TFA/H₂O for 2 hr. After solvent removal, the crude material was re-dissolved

in 10 mL acetonitrile/H₂O (2:3) solution and purified via RP-HPLC yielding a white solid after lyophilization (85 mg, 35% yield over three steps). ¹H NMR (Methanol-*d*₄) δ 7.99 (d, *J* = 8.6 Hz, 1H), 7.00 (dd, *J* = 8.6, 2.6 Hz, 1H), 6.94 (d, *J* = 2.5 Hz, 1H), 4.14 (t, *J* = 6.2 Hz, 2H), 3.68 (s, 2H), 3.38 (t, *J* = 6.7 Hz, 2H), 2.59 (s, 3H), 2.01 (m, *J* = 6.5 Hz, 2H). ¹³C NMR (Methanol-*d*₄) δ 200.46, 170.09, 163.52, 132.59, 131.19, 116.14, 113.61, 65.37, 36.38, 28.33, 22.81, -3.50. MS-ESI⁺: *m/z* calculated for C₁₃H₁₆BINO₄ [M-H₂O+H]⁺ 388.0217, found 388.0473.

3.5.3 Modification of C7C Library

The Ph.D.TM-C7C Phage Display Peptide Library (5 μL, ~1x10¹³ pfu/mL) was subjected to reduction in the presence of iTCEP (25 μL), in a total volume of 200 μL in tris-buffered saline (TBS, pH 8.5) for 48 hr at 4 °C. APBA-IA (2 mM, 2 μL from a 200 mM dimethylsulfoxide (DMSO) stock) was added to the reduced phage and allowed to conjugate for 2 hr at room temperature. The labeled phage was removed from iTCEP and precipitated to remove excess labeling reagent with 1/6 volume 20% (w/v) polyethylene glycol (PEG)-8000, 2.5 M sodium chloride (NaCl) for 5 hr at 4 °C. Precipitated phage was re-dissolved in PBS (pH 7.4, 100 μL) and the phage titer was calculated according to the M13 Titer Protocol provided by NEB.

3.5.4 Streptavidin Capture Assay

For confirmation of APBA-IA labeling on phage, streptavidin agarose resin (25 μL/sample) was washed with PBS (pH 7.4) and blocked with 10 mg/mL BSA via incubation for 1 hr. APBA-IA labeled library was subjected to subsequent labeling with Biotin-IA (2 mM) for 2 hr followed by dilution to minimize small molecule concentration. Biotin-IA labeled and

APBA-IA/Biotin-IA labeled phage (200 μ L, $\sim 1 \times 10^{10}$ pfu/mL) were subjected to the streptavidin resin for 1 hr. Non-reduced and reduced phage, without small molecule labeling, were also analyzed. Unbound phage was removed from resin and the phage titer was calculated. The titer was compared to that of phage not subjected to streptavidin to generate a percent capture. The average percent capture and standard deviation of three trials was plotted. Wild-type phage, with no library insert, was subjected to the same analysis for comparison.

3.5.5 Synthesis of Biotin-Lipid II Pentapeptide

The synthesis, on a 0.1 mmol scale, was accomplished by first attaching D-Ala to Wang resin using a symmetrical anhydride and a catalytic amount of 4-dimethylaminopyridine (DMAP). Fmoc-D-Ala-OH (10 equivalents) was dissolved in minimal DMF (500 μ L) and anhydrous DCM (5 mL). N,N'-diisopropylcarbodiimide (DIC, 5 equivalents) was added and the reaction was allowed to stir on ice for 20 min under argon. DCM was evaporated, the activated anhydride was dissolved in DMF (2 mL), added to Wang resin (swelled in DMF) with DMAP (0.1 equivalent) and stirred for 1 hr. The Fmoc-loading capacity was calculated to be 0.35 mmol/g using 2% 1,8-diazabicyclo[5.4.0]undec-7-ene (DBU) in DCM and measuring the optical density at 304 nm. Upon attachment of the first D-Ala to the Wang resin, the remainder of the peptide (D-Ala, L-Lys, D- γ -Glu and L-Ala) was attached via Fmoc-based SPPS with 5 equivalents of each amino acid and equal equivalents of HBTU. A 6-aminohexanoic acid (3 equivalents activated with HBTU) was attached as a linker and biotin (3 equivalents activated with HBTU) was subsequently reacted on resin. The peptide was cleaved off resin and globally deprotected with Reagent B (88% TFA, 5%

water, 2% triisopropylsilane, 5% phenol). Crude peptide was obtained through ether precipitation and purified by RP-HPLC.

3.5.6 Panning Against Lipid II Pentapeptide

Streptavidin agarose resin (binding capacity: 20 µg/mL, 50 µL) was washed with 0.1% Tween in TBS (TBST) and incubated in 1 mL blocking buffer (0.1 M NaHCO₃ (pH 8.6), 5 mg/mL BSA) for 1 hr at 4 °C. The blocked resin was subsequently washed with TBST (4x). Excess Biotin-Lipid II (5 µg) was added to streptavidin resin in TBST (200 µL) and allowed to incubate for 30 min. The Biotin-Lipid II bound resin was washed with TBST (2x) to eliminate excess unbound pentapeptide. The APBA-labeled phage library (~1x10¹⁰ pfu) was added to the resin with 1 mg/mL in TBST (200 µL total volume) and incubated for 30 min. The resin was washed with TBST (5x) to remove unbound phage. Resin-bound phage were incubated with 200 µL elution buffer (Glycine-HCl, pH 2.2, 1 mg/mL) for 15 min followed by centrifugation. The supernatant was removed and neutralized with 150 µL Tris-HCl (pH 9.1). The eluted bound phage solution was added to early-log phase ER2738 and amplified for 4.5 hr followed by precipitation to isolate the amplified phage. The amplified phage were labeled with APBA-IA and subjected to the next round of panning. A negative screen was performed in the second and third rounds of panning in which the phage library was incubated with Biotin-bound streptavidin beads for 1 hr, the supernatant was removed and subsequently subjected to the positive screen against Biotin Lipid II-bound beads. The phage titer was calculated before and after each round of panning to determine the input and output population. Individual phage colonies from

each round of panning were amplified in ER2738. Phage DNA was isolated using a Qiagen miniprep kit and sent for sequencing analysis by Eton Bioscience, Inc.

3.5.7 Synthesis of Peptide Repeats

SPPS was performed on a Rink Amide MBHA solid support using Fmoc/*t*Bu chemistry on a 0.05 mmol scale. Five equivalents of commercially available amino acids were used for the coupling reaction with HBTU as an activating reagent. An Alloc-protected Dap residue was installed at the C-terminus for on-resin coupling of a fluorophore, followed by a triple glycine linker and the peptide hit sequence at the N-terminus. 5(6)-carboxyfluorescein (FAM) was conjugated to the peptide on resin by first removing the Alloc protecting group, as described in chapter 2, followed by subsequent HBTU-mediated amide bond coupling in 0.4 M NMM/DMF. The peptides were cleaved off resin and globally deprotected with Reagent B. Crude peptides were obtained via ether precipitation and purified by RP-HPLC. For cysteine alkylation, each peptide hit was treated with 3 equivalents of APBA-IA in the presence of TCEP (2 equivalents) in 2 M NMM/DMF for 3 hr and purified via RP-HPLC. All peptides were characterized via LC-MS for excellent purity (>95%) and correct masses (Table 3-2).

Table 3-2 MS data of Lipid II Pentapeptide Screen Hits.

Peptide	Calculated m/z	Observed m/z
KAM-GPT	1089.49 [M-H ₂ O+2H] ²⁺	1089.43
KAM-SKM	1135.06 [M-2H ₂ O+2H] ²⁺	1134.97
KAM-NIK	1115.99 [M-H ₂ O+H] ²⁺	1115.95

3.5.8 Fluorescence Microscopy Analysis of Lipid II-Bound Streptavidin Beads

Streptavidin agarose resin (40 μ L) was incubated with excess Biotin-Lipid II or excess biotin (1 μ g) for 1 hr in TBS and subsequently washed with TBS (2x) to remove excess reagent. Each peptide was incubated at 1000 nM and 100 nM (40 μ L total volume) for 1 hr. White light and fluorescent images were obtained on the Zeiss microscope equipped with filter set 44 (excitation: BP 475/40, emission: BP 530/50) suitable for detection of fluorescein fluorescence. Images were captured using the 10X objective with a 300 ms exposure time. All images were processed consistently using ImageJ software.

3.5.9 Fluorescence Anisotropy Analysis of Lipid II-Bound NeutrAvidin Protein

Biotin-Lipid II or biotin was bound to NeutrAvidin in a 4:1 ratio, the amount of biotin binding pockets per molecule of NeutrAvidin. Biotin-NeutrAvidin or Lipid II-NeutrAvidin was added at various concentrations to a Costar black/clear-bottom 96-well plate from a stock solution in PBS (pH 7.4). The FAM-labeled peptides (1 μ M) were added to the 96-well plate in triplicate. Endpoint fluorescence polarization readings were obtained hourly until they leveled off. Anisotropy generated saturation binding curves of peptides were plotted with Origin software.

3.5.10 Minimum Inhibitory Concentration Determination

MIC values for each peptide and positive control were determined using the broth microdilution method.²⁰ *S. aureus* was grown to an $OD_{600} \approx 0.6$ and diluted in LB media to a concentration of $\sim 5 \times 10^5$ cfu/mL. The cell suspension (200 μ L) was added to each well of a Costar 96-well plate. To each well, serial diluted (2-fold) peptides in DMSO (2 μ L) were added in triplicate. The plate was allowed to incubate at 37 $^{\circ}$ C while OD_{600} readings were

obtained every 20 min for 12 hr on the microtiter plate reader. The averaged OD₆₀₀ readings were plotted over time for each peptide. To generate MIC graphs, the OD₆₀₀ readings at the time point where an untreated sample began to level off were plotted versus concentration of peptide.

3.5.11 Flow Cytometry Analysis of S. aureus Binding

S. aureus was grown to an OD₆₀₀ ≈ 0.5, washed and diluted with PBS (pH 7.4). The cells (~1 × 10⁷ cfu/mL) were incubated with various concentrations of FAM-labeled peptide in PBS. After incubation for 1 hr, samples were subjected to cytometric analysis. Data obtained were analyzed via BD FACSDiva software and median fluorescent values were computed from the generated histograms. All flow cytometry experiments were repeated and generated consistent results.

3.6 References

1. Koch, A. L. Bacterial Wall as Target for Attack: Past, Present, and Future Research. *Clin. Microbiol. Rev.* **16**, 673–687 (2003).
2. Heijenoort, J. Van & Gutmann, L. Correlation between the structure of the bacterial peptidoglycan monomer unit, the specificity of transpeptidation, and susceptibility to β-lactams. *Proc. Natl. Acad. Sci.* **97**, 5028–5030 (2000).
3. Ng, V. & Chan, W. C. New Found Hope for Antibiotic Discovery: Lipid II Inhibitors. *Chem. Eur. J.* **22**, 12606–12616 (2016).
4. Münch, D. & Sahl, H. Structural variations of the cell wall precursor lipid II in Gram-positive bacteria — Impact on binding and efficacy of antimicrobial peptides. *Biochim. Biophys. Acta* **1848**, 3062–3071 (2015).
5. Fair, R. J. & Tor, Y. Antibiotics and Bacterial Resistance in the 21st Century. *Perspect. Medicin. Chem.* **6**, 25–64 (2014).

6. Breukink, E. & Kruijff, B. De. Lipid II as a target for antibiotics. *Nat. Rev. Drug Discov.* **5**, 321–323 (2006).
7. Smith, G. P. Filamentous Fusion Phage: Novel Expression Vectors That Display Cloned Antigens on the Virion Surface. *Science.* **228**, 1315–1317 (1985).
8. Hamzeh-mivehroud, M., Alizadeh, A. A., Morris, M. B., Church, W. B. & Dastmalchi, S. Phage display as a technology delivering on the promise of peptide drug discovery. *Drug Discov. Today* **18**, 1144–1157 (2013).
9. Wu, C. H., Liu, I. J., Lu, R. M. & Wu, H. C. Advancement and applications of peptide phage display technology in biomedical science. *J. Biomed. Sci.* **23**, (2016).
10. Ng, S., Jafari, M. R. & Derda, R. Bacteriophages and Viruses as a Support for Organic Synthesis and Combinatorial Chemistry. *ACS Chem. Biol.* **7**, 123–138 (2012).
11. Mohan, K. & Weiss, G. A. Chemically Modifying Viruses for Diverse Applications. *ACS Chem. Biol.* **11**, 1167–1179 (2016).
12. Day, J. W., Hyuk, C., Smider, V. V & Schultz, P. G. Identification of metal ion binding peptides containing unnatural amino acids by phage display. *Bioorg. Med. Chem. Lett.* **23**, 2598–2600 (2013).
13. Tian, F., Tsao, M. & Schultz, P. G. A Phage Display System with Unnatural Amino Acids. *J. Am. Chem. Soc.* **126**, 15962–15963 (2004).
14. Heinis, C., Rutherford, T., Freund, S. & Winter, G. Phage-encoded combinatorial chemical libraries based on bicyclic peptides. *Nat. Chem. Biol.* **5**, 502–507 (2009).
15. Ng, S., Jafari, M. R., Matochko, W. L. & Derda, R. Quantitative Synthesis of Genetically Encoded Glycopeptide Libraries Displayed on M13 Phage. *ACS Chem. Biol.* **7**, 1482–1487 (2012).
16. Jafari, M. R., Deng, L., Kitov, P. I., Ng, S., Matochko, W. L., Tjhung, K. F., Zebero, A., Elias, A. Klassen, J. S. & Derda, R. Discovery of Light-Responsive Ligands through Screening of a Light- Responsive Genetically Encoded Library. *ACS Chem. Biol.* **9**, 443–450 (2014).

17. McCarthy, K. A., Kelly, M. A., Li, K., Cambray, S., Hosseini, A. S., van Opijnen, T. & Gao, J. Phage Display of Dynamic Covalent Binding Motifs Enables Facile Development of Targeted Antibiotics. *J. Am. Chem. Soc.* **140**, 6137–6145 (2018).
18. Bandyopadhyay, A., Cambray, S. & Gao, J. Fast Diazaborine Formation of Semicarbazide Enables Facile Labeling of Bacterial Pathogens. *J. Am. Chem. Soc.* **139**, 871–878 (2017).
19. van Wezenbeek, P. M. G. F., Hulsebos, T. J. M. & Schoenmakers, J. G. G. Nucleotide sequence of the filamentous bacteriophage M13 DNA genome: comparison with phage fd. *Gene* **11**, 129–148 (1980).
20. Wiegand, I., Hilpert, K. & Hancock, R. E. W. Agar and broth dilution methods to determine the minimal inhibitory concentration (MIC) of antimicrobial substances. *Nat. Protoc.* **3**, 163–175 (2008).

CHAPTER 4

TARGETING LIVE BACTERIAL CELLS WITH APBA-MODIFIED PHAGE DISPLAY LIBRARY FOR DEVELOPMENT OF TARGETED ANTIBIOTICS

4.1 Introduction

4.1.1 Live Cell Panning

Panning phage libraries directly against live bacterial cells presents an intriguing alternative to panning against target biomolecules. Multiple bacterial strains have been pursued as whole-cell targets with phage display libraries resulting in peptide therapeutics for both diagnostic and antimicrobial purposes.¹ However, earlier efforts on this front have only yielded low affinity (sub to low millimolar) peptide probes.^{1,2} Although target elucidation is required to fully understand the binding mechanism of probes discovered via live cell panning, the entire cell can be pursued instead of a single, chosen target. We hypothesized that panning the APBA-dimer library directly against bacterial strains that are known to present amine surface modifications, such as *S. aureus* and mutant *A. baumannii* strains, would allow for the discovery of highly potent and selective peptide probes for the bacteria.

4.1.2 Amine Surface Modifications: A Mechanism of Resistance

As discussed in the introduction, bacteria exhibit numerous mechanisms to evade CAMPs, a key component of the host's innate immune system to combat pathogenic bacteria.³ In addition to proteolytic degradation or sequestration by secreted proteins, bacteria present many cell surface modification strategies to interfere with the activity of CAMPs.⁴ Due to the characteristic cationic nature of these peptides, the surface modifications typically introduce primary amines, creating electrostatic repulsion (Figure 4-1). Amino acid modification of phospholipids, such as Lys-PG synthesis in *S. aureus*, which presents a high abundance of both α - and ϵ -amines of lysine on

phosphatidylglycerol, have been reported as a resistance mechanism to CAMPs and neutrophil clearance.⁴⁻⁶ Lys-PG synthesis is one of the critical features of *S. aureus* that makes it a prevalent pathogen.⁵ Similarly, negatively charged teichoic acids, the most abundant component of a Gram-positive cell wall, are often alanylated on free hydroxyls, affording electrostatic repulsion of CAMPs.^{4,7} In Gram-negative bacteria, lipopolysaccharide (LPS) or lipooligosaccharide (LOS) is the most abundant component of the cell wall and often subjected to alteration with positive charge to evade CAMPs.⁴ For example, modification of the Lipid A portion of LPS with phosphoethanolamine or 4-aminoarabinose leads to polymyxin resistance for many bacterial species, including *A. baumannii*.⁸ *A. baumannii* has emerged as a major healthcare-associated pathogen, which can cause severe infections in the lungs and blood in which polymyxins are used as last-resort antibiotics for its treatment.⁹ In addition to LOS amine-modification, some polymyxin resistant strains completely shut down LOS biosynthesis, replacing the exterior leaflet of the outer membrane with amine-presenting lipoproteins.^{10,11} We hypothesized that the iminoboronate-capable APBA-dimer library could be utilized to discover potent peptide probes of these amine-presenting bacterial species, particularly those which display CAMP resistance.

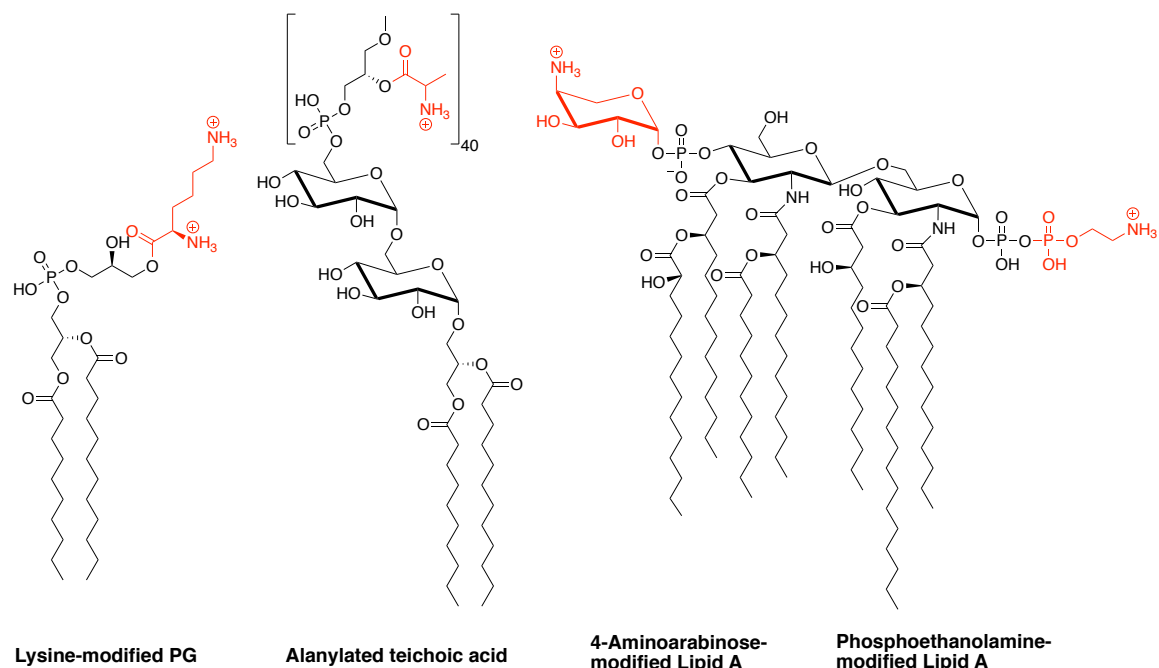


Figure 4-1 Illustration of targeted amine modifications on the bacterial cell surface.

4.2 Panning Against *S. aureus* with the APBA-Dimer Library

4.2.1 Screening Protocol Against *S. aureus*

The APBA-dimer library, discussed in Chapter 3, was screened against live *S. aureus* cells in an effort to discover peptide probes of *S. aureus*. To avoid interference of endogenous proteins, which can compete for iminoboronate formation, the APBA-dimer library was screened against *S. aureus* cells in a suspension containing 10 mg/mL BSA as an internal competitor (Figure 4-2). Three rounds of affinity selection were initiated with an input population of 10^{10} pfu in each round along with extensive washing steps to eliminate non-binders and strong albumin binders by centrifugation. Acid treatment, which is known to disrupt iminoboronate formation, was used to release bound phage

from *S. aureus*. The output population typically ranged from 10^3 to 10^5 pfu for *S. aureus* panning. The recovered phage were amplified, labeled with APBA-IA and subjected to the next round of panning.

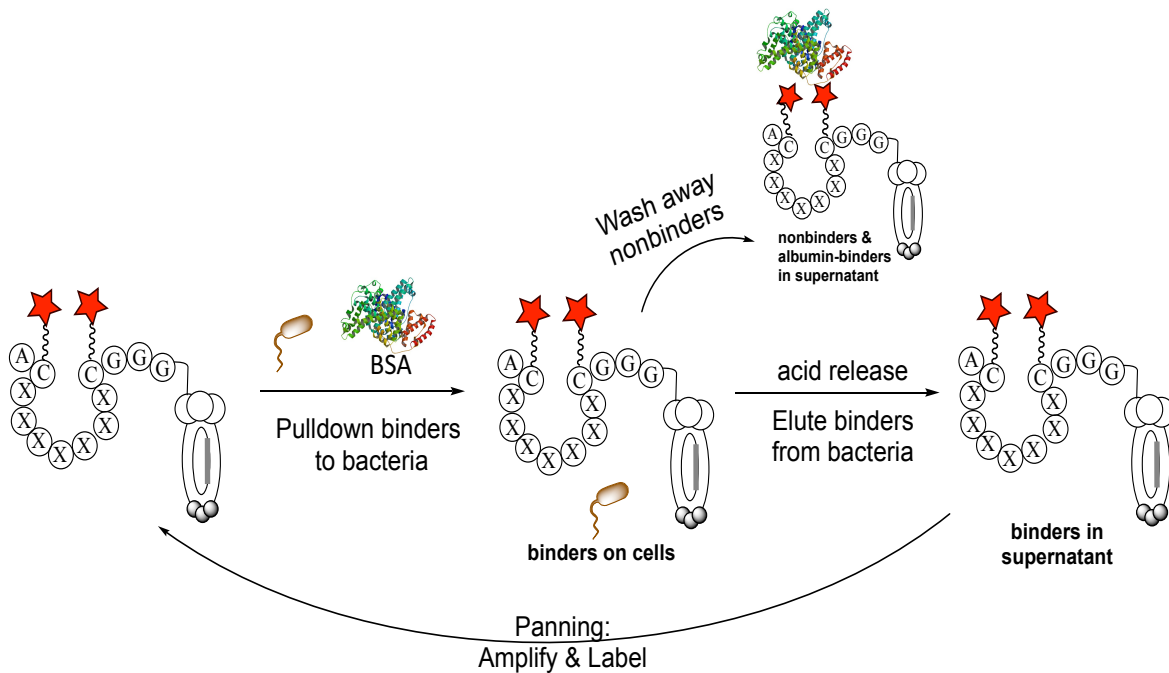


Figure 4-2 Illustration of live bacterial cell panning protocol. Stars represent APBA.

After each round of panning, 10–20 colonies were randomly selected from the output population and subjected to sequencing. Several peptide sequences were observed repeatedly in round 2 and round 3, even within this small set of colonies subjected for sequencing (Table 4-1).

Table 4-1 Sequences of the peptide hits for *S. aureus* binding (a) From round 2. (b) From round 3. (c) Recurring sequences and frequency.

a)

Hit #	DNA Sequence	Peptide Sequence
1	GCTTGTACGACTGCTGCGTCGCGTTTGTGC	ACTTAASRLC
2	GCTTGTCTGATGGTTTGAGTCCGCGTTGC	ACPDGLSPRC
3	GCTTGTCCGACGAGTAATAATCGGGAGTGC	ACPTSNNREC
4	GCTTGTAAATTTACTAAGACGTTTCGTTGC	ACNFTKFR
5	GCTTGTAAAGTGAGTAAGATGGAGCGTTGC	ACKVSKMERC
6	n/a	Blank
7	GCTTGTAAAGTTTGATTGACGAGGTATTGC	ACKFDSTRYC
8	GCTTGTCTTGAGCTTTTTCATTGTCGTCGTC	ACLELFHSSC
9	GCTTGTACGAATCCTGTGACTGCTCGGTGC	ACTNPVTARC
10	GCTTGTACGAATACGCTGCCTAAGCTGTGC	ACTNTPKLC
11	GCTTGTACGAGGGAGATGACGCATATGTGC	ACQREMTTHMC
12	GCTTGTATGAATCCGCGGGTAATTTGTGC	ACMNPGRNLC
13	GCTTGTATGTTCTATGTCGAGTATGTGC	ACYGSMSSMC
14	n/a	Blank
15	GCTTGTACGAGGGAGATGACGCATATGTGC	ACQREMTTHMC
16	GCTTGTACGACTGCTGCGTCGCGTTTGTGC	ACTTAASRLC
17	GCTTGTCTAGGGTTTCATTGTTGGGTTGC	ACARVHSLGC
18	GCTTGTAAATCCGACTTCGCTAATTCGTGC	ACNPTSLNSC
19	GCTTGTAGTACGAATAGTAATATTGTGTGC	ACSTNSNIVC
20	GCTTGTAACTCAGTCGAAGCATGAGTGC	ACNTQSKHEC

b)

Hit #	DNA Sequence	Peptide Sequence
1	GCTTGTACGACTGCTGCGTCGCGTTTGTGC	ACTTAASRLC
2	GCTTGTAAAGTGAGTAAGATGGAGCGTTGC	ACKVSKMERC
3	GCTTGTACGACTGCTGCGTCGCGTTTGTGC	ACTTAASRLC
4	GCTTGTAGTGAGGGTAGGGCTTATGCTTGC	ACSEGRAYAC
5	GCTTGTCAATGGTATTCTAGTAAGGCTTGC	ACHWYSSKAC
6	GCTTGTCAATGGTATTCTAGTAAGGCTTGC	ACHWYSSKAC
7	GCTTGTGTTTCTCCGAGGAGTCATGAGTGC	ACVSPRSHEC
8	GCTTGTACGAGGGAGATGACGCATATGTGC	ACQREMTTHMC
9	GCTTGTACGACTGCTGCGTCGCGTTTGTGC	ACTTAASRLC
10	GCTTGTACGACTGCTGCGTCGCGTTTGTGC	ACTTAASRLC
11	GCTTGTACGACTGCTGCGTCGCGTTTGTGC	ACTTAASRLC
12	GCTTGTATGTTCTATGTCGAGTATGTGC	ACYGSMSSMC
13	GCTTGTGTTTCTCCGAGGAGTCATGAGTGC	ACVSPRSHEC
14	GCTTGTGTTTCTCCGAGGAGTCATGAGTGC	ACVSPRSHEC
15	GCTTGTGTTTCTCCGAGGAGTCATGAGTGC	ACVSPRSHEC
16	GCTTGTAGTGAGGGTAGGGCTTATGCTTGC	ACSEGRAYAC
17	GCTTGTAAAGTATTCTATTCTAGTCTTGC	ACKYSHSSC
18	GCTTGTCAATGGTATTCTAGTAAGGCTTGC	ACHWYSSKAC
19	GCTTGTACGAAGTTGATGATGTTGGTGC	ACTKLMHWGC
20	GCTTGTAGTGAGGGTAGGGCTTATGCTTGC	ACSEGRAYAC

c)

Peptide Sequence	Round 2 Frequency	Round 3 Frequency
ACTTAASRLC	2	5
ACKVSKMERC	1	1
ACQREMTTHMC	2	1
ACYGSMSSMC	1	1
ACSEGRAYAC	0	3
ACHWYSSKAC	0	3
ACVSPRSHEC	0	4

To determine which sequences merited further pursuit, a phage-based microscopy experiment was performed. The individual phage hits were modified with APBA-IA, incubated with *S. aureus*, and subsequently treated with a FITC-labeled anti-M13 antibody, which binds to the pVIII protein of the M13 phage. The phage-bound *S. aureus* was imaged via fluorescence microscopy to determine which phage sequences elicited the most potent bacterial labeling (Figure 4-3). The phage-displayed peptide sequences that elicited the strongest fluorescence signal were pursued.

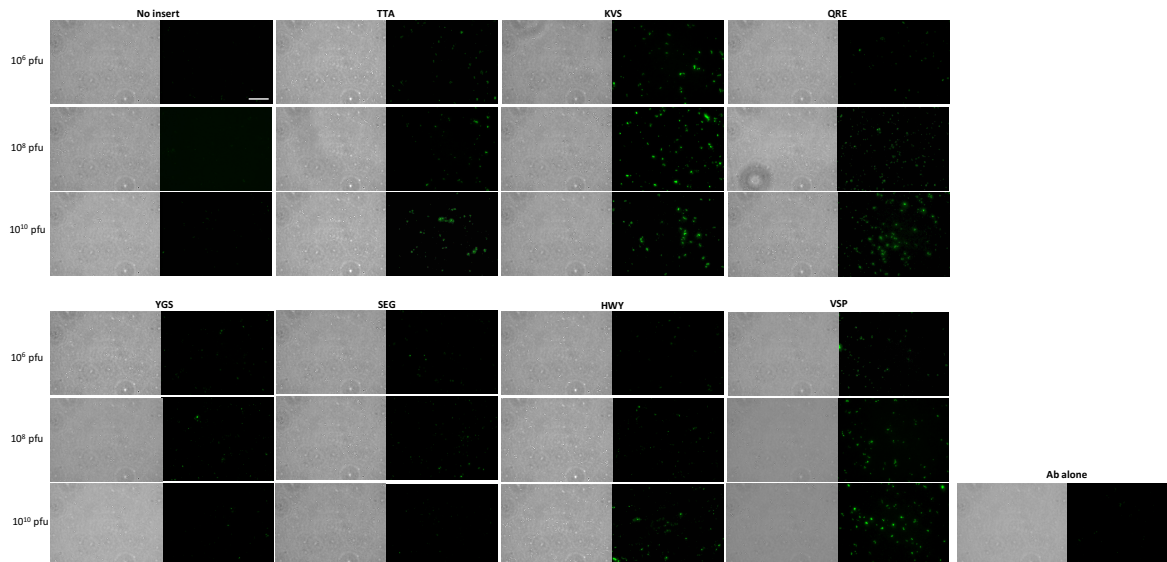


Figure 4-3 Fluorescence microscopy of phage binding *S. aureus* with FITC-anti-M13 antibody. Each phage variant is designated as the first three letters of the heptapeptide sequence. Scale bar: 10 μ m.

The phage-based microscopy experiment demonstrated that multiple peptides elicited strong binding to *S. aureus*. The five peptide hits that displayed the brightest images, given the names KAM1-KAM5, were selected and synthesized via SPPS (Table 4-2). Synthesis was performed on a rink amide resin incorporating an orthogonally protected Dap residue on the C-terminus, which allowed for on-resin coupling of fluorescein or rhodamine as a fluorescent reporter. A triple glycine linker was installed between Dap and the core C7C peptide to minimize interference of the fluorophore. After peptide synthesis, each cysteine was subsequently modified with APBA-IA.

Table 4-2 Synthesized peptide hits from *S. aureus* screening.
 C_m: APBA-IA modified Cys, Dap*: Fluorophore modified Dap residue.

NAME	PEPTIDE SYNTHESIZED
KAM1	AC _m TTAASRLC _m GGGDap*
KAM2	AC _m KVKMERC _m GGGDap*
KAM3	AC _m QRETHMC _m GGGDap*
KAM4	AC _m HWYSSKAC _m GGGDap*
KAM5	AC _m VSPRSHEC _m GGGDap*

4.2.2 Characterization of Binding to *S. aureus*

To assess *S. aureus* binding, flow cytometry was used to measure the median fluorescence intensity of the cells that each FAM-labeled peptide hit gave. All five peptide hits showed significant binding to *S. aureus* cells at submicromolar concentrations (Figure 4-4). Interestingly, all peptides except KAM2 afforded even stronger fluorescence staining of the bacteria in the presence of 1 mg/mL BSA than otherwise. KAM3 and KAM5, the most promising binders, were further analyzed via flow cytometry up to 10 μ M (Figure 4-5). Analysis of the bacterial binding curve of KAM5 gave an estimated EC₅₀ of \sim 1.5 μ M for staining *S. aureus* cells. The bacterial binding potency displayed by KAM5 is orders of magnitude better than the peptides borne out of previous phage display efforts with natural peptide libraries, which only yielded sub to low mM binders.^{1,2} The *S. aureus* binding potency of KAM5 is also much greater than that of Hlys-AB1, a previously reported¹² rationally designed peptide that incorporates a single APBA motif (Figure 4-6).

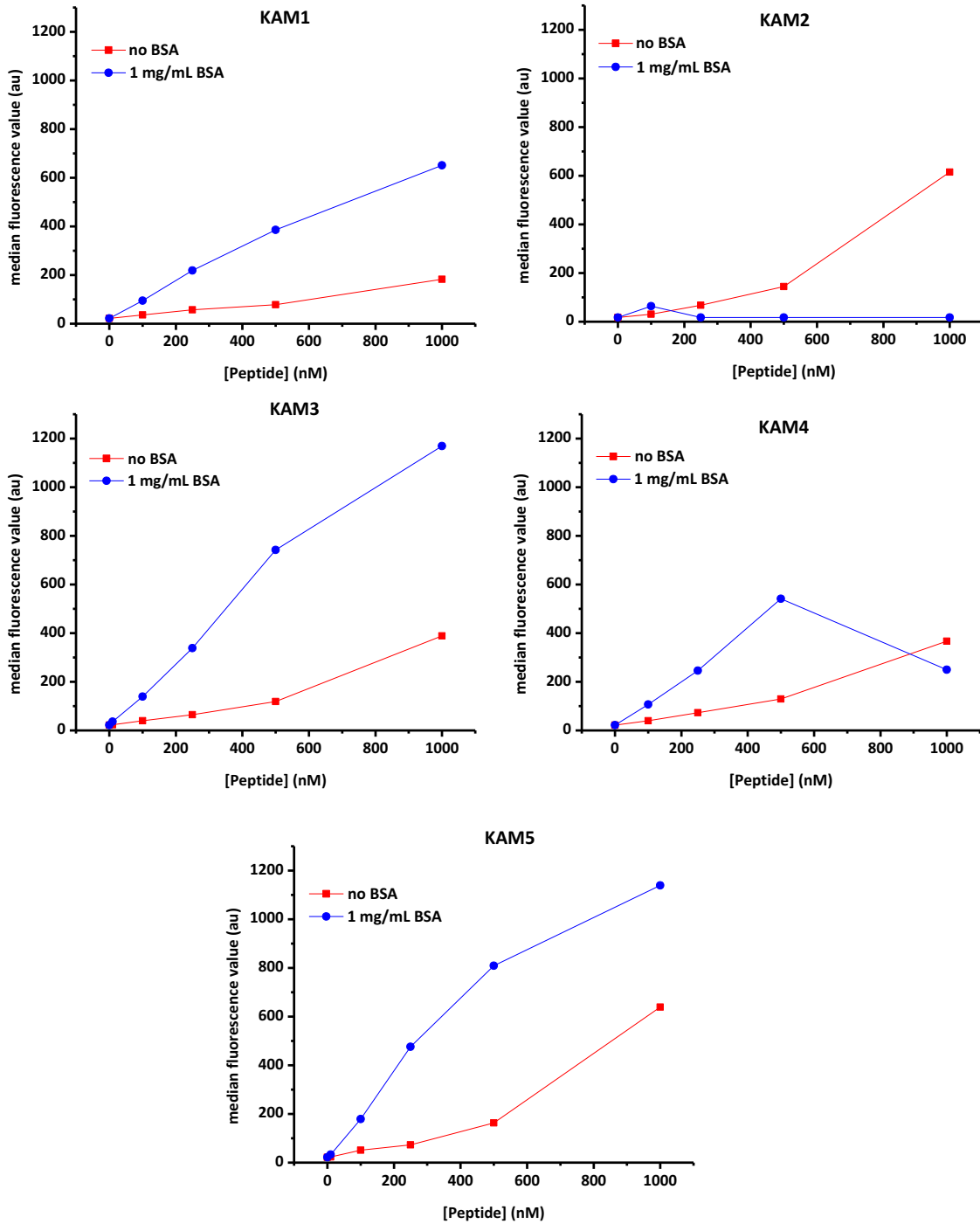


Figure 4-4 Flow cytometry analysis of *S. aureus* staining by KAM1-5 in the presence and absence of BSA.

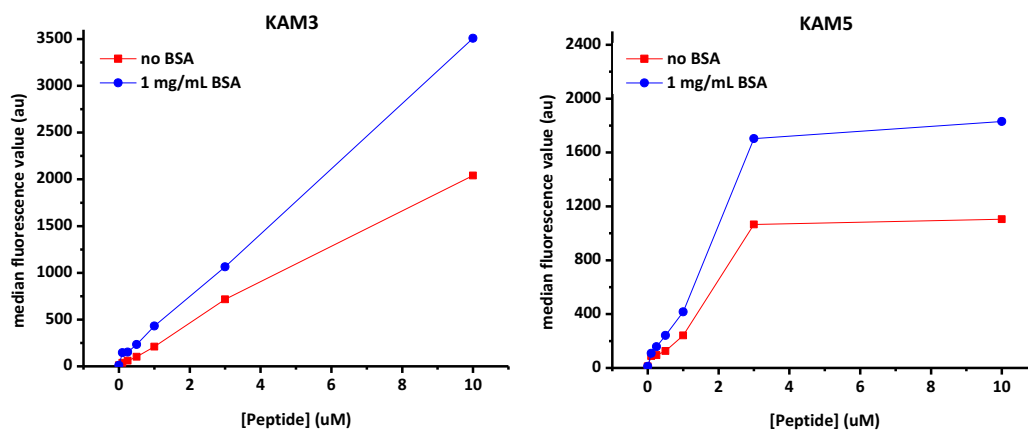


Figure 4-5 Flow cytometry analysis of *S. aureus* staining by KAM3 and KAM5 up to 10 μM in concentration in the presence and absence of BSA.

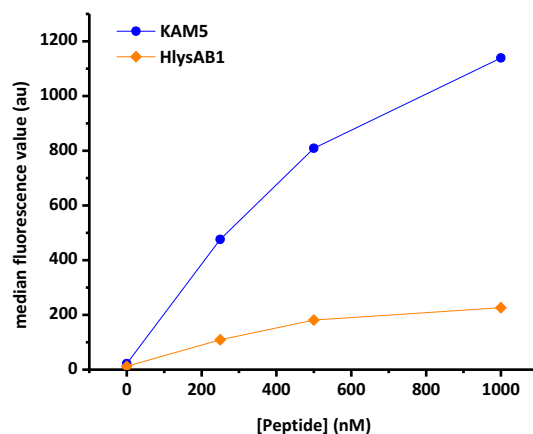


Figure 4-6 Flow cytometry comparison of *S. aureus* staining by KAM5 versus Hlys-AB1 prepared in 1 mg/mL BSA.

Importantly, a negative control peptide KAM6 (reported in Chapter 3 as KAM-GPT), which was not selected from the screen and contains a random heptapeptide sequence, showed no bacterial staining under the same experimental conditions (Figure 4-7). Furthermore, the cyclic precursor of KAM5 (KAM5-Cyclic which has no APBA

moieties) elicited little *S. aureus* staining as well, demonstrating the importance of the APBA warhead (Figure 4-7).

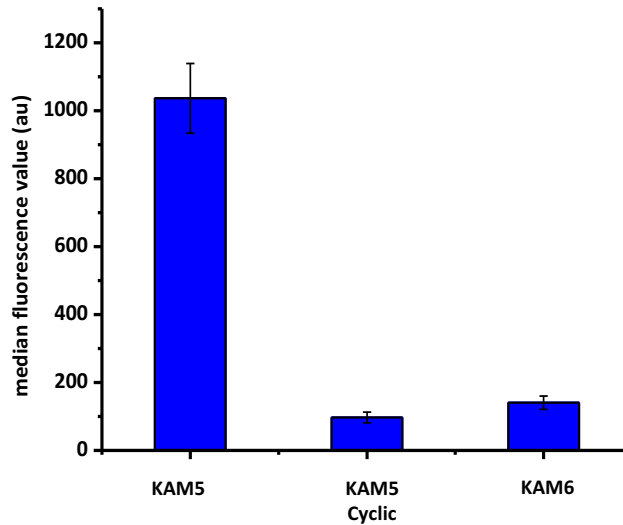


Figure 4-7 Flow cytometry comparison of *S. aureus* staining by KAM5 versus controls at 1 μ M in concentration prepared in 1 mg/mL BSA.

The cell staining ability of KAM5 was also evaluated via fluorescence microscopy with a tetramethylrhodamine (TAMRA) labeled peptide due to better stability of the fluorophore. The microscopy studies yielded results consistent with those of flow cytometry: KAM5 at 2 μ M concentration gave strong fluorescence staining of *S. aureus* cells and the addition of BSA up to 10 mg/mL did not inhibit the bacterial staining by KAM5. On the contrary, the BSA addition elicited stronger fluorescence staining of the bacteria, consistent with the flow cytometry results (Figure 4-8).

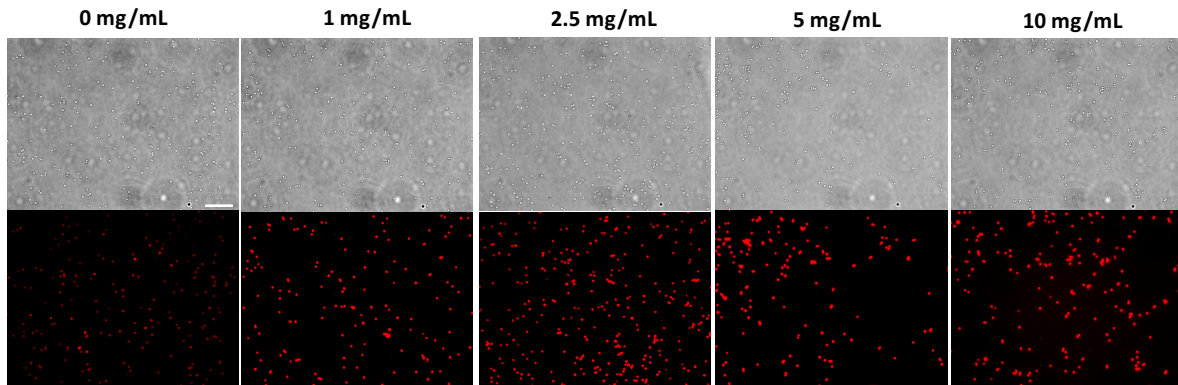


Figure 4-8 Fluorescence microscopy analysis of *S. aureus* staining by KAM5-TAMRA (2 μ M) with increasing concentration of BSA. Scale bar: 10 μ m.

The protein-enhanced bacterial binding by KAM5 is not BSA-specific as similar enhancement was observed with HSA as well (Figure 4-9a). To better understand this phenomenon, the binding of KAM5 to these serum proteins was assessed via fluorescence anisotropy (Figure 4-9b). KAM5 did show binding to both BSA and HSA at high protein concentrations, which is perhaps not surprising given these proteins display a large number of surface lysine residues. These results suggest that BSA/HSA may enhance KAM5 binding to *S. aureus* by forming ternary complexes, although the detailed mechanism requires further investigation.

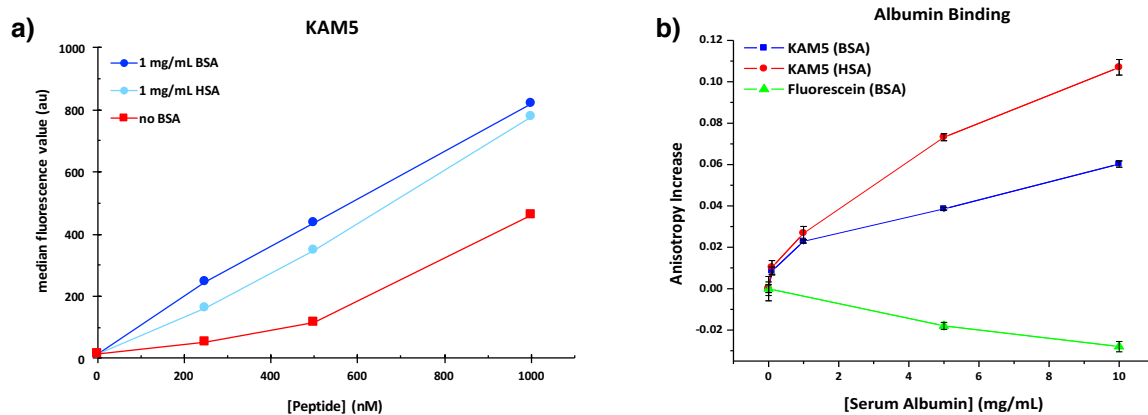


Figure 4-9 (a) Flow cytometry analysis of *S. aureus* staining by KAM5 in the presence of either BSA or HSA. (b) Fluorescence anisotropy increase of KAM5 (500 nM) against each serum protein compared to fluorophore alone.

Further analysis of KAM5 via fluorescence microscopy showed equally potent staining of a methicillin-resistant strain of *S. aureus* (MRSA) in comparison to the strain used in phage display (Figure 4-10). This is consistent with our hypothesis that KAM5 binds the bacteria via covalent conjugation to Lys-PG, which is present on essentially all *S. aureus* strains, although its percentage may vary.⁶

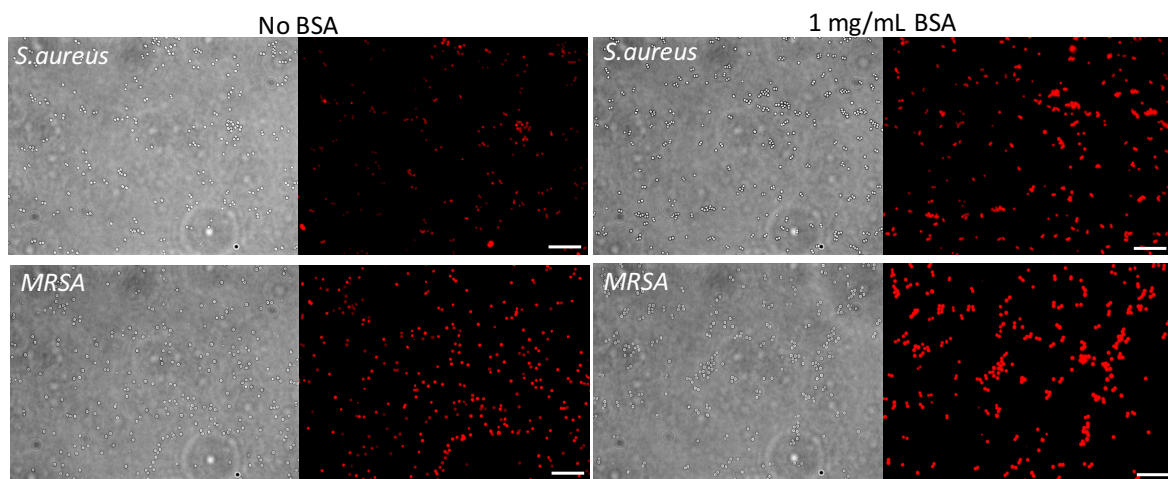


Figure 4-10 Fluorescence microscopy comparison of KAM5 (2 μ M) binding to *S. aureus* and MRSA. Scale bar: 10 μ m.

The bacterial selectivity of KAM5 toward different bacterial species was also analyzed. Specifically, KAM5 labeling of *E. coli*, a model Gram-negative bacterium, and *B. subtilis*, a model Gram-positive bacterium, was assessed via flow cytometry (Figure 4-11a) and fluorescence microscopy (Figure 4-11b). The data revealed negligible staining of these control bacterial species with up to 10 μ M peptide, highlighting the desirable species selectivity toward *S. aureus*.

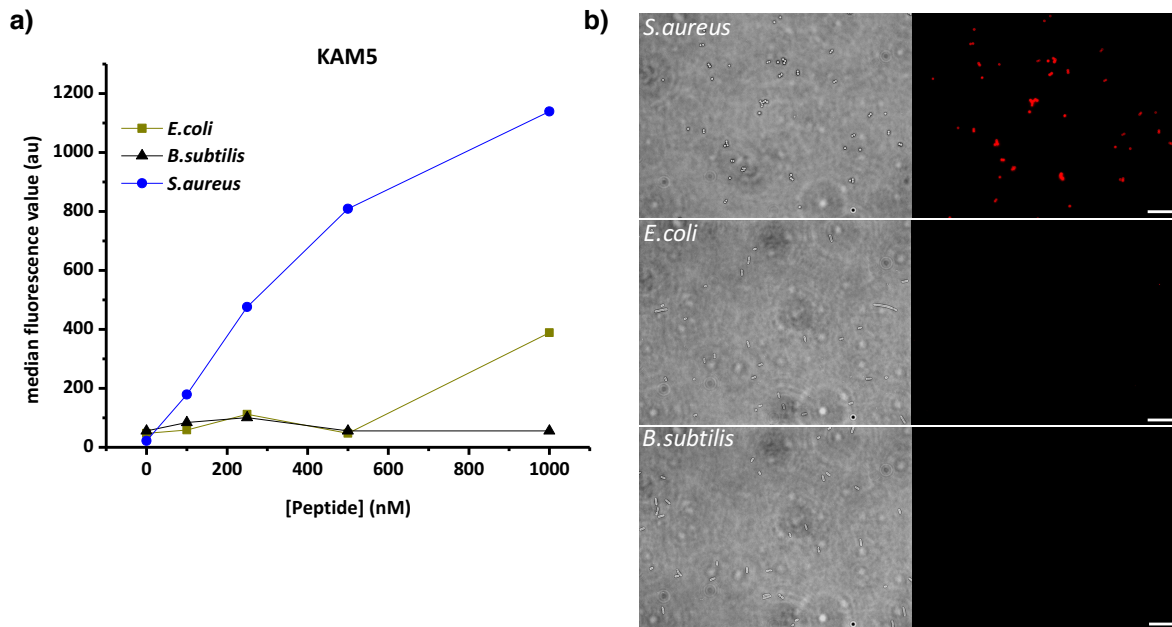


Figure 4-11 Comparison of KAM5 binding different species of bacteria in the presence of 1 mg/mL BSA via (a) flow cytometry and (b) fluorescence microscopy with 10 μ M peptide. Scale bar: 10 μ m.

4.2.3 Comparison to Control Phage Libraries

To directly assess the advantage of the APBA-modified phage library, parallel screening for *S. aureus* binding was performed using the unmodified C7C library, as well as a C7C-derived library in which the reduced cysteines were alkylated with simple iodoacetamide (C7C-IA library). The *S. aureus* panning experiments were performed by following the same protocol used for the APBA-dimer library. Sequencing results after three rounds of panning of the unmodified C7C library did yield two repeating sequences (Table 4-3a). However, when synthesized (Table 4-4a) and characterized using flow cytometry, neither of these peptides showed significant bacterial staining up to 10 μ M (Figure 4-12). Even if they did bind *S. aureus* at higher concentrations, their affinity for the bacteria would be much lower than that of KAM5. It is worth noting that the final output

population of the C7C library, in comparison to the APBA-dimer library, contains a proportionally larger number of blank sequences (no peptide displayed), which presumably came from the original, imperfectly created C7C library and did not get selected out during the panning process. The higher percentage of blank sequences suggests that the unmodified C7C library offers few potent binders or “real hits” for *S. aureus*. Similarly, after three rounds of panning, the C7C-IA library gave a larger number of blank sequences as well, yet only one sequence showing repeats (Table 4-3b). Characterization of this recurring sequence in addition to a randomly picked sequence out of the round 3 output population (Table 4-4b) failed to show bacterial staining up to 10 μ M (Figure 4-12). The failure of these control libraries is consistent with earlier phage display efforts where screening of natural peptide libraries was only able to yield sub-to-low millimolar binders of bacteria at best. Collectively, the comparative study presented here clearly showcases the advantage of phage display with dynamic covalent binding motifs.

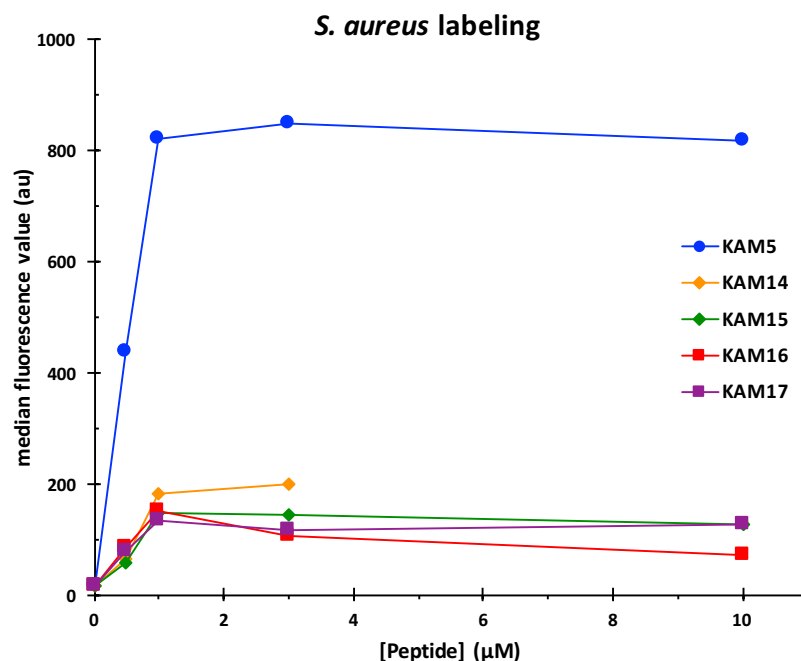


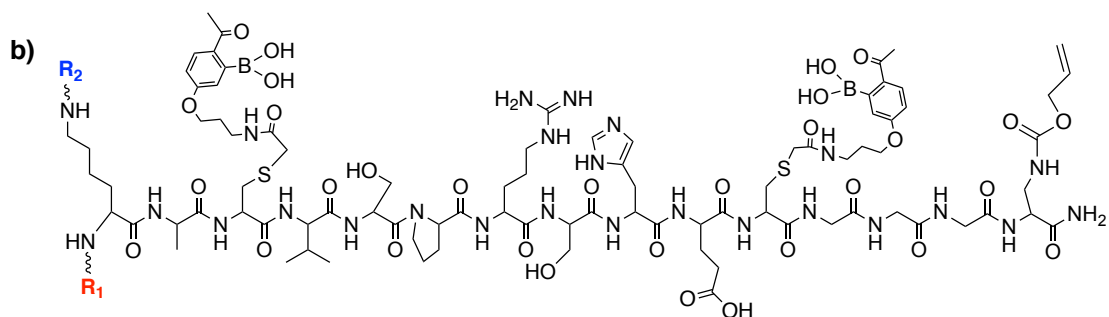
Figure 4-12 Flow cytometry comparison of KAM5 to peptide “hits” from control libraries (KAM14-17) with 1 mg/mL present. *Note: KAM14 only analyzed up to 3 μM due to aggregation at higher concentrations.

4.3 Generating a Targeted Antibiotic for *S. aureus*

A potent and selective *S. aureus* binder has the potential to serve as a directing element to develop targeted antibiotics. The preferential binding of KAM5 toward *S. aureus* over serum proteins as well as other bacterial species makes it an excellent candidate for delivering a bactericidal agent to target cells.

4.3.1 Conjugation of Various Hydrophobic Groups

First, a panel of KAM5 derivatives were synthesized with various hydrophobic moieties in an effort to cause selective membrane disruption, using the KAM5 peptide as a directing entity to the *S. aureus* cell membrane. Long hydrocarbon chains were conjugated to the N-terminal amine and/or Dap residue via amide bond linkages (Figure



Peptide name	R1	R2	ClogP
Bn-KAM5			1.28
Ad-KAM5			3.01
TP-K-KAM5		H_3N^+	3.53
TP-KAM5			8.83

Figure 4-13 (a) Panel of lipid tail-KAM5 conjugates synthesized. (b) Panel of bulky, hydrophobic KAM5 conjugates synthesized on additional N-terminal lysine residue.

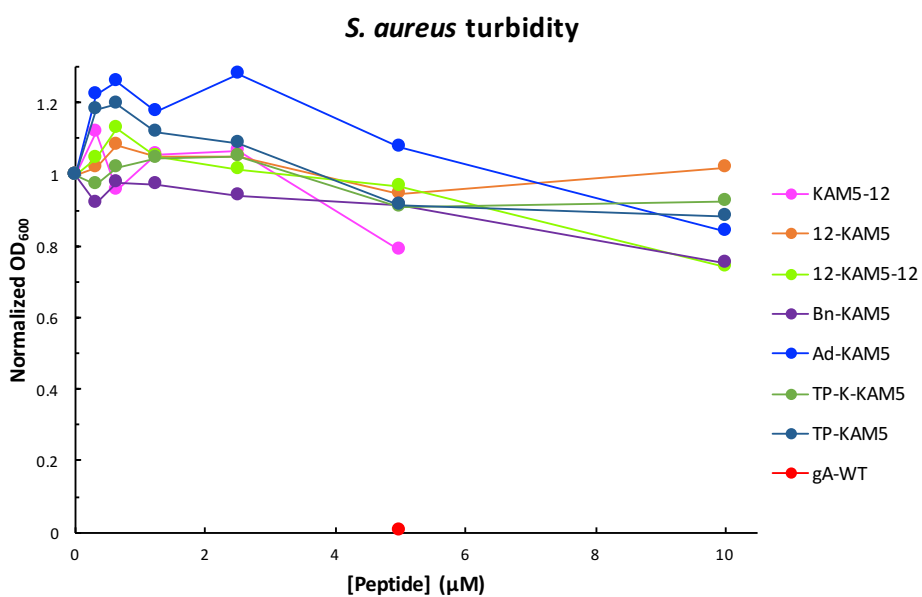
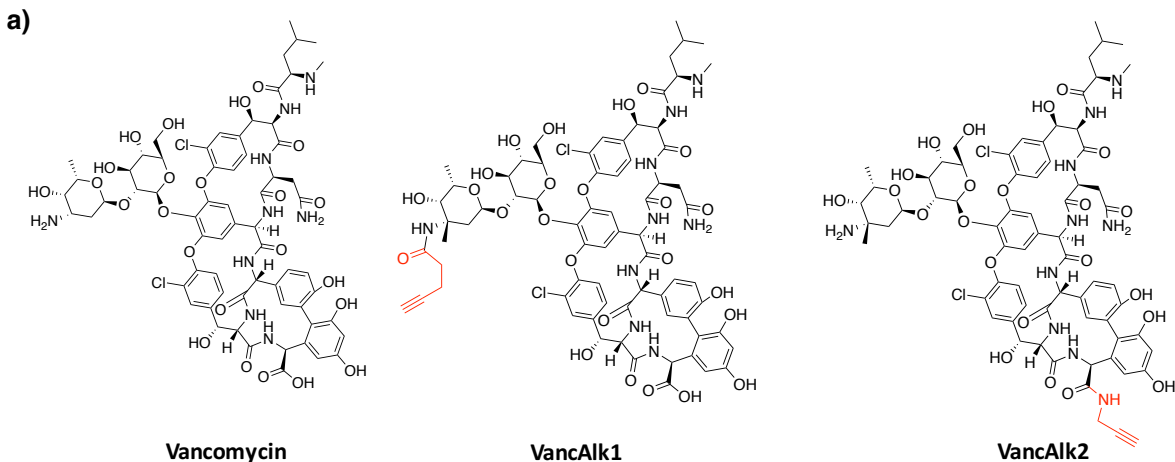


Figure 4-14 MIC assay of hydrophobic KAM5 conjugates against *S. aureus* compared to a positive control, gramicidin (gA-WT, red marker).

4.3.2 Conjugation to Vancomycin

Since conjugation of a generic hydrophobic molecule to KAM5 did not elicit bactericidal activity, conjugation of a known antibiotic was then explored. We hypothesized that conjugation of an antimicrobial peptide, such as vancomycin, to KAM5 would result in increased potency of vancomycin towards *S. aureus*. Previous studies have shown that multiple sites on vancomycin can be modified without loss of bactericidal activity, including the vancosamine sugar amine and the C-terminal carboxylic acid.¹³⁻¹⁶ Copper-catalyzed azide-alkyne cycloaddition (CuAAC) was exploited for the synthesis of various KAM5-Vancomycin conjugates, connected via various linkers. Accordingly, an alkyne handle was attached to vancomycin on either the vancosamine sugar amine or C-terminal carboxylic acid via amide bond formation (Figure 4-15a). The alkyne-modified Vancomycin derivatives (VancAlk1 and VancAlk2) were assessed for staphylocidal activity via an MIC assay alongside unmodified Vancomycin (Figure 4-15b). Conjugation of the alkyne at either site did not significantly effect *S. aureus* cell killing.



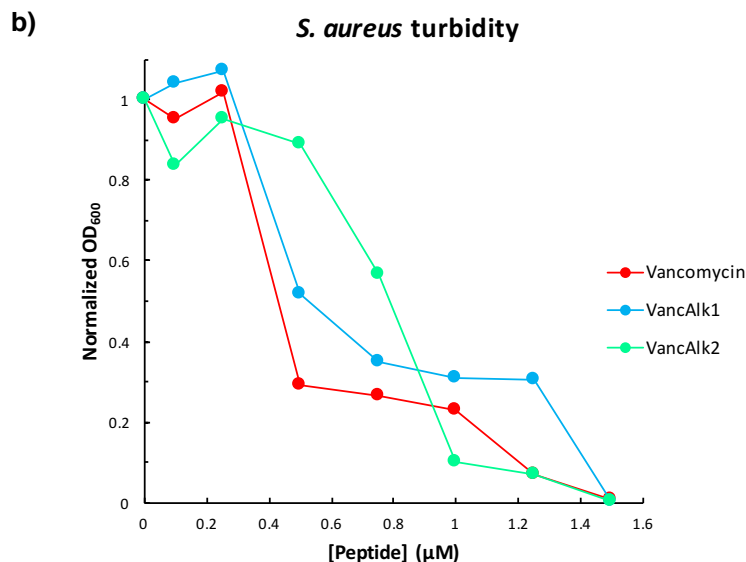
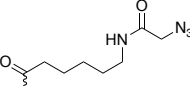
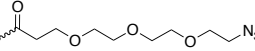


Figure 4-15 (a) Alkyne-modified vancomycin derivatives synthesized (b) MIC assay of vancomycin and derivatives against *S. aureus*.

KAM5 was derivatized with multiple azido functionalities with various linker lengths and compositions on the Dap residue via amide bond formation. An alkyne-functionalized Vancomycin and azide-modified KAM5 were subjected to the CuAAC reaction and subsequently labeled with APBA-IA. Four different KAM5-Vancomycin conjugates were synthesized (Table 4-5). One major synthetic obstacle to overcome with the vancomycin conjugates was that treatment with TFA and cold temperature, for example the acidic eluent of RP-HPLC followed by freeze drying, removes the vancosamine amine and therefore the clicked portion of KAM5. In fact, Schabel and coworkers treated vancomycin with TFA at -15°C to selectively cleave the vancosamine amino sugar from vancomycin.¹⁷ To prevent the sugar ring from falling off, slightly less acidic formic acid was utilized for purification via HPLC. Once synthesized, the vancomycin conjugates were subjected to an MIC assay against *S. aureus*; however, none of the

conjugates elicited any Staphylocidal activity with treatment of up to 1.5 μM (Figure 4-16). KAM5-Vanc4 was analyzed up to 5 μM ; however, no *S. aureus* cell killing was observed even with this considerably higher concentration.

Table 4-5 KAM5-azide and Vancomycin-alkyne derivatives subjected to CuAAC to yield various KAM5-Vancomycin conjugates.

Peptide name	Azido-modified Dap	Vancomycin Derivative
KAM5-Vanc1		VancAlk1
KAM5-Vanc2		VancAlk2
KAM5-Vanc3		VancAlk1
KAM5-Vanc4		VancAlk1

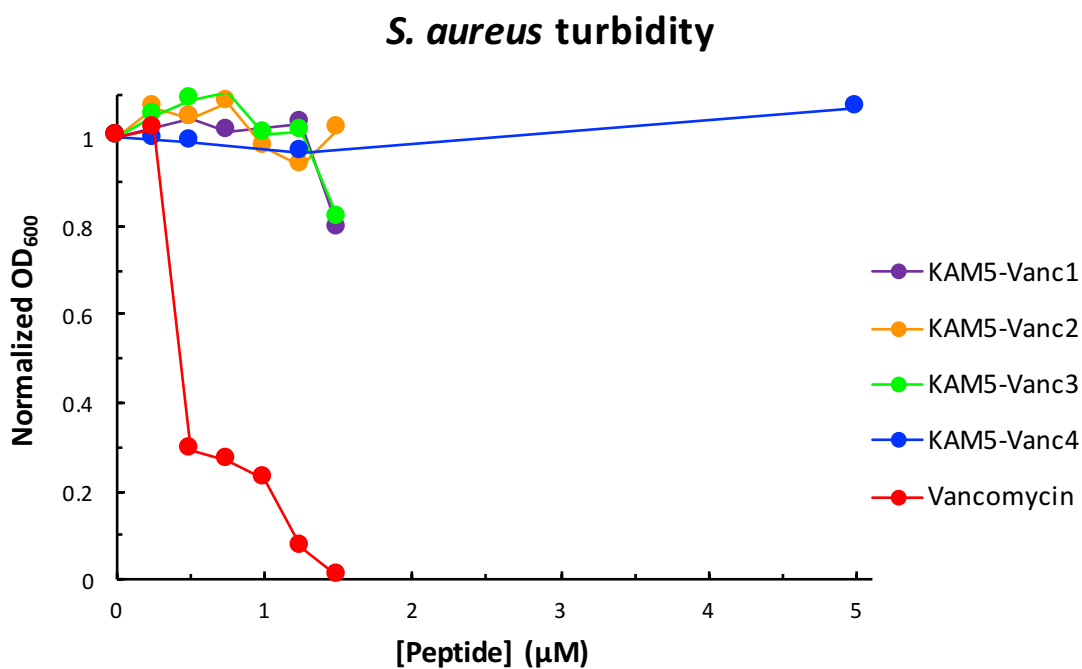


Figure 4-16 MIC assay of KAM5-Vancomycin conjugates compared to vancomycin.

In an effort to determine if the linkages to vancomycin were tolerated for retention of antimicrobial function, additional studies were performed. KAM5-Vanc4 was synthesized without the KAM5 peptide portion to ensure that the PEG linker and triazole were tolerated (Figure 4-17a). An MIC assay against *S. aureus* was performed to compare vancomycin to Vanc(tri)PEG (Figure 4-17b). Although a slight decrease in MIC was determined for this control peptide (~2 μ M compared to ~1.5 μ M for Vancomycin), the antimicrobial function was not completely lost, suggesting that the triazole linker is not causing the lack of antimicrobial function of the KAM5-Vancomycin conjugates. This data suggests that the KAM5 portion of the peptide is effecting the antimicrobial activity of vancomycin. Cooper and coworkers conjugated a directing peptide, a positively charge effector sequence, along with a lipophilic tail onto vancomycin and were able to achieve more than 100-fold increase in potency towards *S. aureus* compared to vancomycin.¹⁶ Perhaps the addition of a lipid tail to KAM5 could have a similar effect, where KAM5 serves as the effector peptide sequence, to overcome the lack of antimicrobial activity of the conjugates.

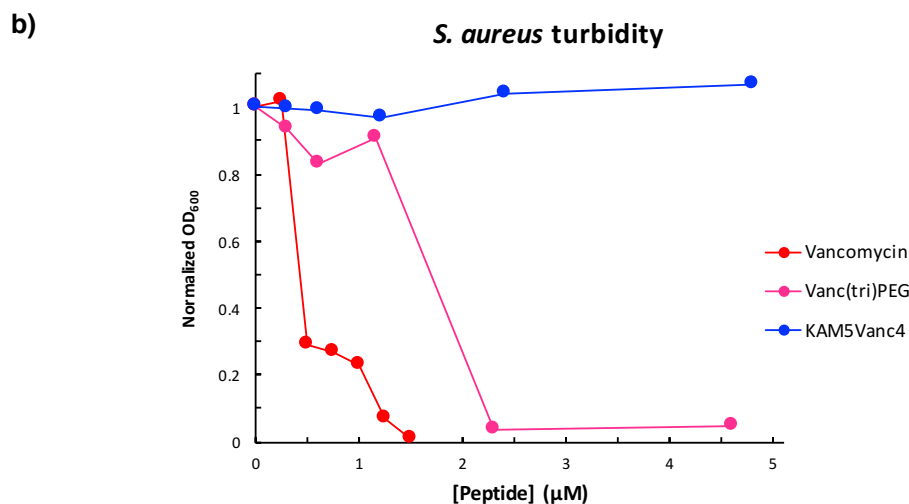
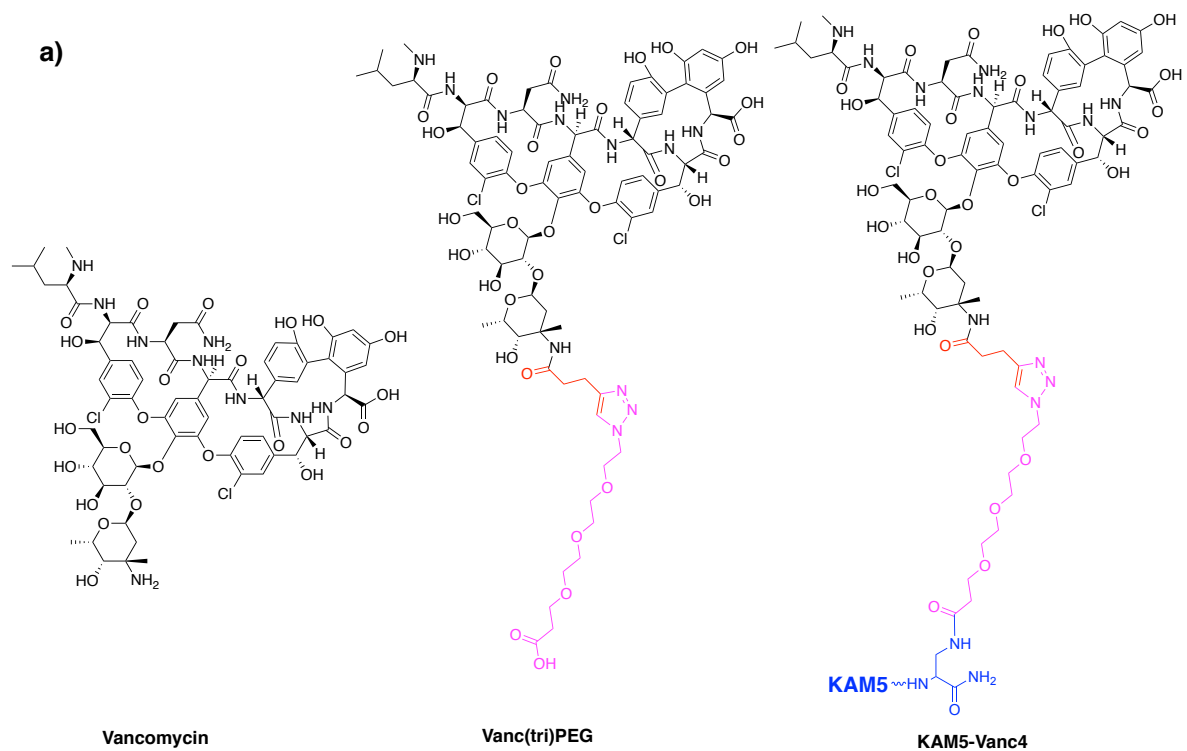


Figure 4-17 (a) Structures of vancomycin derivatives (b) MIC assay of vancomycin compared to derivatives against *S. aureus*.

4.3.3 Conjugation to Other Antimicrobials

Two final antimicrobial agents were conjugated to KAM5 in a similar approach as vancomycin. First, Hlys was synthesized with an alkyne handle via an additional C-terminal

Dap residue and was conjugated to KAM5-azide, specifically the derivative with the short azidoacetic acid moiety, via CuAAC (Figure 4-18). Hlys, previously mentioned in Chapter 2, is the bactericidal portion of a cationic antimicrobial peptide with a relatively high reported MIC value of 24 μM against *S. aureus*.¹⁸ It was hypothesized that conjugation to KAM5 could direct Hlys to the *S. aureus* cell membrane to increase its cell killing potency. Second, a small molecule reduced amide membrane disruptor from the Cai lab¹⁹, m-146, was provided to us as an alkyne and conjugated to KAM5-azide, specifically the derivative with the PEG linker, via CuAAC (Figure 4-18). We also hypothesized that conjugation to KAM5 could allow for increased potency of m-146, of which the alkyne-deficient molecule has a reported MIC of 1.56 $\mu\text{g}/\text{mL}$ against *S. aureus*.¹⁹

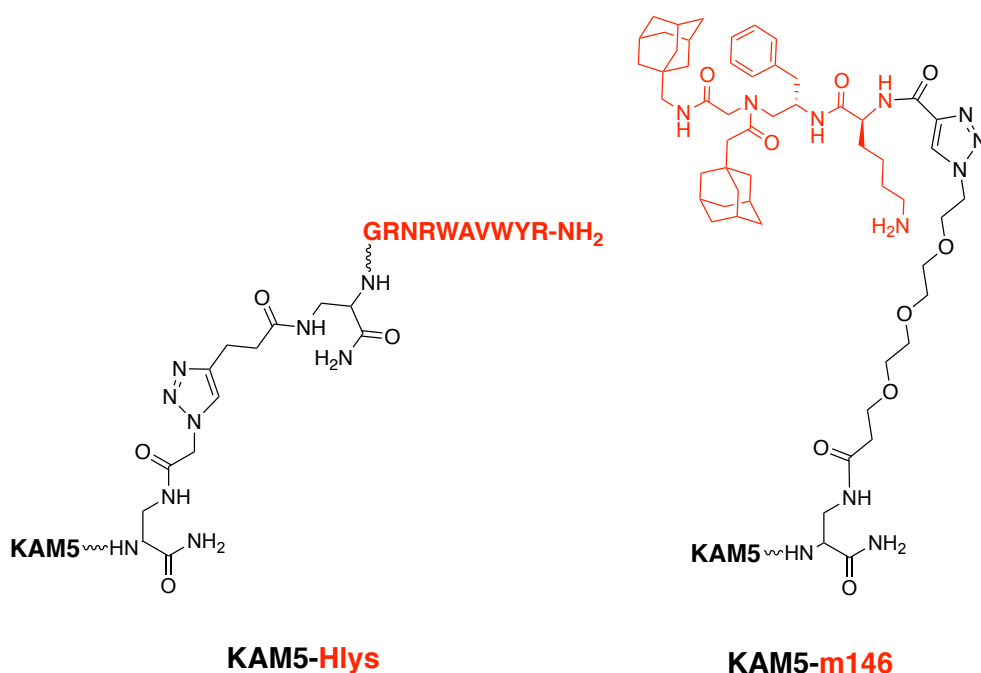


Figure 4-18 Structures of KAM5-Hlys and KAM5-m146 conjugates.

KAM5-Hlys exhibited a similar, but slightly higher MIC value than Hlys-alkyne (Figure 4-19a). As observed with the vancomycin conjugates, KAM5-m146 did not exhibit any Staphylocidal activity compared to its respective alkyne antimicrobial agent (Figure 4-19b). The lack of bactericidal activity enhancement of one KAM5 conjugate and the complete loss of staphylocidal activity by the other two molecules thus far established that a different approach should be taken to achieve selective antimicrobial activity of KAM5.

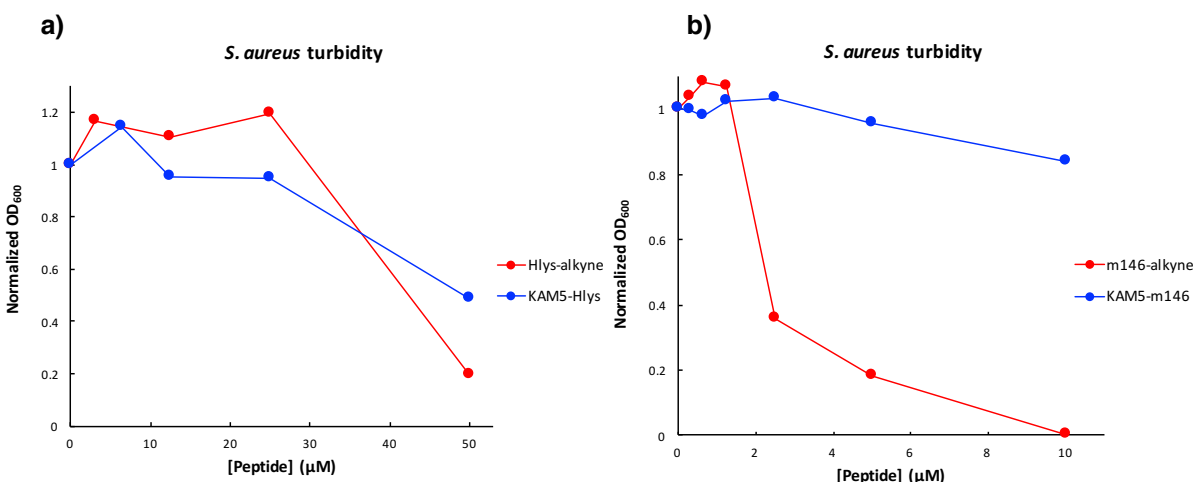


Figure 4-19 MIC assay against *S. aureus* with (a) KAM5-Hlys and (b) KAM5-m146.

4.3.4 Co-treatment with Antimicrobial Peptides

Our working hypothesis is that KAM5 binds to the highly abundant Lys-PG phospholipid on the *S. aureus* cell membrane. Therefore, we postulated that pre-treatment of the bacteria with KAM5 could cap the resistance-causing Lys-PG, further sensitizing the bacteria to CAMPs, such as Protegrin 1 (PG1). PG1 is a cysteine rich CAMP isolated from porcine leukocytes with broad-spectrum antimicrobial activity²⁰ previously synthesized in our lab by Chelsea Weidman. An MIC assay was performed against *S.*

aureus on PG1 alone along with *S. aureus* pretreated with KAM5 (3 μ M) for 15 min followed by PG1 treatment (Figure 4-20a). Unfortunately, no increase in Staphylocidal activity was observed upon the pretreatment with KAM5. This concept was also applied to Daptomycin, a Gram-positive acting lipopeptide antibiotic²¹; however, as with PG1, no increase in Staphylocidal activity was observed upon the pretreatment with KAM5.

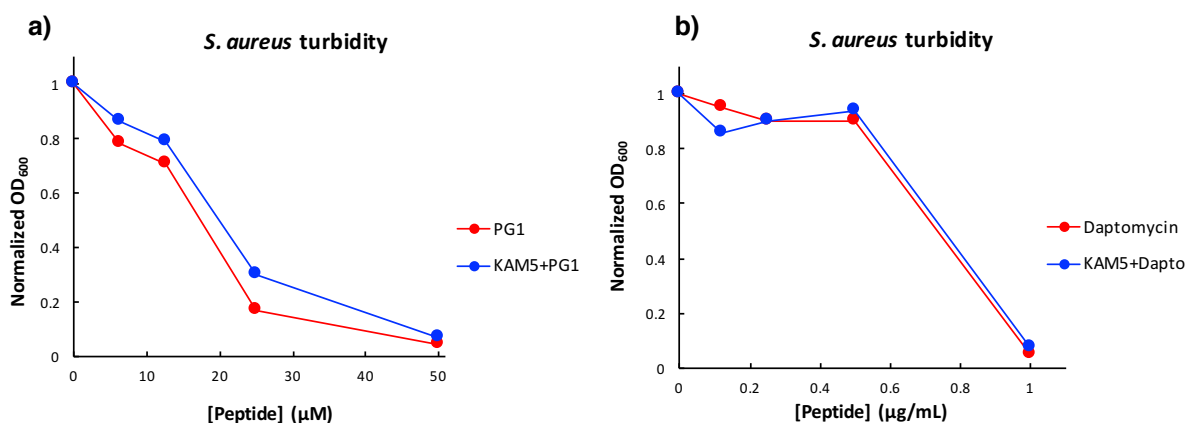


Figure 4-20 MIC assay with and without KAM5 pretreatment of *S. aureus* with (a) PG1 and (b) Daptomycin

4.3.5 Conjugation of ATCUN Motif

Since conjugation of KAM5 to membrane disrupting entities such as hydrophobic groups and antimicrobial peptides was not effectively allowing for *S. aureus* cell killing, another type of chemistry was explored. Amino-terminal copper and nickel (ATCUN) binding motifs are known to bind metals and actively form reactive oxygen species (ROS), causing localized oxidative damage.²²⁻²⁴ The presence of ATCUN motifs, with the general sequence H₂N-AA₁-AA₂-His, on antimicrobial peptides has been reported to increase their bactericidal activity by causing oxidative damage to the lipids, leading to bacterial cell death.²⁴ We hypothesized that addition of an ATCUN motif to KAM5 would allow for

selective oxidative damage of the *S. aureus* cell membrane upon metal binding. Towards this end, the ATCUN derivative VIH-KAM5 was synthesized by simple addition of three amino acids to the N-terminus of KAM5 (Figure 4-21a). The motif “H₂N-Val-Ile-His” was chosen since it was previously reported by Angeles-Boza and coworkers as a potent Cu-ATCUN motif that allowed for increased antimicrobial activity of various antimicrobial peptides against a panel of bacterial species and lead to the most rapid production of ROS.²³ An MIC assay against *S. aureus* was performed with VIH-KAM5 in media supplemented with Cu^{II} to form Cu^{II}-peptide complexes for ROS production (Figure 4-21b). Unfortunately, no antimicrobial activity was observed with up to 50 μM VIH-KAM5. Most reported examples of this concept involve conjugation of an ATCUN motif to α-helical antimicrobial peptides. Perhaps the helicity of the peptide is important to insert into the membrane and strategically position the ATCUN motif to cause ROS upon metal binding.

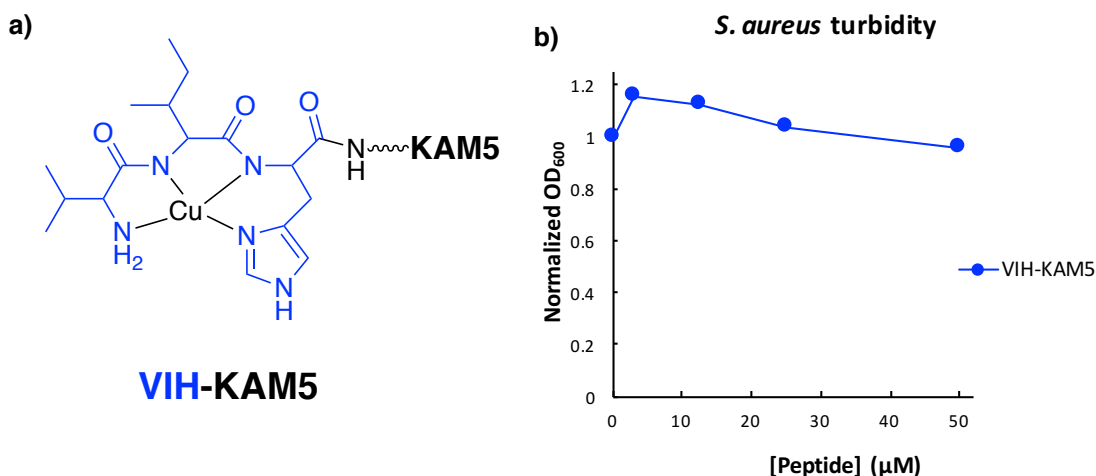


Figure 4-21 (a) Structure VIH-KAM5 bound to copper (b) MIC assay of ATCUN binding motif conjugate in presence of copper against *S. aureus*.

4.3.6 Conjugation of a Phototoxin Elicits Cell Death Upon Light Exposure

Exploring a similar bactericidal mechanism as previously described with the ATCUN binding motifs, KAM5 was conjugated to a photosensitizer. Specifically, KAM5 was conjugated to Eosin (Figure 4-22a), a phototoxin that upon photoirradiation triggers the production of ROS, killing cells in close proximity (Figure 4-22b).²⁵ There has been considerable interest in developing photoinactivation strategies for pathogenic bacteria,²⁵⁻²⁸ which has been encouraged by the technological advances and therapeutic successes achieved in photodynamic therapy.²⁹ Delivery of a photosensitizer in a species-specific manner would maximize the benefit and minimize the side effect of photodynamic therapy in treating bacterial infections, particularly when the infection site hosts human commensal bacteria.

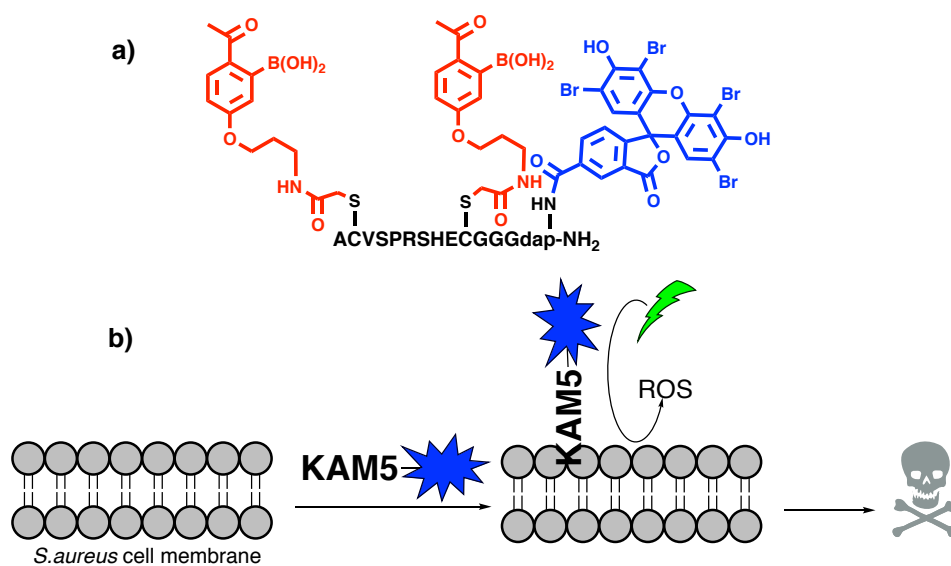


Figure 4-22 (a) Structure of KAM5-Eosin (b) Cartoon representation of photodynamic therapy with KAM5-Eosin.

The conjugate was assessed for photodynamic inactivation of *S. aureus* via a titering assay. When *S. aureus* was mixed with 1 μ M and 2 μ M KAM5-Eosin and then

exposed to blue light for 15 min, 74% and 92% cell killing was observed, respectively (Figure 4-23a). Importantly, eosin alone at these concentrations did not elicit cell death nor did KAM5 without the photosensitizer. Extending the bactericidal assay into other strains of *S. aureus* revealed that KAM5-Eosin worked equally well against the MRSA strain with comparable percentage of cell killing under the same experimental conditions (Figure 4-23b). As expected from the cell binding specificity of KAM5, the cell killing of KAM5-Eosin was specific to *S. aureus* as no significant cell death was observed for *B. subtilis* and *E. coli* treated with 2 μ M peptide followed by photoirradiation (Figure 4-23c).

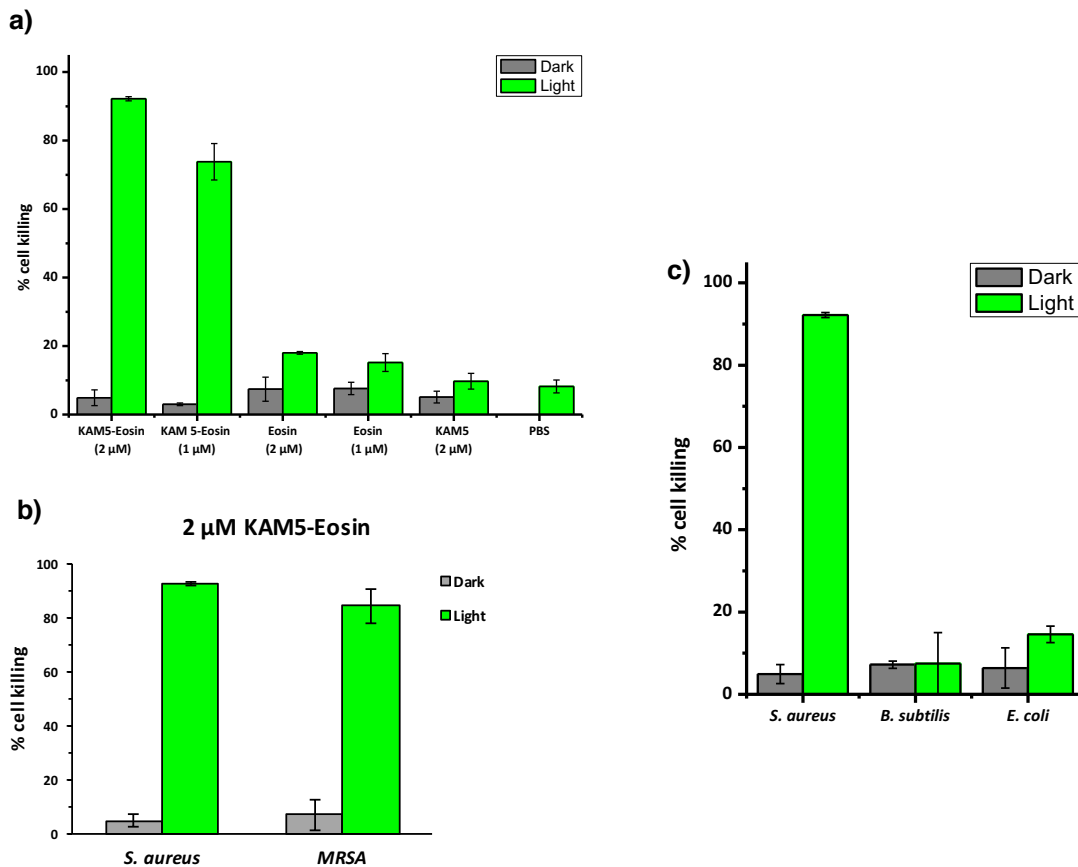


Figure 4-23 (a) Percent killing by KAM5-Eosin and controls with and without photoirradiation. (b) Comparable killing of MRSA by KAM5-Eosin. (c) Percent killing of several bacterial species with KAM5-Eosin (2 μ M).

Furthermore, no mammalian cell toxicity by KAM5-Eosin was observed via an MTT assay against HEK 293T cells and Jurkat cells with or without photoirradiation (Figure 4-24). For HEK 293T cells, photoirradiation alone resulted in some extent of cell killing; however, the peptide addition elicited no additional cell killing indicating lack of toxicity. Camptothecin (50 μ M), a topoisomerase inhibitor, was used as a positive control for mammalian cell death.

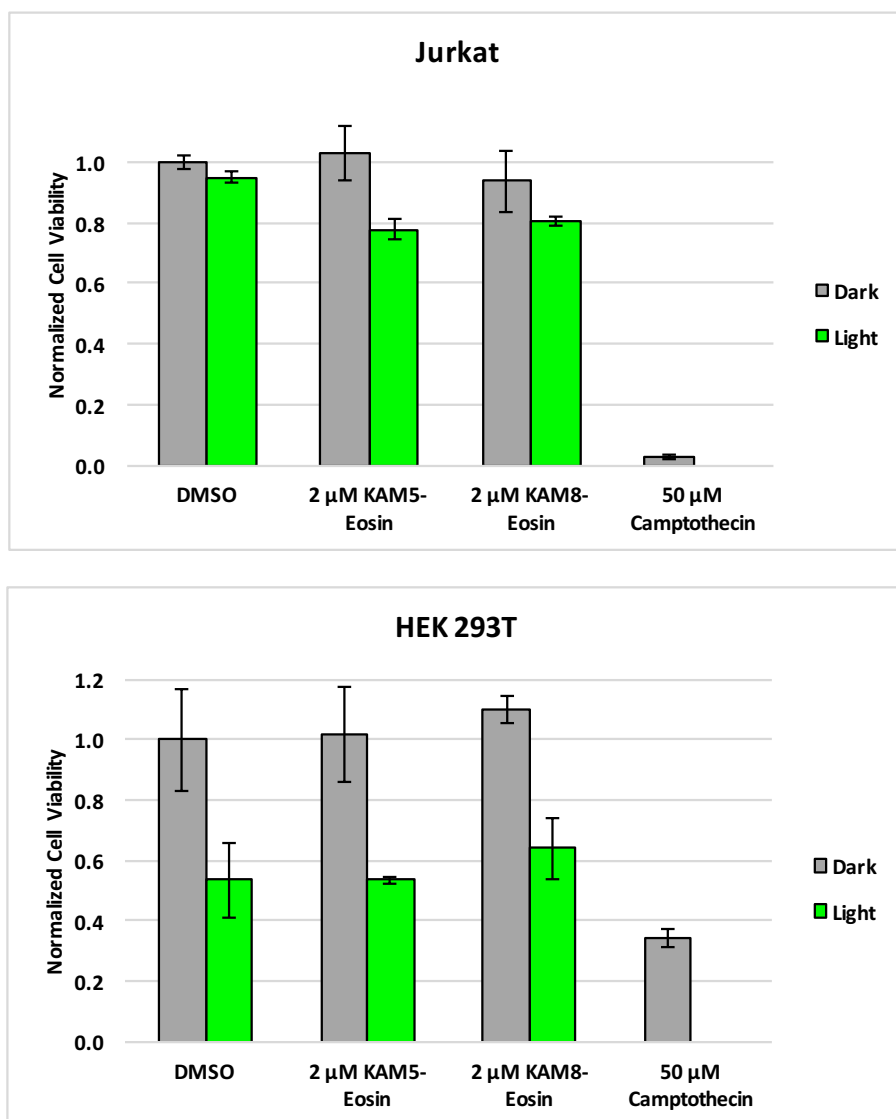


Figure 4-24 MTT assay to assess mammalian cell toxicity after treatment for 24 hours.

4.4 Strain-Specific Targeting of *A. baumannii*

4.4.1 Screening Against *A. baumannii* (LOS-)

To probe the general applicability of this approach, the APBA-dimer library was panned against a colistin-resistant, LOS-deficient strain of *A. baumannii* described previously. Three rounds of panning against the LOS- *A. baumannii* were executed following the same panning procedure described above for *S. aureus* except with the addition of a negative screen against the wild-type (LOS+) *A. baumannii* in the second round. After each round of panning, 15 colonies were isolated from the output population and subjected to sequencing, in which convergence was detected starting in round 2 (Table 4-6). Four different peptide sequences (KAM7–10) were observed repeatedly and synthesized via SPPS following the same procedure used for the *S. aureus* binding peptides (Table 4-7).

Table 4-6 Sequences of the peptide hits for *A. baumannii* (LOS-) binding (a) From round 2. (b) From round 3.

a)			b)		
Hit #	DNA Sequence	Peptide Sequence	Hit #	DNA Sequence	Peptide Sequence
1	GCTTGATTCGACTCATGCTAATTCGTGC	ACIPTHANSC	1	GCTTGAATATGCATACGCCTATGGTGTGC	ACNMHTPMVC
2	GCTTGACGTTGCCGAATGGGCCTAGGTGC	ACTLPNGPRC	2	GCTTGATTCGACTCATGCTAATTCGTGC	ACIPTHANSC
3	GCTTGTGAGCCGGGCTGGCGAGGTTTGC	ACEPGLARFC	3	GCTTGAATATGCATACGCCTATGGTGTGC	ACNMHTPMVC
4	GCTTGACGTTGCCGAATGGGCCTAGGTGC	ACTLPNGPRC	4	GCTTGAAGCTGTCGGGTATGCGCCTTGC	ACKLSGHAPC
5	GCTTGACGTTGCCGAATGGGCCTAGGTGC	ACTLPNGPRC	5	GCTTGACGTTGCCGAATGGGCCTAGGTGC	ACTLPNGPRC
6	GCTTGATTCGACTCATGCTAATTCGTGC	ACIPTHANSC	6	GCTTGATTCGACTCATGCTAATTCGTGC	ACIPTHANSC
7	GCTTGAAGCTGTCGGGTATGCGCCTTGC	ACKLSGHAPC	7	GCTTGACGTTGCCGAATGGGCCTAGGTGC	ACTLPNGPRC
8	GCTTGAAGCATTGCGCGCCGAATTGC	ACKHLPAPNC	8	GCTTGATTCGACTCATGCTAATTCGTGC	ACIPTHANSC
9	GCTTGAAGCTGTCGGGTATGCGCCTTGC	ACKLSGHAPC	9	GCTTGAAGCTGTCGGGTATGCGCCTTGC	ACKLSGHAPC
10	GCTTGACGTTGCCGAATGGGCCTAGGTGC	ACTLPNGPRC	10	GCTTGACGTTGCCGAATGGGCCTAGGTGC	ACTLPNGPRC
11	GCTTGACGTTGCCGAATGGGCCTAGGTGC	ACTLPNGPRC	11	GCTTGACGTTGCCGAATGGGCCTAGGTGC	ACTLPNGPRC
12	GCTTGAATATGCATACGCCTATGGTGTGC	ACNMHTPMVC	12	GCTTGACGTTGCCGAATGGGCCTAGGTGC	ACTLPNGPRC
13	n/a	Blank	13	GCTTGATTCGACTCATGCTAATTCGTGC	ACIPTHANSC
14	GCTTGACGTTGCCGAATGGGCCTAGGTGC	ACTLPNGPRC	14	GCTTGACGTTGCCGAATGGGCCTAGGTGC	ACTLPNGPRC
15	GCTGTTGGAGCAGAGGGGGCCGATTGC	ACLEQRGPDC	15	GCTTGATTCGACTCATGCTAATTCGTGC	ACIPTHANSC

Table 4-7 Synthesized peptide hits and frequency from *A. baumannii* (LOS-) screening.
 C_m: APBA-IA modified Cys, Dap*: Fluorophore modified Dap residue.

NAME	PEPTIDE SYNTHESIZED	Round 2 Frequency	Round 3 Frequency
KAM7	AC _m IPTHANSC _m GGGDap*	2	5
KAM8	AC _m TLPNGPRC _m GGGDap*	6	6
KAM9	AC _m KLSGHAPC _m GGGDap*	2	2
KAM10	AC _m NMHTPMVC _m GGGDap*	1	2

4.4.2 Characterization of *A. baumannii* (LOS-) Binding

Flow cytometry analysis of the peptide hits showed potent binding at sub- μ M concentrations (Figures 4-25). Similar to what was observed for *S. aureus*, the presence of BSA did not inhibit the peptides' binding to the bacteria. Instead, it actually enhanced bacterial staining by KAM8 at sub- μ M concentrations to some extent. Analysis of the concentration profile of the bacterial staining by KAM8 gave an estimated EC₅₀ of \sim 0.3 μ M. Also similar to the *S. aureus* binders, KAM8 binding to *A. baumannii* requires both the two APBA warheads as well as the specific peptide sequence in between, since the negative controls (KAM6 and the cyclic precursor KAM8-Cyclic) showed much reduced binding to the bacteria (Figure 4-26).

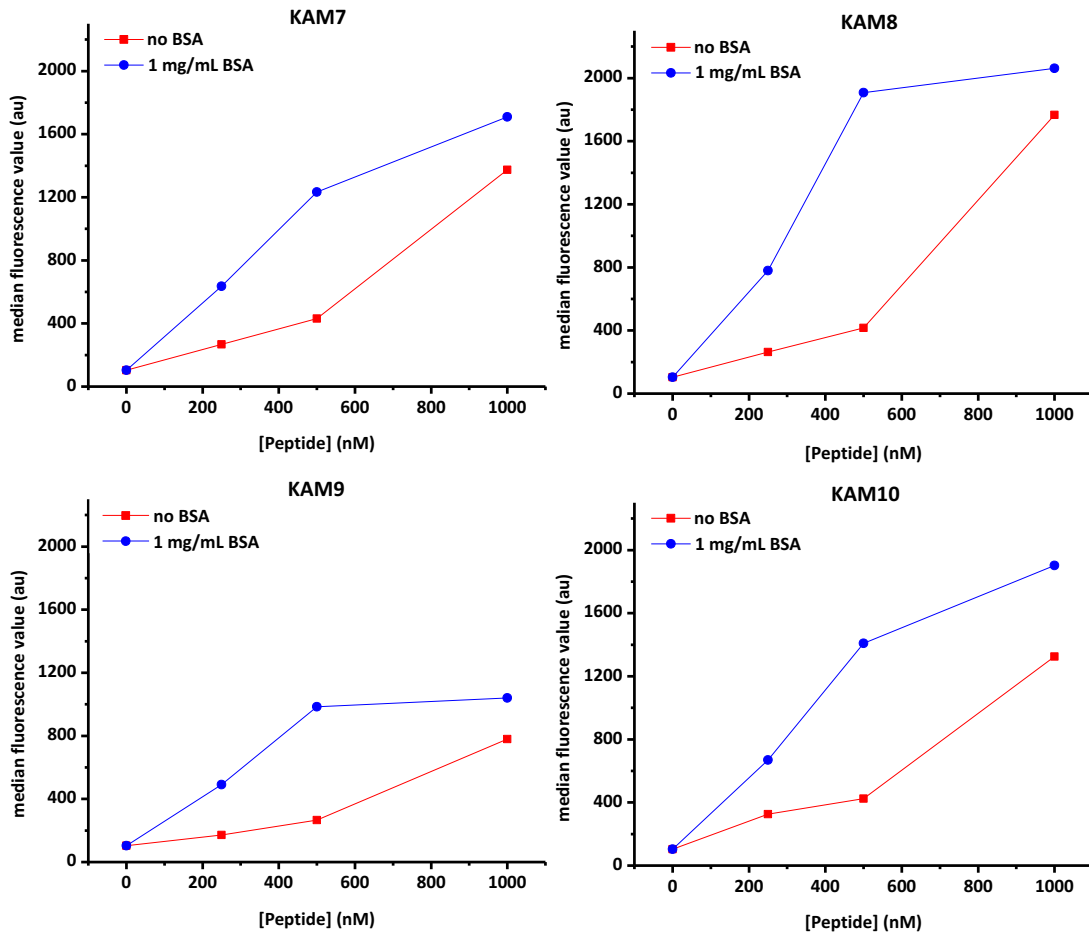


Figure 4-25 Flow cytometry analysis of *A. baumannii* (LOS-) staining by KAM7-10 in the presence and absence of BSA.

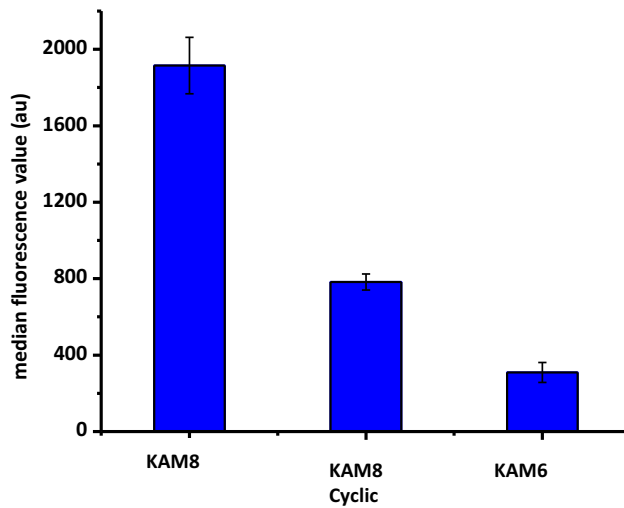


Figure 4-26 Flow cytometry analysis of *A. baumannii* (LOS-) staining by KAM8 compared to KAM8-Cyclic and KAM6 at 1 μM with 1 mg/mL present.

The flow cytometry results were further corroborated with fluorescence microscopy studies, which showed bright fluorescence staining of the LOS- *A. baumannii* with 2 μ M KAM8 (Figure 4-27).

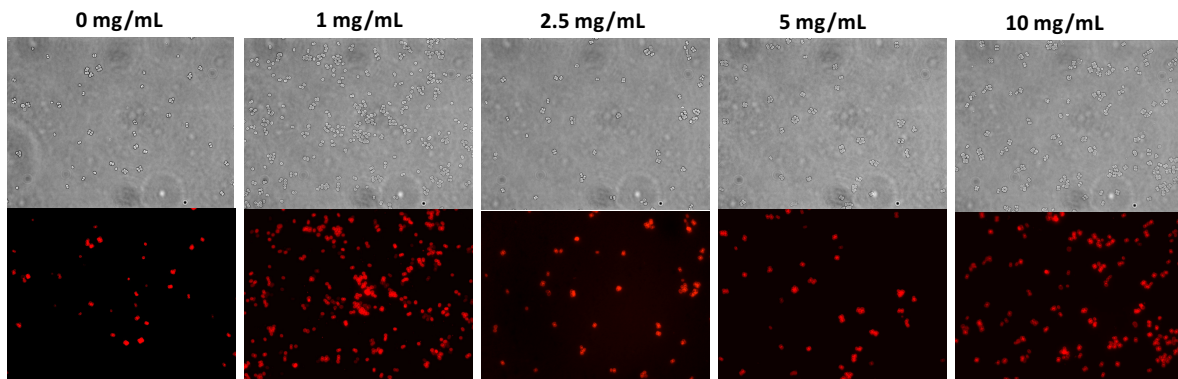


Figure 4-27 Fluorescence microscopy analysis of *A. baumannii* (LOS-) staining by KAM8-TAMRA (2 μ M) with increasing concentration of BSA. Scale bar: 10 μ m.

The bacterial selectivity of KAM8 toward different bacterial species, including wild-type *A. baumannii*, was analyzed. The wild-type *A. baumannii* (LOS+) showed little fluorescence staining under the same conditions that gave strong fluorescence staining of the LOS- strain via flow cytometry (Figure 4-28a) and fluorescence microscopy (Figure 4-28b). As expected, KAM8 showed no binding to *S. aureus* or *E. coli*, which were used as controls to represent Gram-positive and Gram-negative bacteria, respectively (Figure 4-28c).

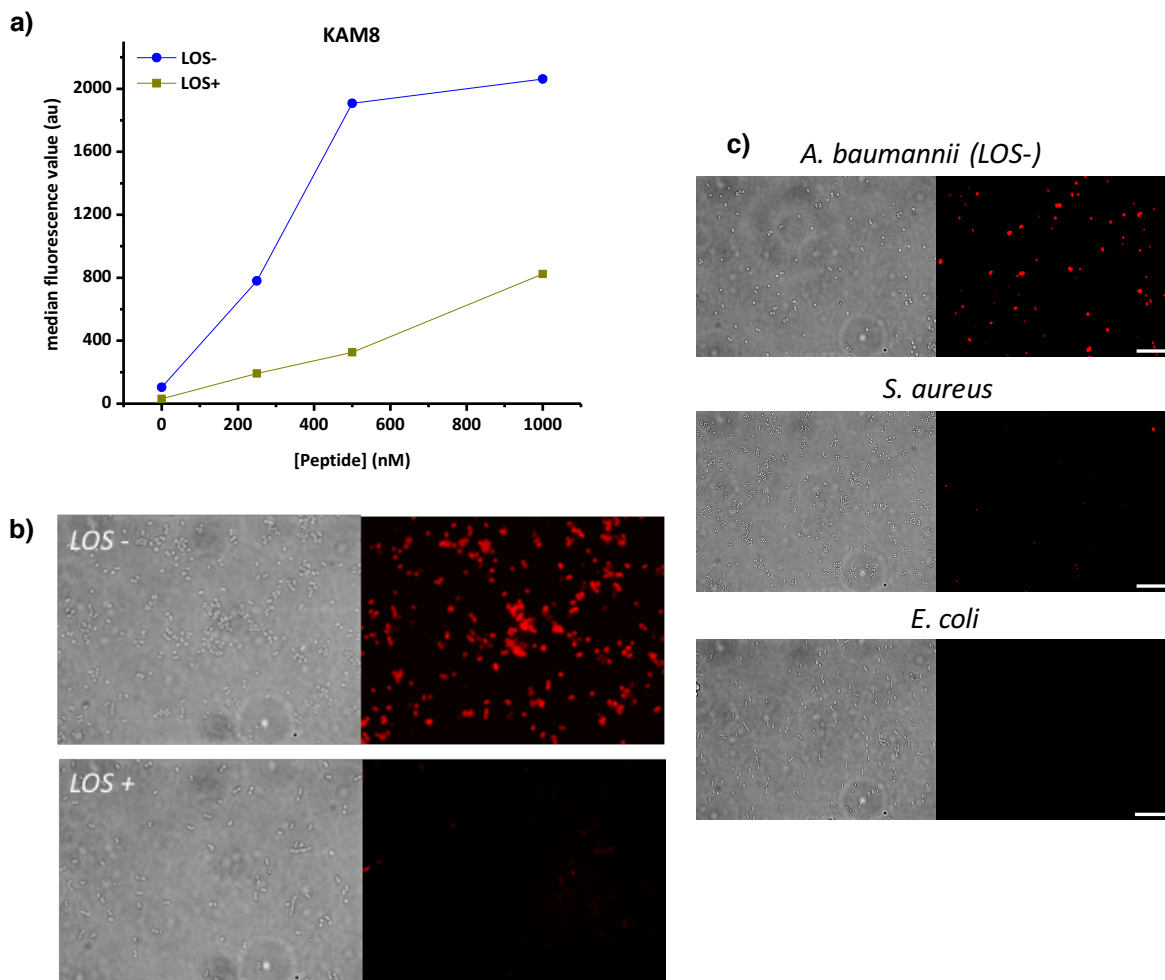


Figure 4-28 (a) Flow cytometry concentration profile of KAM8 against *A. baumannii* strains. (b) Fluorescence microscopy of KAM8 (2 μ M) staining LOS- versus LOS+ *A. baumannii*. (c) Fluorescence microscopy of KAM8 (2 μ M) staining of other bacterial species. Scale bar: 10 μ m.

4.4.3 Generating a Strain-Specific Antibiotic for *A. baumannii* (LOS-)

The feasibility of converting KAM8 into a targeted antibiotic for the LOS- strain of *A. baumannii* via phototoxin conjugation was explored. Toward this end, the KAM8-Eosin conjugate was synthesized, which upon photoirradiation effectively killed the LOS- *A. baumannii* cells (2 μ M, 15 min light, > 90% cell killing, Figure 4-29a). In contrast, eosin alone at these concentrations did not elicit *A. baumannii* cell death nor did KAM8 without

the photosensitizer. KAM8-Eosin was established as a strain-specific antibiotic of the LOS- *A. baumannii* as it demonstrated little killing of the wild-type (LOS+) strain under the same conditions (Figure 4-29b). Collectively, these data showcase that strain-specific bacterial cell killing can be achieved through phage display and selection of the APBA-presenting peptides.

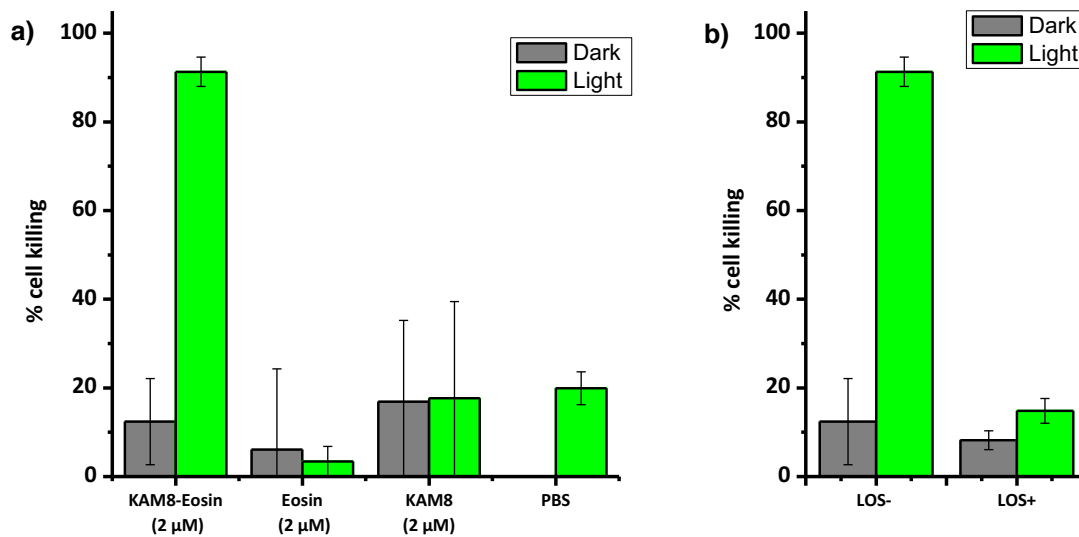


Figure 4-29 (a) Percent killing by KAM8-Eosin and controls with and without photoirradiation. (b) Percent killing of LOS- versus LOS+ strains with KAM8-Eosin (2 μM).

4.4.4 Screening Against Other Mutant *A. baumannii* Strains

We hypothesized that our previously reported APBA-dimer library and live cell screening protocol could be applied to mutant *A. baumannii* strains. Two *A. baumannii* strains, EGA-407 and EGA-408, were sequenced by our collaborators in Professor Tim van Opijnen's lab and displayed mutations in the *pmrAB* system, which controls the *pmrC* gene responsible for the addition of phosphoethanolamine to Lipid A (see Figure 4-1).⁸

Three rounds of panning against the mutant *A. baumannii* strains were executed following the same panning procedure described above for *S. aureus*. After each round of panning, 20 colonies were isolated from the output population and subjected to sequencing, in which convergence was detected starting in round 3 for each strain (Table 4-8). Two peptides from the screen against mutant EGA-407 (KAM18-19) and two peptides from the screen against mutant EGA-408 (KAM20-21) were observed repeatedly and were synthesized via SPPS following the same procedure used for the *S. aureus* binding peptides (Table 4-9).

Table 4-8 Round 3 sequences of the peptide hits for mutant *A. baumannii* binding (a) EGA-407 strain (b) EGA-408 strain. Repeating sequences are color-coded.

a)

Hit #	DNA Sequence	Peptide Sequence
1	GCTTGTGGTTATAGTAGTTTTAATCGGTGC	ACGYSSFNRC
2	GCTTGTGATGCGGTGTTCCGCAGATGTGC	ACDAVFPQMC
3	GCTTGTGATAAGCAGATGCAGTTTGTGTGC	ACHKQMQFVC
4	GCTTGTATACGGAGACTAATGCTCAGTGC	ACYTETNAQC
5	GCTTGTACGCAGGTTCTTATCATTATTGC	ACTQGSYHYC
6	GCTTGTACTAAGCCTACGAATCTGGCGTGC	ACTKPTNLAC
7	GCTTGTATCCGTATACGAAGAGTTATTGC	ACHPYTKSYC
8	n/a	Blank
9	n/a	Blank
10	GCTTGTAGTTGGTTTACGTCTAATCGTTGC	ACSWFTSNRC
11	GCTTGTAGTTGGTTTACGTCTAATCGTTGC	ACSISSLTHC
12	n/a	Blank
13	GCTTGTGGTTATAGTAGTTTTAATCGGTGC	ACGYSSFNRC
14	n/a	Blank
15	n/a	Blank
16	n/a	Blank
17	GCTTGTCTGCCTAATGGGCATGTTACGTGC	ACLPNGHVTC
18	GCTTGTAAATCTAATCCGAAGTCTGCGTGC	ACNLNPKSAC
19	GCTTGTATGATCTGAATGGTAGTATGTGC	ACHDLNGSMC
20	GCTTGTAGTTGGTTTACGTCTAATCGTTGC	ACSWFTSNRC

b)

Hit #	DNA Sequence	Peptide Sequence
1	GCTTGTACTAATGCTAATCATTATTTTGC	ACTNANHYFC
2	GCTTGTACTAATGCTAATCATTATTTTGC	ACTNANHYFC
3	GCTTGTACTCAGAAGCCGTCGACTGTTTGC	ACTQKPSTVC
4	GCTTGTTCGTATTGGTTGAGTGCACGTGC	ACSYWLSATC
5	GCTTGTAACTACTGGTTCGCCTTATGAGTGC	ACNTGSPYEC
6	GCTTGTACTAATGCTAATCATTATTTTGC	ACTNANHYFC
7	n/a	Blank
8	GCTTGTGGTTGGAGAGGACTTCGGCTTGC	ACGLERTSAC
9	GCTTGTAAAGTTGACTACTCAGATGATGTGC	ACKLTTQMMC
10	GCTTGTACTAATGCTAATCATTATTTTGC	ACTNANHYFC
11	GCTTGTATTCTAGTCTTCTCATTATTTTGC	ACYSSPSHFC
12	n/a	Blank
13	GCTTGTATTCTAGTCTTCTCATTATTTTGC	ACYSSPSHFC
14	GCTTGTACTAATGCTAATCATTATTTTGC	ACTNANHYFC
15	GCTTGTACTAATGCTAATCATTATTTTGC	ACTNANHYFC
16	GCTTGTGCGGTGGCCGATTCCGCTGTGTGC	ACRWPDSRLC
17	GCTTGTACTAATGCTAATCATTATTTTGC	ACTNANHYFC
18	GCTTGTCTTTGGAGTACGGGTGCGACTTGC	ACLWSTGATC
19	GCTTGTATTCTAGTCTTCTCATTATTTTGC	ACYSSPSHFC
20	GCTTGTACTAATGCTAATCATTATTTTGC	ACTNANHYFC

Table 4-9 Synthesized peptide hits from mutant *A. baumannii* screening.

C_m: APBA-IA modified Cys, Dap*: Fluorophore modified Dap residue

NAME	PEPTIDE SYNTHESIZED
KAM18	AC _m GYSSFNRC _m GGGDap*
KAM19	AC _m SWFTSNRC _m GGGDap*
KAM20	AC _m TNANHYFC _m GGGDap*
KAM21	AC _m YSSPSHFC _m GGGDap*

Interestingly, a parallel screen against wild-type *A. baumannii* yielded 90% blank sequences after the third round of panning, suggesting no peptide hits could be isolated for the wild-type strain, even though the screen was performed in parallel with the mutant *A. baumannii* selections (Table 4-10). These results are consistent with the fact that wild-type *A. baumannii* does not have amine modification to its LPS, and therefore has no target for the iminoboronate-capable APBA-dimer library. This concept is similar to the previously observed results that no true peptide hits could be discovered with control libraries which do not contain the APBA warheads.

Table 4-10 Sequencing results from round 3 of wild-type *A. baumannii* panning.

Hit #	DNA Sequence	Peptide Sequence
1	GCTTGTAATACTGGTTCGCCTTATGAGTGC	ACNTGSPYEC
2	n/a	Blank
3	n/a	Blank
4	n/a	Blank
5	n/a	Blank
6	n/a	Blank
7	n/a	Blank
8	n/a	Blank
9	n/a	Blank
10	n/a	Blank
11	n/a	Blank
12	n/a	Blank
13	n/a	Blank
14	n/a	Blank
15	n/a	Blank
16	GCTTGTAGGGGTGCTACGCCGATGAGTTGC	ACRGATPMSC
17	n/a	Blank
18	n/a	Blank
19	n/a	Blank
20	n/a	Blank

4.4.5 Characterization of a Colistin-Resistance Sensor Peptide

The mutant *A. baumannii* peptide hits were first assessed for *A. baumannii* binding via flow cytometry. Four strains of *A. baumannii* were analyzed: wild-type (WT), EGA-407, EGA-408, and LOS-. KAM8, the peptide selected from the *A. baumannii* (LOS-) screen, was assessed for binding against the panel of *A. baumannii* species, alongside KAM18-21 in the presence of 1 mg/mL BSA. Flow cytometry revealed staining of the three mutant species with all five peptides, yet no staining of the wild-type strain (Figure 4-30). From these results, it is evident that the APBA-dimer peptides can elicit strong binding with both the amine-modified LPS of *A. baumannii* as well as the lipoprotein-enhanced surface of the LOS- strain.

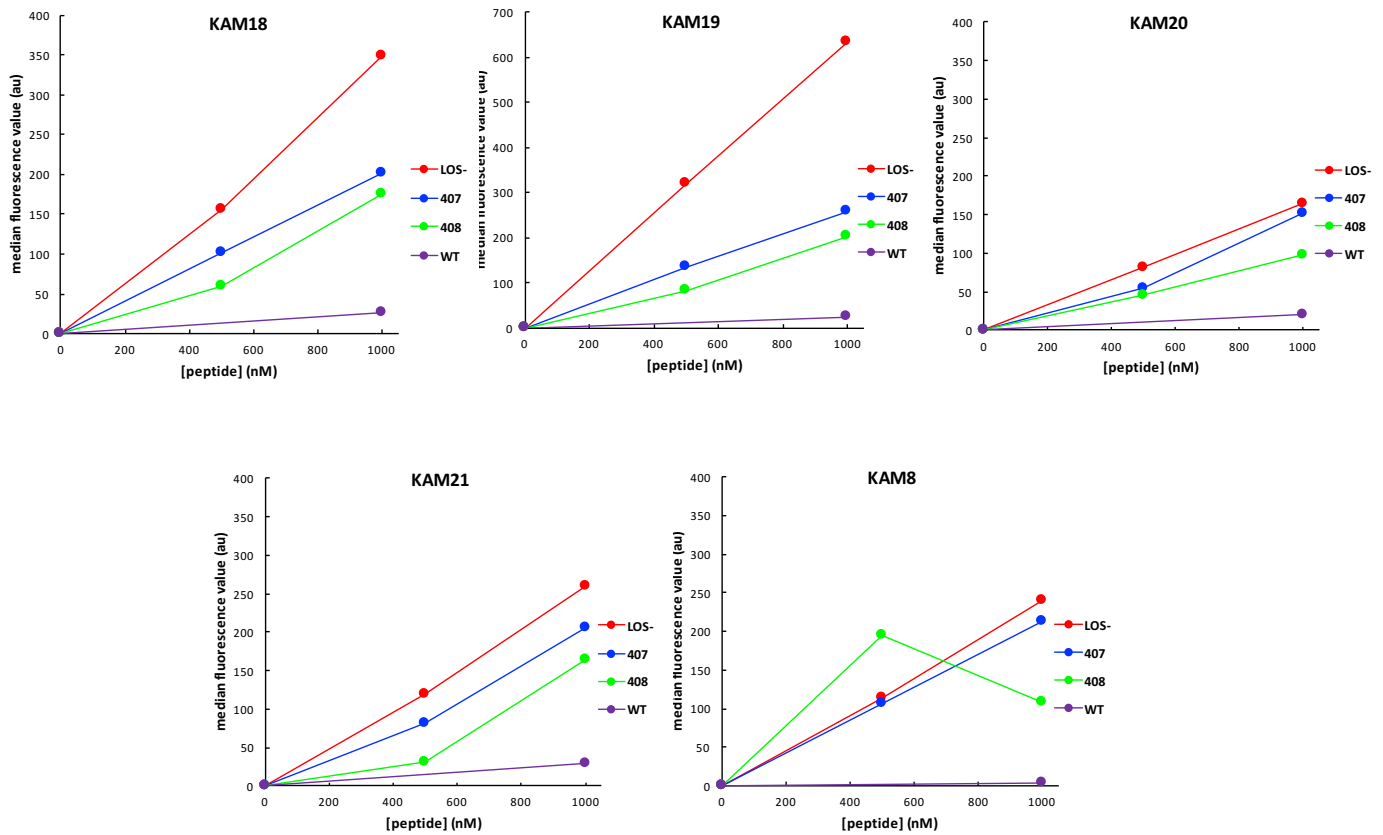


Figure 4-30 Flow cytometry concentration profiles against all four *A. baumannii* strains in presence of 1 mg/mL BSA.

Of particular interest was KAM19, which prompted the strongest response against all mutants. Importantly, the cyclic precursor of KAM19 (KAM19-Cyclic which has no APBA moieties) did not elicit considerable binding to any of the three mutant strains, nor did a negative control peptide KAM6, which was not selected for in this screen and mentioned previously (Figure 4-31).

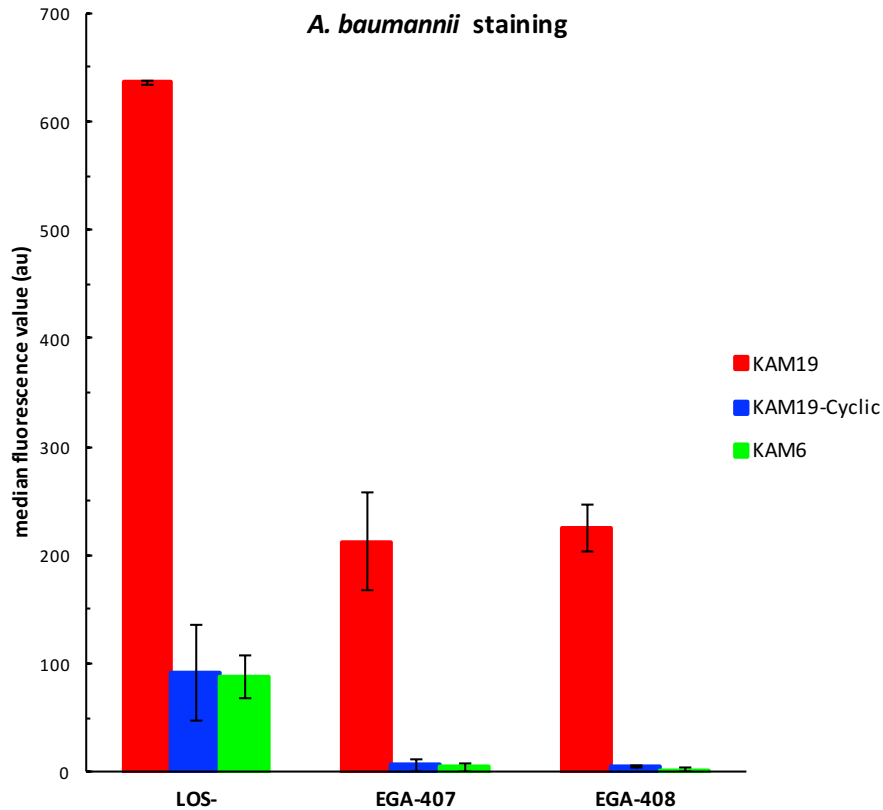


Figure 4-31 Flow cytometry of KAM19 (1 μ M, +1 mg/mL BSA) compared to controls.

Although the medium fluorescent values for the EGA-407 and EGA-408 mutant strains are lower than the values for the LOS- strain, they are still significantly higher than the wild-type screen. Additionally, fluorescence microscopy analysis of TAMRA-labeled KAM19 corroborated flow cytometry data, indicating potent staining of the mutant strains compared to the wild-type strain of *A. baumannii*, which demonstrated no staining (Figure 4-32). It is evident that KAM19 stains the LOS- strain in a consistent manner, while the staining of the EGA-407 and EGA-408 mutants is more uneven between colonies. It is speculated that the EGA-407 strain is a mixture of clones, demonstrating approximately 50% frequency of the *pmrAB* mutation; therefore, it is not surprising that the EGA-407 visibly shows even less staining via microscopy. Perhaps this noticeably variable staining

via fluorescence microscopy rationalizes the lower median fluorescent values from flow cytometry analysis for the EGA-407 and EGA-408 mutants.

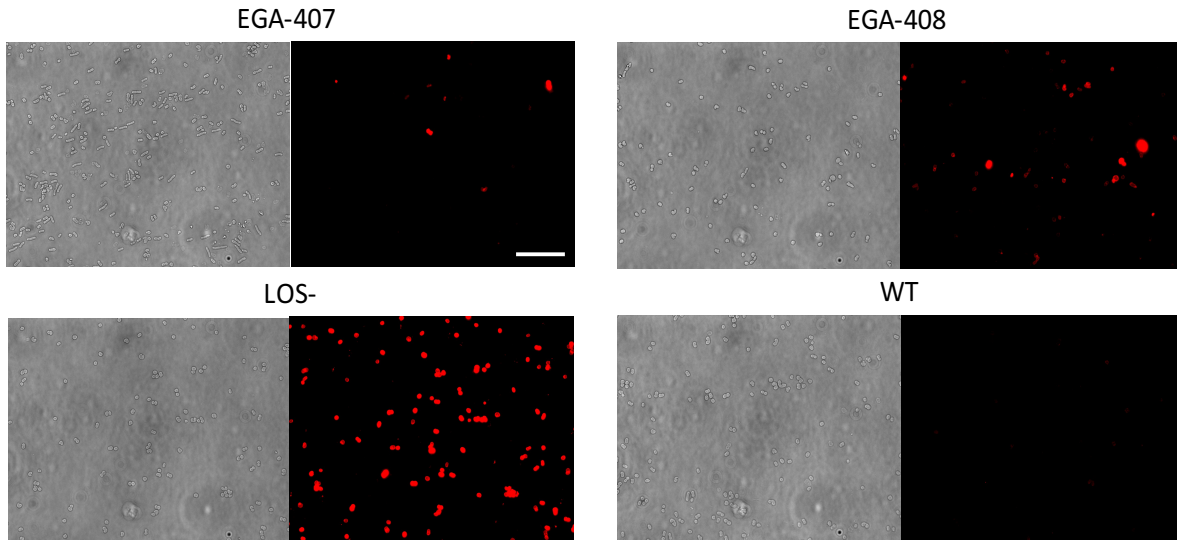


Figure 4-32 Fluorescence microscopy of KAM19 (2 μ M) staining various *A. baumannii* strains in 1 mg/mL BSA. Scale bar: 10 μ m.

4.4.6 Detection of Colistin Resistance in Blood Serum

A clinically relevant peptide must be able to detect colistin resistant *A. baumannii* from colistin sensitive *A. baumannii* in complex biological milieu. Therefore, KAM19 was analyzed for its binding activity in the presence of blood serum. Fluorescence microscopy analysis of a co-culture containing various percentage of wild-type *A. baumannii* to LOS-*A. baumannii* visibly depicts that the amount of cells stained by KAM19 increases as ratio of wild-type: mutant decreases (Figure 4-33). This data demonstrates that the mutant strains of *A. baumannii* can be detected with our selective peptide probes over wild-type *A. baumannii* and in a complex biological setting.

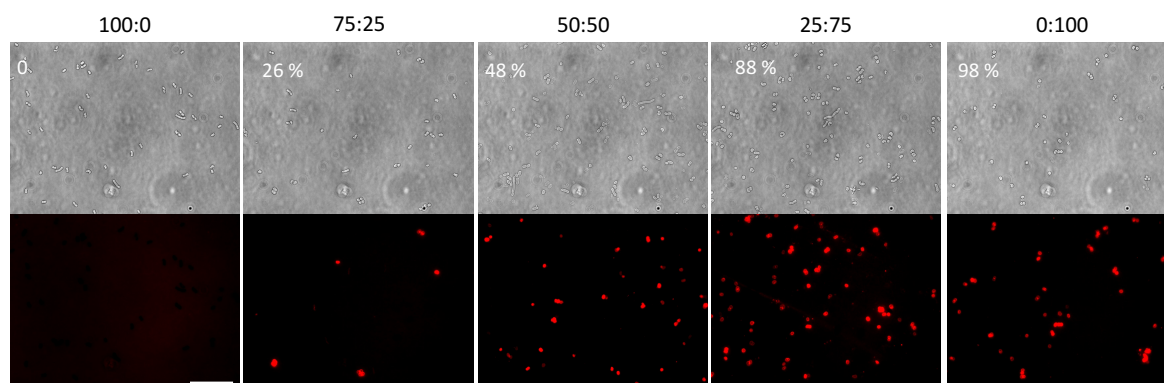


Figure 4-33 Fluorescence microscopy of KAM19 (2 μ M) against co-culture of *A. baumannii* (wild-type: LOS- ratio displayed) in 25% human serum. A percent staining estimation based on the amount of colonies stained is indicated on each image. Scale bar: 10 μ m.

4.5 Serum Stability of APBA-Dimer Peptides

4.5.1 Serum Stability Assessment of APBA-Presenting Peptides

A general problem associated with peptide therapeutics is their susceptibility to protease degradation in the blood stream.³⁰ The stability of these APBA-dimer peptides was assessed via analytical HPLC after treatment with 25% human blood serum. KAM5-Eosin (25 μ M) was subjected to 25% serum and incubated at 37 $^{\circ}$ C. Aliquots were removed and analyzed via HPLC for peptide purity. An iodoacetamide-capped KAM5 (KAM5-IA, no APBA moieties) was analyzed in parallel to observe the effect of the APBA warheads. Excitingly, KAM5 displayed excellent serum stability after 24 hr of incubation in serum with only 20% peptide degradation observed. Conversely, KAM5-IA showed complete degradation after just 6 hr of incubation (Figure 4-34).

Serum Stability

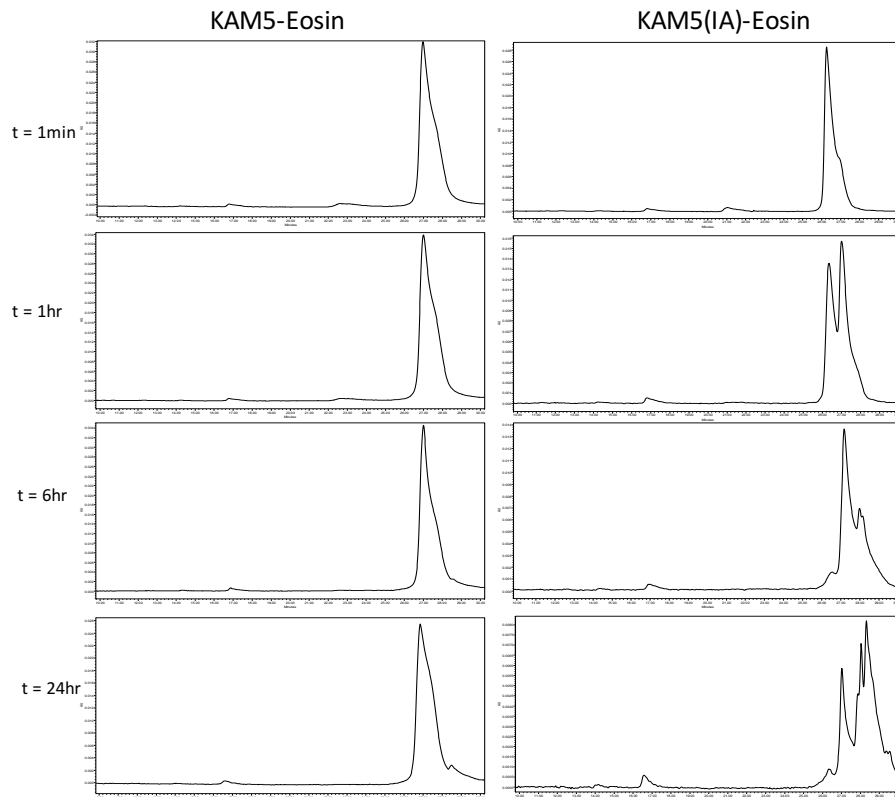
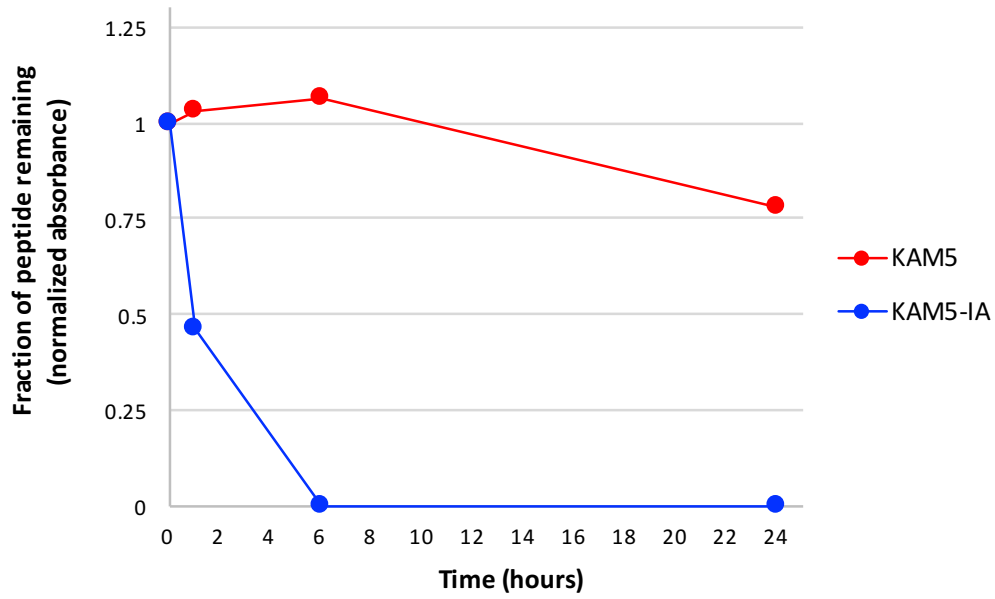


Figure 4-34 Serum stability of KAM5-Eosin compared to KAM5(IA)-Eosin. (a) Graphical representation displaying fraction of peptide remaining over time, calculated via normalized absorbance values. (b) HPLC chromatograms analyzing peptide integrity at various time points.

We hypothesized that the serum stability of KAM5 is due to the ability of the APBA-dimer peptides to bind albumin (see Figure 4-9), which could provide a protective effect against protease degradation. The serum stability was not specific to KAM5, as KAM8-Eosin and KAM19-FAM were significantly more stable than their iodoacetamide-capped derivative as well (Figure 4-35).

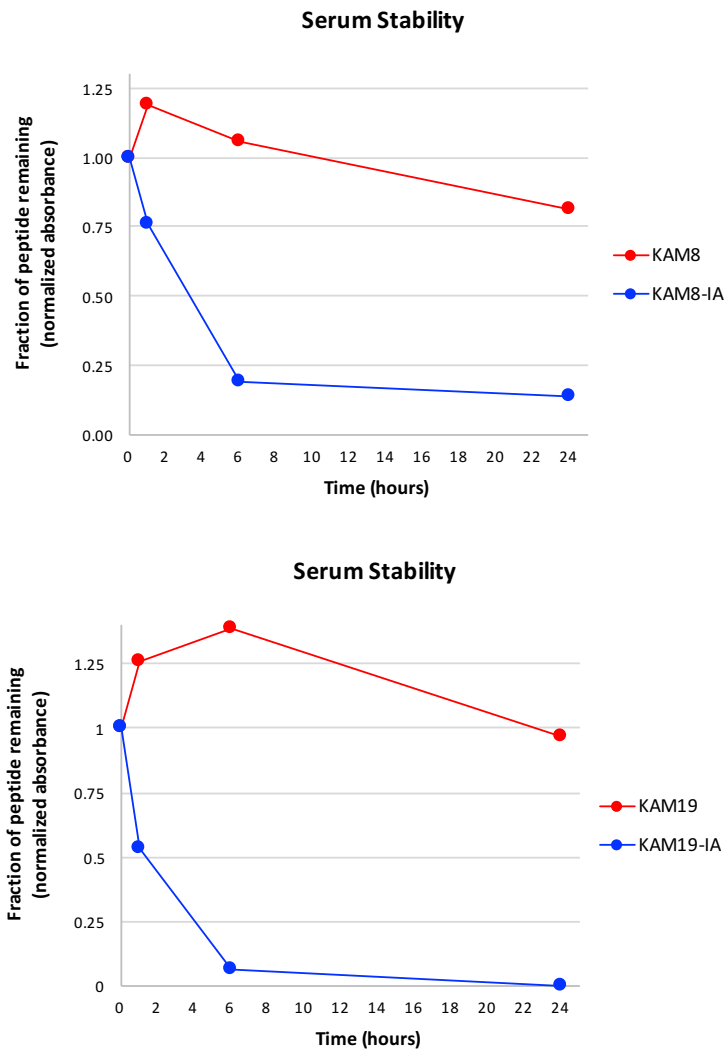


Figure 4-35 Serum stability of KAM8-Eosin and KAM19-FAM compared to KAM8(IA)-Eosin and KAM19(IA)-FAM.

4.6 Conclusions

The APBA-dimer library was able to successfully yield submicromolar peptide binders of specific species, and even strains, of bacteria via live cell panning. Specifically, a peptide probe for *S. aureus*, KAM5, and a peptide probe for LOS deficient *A. baumannii*, KAM8, were discovered. The phage panning against intact cells is remarkably convenient and powerful, allowing facile incorporation of negative screens and internal competitors. Abundant endogenous protein could compete for iminoboronate conjugation, thereby inhibiting the bacterial binding of an APBA-containing peptide.¹² This data clearly demonstrates that this protein interference problem can be overcome by including serum albumin in the screening mixture and the reversible covalent binding mechanism can afford highly selective binders in complex biological milieu.

With KAM5, the ability of creating a *S. aureus* selective antimicrobial agent was explored. Unfortunately, conjugation of various hydrophobic groups and antimicrobial peptides did not elicit or improve upon *S. aureus* cell killing. However, the conjugation of a phototoxin, eosin, allowed for selective *S. aureus* cell death upon irradiation with visible light. This phototoxin conjugation strategy was applied to KAM8 as well, allowing for eradication of the targeted LOS-deficient *A. baumannii* strain. The facile generation of targeted antibiotics is of contemporary importance given the undesirable consequences of broad-spectrum antibiotics, which inevitably cultivate antibiotic resistance and cause damage to human microbiota. Further investigation is needed to elucidate the binding mechanisms and targets of the peptide binders to fully understand the lack of activity of the other KAM5 conjugates.

Panning the APBA-dimer library against other colistin resistant strains of *A. baumannii*, which exhibit mutations responsible for the addition of phosphoethanolamine to the LPS outer membrane, demonstrates the capability of the library to discover potent peptide probes of various relevant bacterial pathogens, particularly those that show antibiotic resistance (see Figure 4-1). The iminoboronate-capable APBA-dimer library elucidated KAM19, a peptide probe with the ability to distinguish colistin resistant strains of *A. baumannii* (EGA-407, EGA-408 and LOS-) versus wild-type *A. baumannii*. Additionally, the peptide was able to make this distinction in the presence of human blood serum. The robust APBA-dimer peptides that are borne out of the APBA-dimer phage library not only elicit strong binding to their target bacteria, but they also exhibit excellent serum stability. The data presented here demonstrates the promise of chemically modified phage libraries. It is intriguing to speculate that even higher potency binding could be accomplished with better designed phage libraries with reversible covalent warheads.

4.7 Experimental Procedures

4.7.1 General Methods

The Ph.D.[™]-C7C Phage Display Peptide Library Kit and the *E. coli* K12 ER2738 strain were purchased from NEB. All ER2738 strains were grown with 20 µg/mL tetracycline. Chemical reagents for library modification and peptide synthesis were purchased from various vendors and used as received. *S. aureus* (ATCC 6538) and *B. subtilis* (ATCC 663) were purchased as lyophilized pellets from Microbiologics (Cloud, MN). MRSA (ATCC 43300) was purchased from ATCC (Manassas, VA). *E. coli* (BL21) was a gift from the laboratory of

Professor Mary Roberts. Wild-type *A. baumannii* (AB5075³¹) and mutant *A. baumannii* strains (LOS-, EGA-407 and EGA-408) were provided by the laboratory of Professor Tim van Opijnen. Strains EGA-407 and EGA-408 were grown in the presence of 8 µg/mL colistin. All titering experiments were plated on IPTG/Xgal-containing agar. Mass spectrometry data were generated by using an Agilent 6230 LC TOF mass spectrometer. Peptide synthesis was carried out on a Tribute peptide synthesizer from Protein Technologies and purified via RP-HPLC on a Waters Prep LC with a Jupiter C18 column (Phenomenex) with acetonitrile/water (0.1% TFA) eluent unless specified otherwise. The peptide concentration of all samples used in these studies were determined by measuring their absorbance at 495 nm ($\epsilon = 75,000 \text{ M}^{-1} \text{ cm}^{-1}$ for fluorescein), at 556 nm ($\epsilon = 89,000 \text{ M}^{-1} \text{ cm}^{-1}$ for TAMRA) or at 525 nm ($\epsilon = 95,000 \text{ M}^{-1} \text{ cm}^{-1}$ for Eosin) on a Nanodrop 2000c UV/VIS spectrometer or by weight when no fluorophore present. Fluorescence images were taken on a Zeiss Axio Observer A1 inverted microscope. Flow cytometry analysis was carried out on a BD FACSAria cell sorter housed in the Biology Department at Boston College. Photoinactivation was performed with a X-Cite 120Q (120-W lamp) excitation light source accompanied by the Zeiss microscope. Jurkat T lymphocytes were a gift from the Johnson lab at Boston College, HEK293T cells were a gift from the Weerapana lab at Boston College, and mammalian cell cytotoxicity was evaluated on a SpectraMax M5 plate reader along with fluorescence anisotropy and MIC assays. Serum stability was assessed on a Waters Analytical LC with a Jupiter C18 column (Phenomenex).

4.7.2 Panning Against Live Cells

S. aureus was grown to an $OD_{600} \approx 1.0$ ($\sim 1 \times 10^9$ cfu/mL) in LB medium. The cells (1 mL) were washed with chilled PBST (0.05%) twice and resuspended in PBS (pH 7.4) with 10 mg/mL BSA present. The APBA-labeled phage library ($\sim 1 \times 10^{10}$ pfu) was added to the cell suspension and allowed to incubate on ice for 1 hr. The cells were washed with PBST (3x) and PBS (3x) to remove unbound phage. Cell-bound phage were incubated with 200 μ L elution buffer (Glycine-HCl, pH 2.2, 1 mg/mL) for 15 min followed by centrifugation of the cells. The supernatant was removed and neutralized with 150 μ L Tris-HCl (pH 9.1). All Eppendorf tubes utilized in the panning procedure were blocked with 10 mg/mL BSA before use. Centrifugation of cells was performed at 5000 rcf for 5 min. The eluted bound phage solution was added to early log phase ER2738 and amplified for 4.5 hr followed by precipitation to isolate the amplified phage. The amplified phage were labeled with APBA-IA and subjected to the next round of panning. The phage titer was calculated before and after each round of panning to determine the input and output population. Individual phage colonies from each round of panning were amplified in ER2738. Phage DNA was isolated using a Qiagen miniprep kit and sent for sequencing analysis by Eton Bioscience, Inc. The screens against *S. aureus* with the unmodified C7C library and the IA-alkylated library (C7C-IA) were performed following the same protocol. The C7C-IA library was prepared using the same protocol described for the APBA-dimer library preparation except with simple iodoacetamide. The screen against *A. baumannii* (LOS-) was performed following the same protocol; however, a negative screen was introduced against wild-type *A. baumannii* starting in the second round. In the negative screen, the

phage library was incubated with wild-type *A. baumannii* for 1 hr, the supernatant was removed and subsequently subjected to the positive screen against *A. baumannii* (LOS-). The screens against wild-type *A. baumannii*, EGA-407 and EGA-408 were performed following the same protocol for the *S. aureus* screen.

4.7.3 Phage-binding Microscopy

For the screen against *S. aureus*, individual phage variants in which sequence repetition was observed were reduced and labeled with APBA-IA. *S. aureus* was grown to an $OD_{600} \approx 1.0$, washed and diluted with PBS (pH 7.4). The cells ($\sim 1 \times 10^9$ cfu/mL) were incubated with 10^6 , 10^8 and 10^{10} pfu/mL of each labeled phage hit for 1 hr in the presence of 10 mg/mL BSA. Fluorescein labeled anti-M13 major coat protein antibody (1 μ g, Santa Cruz Biotechnology) was added to the bacterial suspension, incubated for 30 min and directly subjected to fluorescence microscopy analysis. Antibody binding to *S. aureus*, with no phage present, was also analyzed to assess any background fluorescence. White light and fluorescent images were obtained on the Zeiss microscope equipped with filter set 44 (excitation: BP 475/40, emission: BP 530/50) suitable for detection of fluorescein fluorescence. Images were captured using the 100X oil immersion objective with a 500 ms exposure time. All images were processed consistently using ImageJ software.

4.7.4 Synthesis of Peptide Repeats

SPPS was performed on a Rink Amide MBHA solid support using Fmoc/*t*Bu chemistry on a 0.05 mmol scale. Five equivalents of commercially available amino acids were used for the coupling reaction with HBTU as an activating reagent. An Alloc-protected Dap residue was installed at the C-terminus for on-resin coupling of a fluorophore, followed by a triple

glycine linker and the peptide hit sequence at the N-terminus. 5(6)-carboxyfluorescein, 5(6)-carboxytetramethylrhodamine or 5(6)-carboxyeosin was conjugated to the peptide on resin by first removing the Alloc protecting group, as described in Chapter 2, followed by subsequent HBTU-mediated amide bond coupling in 0.4 M NMM/DMF. The peptides were cleaved off resin and globally deprotected with Reagent B (88% TFA, 5% water, 2% triisopropylsilane, 5% phenol). Crude peptides were obtained via ether precipitation and purified by RP-HPLC. For cysteine alkylation, each peptide hit was treated with 3 equivalents of APBA-IA (or IA for controls) in the presence of TCEP (2 equivalents) in 2 M NMM/DMF for 3 hr and purified via RP-HPLC. All peptides were characterized via LC-MS for excellent purity (>95%) and correct masses (Tables 4-11 – 4-14).

Table 4-11 Mass spec data of *S.aureus* peptide hits.

Peptide	Calculated m/z	Observed m/z
KAM1-FAM	1073.93 [M-H ₂ O+H] ²⁺	1073.92
KAM2-FAM	1144.48 [M-2H ₂ O+H] ²⁺	1144.46
KAM3-FAM	1180.59 [M-H ₂ O+H] ²⁺	1180.92
KAM4-FAM	1153.44[M-H ₂ O+H] ²⁺	1153.92
KAM5-FAM	1120.43 [M-H ₂ O+H] ²⁺	1120.42
KAM5-Cyclic (FAM)	1703.64 [M+H] ⁺	1703.63
KAM5-TAMRA	1138.48 [M-2H ₂ O+H] ²⁺	1138.44
KAM5-Eosin	1268.78 [M-2H ₂ O+H] ²⁺	1268.71
KAM5-IA (Eosin)	2134.49 [M+H] ⁺	2134.28

Table 4-12 Mass spec data of peptides from control library screen.

Peptide	Calculated m/z	Observed m/z
KAM14-FAM	1628.83 [M+H] ⁺	1628.53
KAM15-FAM	1714.80 [M+H] ⁺	1714.53
KAM16-FAM	1883.69 [M+H] ⁺	1883.64
KAM17-FAM	1751.92 [M+H] ⁺	1751.67

Table 4-13 Mass spec data of *A. baumannii* (LOS-) peptide hits.

Peptide	Calculated m/z	Observed m/z
KAM7-FAM	1083.45 [M-H ₂ O+H] ²⁺	1083.90
KAM8-FAM	1091.48 [M-H ₂ O+H] ²⁺	1091.92
KAM8-Cyclic (FAM)	1645.65 [M+H] ⁺	1645.63
KAM8-TAMRA	1109.49 [M-2H ₂ O+H] ²⁺	1109.98
KAM8-Eosin	1258.30 [M-H ₂ O+H] ²⁺	1258.26
KAM8-IA (Eosin)	2077.49 [M+H] ⁺	2077.30
KAM9-FAM	1078.46 [M+H] ²⁺	1078.41
KAM10-FAM	1129.44 [M-2H ₂ O+H] ²⁺	1129.39

Table 4-14 Mass spec data of *A. baumannii* (EGA-407 and EGA-408) peptide hits.

Peptide	Calculated m/z	Observed m/z
KAM18-FAM	1129.99 [M-H ₂ O+2H] ²⁺	1129.92
KAM19-FAM	1163.53 [M-H ₂ O+H] ²⁺	1163.42
KAM19-Cyclic (FAM)	1790.90 [M+H] ⁺	1790.65
KAM19-TAMRA	1190.13 [M-2H ₂ O+H] ²⁺	1190.46
KAM19-IA (FAM)	952.05 [M+H] ²⁺	952.32
KAM20-FAM	1147.50 [M-H ₂ O+H] ²⁺	1147.91
KAM21-FAM	1126.48 [M-H ₂ O+H] ²⁺	1126.88

4.7.5 Flow Cytometry Analysis

Each bacterial strain was grown to an OD₆₀₀ ≈ 0.5, washed and diluted with PBS (pH 7.4). The cells (~1 × 10⁷ cfu/mL) were incubated with various concentrations of FAM-labeled peptide in PBS or with 1 mg/mL BSA in PBS as indicated in each experiment. After incubation for 1 hr, samples were subjected to cytometric analysis. Data obtained were analyzed via BD FACSDiva software and median fluorescent values were computed from the generated histograms. All flow cytometry experiments were repeated and generated consistent results.

4.7.6 Fluorescence Microscopy

Each bacterial strain was grown to an OD₆₀₀ ≈ 1.0, washed and diluted with PBS (pH 7.4). The cells (~1 × 10⁹ cfu/mL) were incubated with various concentrations of TAMRA-labeled

peptide in PBS alone or with BSA/human serum in PBS for 1 hr. White light and fluorescent images were obtained on the Zeiss microscope equipped with filter set 20 HE (excitation: BP 546/12, emission: BP 607/80) suitable for detection of TAMRA fluorescence. Images were captured using the 100X oil immersion objective with a 500 ms exposure time. All images were processed consistently using ImageJ software.

4.7.7 Fluorescence Anisotropy

BSA or HSA was added at various concentrations to a Costar black/clear-bottom 96-well plate from a stock solution in PBS (pH 7.4). The FAM-labeled peptides or FAM (500 nM) were added to the 96-well plate in triplicate. Endpoint fluorescence polarization readings were obtained hourly until they leveled off. Anisotropy generated saturation binding curves were plotted as an average of three trials with standard deviation error.

4.7.8 KAM5 Conjugate Synthesis

Synthesis of Hydrophobic Conjugates. Fmoc-ACVSPRSHECGGG-Dap(Alloc) was synthesized via SPPS as described above. For KAM5-12, the Alloc group was removed and subjected to HBTU-mediated amide bond coupling with 5 equivalents of lauric acid in 0.4 M NMM/DMF on the Dap amine followed by Fmoc removal. For 12-KAM5, the Fmoc protecting group was removed and subjected to HBTU-mediated amide bond coupling with 5 equivalents of lauric acid in 0.4 M NMM/DMF on the N-terminal amine. For 12-KAM5-12, the Alloc and Fmoc protecting groups were removed and subjected to HBTU-mediated amide bond coupling with 10 equivalents of lauric acid in 0.4 M NMM/DMF on both amines. For Bn-KAM5, Ad-KAM5 and TP-KAM5, Fmoc-Lys(Fmoc)-OH was first conjugated to the N-terminus of KAM5. The Fmoc protecting groups were removed and

subjected to 10 equivalents of benzoyl chloride in DCM and DIPEA or 10 equivalents of adamantane carbonyl chloride in DCM and DIPEA for Bn-KAM5 and Ad-KAM, respectively. For TP-KAM5 the amines were subjected to HBTU-mediated amide bond coupling with 10 equivalents of *p*-terphenyl-4-carboxylic acid in pyridine with minimal DMF (for solubility). For TP-K-KAM5, Fmoc-Lys(Boc)-OH was instead conjugated to the N-terminus of the peptide. The Fmoc group was removed and 5 equivalents of *p*-terphenyl-4-carboxylic acid were coupled to the N-terminal amine as described above. Upon conjugation of the hydrophobic groups, each peptide was subjected to cleavage from resin and global deprotection with Reagent B and purified via RP-HPLC. Cysteine alkylation with APBA-IA was performed as described above and purified via RP-HPLC. All peptides were characterized via LC-MS for excellent purity (>95%) and correct masses (Table 4-15). ClogP values were generated via ChemDraw software, focusing on the terminal portion of the peptide incorporating the hydrophobic entity.

Table 4-15 Mass spec data of hydrophobic KAM5 peptides.

Peptide	Calculated m/z	Observed m/z
KAM5-12	1022.98 [M-2H ₂ O+H] ²⁺	1023.03
12-KAM5	1074.02 [M-H ₂ O+H] ²⁺	1074.07
12-KAM5-12	1124.57 [M+H] ²⁺	1123.56
Bn-KAM5	1151.06 [M-H ₂ O+H] ²⁺	1151.48
Ad-KAM5	1209.19 [M-H ₂ O+H] ²⁺	1209.55
TP-K-KAM5	1166.11 [M-2H ₂ O+H] ²⁺	1166.49
TP-KAM5	1303.26 [M-H ₂ O+H] ²⁺	1303.54

Synthesis of Vancomycin Conjugates. CuAAC was employed to conjugate KAM5 to vancomycin; therefore, various KAM5-azide and vancomycin-alkyne derivatives were synthesized. Three different KAM5-azide derivatives were synthesized. Fmoc-ACVSPRSHECGGG-Dap(Alloc) was synthesized via SPPS as described above and subjected to Alloc deprotection. For the derivative used in KAM5-Vanc1 and KAM5-Vanc2, 5 equivalents of 2-azidoacetic acid were coupled to the Dap residue via HBTU-mediated amide bond coupling in 0.4 M NMM/DMF. For the derivative used in KAM5-Vanc3, 5 equivalents of 6-aminohexanoic acid were coupled to the Dap residue via HBTU-mediated amide bond coupling in 0.4 M NMM/DMF followed by subsequent coupling of 5 equivalents of 2-azidoacetic acid. For the derivative used in KAM5-Vanc4, 3 equivalents of azido-PEG3-NHS were coupled to the Dap residue in DMF and DIPEA. Upon attachment of the azide, each peptide was subjected to cleavage from resin and global deprotection with Reagent B followed by purification via RP-HPLC. Two vancomycin derivatives were synthesized with the alkyne attached to the vancosamine amine or the C-terminal carboxylic acid, denoted VancAlk1 and VancAlk2, respectively. For VancAlk1, 4-pentynoic acid (10 mg, 0.1 mmol), N-hydroxysuccinimide (28 mg, 0.25 mmol) and N,N'-dicyclohexylcarbodiimide (21 mg, 0.1 mmol) were dissolved in DMSO (600 μ L) and stirred at room temperature for 1 hr. Vancomycin-HCl (60 mg, 0.04 mmol) was added to the NHS-activated alkyne along with DIPEA (35 μ L, 0.2 mmol) and allowed to stir at room temperature for 24 hr. Upon reaction completion, monitored via LC-MS, the product was purified via RP-HPLC using acetonitrile/water (0.1% formic acid) as the eluent. For VancAlk2, Vancomycin-HCl (100 mg, 0.07 mmol) was dissolved in DMF/DMSO (1:1, 2 mL)

and stirred in 3 Å molecular sieves for 30 min. Sieves were removed and propargylamine (10 µL, 0.14 mmol) was added and the reaction was allowed to cool on ice. HBTU (38 mg, 0.1 mmol) and DIPEA (67 µL, 0.4 µmol) were added and the reaction mixture was allowed to stir at room temperature overnight. Upon reaction completion, monitored via LC-MS, the product was purified via RP-HPLC using the 0.1% formic acid buffer system. CuAAC was performed by mixing KAM5-azide and Vancomycin-alkyne in a 1:1 ratio with CuSO₄ (2 equivalents) and NaAsc (4 equivalents) in water with minimal DMF (~2 mM reaction) for 1 hr. The clicked products were purified via RP-HPLC using the 0.1% formic acid buffer system. Cysteine alkylation with APBA-IA was performed as described above and purified via RP-HPLC with the 0.1% formic acid system. All peptides were characterized via LC-MS for excellent purity (>95%) and correct masses (Table 4-16).

Synthesis of KAM5-Hlys. CuAAC was also employed to synthesize KAM5-Hlys. For Hlys, Fmoc-RYWVAWRNR-Dap(Alloc) was synthesized via SPPS on a Rink Amide MBHA resin. Upon Alloc deprotection, HBTU-mediated amide bond coupling was utilized to conjugate 5 equivalents of 4-pentynoic acid to the Dap residue in 0.4 M NMM/DMF. The N-terminus was Fmoc deprotected and the peptide was subjected to cleavage from resin and global deprotection with Reagent B. Hlys-alkyne was purified via RP-HPLC. The shortest KAM5-azide derivative, used for KAM5-Vanc1/2, was subjected to CuAAC with Hlys-alkyne and subsequent cysteine alkylation following the same protocol as described above and purified via RP-HPLC. KAM5-Hlys was characterized via LC-MS for excellent purity (>95%) and correct mass (Table 4-16).

Synthesis of KAM5-m146. CuAAC was also employed to synthesize KAM5-m146. The m-146 compound was provided as an alkyne by the laboratory of Professor Jianfeng Cai. The KAM5-azide derivative with the PEG linker, used for KAM5-Vanc4, was subjected to CuAAC with m-146 and subsequent cysteine alkylation with APBA-IA following the same protocol as described above and purified via RP-HPLC. KAM5-m146 was characterized via LC-MS for excellent purity (>95%) and correct mass (Table 4-16).

Synthesis of VIH-KAM5. Fmoc-ACVSPRSHECGGG-Dap(Alloc) was synthesized via SPPS as described above. The tripeptide segment Val-Ile-His was added to the N-terminus of the peptide via SPPS. The peptide was Fmoc deprotected, cleaved from resin/globally deprotected and purified via RP-HPLC as described above. The peptide was labeled with APBA-IA and purified as described above. VIH-KAM5 was characterized via LC-MS for excellent purity (>95%) and correct mass (Table 4-16).

Table 4-16 Mass spec data of KAM5 conjugates.

Peptide	Calculated m/z	Observed m/z
KAM5-Vanc1	1165.02 [M-H ₂ O+H] ³⁺	1165.09
KAM5-Vanc2	1150.68 [M-H ₂ O+H] ³⁺	1150.76
KAM5-Vanc3	1216.75 [M-H ₂ O+H] ³⁺	1216.68
KAM5-Vanc4	1213.75 [M-H ₂ O+H] ³⁺	1213.76
KAM5-Hlys	1164.88 [M-H ₂ O+H] ³⁺	1164.85
KAM5-m146	1402.44 [M-2H ₂ O+H] ²⁺	1402.66
VIH-KAM5	1157.53 [M-H ₂ O+H] ²⁺	1157.99

4.7.9 Minimum Inhibitory Concentration Determination

MIC values for each peptide and positive control were determined using the broth microdilution method.³² *S. aureus* was grown to an $OD_{600} \approx 0.6$ and diluted in LB media to a concentration of $\sim 5 \times 10^5$ cfu/mL. The cell suspension (200 μ L) was added to each well of a Costar 96-well plate. To each well, serial diluted (2-fold) peptides in DMSO (2 μ L) were added in triplicate. The plate was allowed to incubate at 37 °C while OD_{600} readings were obtained every 20 min for 12 hr on the microtiter plate reader. The averaged OD_{600} readings were plotted over time for each peptide. To generate MIC graphs, the OD_{600} readings at the time point where an untreated sample began to level off were plotted versus concentration of peptide. For co-treatment assays, the bacterial suspensions were first incubated with KAM5 (3 μ M) for 15 min before antibiotic treatment and OD_{600} readings.

4.7.10 Photoinactivation of Bacteria

Each bacterial strain was grown to an $OD_{600} \approx 0.7$, washed and diluted with PBS (pH 7.4). The cells ($\sim 1 \times 10^8$ cfu/mL) were incubated with eosin-conjugated peptides and various controls for 15 min. Half of the bacterial suspension was removed and placed in a 96-well plate (Corning 3595). The well was subjected to photoirradiation on the Zeiss microscope using the 20 \times objective and fluorescein filter to emit blue light for 15 min. Cells were diluted in LB media, spread on LB agar plates and incubated overnight at 37 °C. The *A. baumannii* (LOS-) strain was spread on LB agar (+10 μ g/mL polymyxin b) and incubated for 24 hr. The amount of cell killing was calculated by comparing the amount of colonies

of treated bacteria to an untreated PBS control. All experiments were repeated, and the average cell killing of two trials was plotted.

4.7.11 MTT Assay to Assess Mammalian Cell Toxicity

Jurkat cells were cultured in RPMI 1640 (containing 10% FBS, 2 mM glutamine, 1% Penicillin/Streptomycin) and maintained at 5×10^5 cells/mL. Cells were diluted in RPMI and distributed to a 96-well plate (Corning 3595) at 50,000 cells/well (200 μ L/well). 2 μ L of a 100X DMSO solution of KAM5-Eosin (200 μ M) and KAM8-Eosin (200 μ M) was added to each well and incubated for 24 hr. A positive control for viability of DMSO treated cells along with a positive control for cytotoxicity of camptothecin at 50 μ M (5 mM DMSO stock) were included. For photoirradiation, the cells were incubated with the compound of interest for 15 min, each well was irradiated for 15 min (see photoinactivation protocol) and the plate was returned to the incubator for the remainder of the 24 hr incubation. Cells were centrifuged for 5 min (180 rcf) and the supernatant culture medium was carefully removed. 100 μ L of 3-(4,5-dimethylthiazol-2-yl)-2,5-diphenyltetrazolium bromide (MTT, 0.5 mg/mL in RPMI) was added to each well and incubated for 4 hr followed by the addition of 10% SDS in 0.01 M HCl (100 μ L) and incubation overnight. HEK293T cells were grown in complete DMEM (containing 10% FBS, 2 mM glutamine and 1% Penicillin/Streptomycin) to about 80% confluency in a 150 mm dish. Cells were removed from the plate with 0.25% trypsin protease solution (containing EDTA) at 37 °C for 5 min and pelleted (3,500 rpm, 5 min). Cells were diluted in DMEM, distributed to a 96-well plate (Corning 3595) at 30,000 cells/well (100 μ L/well) and incubated for 24 hr to allow for cell adherence. 1 μ L of 100X DMSO solutions were added to each well and

incubations/photoirradiation were performed as described above. After 24 hr, the supernatant culture medium was carefully removed and the cells were incubated with 100 μ L MTT (0.5 mg/mL in RPMI) for 4 hr followed by the addition of 10% SDS in 0.01 M HCl (100 μ L) and incubation overnight. All incubations were performed at 37 °C and 5% CO₂. Absorbance readings were measured at 570 nm and cell viability was normalized to the DMSO control as an average of three trials for non-irradiated samples and an average of two trials for photoirradiated samples with standard deviations.

4.7.12 Analytical HPLC Analysis of Serum Stability

Human serum was diluted to 25% in RPMI medium and temperature equilibrated at 37 °C for 10 min. KAM5 or KAM5-IA was added to serum at a concentration of 25 μ M. Aliquots were removed at various time points: 1 min, 1 hr, 6 hr and 24 hr. Each aliquot was centrifuged (1 min, 14 000 rpm) and the supernatant was directly analyzed via analytical HPLC. A plot of the fraction of intact peptide remaining versus time was established for each peptide based on the initial (t = 1 min) absorbance value. The same protocol was used for KAM8 and KAM19.

4.8 References

1. Huang, J. X., Bishop-Hurley, S. L. & Cooper, M. A. Development of Anti-Infectives Using Phage Display : Biological Agents against Bacteria, Viruses, and Parasites. *Antimicrob. Agents Chemother.* **56**, 4569–4582 (2012).
2. Gasanov, U., Koina, C., Beagley, K. W., Aitken, R. J. & Hansbro, P. M. Identification of the Insulin-Like Growth Factor II Receptor as a Novel Receptor for Binding and Invasion by *Listeria monocytogenes*. *Infect. Immun.* **74**, 566–577 (2006).

3. Hancock, R. E. W. & Sahl, H. Antimicrobial and host-defense peptides as new anti-infective therapeutic strategies. *Nat. Biotechnol.* **24**, 1551–1557 (2006).
4. Joo, H., Fu, C., Otto, M. & Otto, M. Bacterial strategies of resistance to antimicrobial peptides. *Philos. Trans. B* **371**, (2016).
5. Slavetinsky, C., Kuhn, S. & Peschel, A. Bacterial aminoacyl phospholipids – Biosynthesis and role in basic cellular processes and pathogenicity. *Biochim. Biophys. Acta* **1862**, 1310–1318 (2017).
6. Peschel, B. A. *et al.* Staphylococcus aureus Resistance to Human Defensins and Evasion of Neutrophil Killing via the Novel Virulence Factor MprF Is Based on Modification of Membrane Lipids with L-Lysine. *J. Exp. Med.* **193**, 1067–1076 (2001).
7. Brown, S., Santa, J. P., Jr, M. & Walker, S. Wall Teichoic Acids of Gram-Positive Bacteria. *Annu. Rev. Microbiol.* **67**, 313–336 (2013).
8. Needham, B. D. & Trent, M. S. Fortifying the barrier: the impact of lipid A remodelling on bacterial pathogenesis. *Nat. Rev.* **11**, 467–481 (2013).
9. Peleg, A. Y., Seifert, H. & Paterson, D. L. *Acinetobacter baumannii* : Emergence of a Successful Pathogen. *Clin. Microbiol. Rev.* **21**, 538–582 (2008).
10. Boll, J. M. *et al.* A penicillin-binding protein inhibits selection of colistin-resistant, lipooligosaccharide-deficient *Acinetobacter baumannii*. *Proc. Natl. Acad. Sci.* **113**, 6228–6237 (2016).
11. Powers, M. J. & Trent, M. S. Expanding the paradigm for the outer membrane: *Acinetobacter baumannii* in the absence of endotoxin. *Mol. Microbiol.* **107**, 47–56 (2018).
12. Bandyopadhyay, A., McCarthy, K. A., Kelly, M. A. & Gao, J. Targeting bacteria via iminoboronate chemistry of amine-presenting lipids. *Nat. Commun.* **6**, (2015).
13. Cochrane, S. A. *et al.* Synthesis of Tridecaptin – Antibiotic Conjugates with in Vivo Activity against Gram-Negative Bacteria. *J. Med. Chem.* **58**, 9779–9785 (2015).
14. Enterococci, R. *et al.* The Vancomycin - Nisin (1 - 12) Hybrid Restores Activity against Vancomycin. *Biochemistry* **47**, 12661–12663 (2008).

15. Okano, A., Nakayama, A., Schammel, A. W. & Boger, D. L. Total Synthesis of [Ψ [C(=NH)NH] Tpg⁴]Vancomycin and its (4-Chlorobiphenyl)methyl Derivative: Impact of Peripheral Modifications on Vancomycin Analogues Redesigned for Dual D-Ala-D-Ala and D-Ala-D-Lac Binding. *J. Am. Chem. Soc.* **136**, 13522–13525 (2014).
16. Blaskovich, M. A. T. *et al.* Protein-inspired antibiotics active against vancomycin- and daptomycin-resistant bacteria. *Nat. Commun.* **9**, (2018).
17. Nagarajan, R. & Schabel, A. A. Selective Cleavage of Vancosamine, Glucose, and N-Methyl-leucine from Vancomycin and Related Antibiotics. *J. Chem. Soc. Chem. Commun.* 1306–1307 (1988).
18. Gonzalez, R., Albericio, F., Cascone, O. & Iannucci, N. B. Improved antimicrobial activity of h-lysozyme (107 – 115) by rational Ala substitution. *J. Pept. Sci.* **16**, 424–429 (2010).
19. Teng, P. *et al.* Small Antimicrobial Agents Based on Acylated Reduced Amide Scaffold. *J. Med. Chem.* **59**, 7877–7887 (2016).
20. Steinberg, D. A. *et al.* Protegrin-1 : a Broad-Spectrum , Rapidly Microbicidal Peptide with In Vivo Activity. *Antimicrob. Agents Chemother.* **41**, 1738–1742 (1997).
21. Baltz, R. H. Daptomycin : mechanisms of action and resistance , and biosynthetic engineering. *Curr. Opin. Chem. Biol.* **13**, 144–151 (2009).
22. Alexander, J. L., Yu, Z. & Cowan, J. A. Amino Terminal Copper and Nickel Binding Motif Derivatives of Ovispirin - 3 Display Increased Antimicrobial Activity via Lipid Oxidation. *J. Med. Chem.* **60**, 10047–10055 (2017).
23. Libardo, M. D., Cervantes, J. L., Salazar, J. C. & Angeles-boza, A. M. Improved Bioactivity of Antimicrobial Peptides by Addition of Amino-Terminal Copper and Nickel (ATCUN) Binding Motifs. *ChemMedChem* **9**, 1892–1901 (2014).
24. Libardo, M. D., Gorbatyuk, V. Y. & Angeles-boza, A. M. Central Role of the Copper-Binding Motif in the Complex Mechanism of Action of Ixosin: Enhancing Oxidative Damage and Promoting Synergy with Ixosin B. *ACS Infect. Dis.* **2**, 71–81 (2016).

25. Johnson, G. A., Muthukrishnan, N. & Pellois, J. Photoinactivation of Gram Positive and Gram Negative Bacteria with the Antimicrobial Peptide (KLAKLAK) 2 Conjugated to the Hydrophilic Photosensitizer Eosin Y. *Bioconjug. Chem.* **24**, 114–123 (2013).
26. Dosselli, R., Gobbo, M., Bolognini, E., Campestrini, S. & Reddi, E. Porphyrin-Apidaecin Conjugate as a New Broad Spectrum Antibacterial Agent. *ACS Med. Chem. Lett.* **1**, 35–38 (2010).
27. Liu, F. *et al.* Lipopolysaccharide Neutralizing Peptide–Porphyrin Conjugates for Effective Photoinactivation and Intracellular Imaging of Gram-Negative Bacteria Strains. *Bioconjug. Chem.* **23**, 1639–1647 (2012).
28. Kasimova, K. R., Sadasivam, M., Landi, G., Sarna, T. & Hamblin, M. R. Potentiation of photoinactivation of Gram-positive and Gram-negative bacteria mediated by six phenothiazinium dyes by addition of azide ion. *Photochem. Photobiol. Sci.* **13**, 1541–1548 (2014).
29. Sperandio, F. F., Huang, Y. & Hamblin, M. R. Antimicrobial Photodynamic Therapy to Kill Gram-negative Bacteria. *Recent Pat Antiinfect Drug Discov* **8**, 108–120 (2013).
30. McGregor, D. P. Discovering and improving novel peptide therapeutics. *Curr. Opin. Pharmacol.* **8**, 616–619 (2008).
31. Jacobs, A. C. *et al.* AB5075, a Highly Virulent Isolate of *Acinetobacter baumannii*, as a Model Strain for the Evaluation of Pathogenesis and Antimicrobial Treatments. *MBio* **5**, e01076-14 (2014).
32. Wiegand, I., Hilpert, K. & Hancock, R. E. W. Agar and broth dilution methods to determine the minimal inhibitory concentration (MIC) of antimicrobial substances. *Nat. Protoc.* **3**, 163–175 (2008).

CHAPTER 5

CONSTRUCTION OF NOVEL PHAGE DISPLAY LIBRARIES

5.1 Introduction

Designing novel phage display libraries could help achieve more potent peptide binders to a multitude of targets. Incorporating diverse entities onto diverse phage-displayed peptide scaffolds would increase the chemical space that can be explored with chemically modified phage display libraries. The APBA-dimer library yielded peptide probes with sub-micromolar potency against specific strains of bacteria. Perhaps higher potency binding could be accomplished with better designed phage libraries with dynamic covalent warheads; e.g., polyvalent APBA libraries, cyclic/bicyclic libraries, or dually-modified libraries in which APBA is present alongside another diversity element.

5.1.1 Selective N-terminal Cysteine Modification

Our group recently reported the powerful thiazolidino boronate (TzB) formation that selectively occurs between 2-FPBA and N-terminal cysteine residues.¹ The reaction displays rapid kinetics on the order of $10^3 \text{ M}^{-1} \text{ s}^{-1}$ and although the conjugate is relatively stable at neutral conditions, it demonstrates rapid dissociation in acidic environments.

We anticipate that a phage display library presenting an N-terminal cysteine could be modified as a dual-labeled library, incorporating two distinct unnatural residues (Figure 5-1). An FPBA-modified entity could be reacted with an N-terminal cysteine while an iodoacetamide-modified entity could be subsequently reacted with an internal cysteine on a phage-displayed peptide. Thus, a phage library with the sequence IDGRCX₅C, denoted as IDGRC5C, was produced which incorporates a short, cleavable N-terminal leader sequence and five random amino acids between two cysteines. The M13 phage processing mechanism in *E. coli* is negatively affected by cysteine residues at the N-

terminus², hence the commercially available Ph.D.TM-C7C library incorporates an alanine before the C7C sequence³ as do other cysteine-containing libraries⁴. Therefore, the leader sequence was engineered to be recognized and proteolytically cleaved off by Factor XA, which cleaves after the arginine residue in I-D/E-G-R,⁵ post phage isolation from *E. coli*, yielding an N-terminal cysteine.⁶

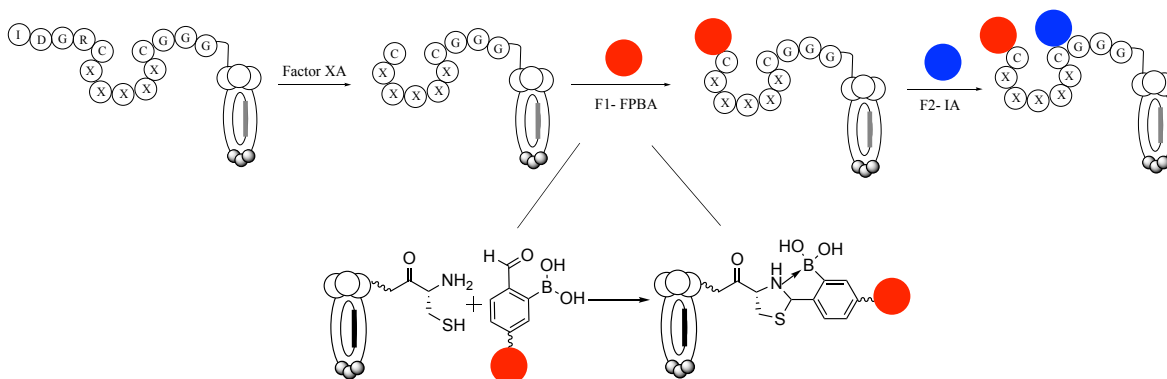


Figure 5-1 Schematic representation of Factor XA cleavage and dual labeling of the IDGRC5C library.

5.2 N-terminal Cysteine Phage Library

5.2.1 Construction of the IDGRC5C Library

The IDGRC5C library was created using the Peptide Display Cloning System from NEB. The first step in phage library synthesis is the preparation of electrocompetent cells to uptake the M13KE cloning vector. The recommended *E. coli* host strain for construction of pIII-displayed peptide libraries using the M13KE vector is the F⁺ strain ER2738.³ The F⁺ ensures that the F-pilus for phage uptake is present, which is important because M13 is a male-specific coliphage and is selected for by growing in the presence of tetracycline. NEB

reports electroporation efficiencies of at least 1×10^9 transformants/ μg with the ER2738 strain. However, the highest electroporation efficiency that I could achieve with prepared ER2738 electrocompetent cells was 6×10^7 transformants/ μg . This is not sufficient for library synthesis since the IDGRC5C diversity is 3.2×10^6 clones and the efficiency is calculated for transformation with undigested M13KE vector, which is expected to decrease by 1-2 orders of magnitude when the library-inserted M13KE vector is used instead. TOP10 is known to be a highly efficient electrocompetent strain of *E. coli*, which is able to achieve electroporation efficiencies $> 1 \times 10^{10}$ transformants/ μg . Although TOP10 is not recommended because it is an F^- strain, the cells can still export the packaged phage, which can consequently infect existent ER2738 cells (F^+ strain). This can be visualized by blue plaques forming on a bacterial lawn of ER2738 cells plated on IPTG/Xgal-containing media, since the M13KE vector contains the *lacZ α* gene, after M13KE transformation into TOP10 cells. Using this rationale, electrocompetent TOP10 cells were prepared and demonstrated a much higher electroporation efficiency of 5×10^{10} transformants/ μg , which is sufficient for library construction.

To achieve ligation of a vector and DNA insert, both entities need to be digested with restriction enzymes. First, the M13KE vector was digested with the restriction enzymes EagI-HF and KpnI-HF followed by agarose gel purification on an ethidium bromide (EtBr) stained gel (Figure 5-2). The gel was visualized under UV light and the digested DNA (top band) was isolated. The first attempt at extracting the DNA from the gel, using a β -agarase protocol, resulted in a very low recovery yield of 3%. However, the second attempt at extracting the DNA from the gel, using a Macherey-Nagel spin

column, resulted in an improved recovery yield of 15%. Although low, this yielded a sufficient amount of DNA to proceed.

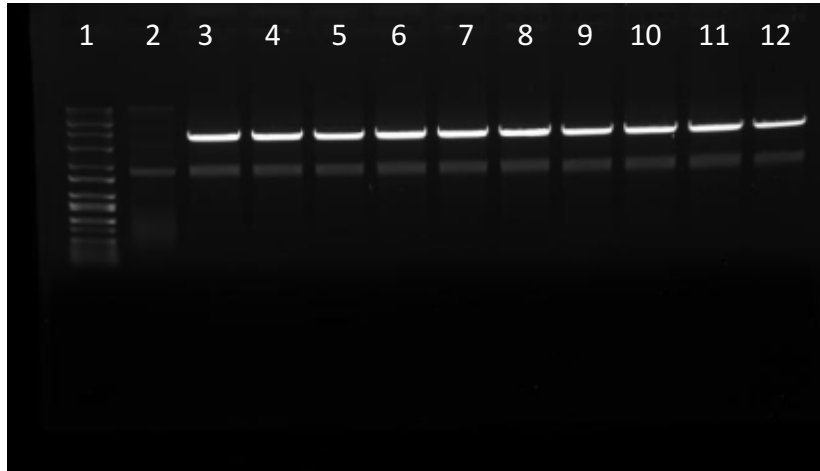


Figure 5-2 Agarose gel (0.45%,+EtBr) of digested M13KE vector. Lane 1: DNA ladder, Lane 2: Undigested M13KE, Lanes 3-12: Digested M13KE.

The library oligonucleotide, designed according to NEB³, was annealed to universal extension primer and the annealed duplex was subjected to an extension reaction with Klenow fragment. The extended duplex was digested with EagI-HF and KpnI-HF and the DNA was purified via phenol/chloroform extraction, chloroform extraction and ethanol precipitation. It was then purified on an 8% non-denaturing polyacrylamide gel (Figure 2-3). The gel was stained with EtBr, visualized under UV light and the digested insert DNA (bottom band) was isolated. The DNA was eluted in gel elution buffer followed by phenol/chloroform extraction, chloroform extraction and ethanol precipitation. A total of 2.3 μg of purified DNA insert was isolated starting from 5 μg of library oligonucleotide.

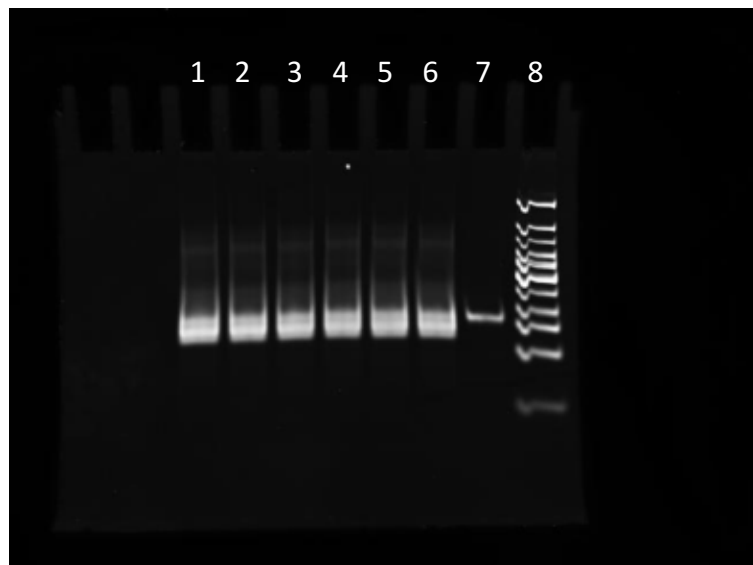


Figure 5-3 Polyacrylamide gel (8%) of digested library insert. Lanes 1-6: Digested insert, Lane 7: Undigested extension reaction, Lane 8: DNA ladder.

The digested M13KE vector and library DNA insert were then ligated and transformed into electrocompetent TOP10 cells. Various conditions were assessed to optimize the ligation conditions, including 3:1, 5:1 and 10:1 molar excess of cut duplex as suggested by NEB. With the assistance of T4 DNA ligase, the ligation reactions were incubated overnight at 16 °C then the enzyme was heat killed. The ligated DNA was electroporated into competent TOP10 cells and plated on IPTG/Xgal-containing media in the presence of ER2738 cells. The 3:1 ratio yielded the highest plaque/ μg ratio of 1×10^8 pfu/ μg . From this test ligation, the DNA from 10 plaques was isolated and sequenced to verify successful ligation. Each of the ten phage particles had a different variable peptide sequence and no blank sequences were observed (Table 5-1). Interestingly, at least one proline residue was present in each sequence. Before scaling up the ligation protocol to

generate a sufficient library to cover the 3.2×10^6 clones of the IDGRC5C library, various test reactions on the IDGRC5C phage and model peptides were performed.

Table 5-1 Sequences of 10 random phage particles from IDGRC5C library preparation.

IDGRCPVPALC	IDGRCPALC
IDGRCSFRFPC	IDGRCSFSYPC
IDGRCPISTKC	IDGRCLPKLVC
IDGRCSPALPC	IDGRCIDPPSC
IDGRCGYPVGC	IDGRCLPPARC

5.2.2 Confirmation of Factor XA Cleavage & FPBA Labeling on Model Peptides

Two model peptides were synthesized based on one of the peptide sequences isolated from the IDGRC5C library electroporation (Figure 5-4). First, a peptide with the sequence IDGRCGYPVGCGW-NH₂ (IDGRC5C peptide), which includes a tryptophan residue for UV monitoring, was synthesized to assess Factor XA cleavage of the leader sequence. Second, a peptide with the sequence CGYPVGCG-FAM (C5C-FAM peptide), which incorporates a C-terminal Dap residue, conjugated to fluorescein as a reporter, was synthesized to assess N-terminal cysteine labeling by FPBA.

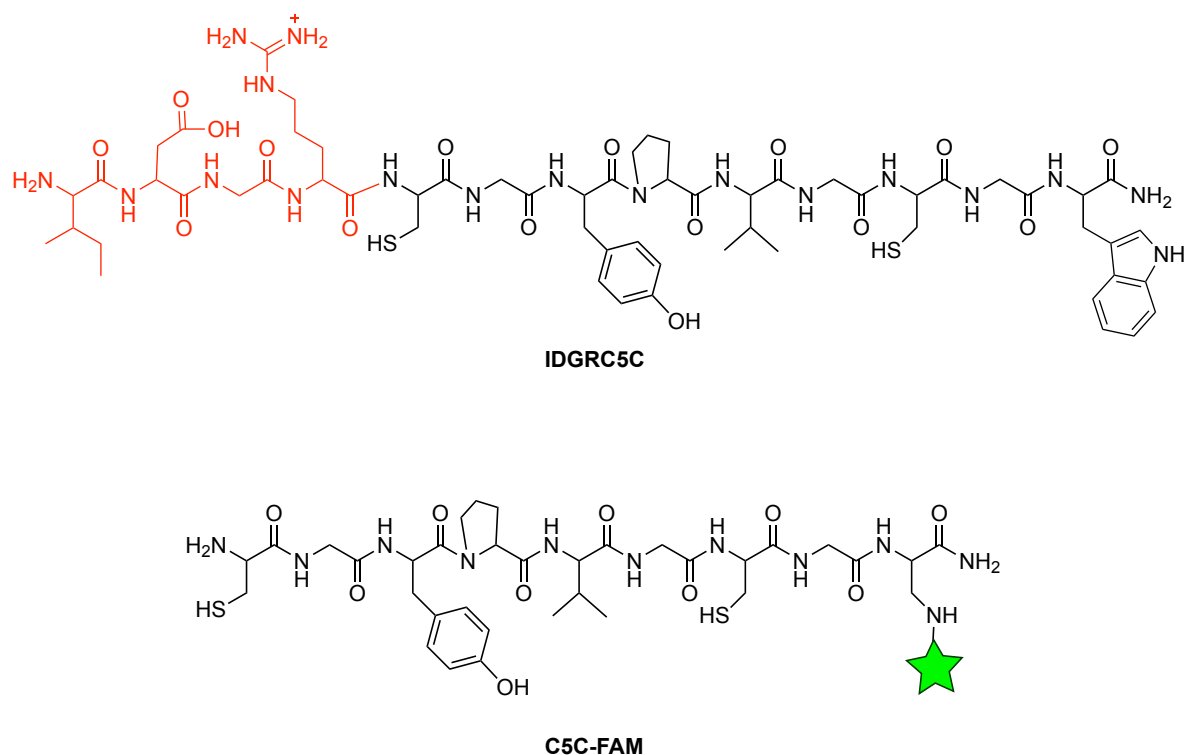


Figure 5-4 Structures of control peptides synthesized.

To mimic the conditions that the phage-displayed peptides would be exposed to for modification, the IDGRC5C peptide was subjected to reduction via iTCEP for 48 hours followed by treatment with Factor XA. The leader sequence cleavage kinetics were monitored via LC-MS. After 40 min, the major product (90%) was the cleaved C5C peptide while only 10% of the uncleaved IDGRC5C peptide remained (Figure 5-5). The leader sequence was completely cleaved after 80 min. These results confirmed that Factor XA could cleave the IDGR leader sequence from an IDGRC5C model peptide.

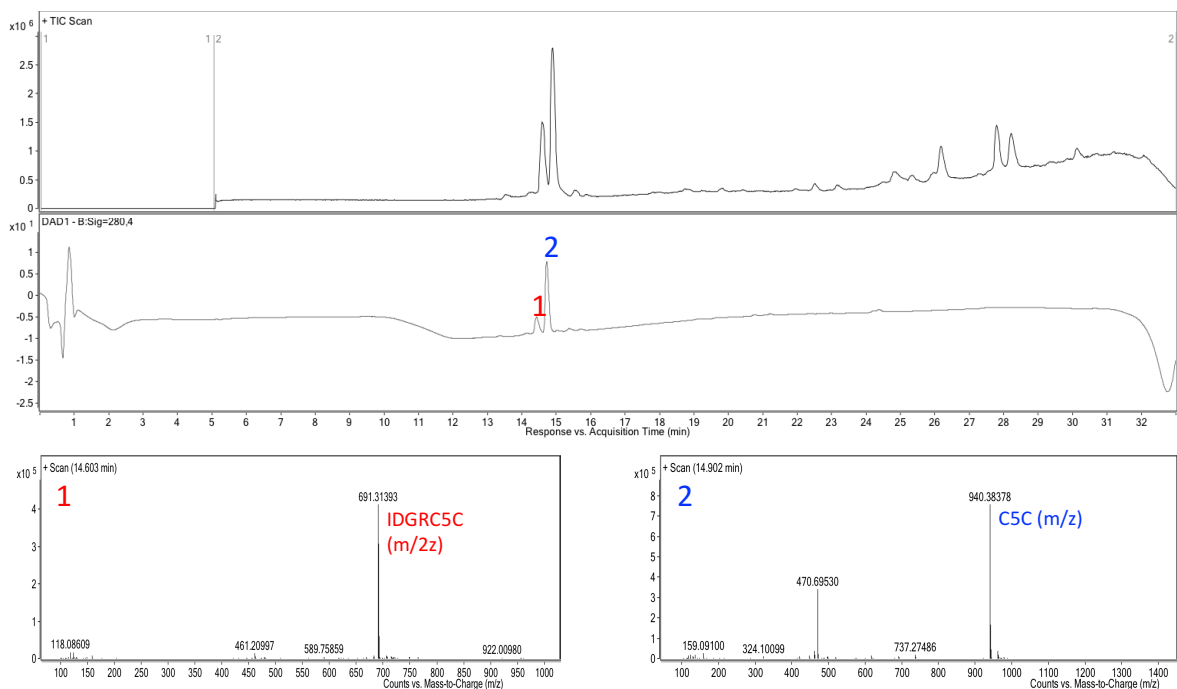


Figure 5-5 LC-MS analysis of Factor XA treated IDGRC5C peptide after 40 min.

The C5C-FAM model peptide was then used to determine if the N-terminal cysteine could be labeled with FPBA, specifically FPBA-Biotin synthesized by Dr. Anupam Bandyopadhyay, which would be used in a streptavidin capture assay to assess FPBA labeling on phage. The C5C-FAM model peptide and FPBA-Biotin were incubated for 30 min in the presence of TCEP and subjected to LC-MS analysis. It is worthy to note that the C5C-FAM peptide could not be treated with iTCEP, as the IDGRC5C peptide was, because the FAM fluorophore sticks to the iTCEP agarose beads; therefore, standard TCEP was used. Although the majority species are the reactants due to the acidic buffer system, some product formation can be observed via LC-MS (Figure 5-6). These results confirm that the N-terminal cysteine on a model peptide can be labeled with FPBA-Biotin, although the exact extent of FPBA labeling cannot be confirmed due to the reversible

nature of TzB formation in the acidic conditions of the LC-MS. The FPBA-Biotin labeling on the IDGRC5C model peptide following Factor XA cleavage generated consistent results, ensuring the FPBA labeling could occur in the exact setting that would be presented on phage with Factor XA present.

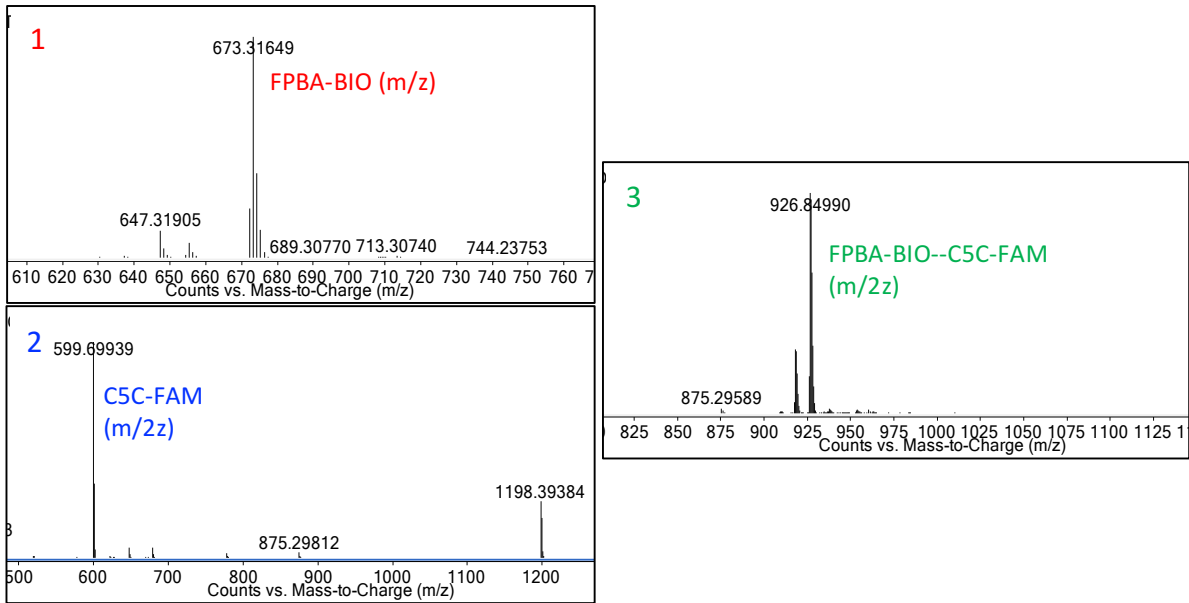
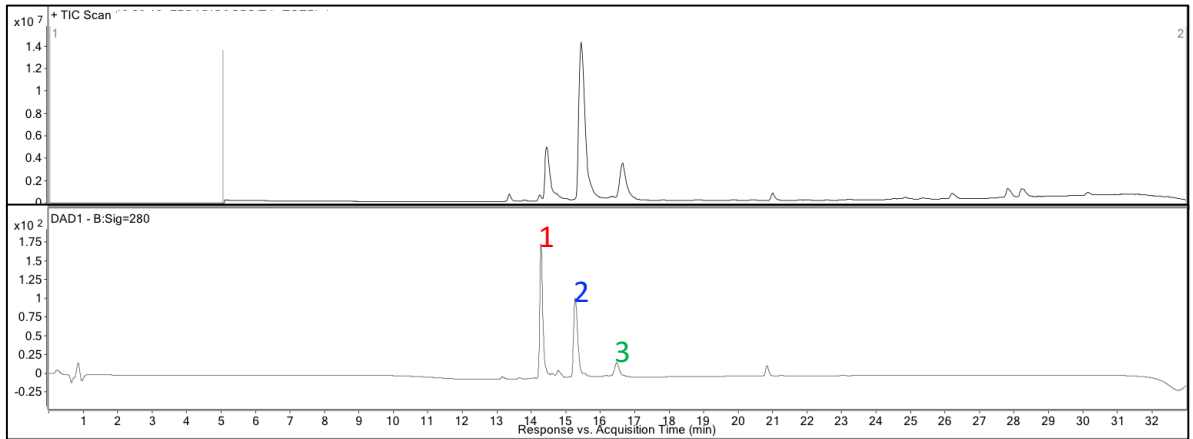


Figure 5-6 LC-MS analysis of TzB formation between FPBA-Biotin and C5C-FAM peptide after 40 min.

5.2.3 Attempt to Confirm Cleavage & Labeling on Phage

Once the desired chemistry was confirmed on the model peptides, the Factor XA cleavage and FPBA labeling on phage was assessed. Since a streptavidin capture experiment with FPBA-Biotin would be desirable to confirm the N-terminal cysteine labeling, the ability of the IDGRC5C phage to be captured via streptavidin pull-down was assessed using a similar assay described for APBA labeling confirmation on Ph.D.TM-C7C (AC7C) phage. When reduced and labeled with biotin-iodoacetamide, the IDGRC5C phage can be captured at a comparable level to the commercially available AC7C phage library (Figure 5-7).

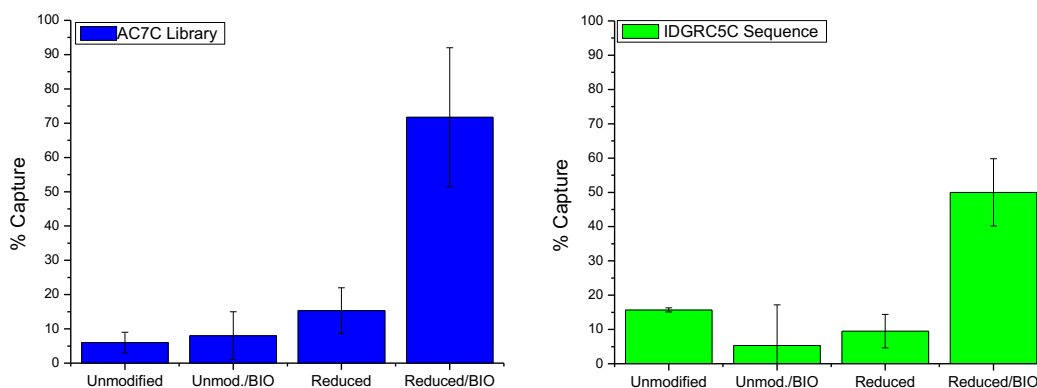


Figure 5-7 Streptavidin capture assay of AC7C library compared to IDGRC5C phage.
BIO: Biotin-IA labeled

Instead of a pulse-chase assay, the labeling of IDGRC5C by FPBA-Biotin would be directly assessed by the amount of streptavidin capture, rather than the lack thereof (Figure 5-8). The amount of capture between Factor XA treated phage, which should generate an N-terminal cysteine for FPBA-Biotin labeling and therefore be captured by

streptavidin, and non-Factor XA treated phage, which should not allow for FPBA-Biotin labeling, could be compared to confirm on Factor XA cleavage and FPBA labeling.

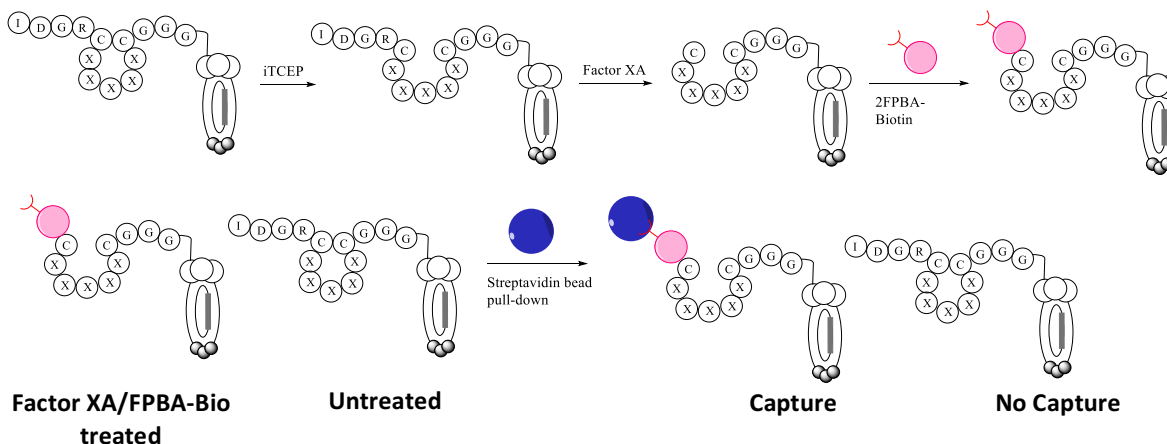


Figure 5-8 Illustration of streptavidin capture assay for Factor XA cleaved and FPBA-Biotin labeled phage.

However, when the IDGRC5C phage was reduced, treated with Factor XA then labeled with FPBA-Biotin, no capture was observed. Various labeling conditions were attempted, including longer/shorter incubation times and an extra reduction step after Factor XA cleavage, but no capture was still observed. The extra reduction step was attempted because oxidation kinetics of the C5C-FAM model peptide revealed that the cysteine residues rapidly oxidized with approximately 50% of the peptide oxidized within 1 hour, and thus could oxidize during Factor XA treatment (Figure 5-9). Although the Factor XA cleavage and FPBA-Biotin labeling were confirmed on model peptides, the confirmation on phage via streptavidin capture was unsuccessful. The two-step process of both cleavage and labeling complicates the analysis and a different, more direct, method of confirmation needed to be explored.

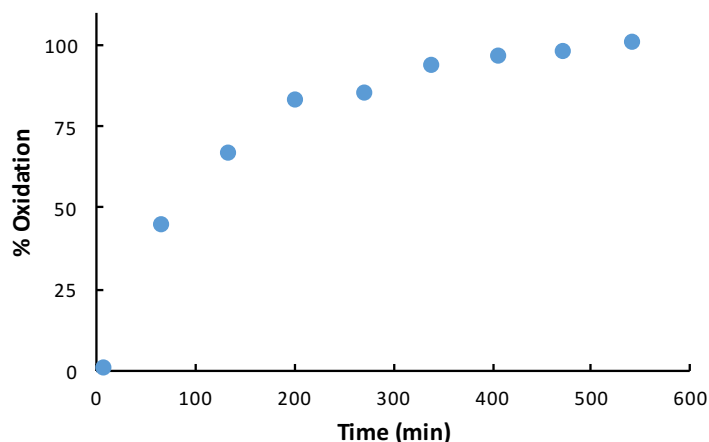
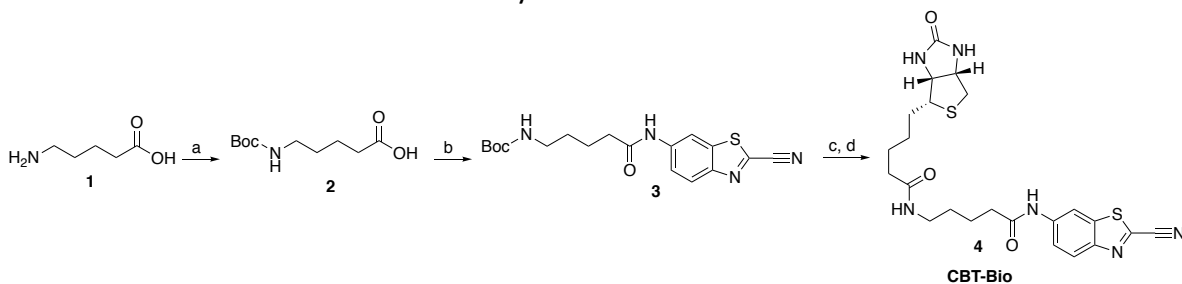


Figure 5-9 Oxidation of C5C-FAM assessed via LC-MS over time.

5.2.4 Exploration of Cyanobenzothiazole Chemistry

Although the TzB formation between FPBA and N-terminal cysteine is reported to be stable at neutral pH, perhaps the reversible nature of conjugation is problematic for the analysis of N-terminal cysteines on phage. Therefore, an irreversible covalent N-terminal cysteine probe was explored. 2-Cyanobenzothiazole (CBT) has been reported to selectively condense with N-terminal cysteine residues and genetically encoded 1,2-aminothiols to allow for site-specific protein labeling.^{7,8} To study this chemistry, a biotin-conjugated CBT molecule, CBT-Bio, was synthesized (Scheme 5-1).

Scheme 5-1 Synthetic route to CBT-Bio.



(a) Boc anhydride, 5% Na₂CO₃, THF; 82% yield. (b) *i*. isobutylchloroformate, NMM, THF *ii*. 2-cyano-6-aminobenzothiazole; 55%. (c) 20% TFA/DCM. (d) Biotin-NHS, DIPEA, DMF; 65% over two steps.

The association kinetics of CBT-Bio and the C5C-FAM model peptide were assessed via LC-MS, demonstrating reaction completion by 40 min (Figure 5-10). This molecule opens up the potential to further investigate the N-terminal cysteine on phage with an irreversible covalent conjugation chemistry.

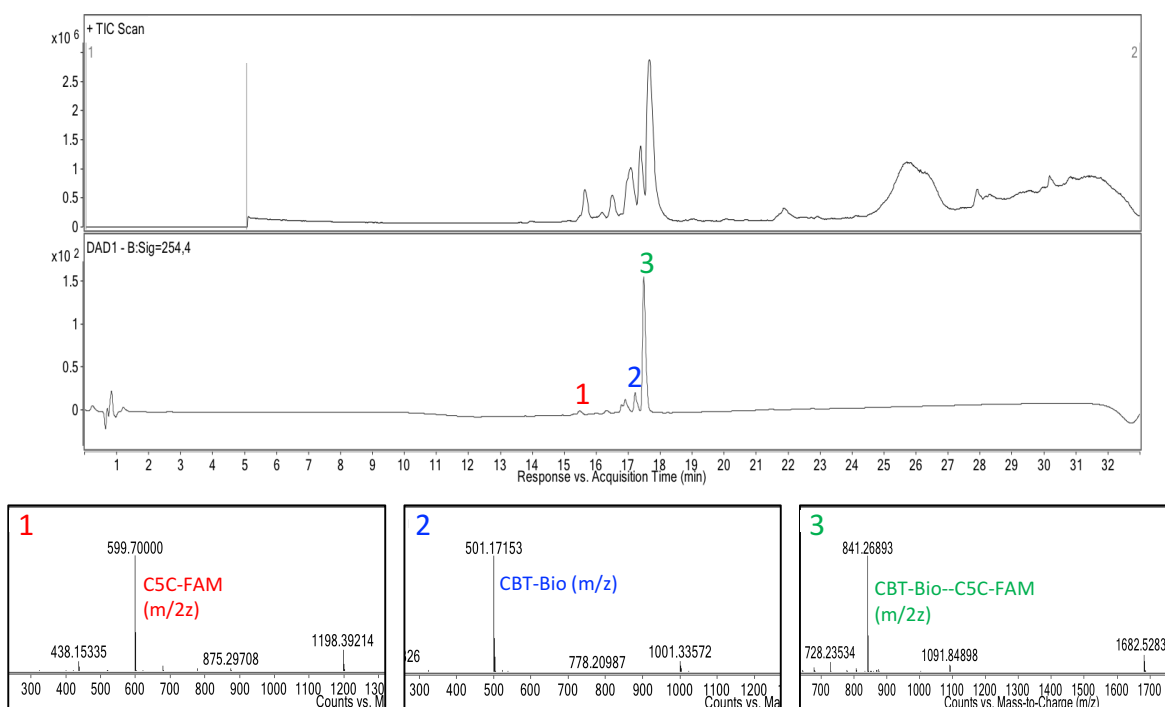


Figure 5-10 LC-MS analysis of complete CBT-Biotin labeling of C5C-FAM peptide.

5.3 Conclusions & Future Work

5.3.1 Conclusions on IDGRC5C Library

Engineering novel phage libraries remains as an innovative approach to achieve more potent peptide probes of a variety of targets. The work herein describes the construction of an IDGRC5C phage library, which has the potential to serve as a dual-labeled library using an N-terminal cysteine specific probe. Presently, the phage library

has been constructed and model peptide studies have confirmed the desired modification chemistries; however, confirmation of the modifications on phage has yet to be achieved.

5.3.2 Future Work on IDGRC5C Library

Samantha Cambray and Wenjian Wang have acquired the IDGRC5C library. Their goal is to confirm on N-terminal cysteine labeling and the ability to conjugate two unnatural functionalities to the library. The CBT-Bio molecule will be used to assist in the N-terminal cysteine labeling; for example, a Western Blot could be performed utilizing a NeutrAvidin antibody after Factor XA cleavage. They are also exploring the advantage of engineering additional epitope tag sequences into the phage-displayed peptide to assist with library confirmation, specifically by encoding a human influenza hemagglutinin (HA) tag before the IDGR sequence, which can be recognized by antibodies. Although these indirect confirmation strategies would be beneficial, mass-spec analysis of protease cleaved peptide insert, similar to a procedure accomplished by Heinis and coworkers⁹, would be an ideal, direct method of library modification confirmation and is additionally being explored.

5.3.3 Additional Proposed Novel Phage Libraries

Besides the N-terminal cysteine library for dual labeling on phage, I can propose additional novel libraries that could be beneficial to achieve more potent or structurally improved peptide therapeutics (Figure 5-11). For one, a cyclic library displaying the APBA warhead on the Ph.D.TM-C7C library could be achieved by alkylating the cysteines with iodoacetamide residues constrained to the same molecule. This idea is currently being explored in the laboratory by Michael Kelly. Additionally, as shown in Chapter 2,

polyvalency of the APBA warhead allows for increased potency against both *S. aureus* and proteins. Perhaps a polyvalent, tetramer library of APBA could be engineered to expose four cysteine residues to be modified with APBA-IA separated by varying random residues to achieve even more potent binders to *S. aureus* than KAM5.

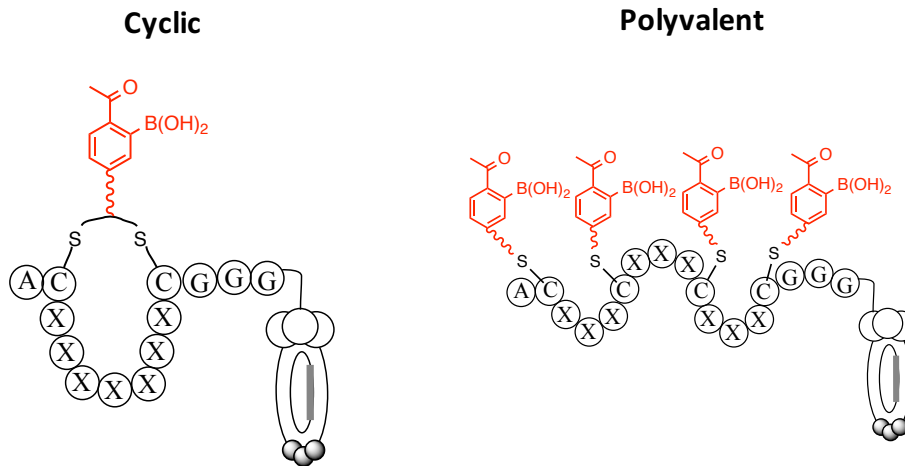


Figure 5-11 Additional unique phage library designs.

5.4 Experimental Procedures

5.4.1 General Methods

The Peptide Display Cloning System, *E. coli* K12 ER2738 strain and all reagents for library cloning (including restriction enzymes) were purchased from NEB. All ER2738 strains were grown with 20 µg/mL tetracycline. TOP10 *E. coli* was provided as a gift from the laboratory of Professor Abhishek Chatterjee. Library DNA oligonucleotide was purchased from Integrated DNA Technologies (IDT). Chemical reagents for gel electrophoresis purifications, small molecule synthesis and peptide synthesis were purchased from various vendors and used as received. Electroporations were performed on a BioRad

Gene Pulser. All titering experiments were plated on IPTG/Xgal-containing agar. Agarose and polyacrylamide gels were imaged on a BioRad ChemiDoc MP Imaging System using EtBr to stain the DNA. DNA concentrations were determined on a Nanodrop 2000c UV/VIS spectrometer. A BioRad C1000 Touch Thermal Cycler was used for library preparation procedures requiring various temperature incubations. Peptide synthesis was carried out on a Tribute peptide synthesizer from Protein Technologies and purified via RP-HPLC on a Waters Prep LC with a Jupiter C18 column (Phenomenex) using acetonitrile/water (0.1% TFA) as the eluent. Mass spectrometry data was generated and peptide modifications and kinetics were monitored using an Agilent 6230 LC TOF mass spectrometer.

5.4.2 Preparation of Electrocompetent Cells

A 10 mL culture of TOP10 *E. coli* was grown overnight from a fresh LB agar plate in sterile SOC media (per liter: 20 g tryptone, 5 g yeast extract, 0.5 g NaCl). SOC media (500 mL) was inoculated with 5 mL of overnight culture and allowed to incubate at 37 °C at 250 rpm until an optimal OD₆₀₀ value of 0.5 – 0.6 was attained (~ 3 hr). Media was transferred to JA-17 centrifuge tubes (autoclaved in advance) and allowed to chill on ice for 20 min. Tubes were centrifuged (6,300 rpm, 4 °C, 10 min) and supernatant was discarded. Cells were resuspended in chilled 15% glycerol (in water) via pipetting, centrifuged again (6,300 rpm, 4 °C, 10 min) and the supernatant was discarded. This process was repeated for a total of 3 washes with 15% glycerol. After the last wash, all of the supernatant, besides ~ 1 mL, was discarded. The cell pellet was resuspended in this 1 mL of 15% glycerol and aliquoted into Eppendorf tubes. Aliquots (50 µL) were immediately subjected to liquid nitrogen to flash freeze the cells and the samples were kept in the -80 °C freezer. The

electrocompetence was assessed by electroporating 1 ng of M13KE into freshly thawed electrocompetent cells according to manufacturer's instruction (25 μ F, 200 OHMS, 2.5 kV). Cells were recovered from the cuvette with 1 mL SOC media and incubated at 37 °C for 45 min. The phage titer was calculated according to the M13 Titer Protocol provided by NEB and blue colonies were counted to calculate the electroporation efficiency (transformants/ μ g).

5.4.3 Preparation of M13KE Vector

M13KE (10 μ g, 10 μ L from 1 mg/mL stock) was incubated at 37 °C for 1 hr with EagI-HF (100 units, 5 μ L from 20,000 units/mL stock) and KpnI-HF (100 units, 5 μ L from 20,000 units/mL stock) in 10X NEB CutSmart Buffer (40 μ L) and water (340 μ L). For gel-purification, 60 μ L of 6X loading dye was added to the digested vector. A 0.45 % agarose gel was made with low melting agarose in 1 X Tris-Acetate-EDTA (TAE) buffer (plus 0.2 μ g/mL EtBr) and the digested M13KE sample was loaded onto the gel alongside undigested vector and a DNA ladder. The gel was run at 90 V for ~ 30 min, until the dye line was ~ 75% of the way down the gel. The gel was imaged under UV and the top band was excised from the gel with a fresh razor blade into a falcon tube. The DNA was extracted from the gel by adding 2 volumes of Macherey-Nagel NTI binding buffer and incubating for 10 min at 50 °C. The solution was transferred in 700 μ L aliquots to a Macherey-Nagel spin column and centrifuged (13,000 rpm, 30 seconds). The spin column was washed with buffer PE (700 μ L, 2x) and dried via centrifugation (13, 000 rpm, 1 min). The spin column was transferred to a collection tube and DNA was eluted with water (30

μL). The concentration of DNA was determined via Nanodrop as 49 ng/μL, or 1.5 μg, from which a 15 % yield could be calculated.

5.4.4 Preparation of Library Insert

Library oligonucleotide was purchased from IDT with the DNA sequence 5'- CAT GTT TCG GCC GAA CCT CCA CCA CAM NNM NNM NNM NNM NNA CAC CTA CCA TCA ATA GAG TGA GAA TAG AAA GGT ACC CGG G -3', incorporating the correct leader peptidase cleavage site and short glycine spacer, flanking the desired IDGRCX₅C sequence, according to NEB. Library oligonucleotide (5 μg, 2 μL of 100 μM stock in water) and universal extension primer (4 μg) were combined in a volume of 50 μL Tris-EDTA (TE) buffer containing 100 mM NaCl. The solution was heated to 95 °C, then cooled to 37 °C over 20 min in a thermal cycler to anneal the two components. The annealed duplex was subjected to extension by adding 10 mM dNTPs (8 μL), Klenow fragment (3 μL), 10X NEBuffer 2 (20 μL) and water (119 μL) followed by incubation at 37 °C for 10 min then 65 °C for 15 min. The extended duplex (196 μL) was then digested with EagI-HF (5 μL) and KpnI-HF (5 μL) in 10X CutSmart Buffer (40 μL) and water (154 μL) by incubating at 37 °C for 1 hr. The DNA was purified by phenol/chloroform extraction, chloroform extraction and ethanol precipitation. An 8% nondenaturing polyacrylamide gel was prepared in TAE buffer and the digested duplex sample was loaded onto the gel alongside undigested duplex and a DNA ladder. The gel was run at 80 V for ~ 60 min, until the dye line was ~ 75% of the way down the gel in 1 X Tris-Borate-EDTA (TBE) buffer. The gel was first stained with EtBr (0.2 μg/mL in 50 mL TBE) for 30 min then imaged under UV. The bottom band was excised from the gel with a fresh razor blade into a falcon tube. The DNA was extracted from the gel by shaking overnight

in several volumes of 100 mM sodium acetate, pH 4.5, 1 mM EDTA, 0.1 % SDS at 37 °C. The gel fragments were separated from elution buffer via centrifugation and the supernatant was transferred to a new tube. The isolated DNA duplex was purified via phenol/chloroform extraction, chloroform extraction and ethanol precipitation. The pellet was resuspended in water (50 µL) and the concentration of DNA was determined via Nanodrop as 46 ng/µL, or 2.3 µg, from which a 46 % yield could be calculated.

5.4.5 Ligation and Electroporation into Competent Cells

The ligation conditions were optimized with NEB-suggested starting parameters of 20 µL ligation reactions with 3:1, 5:1 or 10:1 molar excess of cut duplex. The digested M13KE vector (100 ng, 2.17 µL from 46 ng/µL stock) and the cut insert (various amounts of a 2.8 ng/µL stock according to NEBicalculator) were combined in 10X ligase buffer (2 µL) and 200 units of T4 DNA ligase (1 µL) in water and incubated overnight at 16 °C. The enzyme was heat-killed by heating samples up to 65 °C for 20 min. The ligated samples (2 µL each, 10 ng vector) were electroporated into 50 µL electrocompetent cells, recovered and subjected to titering as described above. The highest plaque/µg ratio was achieved by the 3:1 molar excess reaction (1×10^8 pfu/µg) compared to values on the order of magnitude of 10^7 for 5:1 and 10:1. Ten individual phage colonies from the 3:1 electroporation were selected and amplified in ER2738. Phage DNA was isolated using a Qiagen miniprep kit and sent for sequencing analysis by Eton Bioscience, Inc.

5.4.6 Model Peptide Synthesis

SPPS was performed on a Rink Amide MBHA solid support using Fmoc/tBu chemistry on a 0.05 mmol scale. Five equivalents of commercially available amino acids were used for

the coupling reaction with HBTU as an activating reagent. For the C5C-FAM model peptide, an Alloc-protected Dap residue was installed at the C-terminus for on-resin coupling of a fluorophore. 5(6)-FAM was conjugated to the peptide on resin by first removing the Alloc protecting group, as described in Chapter 2, followed by subsequent HBTU-mediated amide bond coupling in 0.4 M NMM/DMF. The peptides were cleaved off resin and globally deprotected with Reagent B (88% TFA, 5% water, 2% triisopropylsilane, 5% phenol). Crude peptides were obtained via ether precipitation and purified by RP-HPLC. Each peptide was characterized via LC-MS for excellent purity (>95%) and correct masses (Table 5-2).

Table 5-2 Mass-spec data of model peptides.

Peptide	Calculated m/z	Observed m/z
IDGRC5C	691.80 [M+H] ²⁺	691.31
C5C-FAM	599.65 [M+H] ²⁺	599.69

5.4.7 Cleavage and Labeling Confirmation on Model Peptides

The IDGRC5C peptide (50 μM, 200 μL) in 20 mM Tris-HCl (pH 8, 2 mM calcium chloride (CaCl₂)), as recommended for Factor XA use, was subjected to reduction via iTCEP (25 μL) for 48 hr. The peptide was removed from iTCEP and subjected to treatment with Factor XA (2 μL, 1 mg/mL stock) and the leader sequence cleavage kinetics was monitored directly via LC-MS. After 40 min, 90% of the peptide was cleaved by Factor XA. The C5C-FAM peptide (100 μM) and FPBA-Biotin (100 μM) in 20 mM Tris-HCl, pH 8 (200 μL) were incubated for 30 min in the presence of TCEP (2 mM) and subjected to LC-MS analysis. A

small peak corresponding to TzB formation was observed, although the majority species were the reactants due to the acidic buffer system, which readily reverses the TzB. Additionally, the IDGRC5C peptide (100 μ M) in 20 mM Tris-HCl (pH 8, 2 mM CaCl₂) was subjected to reduction via iTCEP (25 μ L) for 48 hr. The peptide was removed from iTCEP and subjected to treatment with Factor XA as described above for 40 min. FPBA-Biotin was directly added to the solution (100 μ M) and stirred at room temperature for 1 hr followed by LC-MS analysis. A small peak corresponding to the Factor XA-cleaved and FPBA-Biotin-labeled IDGRC5C peptide was observed.

5.4.8 Streptavidin Capture Assay

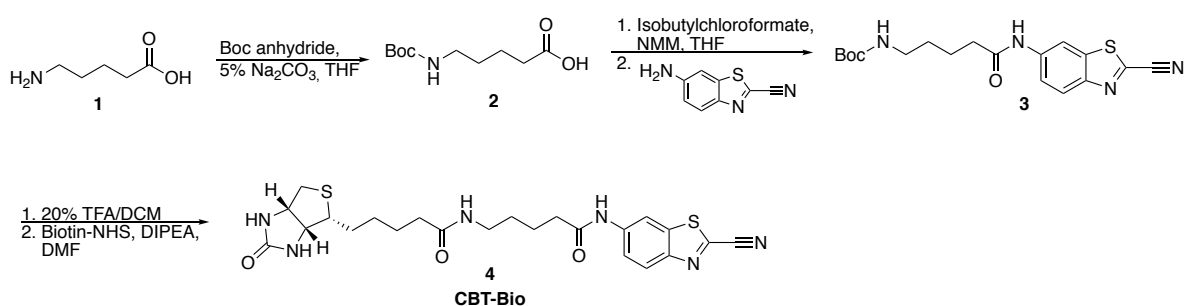
For confirmation of Biotin-IA labeling on phage, streptavidin agarose resin (25 μ L/sample) was washed with PBS (pH 7.4) and blocked with 10 mg/mL BSA via incubation for 1 hr. AC7C or IDGRC5C library phage (200 μ L in TBS, pH 8.5) were reduced with iTCEP (25 μ L) for 48 hr at 4 °C and treated with Biotin-IA (2 mM) for 2 hr. Biotin-IA labeled phage (200 μ L, $\sim 1 \times 10^{10}$ pfu/mL) was removed from iTCEP and subjected to the streptavidin resin for 1 hr. Non-reduced (unmodified), unmodified/biotin-IA labeled and reduced phage (without small molecule labeling) were also analyzed. The titer was compared to that of phage not subjected to streptavidin to generate a percent capture. The average percent capture and standard deviation of three trials was plotted. For the attempt at confirming Factor XA and FPBA-Biotin labeling, streptavidin resin was blocked as described above. IDGRC5C phage was reduced with iTCEP as described above and subjected to cleavage with Factor XA (2 μ L, 1 mg/mL stock, with the addition of 2 mM CaCl₂) for 6 hr at room temperature according to the usage directions by NEB. FPBA-Biotin (2 mM, 2 μ L from a

200 mM DMSO stock) was added to the reduced and Factor XA-treated phage and allowed to conjugate for 2 hr at room temperature. Factor XA/FPBA-Biotin treated phage (200 μ L, $\sim 1 \times 10^{10}$ pfu/mL) was subjected to the streptavidin resin for 1 hr. The titer was compared to that of phage not subjected to streptavidin to generate a percent capture. When no streptavidin capture was observed, various incubation times with Factor XA (including a shorter 40 min incubation) and FPBA-Biotin were assessed, still yielding no streptavidin capture.

5.4.9 Measurement of C5C Peptide Oxidation Kinetics

The C5C-FAM peptide was dissolved in PBS (pH 7.4) at a concentration of 100 μ M. The peptide was directly subjected to LC-MS analysis hourly overnight and the formation of a disulfide bond was observed over time. Oxidation starts to occur within one hour ($\sim 50\%$ oxidized). The kinetics were plotted by comparing the amount of oxidized peptide to reduced peptide at each time-point.

5.4.10 Synthesis of CBT-Bio



Synthesis of Compound 2. 5-aminovaleric acid **1** (1.01 g, 8.6 mmol) was dissolved in 5% Na_2CO_3 (60 mL) and THF (30 mL) and cooled on ice. Boc anhydride (2.06 g, 9.5 mmol) was dissolved in THF (30 mL), added to the reaction mixture on ice and allowed to stir at room temperature overnight. Upon reaction completion, monitored by TLC, the reaction

mixture was acidified with 6 M HCl to pH ~ 2 and extracted with ethyl acetate (3 x 100 mL). The combined organic layer was washed with brine (100 mL) and dried over Na₂SO₄. The resulting crude product was concentrated and purified via silica gel column chromatography using hexane/ethyl acetate (3:2, 0.1% acetic acid) to yield a white solid (1.53 g, 82%); ¹H NMR (CDCl₃) δ 3.15 (m, 2H), 2.31 (t, 2H), 1.68 (m, 2H), 1.55 (m, 2H), 1.45 (s, 9H). MS-ESI⁺: m/z calculated for C₁₀H₁₉NO₄ [M-Boc+H]⁺ 118.13, found 118.08.

Synthesis of Compound 3. Compound 2 (100 mg, 0.46 mmol) and NMM (76 μL, 0.69 mmol) were dissolved in THF (8 mL) on ice. Isobutylchloroformate (45 μL, 0.35 mmol) was added and the reaction mixture was allowed to stir for 20 min on ice under an argon environment. 2-Cyano-6-aminobenzothiazole (40 mg, 0.23 mmol) was added and the reaction mixture was allowed to stir for 2 hr on ice then overnight at room temperature. Saturated NaHCO₃ was added and the product was extracted with ethyl acetate (3 x 30 mL). The combined organic layer was washed with brine (100 mL) and dried over Na₂SO₄. The resulting crude product was concentrated and purified via RP-HPLC. Lyophilization of the final product yielded a white solid (40.7 mg, 55%); ¹H NMR (CDCl₃) δ 8.61 (s, 1H), 8.15 (d, 1H), 7.59 (d, 1H), 3.08 (t, 2H), 2.49 (t, 2H), 1.75 (m, 2H), 1.52 (m, 2H), 1.48 (s, 9H). MS-ESI⁺: m/z calculated for C₁₈H₂₂N₄O₃S [M-Boc+H]⁺ 275.46, found 275.09.

Synthesis of Compound 4. Compound 3 (16 mg, 0.04 mmol) was dissolved in 20% TFA/DCM (3 mL) overnight. Solvent was evaporated and product was precipitated with chilled ether at 4 °C for 6 hr. Crude product was directly combined with Biotin-NHS (15 mg, 0.04 mmol) and DIPEA (17 μL, 0.09 mmol) in DMF (800 μL) and allowed to stir at room temperature for 3 hr. Upon reaction completion, monitored via LC-MS, the product was directly

purified via RP-HPLC. Lyophilization of the final product, confirmed via LC-MS, yielded a white solid (13.8 mg, 65%); MS-ESI⁺: m/z calculated for C₂₃H₂₈N₆O₃S₂ [M+H]⁺ 501.64, found 501.17.

5.4.11 Measurement of CBT-Bio Kinetics with C5C Peptide

Model C5C-FAM peptide (50 μM) and CBT-Bio (100 μM) were combined in 200 μL Tris-HCl (20 mM, 2 mM CaCl₂) in the presence of TCEP (2 mM). The peptide solution was directly subjected to LC-MS analysis for kinetic analysis (every 40 min) of CBT conjugation to the N-terminal cysteine, which was fully conjugated after just 40 min.

5.5 References

1. Bandyopadhyay, A., Cambray, S. & Gao, J. Fast and selective labeling of N-terminal cysteines at neutral pH via thiazolidino boronate formation. *Chem Sci* **7**, 4589–4593 (2016).
2. Nagler, C., Nagler, G. & Kuhn, A. Cysteine Residues in the Transmembrane Regions of M13 Procoat Protein Suggest that Oligomeric Coat Proteins Assemble onto Phage Progeny. *J. Bacteriol.* **189**, 2897–2905 (2007).
3. Noren, K. A. & Noren, C. J. Construction of High-Complexity Combinatorial Phage Display Peptide Libraries. *Methods* **23**, 169–178 (2001).
4. Heinis, C., Rutherford, T., Freund, S. & Winter, G. Phage-encoded combinatorial chemical libraries based on bicyclic peptides. *Nat. Chem. Biol.* **5**, 502–507 (2009).
5. Nagai, K., Perutz, M. F. & Poyartt, C. Oxygen binding properties of human mutant hemoglobins synthesized in Escherichia coli. *Proc. Natl. Acad. Sci. USA* **82**, 7252–7255 (1985).
6. Gentle, I. E., Souza, D. P. De & Baca, M. Direct Production of Proteins with N-Terminal Cysteine for Site-Specific Conjugation. *Bioconjug. Chem.* **15**, 658–663 (2004).

7. Ren, H. *et al.* A Biocompatible Condensation Reaction for the Labeling of Terminal Cysteine Residues on Proteins. *Angew. Chemie Int Ed* **48**, 9658–9662 (2009).
8. Nguyen, D. P., Elliott, T., Holt, M., Muir, T. W. & Chin, J. W. Genetically Encoded 1,2-Aminothiols Facilitate Rapid and Site-Specific Protein Labeling via a Bio-orthogonal Cyanobenzothiazole Condensation. *J. Am. Chem. Soc.* **133**, 11418–11421 (2011).
9. Chen, S., Touati, J. & Heinis, C. Tracking chemical reactions on the surface of filamentous phage using mass spectrometry. *Chem Commun* **50**, 5267–5269 (2014).

CHAPTER 6
CONCLUSIONS

The antibiotic resistance crisis has become a global public health threat, requiring an urgent solution. The continuous overuse and misuse of antibiotics along with the lack of novel antimicrobial drug development has fueled this crisis. According to the CDC, there are several rapidly emerging resistant bacterial species that are recognized as serious threats, including multidrug-resistant *Acinetobacter* and methicillin-resistant *S. aureus*.¹ Bacteria present many mechanisms to evade antibiotics, including cell surface modifications. Both *A. baumannii* and *S. aureus* display resistance mechanisms that add amine functionalities to their surface, causing electrostatic repulsion to cationic antibiotics.² Developing methods to directly target these characteristic surface modifications of resistance poses an excellent strategy to pursue in the field of antibiotics. The work presented in this dissertation offers an intriguing approach to target bacterial cells, particularly those displaying resistance, via dynamic covalent iminoboronate formation between bacterial surface amines and *ortho*-boronyl aryl ketones.

Back in 2014, our group began to investigate iminoboronate formation between 2-APBA and amine-presenting lipids of bacteria, such as Lys-PG, which is known to be expressed on *S. aureus* and contribute to its pathogenicity. We reported an unnatural amino acid, namely AB1, that was able to selectively label Gram-positive bacterial cell membranes over Gram-negative bacteria and mammalian cells.³ Although promising, the interaction of AB1 with the bacterial cell membrane was inhibited by the presence of serum proteins, specifically albumin, which encompasses many surface lysine residues that can engage in iminoboronate formation. Additionally, AB1 suffered from the requirement of high concentrations, effectively staining *S. aureus* at concentrations of

100 μM or higher. We devised two solutions to the concentration and interference problems: conjugation of AB1 to a cationic peptide and increasing the valency of the APBA warhead on a peptide scaffold.

Conjugation of AB1 to Hlys (Hlys-AB1) allowed for a synergistic binding effect where the cationic peptide portion of Hlys directed the conjugate to the bacterial cell surface and AB1 could covalently attach to achieve potent binding.³ Along with increasing the potency of AB1 towards *S. aureus*, effectively labeling the bacteria at sub- μM concentrations, significantly less serum protein interference was observed. Synthesizing multivalent APBA peptides allowed for even more potent labeling of *S. aureus* cells. Unfortunately, the multivalent peptides exhibited more serum protein interference than Hlys-AB1; however, KAM-CT(GRG) was ~ 10 -fold more potent than Hlys-AB1 and exhibited the least amount of serum protein interference. KAM-CT(GRG) demonstrates the promise in being able to achieve potent bacterial-specific peptide probes whose staining is not completely inhibited by serum proteins. The results of the multivalent peptide series establish the limitations of rationally designed peptides.

Although the multivalent peptides are not ideal for real application, their albumin-binding capability could be exploited for improving the pharmacokinetic properties of low molecular weight compounds, which would otherwise be subjected to rapid renal clearance.⁴ The thermodynamics, kinetics and selectivity of albumin binding is presented in this dissertation via *in vitro* studies. *In vivo* studies in mice would be crucial to fully realize the advantage of these multivalent APBA peptides as drug carriers.

As mentioned, KAM-CT(GRG) demonstrates the promise of being able to achieve potent bacterial binders with limited serum protein interference. The addition of three arginine residues reduced the interference from 90% to 70%. It was compelling to speculate what effects other amino acid residues would have on selective and potent binding. Towards this end, a peptide library, specifically phage display, was pursued. Phage display is a screening technique in which a library of peptides is expressed on the outside of a phage virion. Due to recent advances in the field, which offer the chemical and genetic modification of phage libraries, phage display is no longer limited solely to natural, proteinogenic amino acids.⁵ Expanding the chemical space of phage display libraries, our group developed a phage library that was chemically modified with reversible covalent warheads.⁶ Specifically, the library presents two APBA moieties separated by seven random amino acids. We hypothesized that this library could be used to discover potent divalent peptide probes against bacterial cells. By screening against a target of interest in the presence of serum albumin, the experimental setup allows us to incorporate an internal competitor for iminoboronate formation in which peptides with a strong affinity for albumin can be eliminated during washing steps.

The first screening approach we endeavored was panning against a specific bacterial target, immobilized on streptavidin agarose beads. The pentapeptide portion of Lipid II was chosen as the target for screening since it is the target of various antibiotics and has a lysine residue that can be pursued with iminoboronate chemistry. Although the lysine is not a direct effect of resistance, modification of the Lipid II structure is known to contribute to resistance. For example, the D-Ala-D-Ala to D-Ala-D-Lac mutation of the

stem peptide acquires vancomycin resistance in various Gram-positive bacteria such as *S. aureus*.⁷ Although screening against the Lipid II pentapeptide yielded sequence repeats after the third round of panning, upon peptide synthesis off-phage, the peptides did not bind to or cause cell killing of *S. aureus*. Although panning against the Lipid II pentapeptide failed, it educated us in the limitations of library panning. Perhaps the biotinylation and immobilization of the target does not display the Lipid II pentapeptide in an optimal manner to achieve binding. It is conceivable that the linker between the Lipid II pentapeptide and the biotin needs to be longer to properly display the target on the streptavidin beads. In retrospect, it is also plausible that the Lipid II pentapeptide is simply too small to pan against and pull down binders to with such a short heptamer peptide library.

With the failed effort of screening the APBA-dimer library against a specific target, live cell panning was pursued instead. Excitingly, panning directly against *S. aureus* cells allowed for the discovery of potent peptide dimers against *S. aureus*.⁶ Of particular interest was KAM5 which effectively stained *S. aureus* selectively at sub- μ M concentrations over other bacterial species and in the presence of high concentrations of serum albumin. Our peptides are much more potent than peptides borne out of earlier efforts with phage library screens against live cells, which display sub to low millimolar potencies. Additionally, our iminoboronate-capable library is advantageous over libraries not displaying the covalent warheads, indicated by the lack of peptide hits identified in parallel screened control libraries.

With a potent and selective *S. aureus* peptide probe in hand, we sought to conjugate an entity that would allow for targeted cell killing of *S. aureus*. Targeted, narrow-spectrum, antimicrobial agents are currently of particular interest in the field of antibiotics because they allow for selective killing of solely the target bacterium, leading to a lower propensity to accumulate resistance and less disruption to the gut microbiome.⁸ After synthesizing various KAM5 conjugates which failed to elicit *S. aureus* cell death, a KAM5-phototoxin was synthesized that allowed for the selective killing of *S. aureus* upon visible light irradiation. Although a targeted antibiotic with light-responsive activity could be beneficial in certain clinical circumstances, such as in endoscopic procedures or during surgery where light can be easily supplied, it would be ideal to be able to conjugate antibiotics with other modes of action to expand the scope of our strategy to create targeted antibiotics.

One of the major limitations of live cell panning is the lack of knowledge of your target. We can speculate that KAM5 binds to Lys-PG on the *S. aureus* cell surface; however, confirmation of the binding mechanism would be valuable to fully understand these peptides and their capabilities. Future work that could be pursued on this front would include obtaining a *S. aureus* cell line with a MprF-knockdown, the enzyme responsible for Lys-PG production. Lack of staining of this strain of *S. aureus* would indirectly confirm Lys-PG as the target. For more direct evidence, the iminoboronate between KAM5 and the *S. aureus* cell membrane could be reduced and the lipids could be isolated and analyzed via mass spectrometry for any modifications. Understanding exactly how KAM5 binds to the bacterial cell surface would allow us to make more in

depth conclusions regarding the failure of the KAM5 conjugates and their lack of instigating any *S. aureus* cell death.

To probe the general applicability of our library and screening approach, the APBA-dimer library was panned against a colistin-resistant, LOS-deficient strain of *A. baumannii* from the laboratory of Prof. Tim van Opijnen. Incorporating a negative screen against wild-type *A. baumannii*, species selective peptide probes were identified in the screen. Of particular interest was KAM8, which selectively labeled the LOS-deficient *A. baumannii* at sub- μ M concentrations over the wild-type strain and in the presence of high concentrations of serum albumin. KAM8 was similarly converted into a targeted antibiotic via conjugation to a phototoxin, showcasing that strain-specific bacterial cell killing can be achieved through phage display of APBA-presenting peptides.

KAM5 and KAM8 bind their respective target bacterium in the presence of serum albumin, demonstrating that the protein interference problem can be overcome by including serum albumin in the screening mixture. Interestingly, both peptides exhibit enhanced binding with albumin present in the sample. We showed that they do indeed bind albumin via fluorescence anisotropy, leading to the hypothesis that a ternary complex may form between the peptide, bacteria and albumin. This phenomenon deserves to be further investigated to broaden our understanding of the binding mechanism of each peptide to their respective bacterial species/strain.

We additionally panned against two other mutant *A. baumannii* strains from the laboratory of Prof. Tim van Opijnen (EGA-407 and EGA-408), which exhibit mutations in the *pmrC* gene responsible for the addition of phosphoethanolamine to the LPS surface,

known to cause colistin resistance.² These screens revealed peptide hits that labeled all of the colistin-resistant strains (EGA-407, EGA-408 and LOS-) but not the wild-type strain. One particular peptide, KAM19, was further investigated and distinguished as a probe that could detect general colistin resistance in a sample of *A. baumannii* in the presence of human serum. The ability to detect resistance to a certain antibiotic in a bacterial sample would be extremely beneficial in diagnostics for the rapid and accurate treatment of infections. For example, being able to rapidly detect that an infection is resistant to colistin, and will not respond to its treatment, would eliminate the use of colistin entirely and save valuable time, which a patient with a serious infection may not have much of. Although the preliminary work herein demonstrates a peptide probe that can detect colistin resistance over colistin susceptible *A. baumannii*, future work should determine the detection limit and clinical application of this probe. It is feasible that this library and screening approach could be used to develop peptide probes that can recognize other antibiotic resistance traits, further developing the way physicians analyze and treat infections.

Screening the APBA-dimer library allowed for the discovery of potent and selective peptide probes against a particular bacterial species of interest. With the addition of negative screens, even strain specific bacterial targeting was achieved. Using iminoboronate chemistry allowed us to pursue clinically relevant bacterial strains, which exhibit antibiotic resistance, and develop targeted antibiotics for these strains. In addition to allowing for a novel reversible covalent binding mechanism to the bacteria, the APBA warheads on the peptide probes allow for increased serum stability, a typical pitfall for

peptide therapeutics due to protease cleavage. It is intriguing to speculate if we can achieve even more potent peptide probes by improving the design of our phage display libraries. For example, it is conceivable that cyclic, bicyclic, polyvalent, or dually-modified phage libraries can be constructed and screened against a multitude of targets to develop improved peptide probes. The work presented here confirms that we can indeed construct phage libraries; however, future work needs to focus on the development of more effective techniques to analyze modifications on phage.

In conclusion, the work described in this dissertation clearly demonstrates the utility of the APBA warhead to engage in iminoboronate formation with amine-presenting bacterial cell surfaces. Having a multivalent display of these dynamic covalent binding motifs allows us to not only achieve potent bacterial recognition, but also to evolve strain-specific antibiotics. The story of overcoming the protein interference problem with iminoboronate-capable peptide probes, which starts with the investigation of rationally designed multivalent peptides then turns into the successful development of divalent peptide probes via phage display, clearly demonstrates the robust nature of utilizing peptide library screens in drug development.

I believe peptide library screening and library screening in general present a powerful approach to modern drug discovery. Affinity selection techniques, such as phage display, allow researchers to screen hundreds of millions of compounds against a desired target at once. In my dissertation, phage display library screening allowed me to not only achieve potent binders to my desired target, but the experimental setup also allowed me to solve a major problem in the field of iminoboronate chemistry: selectivity

towards a desired amine. With the feasibility to chemically modify phage to present desired ligands, not only do I anticipate our group to achieve improved peptide probes using better designed phage libraries, but I anticipate that the chemical space of phage display will be rapidly expanded in the near future. I am immensely intrigued by the power of selections techniques to the extent that I will be starting my career in the biotechnology industry in a lead discovery and optimization group exploring affinity selections for drug discovery.

References

1. Ventola, C. L. The antibiotic resistance crisis. *P & T* **40**, 277–83 (2015).
2. Steinbuch, K. B. & Fridman, M. Mechanisms of resistance to membrane-disrupting antibiotics in Gram-positive and Gram-negative bacteria. *Med. Chem. Commun.* **7**, 86–102 (2016).
3. Bandyopadhyay, A., McCarthy, K. A., Kelly, M. A. & Gao, J. Targeting bacteria via iminoboronate chemistry of amine-presenting lipids. *Nat. Commun.* **6**, 6561 (2015).
4. Dennis, M. S., Zhang, M., Meng, Y. G., Kadkhodayan, M., Kirchhofer, D., Combs, D. & Damico, L. A. Albumin Binding as a General Strategy for Improving the Pharmacokinetics of Proteins. *J. Biol. Chem.* **277**, 35035–35043 (2002).
5. Mohan, K. & Weiss, G. A. Chemically Modifying Viruses for Diverse Applications. *ACS Chem. Biol.* **11**, 1167–1179 (2016).
6. McCarthy, K. A., Kelly, M. A., Li, K., Cambray, S., Hosseini, A. S., van Opijnen, T. & Gao, J. Phage Display of Dynamic Covalent Binding Motifs Enables Facile Development of Targeted Antibiotics. *J. Am. Chem. Soc.* **140**, 6137–6145 (2018).
7. Walsh, C. T. Vancomycin Resistance: Decoding the Molecular Logic. *Science* **261**, 308–309 (1993).
8. Fischbach, M. A. & Walsh, C. T. Antibiotics for Emerging Pathogens. *Science* **325**, 1089–1094 (2009).